Drug Accumulation in Gram-negative Bacteria is Growth Phase Dependent

by

Emily Elizabeth Whittle

A thesis submitted to the University of Birmingham for the degree of

DOCTOR OF PHILOSOPHY

Institute of Microbiology and Infection
College of Medical and Dental Sciences
University of Birmingham
September 2020

Abstract

For antibiotic classes with intracellular targets, effective treatment of bacterial infections requires the drug to accumulate to a high concentration inside cells. Decreased permeability of the cell envelope and increased efflux pump activity causes low intracellular accumulation of antibiotics, contributing to the development of antimicrobial resistance. Here, the aim was to identify whether the balance between influx and efflux differs depending on bacterial growth phase in *Salmonella enterica* serovar Typhimurium. A novel flow cytometry assay was developed and used to measure accumulation of ethidium bromide (EtBr) in *S.* Typhimurium SL1344 and Δ*acrB* strains during growth. In SL1344, EtBr accumulation remained low, regardless of growth phase and did not correlate with *acrAB* transcription. EtBr accumulation in Δ*acrB* was high in exponential phase but dropped sharply later in growth and by stationary phase, EtBr accumulation was not significantly different from SL1344. Low EtBr accumulation in both strains was shown not to be due to the upregulation of other efflux pumps, but instead, due to decreased permeability of the membrane in stationary phase. RNAseq identified changes in expression of several pathways that are associated with decreased membrane permeability in stationary phase. This study shows that efflux is only important for maintaining low drug accumulation in actively growing cells, and that membrane permeability is the predominant factor in stationary phase. This conclusion means that (i) more consideration may be required when prescribing existing antibiotics that have intracellular targets in complex non-growing or slow-growing bacterial infections where accumulation concentration may be low, and (ii) efflux inhibitors may be successful in potentiating the activity of existing antibiotics, but potentially only for bacterial infections where cells are actively growing.

Acknowledgements

Thank you to the Wellcome Trust for funding this PhD project.

I would like to thank my supervisor, Dr. Jessica Blair for the constant support and advice with my PhD project and thesis and for life in general, and for the continuous supply of biscuits and cakes to keep morale high. I would also like to thank Dr. Tim Overton, for the constant flow cytometry help but also the time spent helping me with advice and ideas when the massive amount of RNAseq gene lists got too overwhelming.

I also greatly appreciate all laboratory-based help from Dr. Helen McNeil, without whose cloning expertise I may have had more failures than I did. Also, to Dr. Alessandro Di Maio, for the time spent teaching me microscopy. Big thanks also to the flow cytometer in T102 for working sometimes (I now know the true meaning of the word temperamental).

Thanks go to the friends I have made throughout my PhD. To the first cohort of the Wellcome Trust AAMR DTP, thanks for getting me through that first year! And a thank you to all Blair lab members, past and present, for the fun and laughs, as well as Costa trips when experiments went wrong.

And to my all-time favourite people - I would like to thank my parents for always inspiring me and for giving me the belief that I could to do whatever I wanted. Thanks to my big brother, for teaching me what DNA meant before I even got to my first Biology lesson. And to Jack, for reading all my thesis drafts, for telling me off when I decided I wanted to quit, and for pretty much everything else.

Clarification of Results produced under Supervision or in Collaboration

The figures detailed below contain results produced in collaboration or as a result of supervision of undergraduate/masters students within the lab.

Chapter 3:

Figure 3-3 Accumulation of Nile Red in WT, Δ*acrB* and *tolC::aph* in *S*. Typhimurium. This assay was optimised and results were obtained by Ilyas Alav under the supervision of Emily Whittle.

Figure 3-4 Accumulation of EtBr in SL1344 in the absence and presence of 100 μM CCCP and 50 μg/mL of PAβN. The PAβN assay was optimised and results were obtained by Simon Legood under the supervision of Emily Whittle.

Chapter 4:

The items listed below were completed in collaboration with Jayant Cherukat, with Emily Whittle acting as laboratory supervisor.

Table 4-4 Susceptibility profiles of SL1344 and Δ*acrB* at 1, 3 and 5 hours.

Figure 4-10 Curli biogenesis of 14028s, SL1344 and SL1344 ΔacrB stained with congo red

Figure 4-11 Biofilm formation by crystal violet staining in S. Typhimurium at 1, 3 and 5 hours.

Chapter 7:

Emily Whittle collaborated with Helen McNeil on preparation of samples for RNAseq. Genewiz was responsible for RNA extraction, sequencing and data analysis.

Table of Contents

List of Figures

List of Tables

List of Abbreviations

ABC - ATP binding cassette
AI-2 - Autoinducer-2
AMR - Antimicrobial resistance
aph - Aminoglycoside phosphotransferase
ATP - Adenosine triphosphate
bp - Base pairs
BSAC - British society of Antimicrobial Chemotherapy
CASP - Constant activity at stationary phase
CCCP - Carbonyl cyanide 3-chlorophenylhydrazone
CFDA-AM - 5-Carboxyfluorescein Diacetate, Acetoxymethyl Ester
CFU - colony forming unit
COG - Clusters of Orthologous genes
DEG - Differentially expressed genes
DNA - Deoxyribonucleic acid
Dps - DNA protection during starvation
ECA - Enterobacterial common antigen
EDPI - energy-dependent phase I
EDPII - energy-dependent phase II
EDTA - Ethylenediaminetetraacetic acid
ESβL - Extended spectrum β-lactamases
EtBr - Ethidium bromide
FDA - Fluorescein diacetate
Fis - Factor for Inversion Stimulation
FSC-H - Forward scatter – Height
GASP - Growth advantage in stationary phase
GFP - Green fluorescent protein
GlcNAc - N-acetyl glucosamine
HBS - HEPES buffered saline
IHF - Integration host factor
IM - Inner membrane
KPC - *Klebsiella pneumoniae* carbapenemases
LB - Luria Bertani
LED - Light-emitting diode
LIC - Ligation independent cloning

Log - logarithmic
LPS - Lipopolysaccharide
Lrp - Leucine responsive regulator protein
MATE - Multidrug and toxic compound extrusion
MDR - Multidrug resistant
MFI - mean fluorescence intensity
MFS - Major facilitator superfamily
MIC - Minimum inhibitory concentrations
mRNA - Messenger RNA
MRSA - Methicillin resistant *Staphylococcus aureus*
msfGFP - Monomeric superfolder GFP
MurNAc - N-acetyl muramic acids
NDM - New Delhi Metallo-β-lactamase
NEB - New England Biolabs
NPN - 1-*N*-phenylnaphthylamine
nm - nanometres
NTS - Non-typhoidal *Salmonella*
OD - Optical density
OM - Outer membrane
PAβN - Phenylalanine-Arginine Beta-Naphthylamide
PACE - Proteobacterial antimicrobial compound efflux
PAP - Periplasmic adaptor proteins
PBP - Penicillin binding proteins
PBS - Phosphate buffered saline
PCR - Polymerase chain reaction
PHE - Public Health England
PMF - proton motive force
PMT - photomultiplier tubes
PPB - Potassium phosphate buffer
ppGpp - guanosine 5',3' bispyrophosphate
QS - Quorum sensing
RFU - Relative fluorescence units
RIN - RNA integrity number
RMF - Ribosome modulation factor
RNA - Ribonucleic acid

RND - Resistance nodulation division
rRNA - Ribosomal RNA
RT-PCR - Reverse transcription polymerase chain reaction
SAM - *S*-adenosyl-L-methionine
SCDI - Stationary phase contact dependent inhibition
SEM - Standard error of the mean
SDS - Sodium dodecyl sulphate
SMR - small multidrug resistance
SRA - stationary-phase-induced ribosome-associated
sRNAs - Small RNAs
SHV - Sulphydryl variant β- lactamase
SSC-H - Side scatter – Height
TCA - Tricarboxylic acid
TEM - Temoneira β- lactamase
ToF-SIMS - Time-of-Flight secondary ion mass spectrometry
TraDIS - Transposon Directed Insertion Site Sequencing
tRNA - Transfer RNA
UTI - Urinary tract infection
UTR - Untranslated region
UV - Ultraviolet
VNBC - Viable non culturable state
VRE - Vancomycin resistant enterococcus
WHO - World Health Organisation
WT - Wild type
1,2-DNA - 1,2-dinapthylamine

Chapter 1 - Introduction

1.1 The burden of Antimicrobial Resistance

Antimicrobial resistance (AMR) is one of the biggest public health threats faced in the 21st century (O' Neill, 2016, Davies, 2011). In 2017, the WHO published a report which prioritised several pathogens including *Acinetobacter baumannii*, *Pseudomonas aeruginosa*, Enterobacteriaceae, *Salmonella* and *Mycobacterium tuberculosis* which are considered to be the biggest challenge when combatting AMR (WHO, 2017b, WHO, 2017a). The O'Neill report predicted that by 2050, there will be 10 million deaths a year due to AMR infections (O' Neill, 2016) if no solutions are found to curb the rise in antimicrobial resistance.

Although the burden of AMR is increasing, the discovery of new antibiotic classes has been limited in this century, with only some new antibiotics introduced clinically. These more recent classes of antibiotics include oxazolidinones, namely linezolid, which became clinically available in 2000 (Senior, 2000), and glycyclines, namely tigecyline, which although related to tetracycline, has an increased spectrum of activity (Greer, 2006). The timeline of the discovery of antibiotic classes is shown in **Figure 1-1**. Antibiotic drug discovery is constantly ongoing, but research has also focused on alternatives to antibiotics, such as inhibitors to the mechanisms of resistance, anti-virulence drugs and vaccines.

Figure 1-1 Timeline of Antibiotic Discovery in the 20th and 21st century.

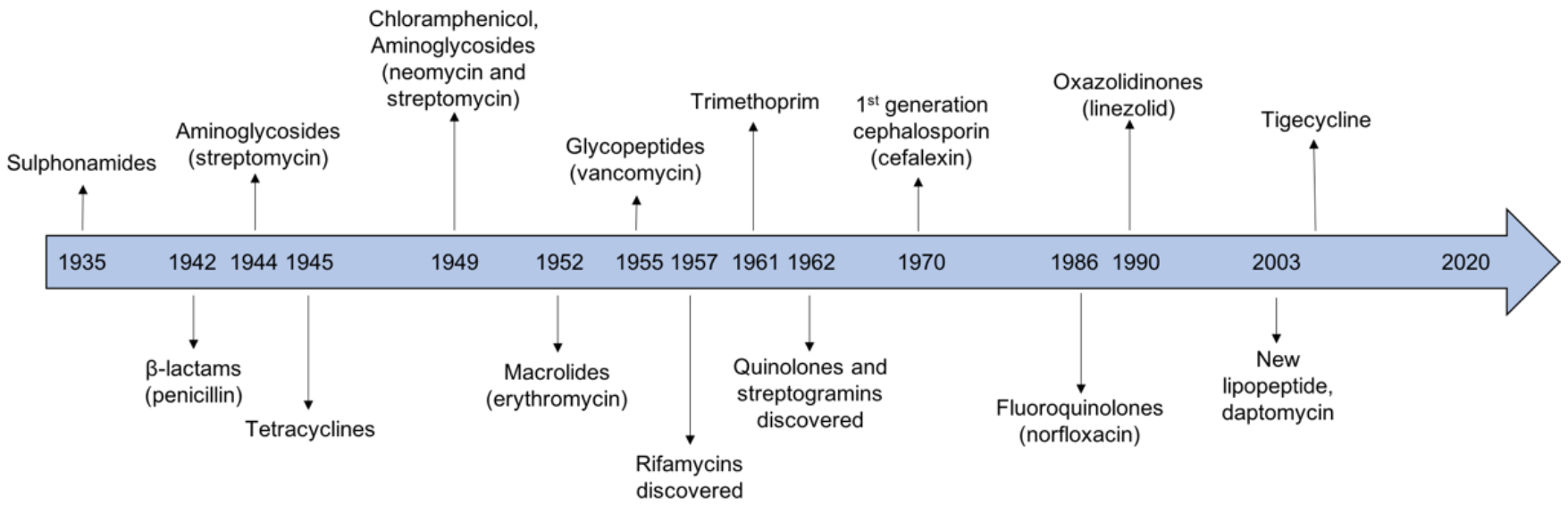

The blue arrow highlights a timeline with key dates for the discovery of the antibiotic classes labelled. In 1935, the first antibiotic class, sulphonamides, were discovered. There was a 'golden age' of antibiotic discovery in the 20th century. In the last decade, no new antibiotic classes have been available for use clinically. Figure is adapted from Hogberg et al. (2010)

1.2 Mechanisms of AMR

There are several mechanisms bacteria use to confer AMR. These include target modification, metabolic bypass, enzymatic degradation, reduced permeability and increased efflux of antibiotics (**Figure 1-2**).

Figure 1-2 Mechanisms of AMR.

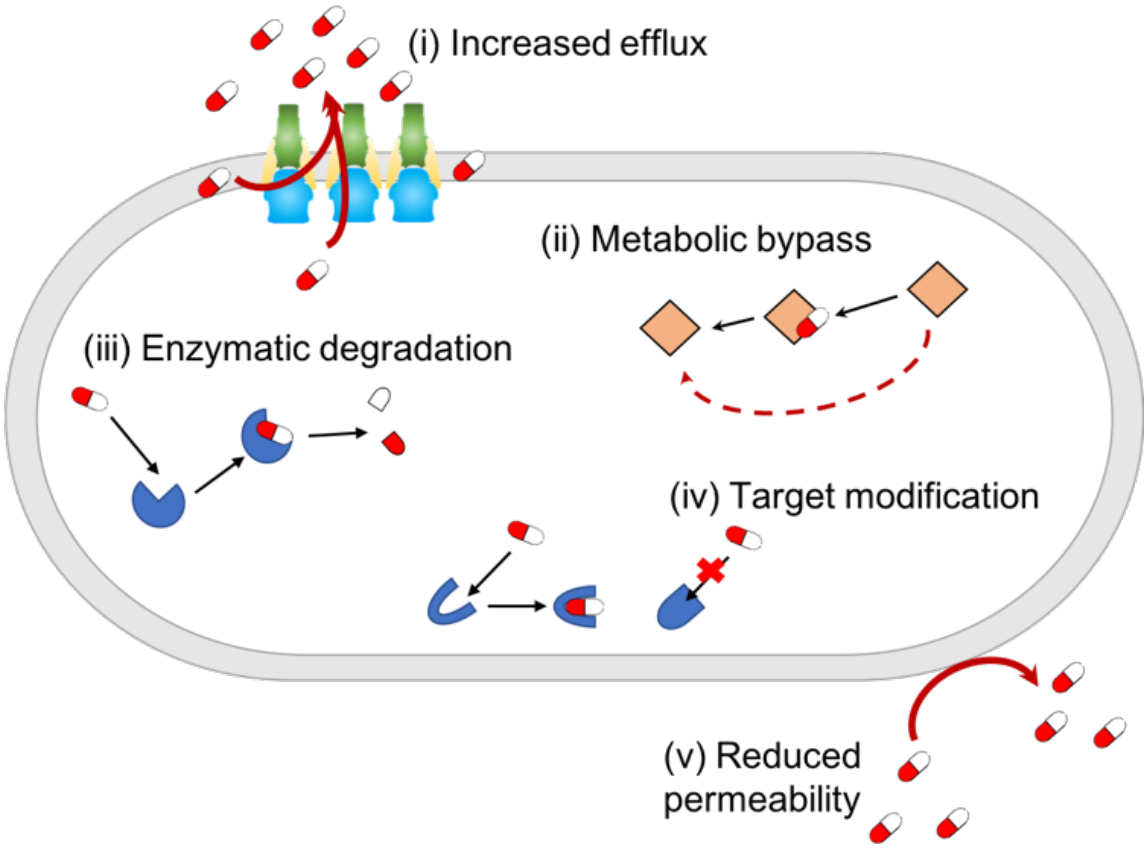

This schematic diagram illustrates the mechanisms by which bacteria develop resistance to antibiotics. (i) Increased expression of efflux pumps leads to an increase in export of antibiotics from cells. (ii) Bacteria can alter metabolic pathways to circumvent the need for the target of the antibiotic. (iii) Enzymes can degrade the antibiotic inside the bacterial cell. (iv) Antibiotic targets can mutate and modify so that antibiotics are not longer effective. (v) Reduced permeability means that antibiotics cannot enter the cell and reach their target. Figure adapted from Singh et al. (2014)

1.2.1 Target modification

The mechanism of action of most antibiotics relies on binding to a specific target within a bacterial cell, either for inhibition of bacterial growth or to kill bacterial cells (Lambert, 2005). Resistance to antibiotics can develop when the gene encoding the target of the antibiotic within bacteria mutates; this mechanism is target modification (**Figure 1-2iv**). This prevents the antibiotic from effectively binding to and inhibiting its target. In *Streptococcus sp.*, the accumulation of mutations in penicillin binding protein 2 (PBP2), a target for β-lactams, reduces the susceptibility to this drug class (Laible and Hakenbeck, 1991). In *Salmonella enterica* serovar Typhimurium (Eaves et al., 2004a) and a large number of *Enterobacteriaceae* clinical isolates (Weigel et al., 1998), mutations in the deoxyribonucleic acid (DNA) gyrase genes, *gyrA* and *gyrB*, confer resistance to fluoroquinolones. Rifampicin targets RNA polymerase, however, substitutions in *Mycobacterium* RNA polymerase confers resistance to rifampicin (Telenti et al., 1993). Modifications in lipopolysaccharides (LPS) in Gram-negative bacteria confer resistance to polymyxins and colistin (Olaitan et al., 2014). The plasmid-mediated *mcr-1* gene, which encodes a phosphoethanolamine transferase, modifies bacterial LPS within the inner membrane by adding phosphoethanolamine to lipid A (Liu et al., 2016, Sabnis et al., 2020). This target modification subsequently leads to bacteria developing resistance to colistin treatment (Liu et al., 2016).

1.2.2 Metabolic bypass

Bacteria have evolved ways to acquire antibiotic resistance by bypassing the target of the drug using a different metabolic pathway to carry out the same function (**Figure**

1-2ii). *Staphylococcus aureus* becomes resistant to methicillin through acquisition of the SSC*mec* chromosomal cassette carrying the *mecA* gene, which encodes for PBP2A (Katayama et al., 2000). The increased expression of *mecA* is linked to an increase in methicillin resistance but a decrease in toxin-mediated virulence (Rudkin et al., 2012). Like other PBPs, PBP2A can form peptidoglycan crosslinks in bacterial cells, but it has low affinity for β-lactams, bypassing the requirement for β-lactam susceptible PBPs (Hartman and Tomasz, 1984), therefore causing Methicillin Resistant *Staphylococcus aureus* (MRSA). Metabolic bypass mechanisms have also been described in *Enterococcus sp.* Glycopeptides such as vancomycin are large antibiotics with activity against Gram-positive bacteria. Their action is to inhibit peptidoglycan synthesis by binding to the D-ala of the peptidoglycan pentapeptide (Bugg et al., 1991). However, the *van* cluster of genes replace D-alanine with D-serine or D-lactate, reducing the susceptibility to glycopeptides (Bugg et al., 1991, Munita and Arias, 2016).

1.2.3 Enzymatic degradation

Degradation of antibiotics is a key mechanism of AMR (**Figure 1-2iii**). Resistance to penicillins, cephalosporins and carbapenems of the β-lactam class has been commonly described in clinical isolates. Enzymes named β-lactamases or carbapenemases degrade the antibiotic by hydrolyzing the β-lactam ring, either through enzyme acylation (serine β-lactamases) or by zinc ions aiding in hydrolysis (metallo-β-lactamases) (Bush, 2018). The first penicillinase was discovered as early as 1940 (Abraham and Chain, 1988). These enzymes are often found on plasmids and are spread by horizontal gene transfer. Examples include Temoneira (TEM)

(Heffron et al., 1975) and Sulphydryl variant (SHV) (Heritage et al., 1999) enzymes, followed by more prevalent CTX-M (Bonnet, 2004) classed as Extended Spectrum β-lactamases (ESβLs). Global dissemination of ESβLs led to increased use of potent carbapenems, leading to the rise in carbapenemases. Of high concern are *Klebsiella pneumoniae* carbapenemases (KPC) and New Delhi β-lactamase (NDM-1) (Yong et al., 2009) disseminating through Enterobacteriaceae.

1.2.4 Outer membrane permeability

Gram-negative bacteria are intrinsically more resistant to antibiotic treatment because they have an outer membrane (OM) barrier which prevents access to larger antibiotics (Blair et al., 2015b). Hydrophilic antibiotics, including commonly used β-lactams and fluoroquinolones, enter Gram-negative bacterial cells through small membrane protein channels called porins (Blair et al., 2015b, Nikaido, 1989, Masi et al., 2019). OmpF and OmpC are the major porins found in Enterobacteriaceae including *Salmonella* (Pratt et al., 1996). Resistance due to membrane permeability can arise in numerous ways including downregulation of porin genes (Dupont et al., 2017), replacement of non-specific porins with more specific porins, substitutions in the porin protein which can change the diameter of the protein channel (De et al., 2001, Bajaj et al., 2016) or by changing the electric field and blocking translocation of the drug across the membrane (Bajaj et al., 2016). OmpF can be replaced with the more specific OmpC, or both can be downregulated or mutated, playing a fundamental role in β-lactam resistance, including resistance to more potent, last line carbapenems (Masi et al., 2019).

1.2.5 Efflux

Bacteria have specialised pumps that are able to remove substrate molecules, including antibiotics, from inside cells to outside. The balance between the prevention of drug entry and the removal of antibiotics can lead to low intracellular accumulation of drugs in bacterial cells (Bolla et al., 2011).

In clinical isolates, overexpression of efflux pumps is commonly described. This leads to increased efflux activity and decreased susceptibility to antibiotics. AcrAB-TolC and MdfA are examples of efflux pumps in *Escherichia coli* that have been overexpressed in clinical isolates, causing resistance to fluoroquinolones (Swick et al., 2011). During tigecycline clinical trials, reduced susceptibility of the drug to *E. coli* clinical isolates was shown to be caused by the overexpression of MarA and therefore the overexpression of AcrAB-TolC (Keeney et al., 2008). *S.* Typhimurium DT104 has been isolated from cattle with overexpression of AcrAB-TolC (Baucheron et al., 2004). A number of studies have shown that overexpression of the AdeABC pump leads to multidrug resistance of clinical isolates of *Acinetobacter baumanii* (Yoon et al., 2013, Rumbo et al., 2013), including one study using isolates from a paediatric intensive care unit (ICU) (Chen et al., 2018). In *Pseudomonas aeruginosa,* multidrug resistant (MDR) isolates overexpress MexAB-OprM (Ziha-Zarifi et al., 1999, Llanes et al., 2004) and SmeABC and SmeDEF are overexpressed in clinical isolates of *Stenotrophomonas maltophila* (Chang et al., 2004). The overexpression of efflux pumps can itself lead to multidrug resistance as certain pumps remove multiple classes of antibiotics from cells.

1.3 *Salmonella*

1.3.1 Classification

Belonging to the family Enterobacteriaceae, *Salmonella sp.* are Gram-negative bacilli and are generally motile due to the presence of peritrichous flagella (Shu-Kee Eng, 2015, Riley et al., 2018). Based on 16S RNA sequence analysis, *Salmonella* are classified into two main species, *S. enterica,* known to infect humans and other mammals, and *S. bongori,* infecting mainly cold-blooded animals (Reeves et al., 1989, Fookes et al., 2011, Giammanco et al., 2002). *Salmonella enterica* is further divided into six subspecies named *S. enterica* subspecies *enterica, S. enterica* subspecies *arizonae, S. enterica* subspecies *salamae, S. enterica* subspecies *indica, S. enterica* subspecies *houtenae* and *S. enterica* subspecies *diarizonae* (Ryan et al., 2017). *Salmonella* is also categorised into serovars, based on the antigens a strain possesses, such as O- antigen on LPS of the bacterial membrane, H- flagellar antigens and K- capsular antigens. This categorisation is known as the Kauffman-White scheme (Salmonella Subcommittee of the Nomenclature Committee of the International Society for, 1934). There are now over 2500 serovars described (Ryan et al., 2017).

1.3.2 Infection and pathogenesis

Salmonella is a common human pathogen and is responsible for disease worldwide. Its most common manifestation is gastroenteritis, prevalent in both developed and developing countries. Salmonellosis, the infection caused by *Salmonella enterica*, can be separated into two clinical diagnoses depending on the serovar. *S.* Typhi and

S. Paratyphi cause enteric fever, classified as Typhoidal infection (Shu-Kee Eng, 2015). In 2014, the WHO estimated that typhoid fever accounts for around 222,000 deaths globally per year (WHO, 2015). Salmonellosis is also caused by non-typhoidal *Salmonella* (NTS) such as *S.* Typhimurium and *S.* Enteritidis (Gal-Mor et al., 2014), with the most common manifestation being gastroenteritis causing nausea and vomiting, abdominal cramps and diarrhoea. Salmonellosis is transmitted by the ingestion of infected food or water and, along with *Campylobacter,* is one of the most frequently isolated pathogens from a gastrointestinal infection, estimated at just over 93 million cases per year (Majowicz et al., 2010).

In 2017, Public Health England (PHE) recorded 306 symptomatic cases of typhoidal *S.* Typhi and *S.* Paratyphi in England, Wales and Northern Ireland, of which 93% were confirmed as imported cases as typhoidal *Salmonella* is not endemic to the UK (PHE, 2017). However, non-typhoidal *Salmonella* infection is more common with 8,558 cases recorded in 2016 in England and Wales (PHE, 2018), the most common causative agents being *S.* Enteritidis and *S.* Typhimurium (**Figure 1-3**). From 2015 to 2016, there was a decrease in the cases of *S.* Enteritidis (from 2495 to 2356 cases) but an increase in *S.* Typhimurium (from 1702 to 1770 cases) (PHE, 2018). This study will use *Salmonella enterica* serovar Typhimurium strain SL1344, both because it is a clinically relevant pathogen that causes a large number of infections in the UK each year (PHE, 2018) and due to the high level of multi-drug resistance in *S.* Typhimurium (Wang et al., 2019).

Figure 1-3 Laboratory confirmed cases of non-typhoidal *Salmonella* in England and Wales from 2007-2016

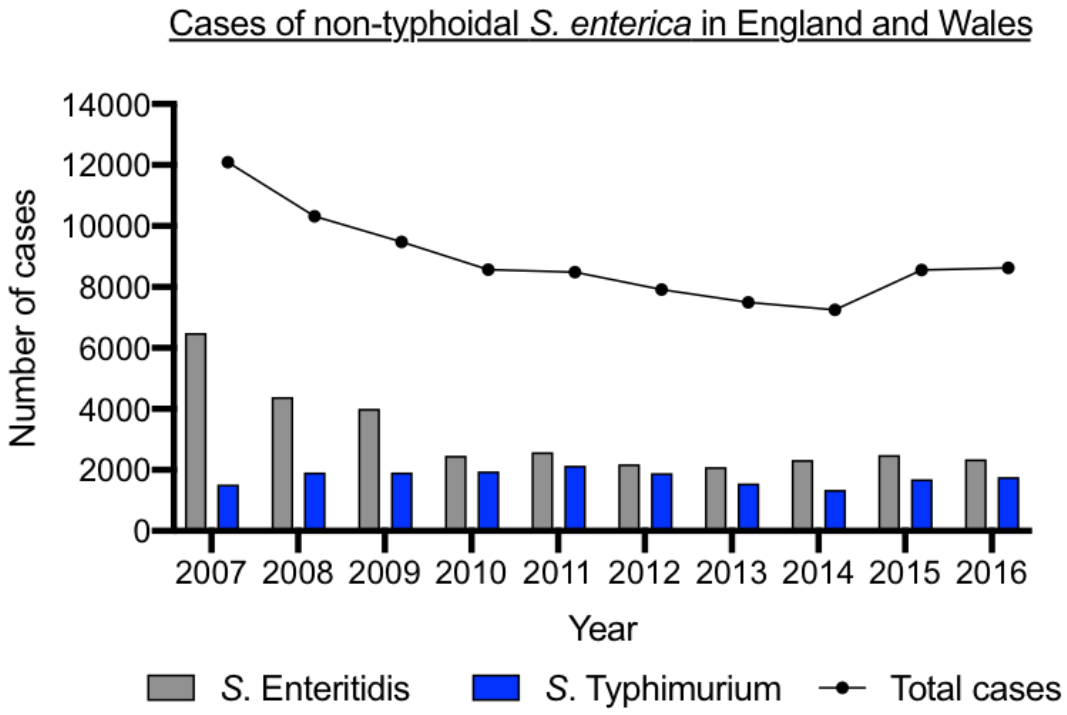

This graph shows the total cases of non-typhoidal *Salmonella* (black dotted line) of which the cases caused by *S*. Enteritidis (grey) and *S*. Typhimurium (blue) are shown. Data is taken from the PHE report on *Salmonella* cases (PHE, 2018).

1.3.3 Antibiotic treatment

Salmonellosis is normally a self-limiting infection and treatment is limited to rehydration unless severe. In more severe cases and for immunocompromised patients at high risk of invasive infection, an antibiotic such as ciprofloxacin or ceftriaxone may be prescribed (Kariuki et al., 2015, Lin et al., 2003).

1.4 The Gram-negative bacterial cell envelope

Gram-positive and Gram-negative bacteria have distinct cell envelopes. Gram-positive bacteria have a single phospholipid membrane with a thick outer layer of peptidoglycan (Silhavy et al., 2010). The Gram-negative envelope is comprised of two membranes separated by a periplasmic space containing a thin peptidoglycan layer (Beveridge, 1999), as shown in **Figure 1-4**.

1.4.1 The inner membrane

Gram-negative bacteria contain an inner membrane (IM) composed of phospholipids, like that of a eukaryotic cell membrane and membrane bound organelles (Ruiz et al., 2008, Silhavy et al., 2010). It also contains proteins with α-helical transmembrane domains and lipoproteins (Ruiz et al., 2008). Functions of membrane proteins located in the IM include energy production and lipid biosynthesis as well as protein secretion and translocation using transport systems such as Sec, YidC and the Tat translocon (Kudva et al., 2013). The IM is key in maintaining the proton motive force (PMF), which is required for a number of cellular processes (Huisman et al., 1996).

Figure 1-4 Schematic of the membrane of Gram-negative bacteria.

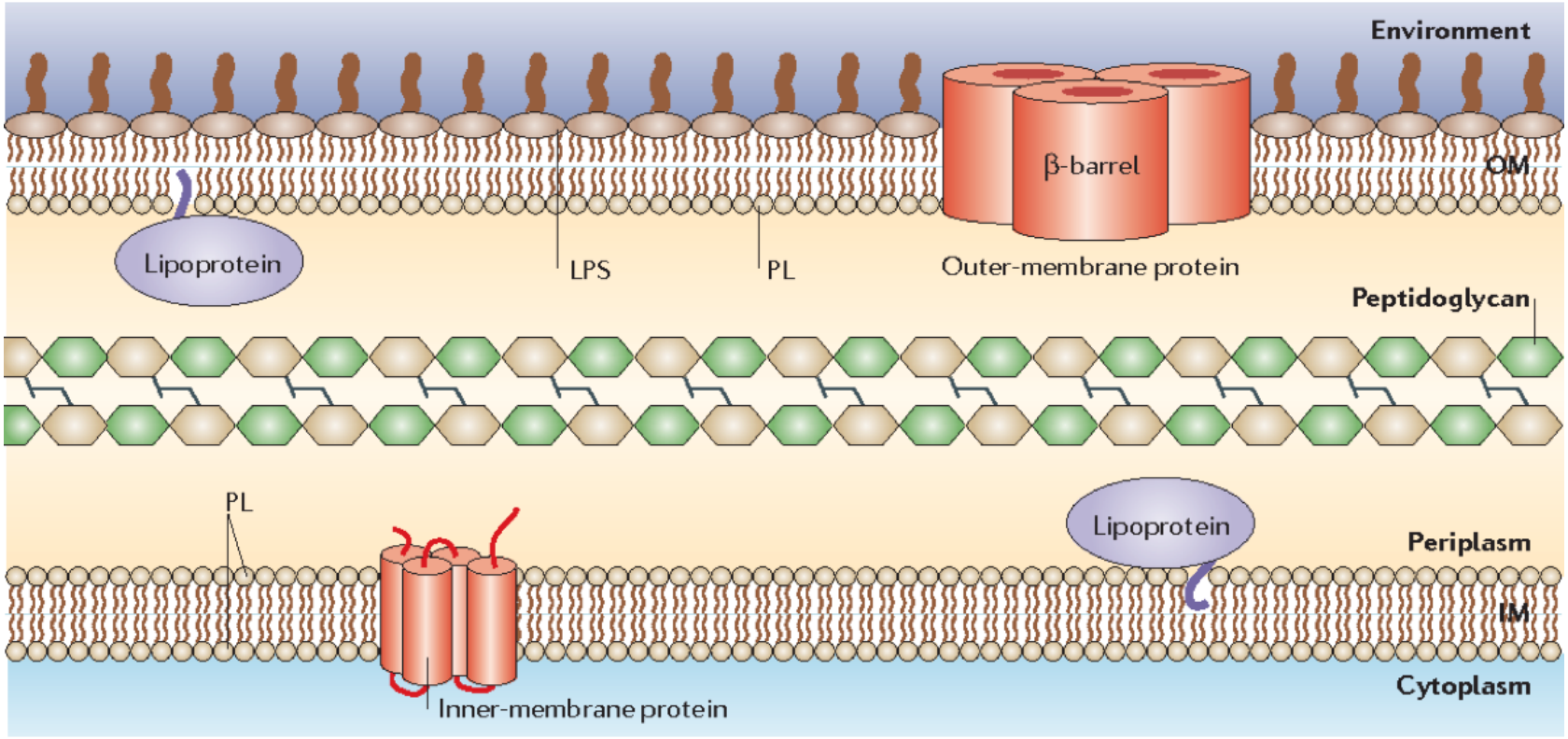

The schematic shows the OM, with LPS on the extracellular side and outer membrane porins. A thin layer of mature peptidoglycan is located in the periplasm. The IM phospholipid bi-layer separates the cytoplasm from the periplasm and also contains membrane proteins (Ruiz et al., 2008). This figure is taken from Ruiz et al. (2008).

1.4.2 The periplasm

The periplasm is the space between the inner and outer membranes of Gram-negative bacteria. The periplasm in both *Salmonella* and *E. coli* contributes 20-40% of the cells total volume (Stock et al., 1977). This compartment is densely populated with enzymes and other proteins (Silhavy et al., 2010). It is important for functions such as protein oxidation, secretion and folding, LPS secretion to the OM and peptidoglycan synthesis (Asmar et al., 2017).

1.4.3 The peptidoglycan layer

The shape and rigidity of a Gram-negative cell envelope is dictated by the thin layer of peptidoglycan located within the periplasm (Silhavy et al., 2010). Peptidoglycan is composed of repeating N-acetyl glucosamine GlcNAc) and N-acetyl muramic acids (MurNAc) that form glycan chains (Vollmer et al., 2008) which are covalently anchored to the OM of Gram-negatives by Lpp, which is an abundant lipoprotein sometimes known as murein or Braun's lipoprotein (Braun, 1975, Suzuki et al., 1978). Penicillin binding proteins (PBPs) are the enzymes required for production of the peptidoglycan macromolecule. PBPs are involved in the reaction to assemble the glycan chains, GlcNAc and MurNAc. Peptidoglycan also relies on crosslinking. MurNAc has a pentapeptide chain, with the final 2 amino acids commonly composed of D-alanine. PBPs involved in the transpeptidation of the penultimate D-ala (position 4) to the amino acid at position 3 on an adjacent strand, therefore forming crosslinks (**Figure 1-5**). Mature peptidoglycan does not have the final D-ala, and PBPs act as carboxypeptidases in this reaction (Macheboeuf et al., 2006, Vollmer et al., 2008).

Figure 1-5 Schematic of the crosslinking of peptidoglycan.

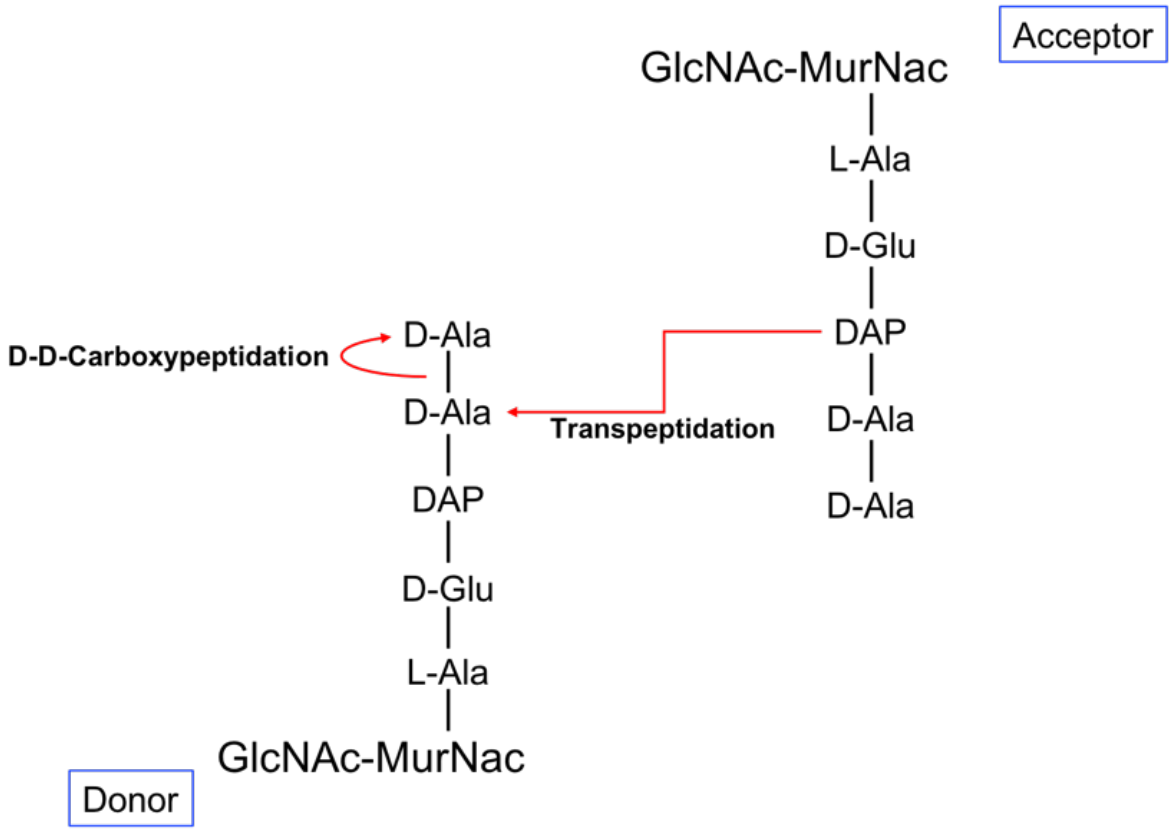

This figure outlines the crosslinking reaction of peptidoglycan. MurNAc has pentapeptide chains which are required for crosslinking. Diaminopimelic acid at position 3 of the pentapeptide crosslinks with the penultimate D-Ala (position 4) of an adjacent pentapeptide, called transpeptidation. D,D-carboxypeptidation results in the loss of the terminal D-Ala, forming mature peptidoglycan. Figure adapted from Macheboeuf et al. (2006).

1.4.4 The outer membrane

The OM of Gram-negative bacteria is an asymmetric protective barrier (Kamio and Nikaido, 1976). The OM contains phospholipids on the periplasmic facing side of the membrane, but is not classed as a phospholipid bilayer because the outer leaflet contains glycolipids such as lipopolysaccharide (LPS) (Silhavy et al., 2010). LPS plays a vital role in decreasing the permeability of the cell to toxic compounds and antibiotics (Nikaido, 2003). LPS has three components: a hydrophobic lipid A attached to the membrane, an O- antigen, and an oligosaccharide which connects them (Bertani and Ruiz, 2018). LPS provides a protective barrier to lipophilic antibiotics. The protective hydrophobic barrier is formed by densely packing the OM with LPS, and by the negative charges of LPS which form crossbridges with divalent cations (Nikaido, 2003).

The majority of proteins in the OM are classed as lipoproteins and β-barrel transmembrane proteins (Silhavy et al., 2010). Transmembrane β-barrels include porins which allow for the diffusion of small molecules through the membrane. In *S.* Typhimurium, OmpC, OmpF and OmpD (Liu and Ferenci, 2001, Santiviago et al., 2003) are considered the major porins, but other porins include OmpS1 and OmpS2 (Rodriguez-Morales et al., 2006).

1.5 How do antibiotics get into cells?

1.5.1 Porins

As discussed, antibiotics can enter cells via porin channels, which are required to control permeability and for the entrance of hydrophilic nutrients through the OM. In

1990, the first structure of a porin was established using X-ray crystallography from *Rhodobacter capsulatus* (Weiss et al., 1990). Porins are β-barrel trimeric structures inserted in the OM. In general, non-substrate specific porins have 16 strands whereas substrate specific porins have 18 strands (Galdiero et al., 2012). Common to all porins is an L3 loop which causes constriction of the barrel structure (Soares et al., 1995), contributing to substrate specificity (Galdiero et al., 2012).

1.5.1.1 The major porins, OmpF and OmpC

OmpF and OmpC are considered major porins in *E. coli* and *Salmonella enterica* (Liu and Ferenci, 2001), and are structurally similar, with OmpF having a larger channel than OmpC. They allow the entrance of small hydrophilic solutes into the bacterial cell, so have been implicated in the development of antibiotic resistance. The main role of OmpF has recently been found to be the entrance of molecules into the cell whereas OmpC was also found to be involved in the maintenance of membrane integrity (Choi and Lee, 2019). These porins are differentially regulated depending on the osmolarity of the environment (Lan and Igo, 1998). This regulation is mainly controlled by the histidine kinase, EnvZ and the response regulator OmpR. EnvZ phosphorylates OmpR, activating the regulator, or dephosphorylates OmpR, deactivating it, dependent on the environmental osmolarity (Aiba and Mizuno, 1990, Lan and Igo, 1998). Phosphorylated OmpR induces expression of OmpC porin under high osmolarity (Yoshida et al., 2006). In low osmolarity, phosphatase activity is higher, meaning OmpR is dephosphorylated and there is increased expression of OmpF (Yoshida et al., 2006). OmpF also appears to have a more enhanced role during glucose limitation, whereas OmpC is upregulated in nitrogen starved

environments (Liu and Ferenci, 2001). Apart from local regulation, upregulation of the multiple antibiotic regulator *marA* leads to the production of *micF*. *micF* is a stress response antisense RNA that binds to *ompF* mRNA, leading to downregulation of the OmpF porin (Cohen et al., 1988, Pratt et al., 1996), reducing permeability and leading to an increase in resistance to hydrophilic antibiotics (Delcour, 2009).

1.5.1.2 OmpS1 and OmpS2

OmpS1 and OmpS2 are porins found in *S. enterica* serovars Typhi and Typhimurium. In comparison to OmpC and OmpF, they are expressed at low levels in normal laboratory growth conditions (Rodriguez-Morales et al., 2006) but they are also regulated by the EnvZ/OmpR system (Rodriguez-Morales et al., 2006). Although OmpS1 and OmpS2 have high sequence similarity (Fernandez-Mora et al., 2004, Flores-Valdez et al., 2003), OmpS1 is also negatively regulated by H-NS (Flores-Valdez et al., 2003) and OmpS2 positively regulated by the LeuO activator (Fernandez-Mora et al., 2004).

1.5.1.3 OmpD

OmpD is the most abundant porin in *S.* Typhimurium, contributing 1% of the total protein found in the cell in laboratory conditions (Santiviago et al., 2003). OmpD differs to the major porins, OmpC and OmpF, because expression does not change in response to osmolarity (Santiviago et al., 2003). Instead, *ompD* expression increases in anaerobic conditions, and is regulated post-transcriptionally by Fnr in this environment (Santiviago et al., 2003). The *ompD* promoter has been shown to be repressed in either low pH or bile rich conditions (Santiviago et al., 2003, Prouty et al., 2004). The chaperone, Hfq, has been implicated in the post-transcriptional

regulation of *ompD*, possibly by binding the 5'-UTR of *ompD* mRNA (Sittka et al., 2007). The roles of the OmpD porin are still disputed, however, it has been shown to be involved in the efflux of methyl viologen in combination with YddG (Santiviago et al., 2002), as well adherence to macrophages and intestinal epithelial cells (Hara-Kaonga and Pistole, 2004). OmpD also facilitates the uptake of hydrogen peroxide, produced in phagocytic oxidative burst (Calderon et al., 2011, Ipinza et al., 2014). More recently, *ompD* has been shown to be downregulated in macrophages. Ipinza et al. (2014) showed that the deletion of the porin increased the bacterial survival within a macrophage.

1.5.1.4 OmpW

OmpW is a small minor porin found in *Salmonella sp, E. coli* and *Vibrio sp* (Gil et al., 2009). OmpW is involved in osmoregulation as well as being affected by environmental signals such as temperature and availability of nutrients (Gil et al., 2009). Although considered to be a porin, OmpW has been implicated in the efflux of the superoxide generating compound, paraquat or methyl-viologen (Gil et al., 2007), and regulation is dependent on the transcriptional regulator, SoxS (Gil et al., 2009). The porin has also been shown to associate with the small multidrug resistance (SMR) efflux protein, EmrE to export quaternary ammonium compounds such as methyl viologen (Beketskaia et al., 2014).

1.5.2 Self-promoted uptake through the outer membrane

Not all antibiotics are hydrophilic and so cannot enter Gram-negative cells through porins; but are able to enter by diffusion across the OM. Self-promoted uptake is a

mechanism of influx that bypasses the use of porins. Polymyxin B, Ethylenediaminetetraacetic acid (EDTA), cationic peptides and the antibiotic class, aminoglycosides, have been shown to use this uptake mechanism (Hancock and Bell, 1988, Delcour, 2009, Hancock et al., 1981).

Cross bridges between the negatively charged regions (phosphate or carboxyl group) of LPS and divalent cations such as Mg^{2+} or Ca^{2+} are essential for the stability of LPS and the OM (Hancock, 1984, Hancock and Bell, 1988). Displacement of these cations results in instability and lateral movement of LPS across the OM (Delcour, 2009). A well-studied disruptor of LPS cross-bridges is the chelator, EDTA, which displaces the divalent cations increasing the permeability of the OM (Leive, 1974, Alakomi et al., 2003) (**Figure 1-6**). Polymyxin B and colistin are also classed as 'permeabilisers' of the OM, as well as aminoglycosides. Although colistin is able to bind LPS in the OM, and allows antibiotic uptake, cell lysis and bactericidal activity is as a result of colistin targeting the LPS in the inner membrane (Sabnis et al., 2020). Fleroxacin, a fluoroquinolone, has also been shown to weaken the membrane in this way to allow for self-promoted uptake (Chapman and Georgopapadakou, 1988). Fluoroquinolones are hydrophilic compounds that enter cells via porins but may also acts as chelators in this case (Chapman and Georgopapadakou, 1988, Delcour, 2009). Permeabilisation of the OM by compounds such as EDTA, may also lead to the uptake of some of the more hydrophobic antibiotics which are otherwise unable to pass the Gram-negative OM (Hancock and Bell, 1988).

In *S.* Typhimurium, a *pmrA* mutant has been described which is resistant to EDTA and polymyxin B, possibly due to alterations in the negative charges of LPS. PmrA is

part of the PmrAB two-component regulatory system, which induces lipid A modification, and therefore resistance to polymyxins and antimicrobial peptides (Gunn et al., 1998). This is important when considering AMR to last-line drugs such as colistin (Vaara et al., 1981, Nikaido, 2003).

Figure 1-6 Self-promoted uptake.

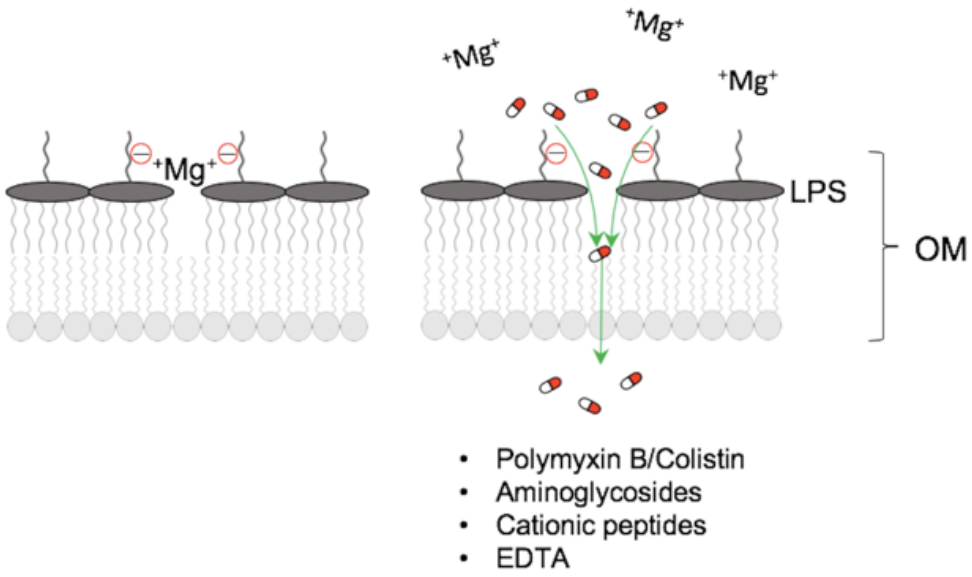

A schematic of the OM of Gram-negative bacteria. LPS usually forms crosslinks for stability using divalent cations. Permeabilisers such as EDTA, displace the cations, permeabilising the membrane and allowing the entrance of some antibiotic compounds through the membrane.

The contribution of Gram-negative impermeability to AMR has led to the concept of synthesising a hybrid of two antibiotics (Gorityala et al., 2016a). The development of a tobramycin-ciprofloxacin hybrid was shown to have anti-pseudomonal properties by tobramycin permeabilising the membrane and allowing ciprofloxacin to reach its target to carry out its bacteriostatic and bactericidal mode of action (Gorityala et al., 2016a). Another hybrid, tobramycin-moxifloxacin has also been produced and studied, suggesting that it can destabilise the membrane and inhibit efflux through dissipation of the PMF (Gorityala et al., 2016b).

1.5.3 Antibiotic transport across the inner membrane

Some antibiotics, such as β-lactams, target the peptidoglycan therefore do not need to pass the cytoplasmic IM (Tipper and Strominger, 1965, Yocum et al., 1980). Other antibiotics do need to cross the IM to reach their target however there are limited studies of this (Hancock and Bell, 1988). It is thought that the majority of antibiotics with targets in the cytoplasm enter by passive diffusion and the IM does not act as a barrier to drugs (Hancock and Bell, 1988). Tetracycline and aminoglycoside transport across the IM have been studied.

The porins, OmpC and OmpF allow tetracycline influx into the periplasm (Chopra and Roberts, 2001). Tetracycline is lipophilic, so can diffuse through the IM via active transport using the PMF (Chopra and Roberts, 2001, Hancock and Bell, 1988). Accumulation of tetracyclines within cells is determined by the pH gradient, and diffusion by this mechanism was found to be similar for fluoroquinolones (Nikaido and Thanassi, 1993).

The aminoglycoside influx mechanism in Gram-negative bacteria is disputed. However, it is accepted that it occurs in three stages: 1. binding and diffusion through the outer membrane, 2. Energy-Dependent Phase I (EDPI), 3. Energy-Dependent Phase II (EDPII) (Bryan and Van Den Elzen, 1977). EDPI involves a slow rate of uptake into the cytoplasm and is dependent on the concentration of antibiotics in the environment (Bryan and Van Den Elzen, 1977). Entrance of aminoglycosides during EDPI, allows the drugs to reach their target (ribosomes) and this is followed by protein translation mismatches leading to the misfolding of membrane proteins, subsequently increasing membrane permeability and the rapid influx of aminoglycosides into the cytoplasm by EDPII, a step clearly dependent on the action EDPI (Davis et al., 1986, Sabeti Azad et al., 2020).

1.6 How are antibiotics removed from cells?

Antibiotics are removed from cells by efflux pumps of which there are 6 classes: small multidrug resistance (SMR) pumps, major facilitator superfamily (MFS), multidrug and toxic compound extrusion (MATE) pumps, proteobacterial antimicrobial compound efflux (PACE) pumps, resistance nodulation division (RND) and ATP binding cassette (ABC) pumps (**Figure 1-7**).

Figure 1-7 A schematic of the efflux pump classes.

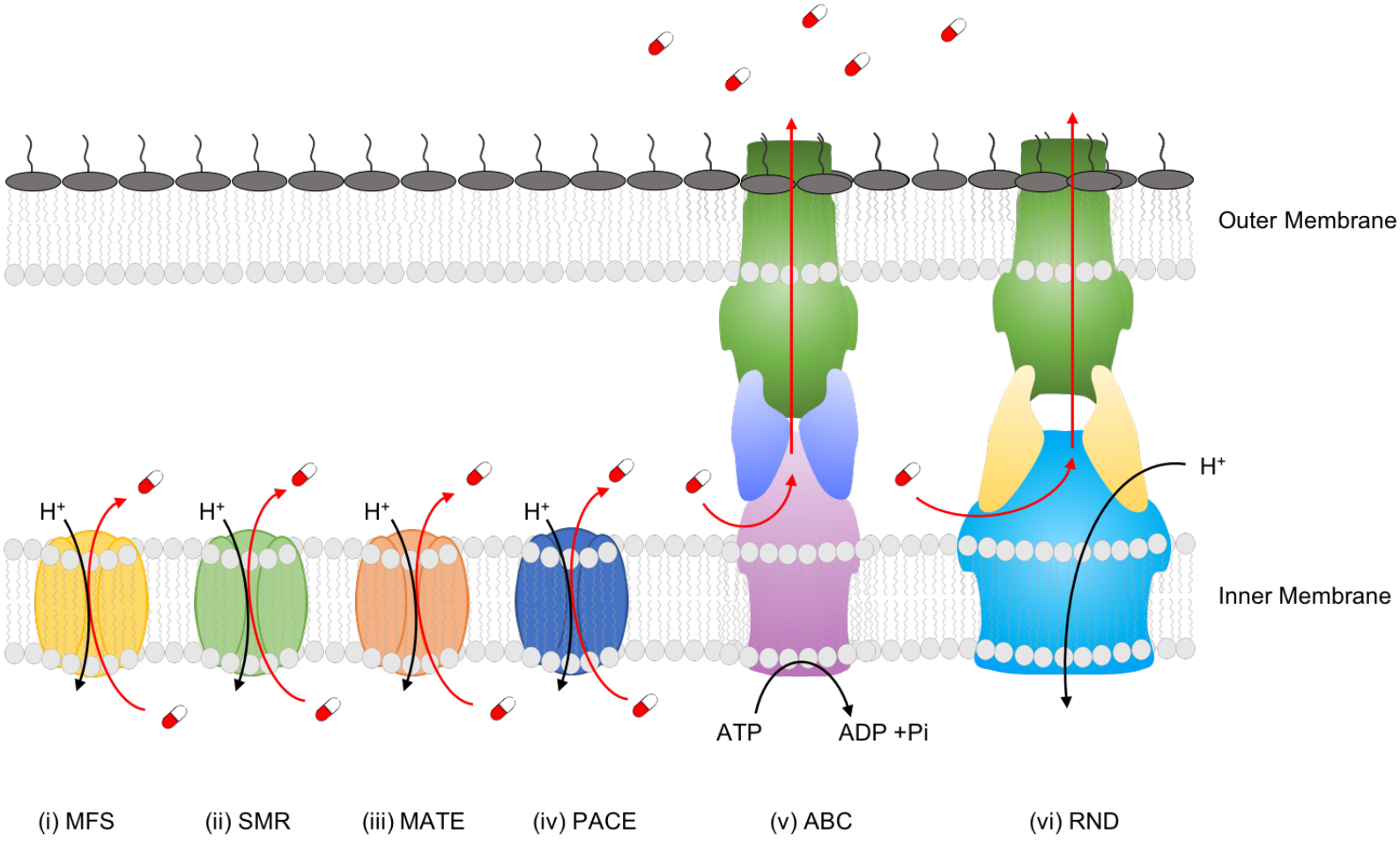

The 6 efflux pump classes and the energy they use to export compounds. (i) MFS, (ii) SMR, (iii) MATE and (iv) PACE are located in the inner membrane and utilise the PMF. (v) The ABC pump, MacAB forms a tripartite complex with TolC which uses ATP hydrolysis for translocation from the periplasm (Greene et al., 2018). (vi) RND pumps also form tripartite complexes with TolC that span the inner and outer membranes but use the PMF.

1.6.1 Major Facilitator Superfamily (MFS) efflux pumps

MFS pumps are small, hydrophobic transmembrane proteins (Kumar et al., 2016) found in Gram-positive bacteria, and the IM of Gram-negatives. The MFS family is one of the two largest classes of transporters and is conserved among bacteria (Pao et al., 1998). MFS pumps use the PMF to export a range of distinct substrates including solutes, sugars, secondary metabolites as well as antimicrobial agents (Kumar et al., 2016). In *S.* Typhimurium, two MFS pumps, EmrAB and MdfA, have been described (Horiyama et al., 2010). The EmrAB pump is dependent on the outer membrane channel, TolC, to provide resistance to antibiotics including novobiocin and nalidixic acid (Horiyama et al., 2010). MdfA is not dependent on TolC but overexpression provides resistance to tetracycline, chloramphenicol, norfloxacin and doxorubicin.

1.6.2 Multidrug and toxic compound extrusion (MATE) pumps

MATE pumps require an electrochemical gradient to extrude substrates (Kuroda and Tsuchiya, 2009). The MATE class of pumps is universal across bacteria with the first, NorM, being identified in *Vibrio parahaemolyticus* (Morita et al., 1998, Brown et al., 1999). Most MATE pumps can extrude fluoroquinolone antibiotics and also the removal of cationic dyes such as ethidium bromide (EtBr) has been described (Kuroda and Tsuchiya, 2009). The only MATE pump in *S.* Typhimurium to be identified is MdtK which has been shown to remove norfloxacin, doxorubicin and the dye, acriflavine (Nishino et al., 2006).

1.6.3 ATP Binding Cassette (ABC) pumps

ABC pumps differ from all other efflux pump classes because they require adenosine triphosphate (ATP) hydrolysis for export of substrates, rather than PMF (Davidson and Chen, 2004). They are a major family of transporters within mammalian cells as well as bacterial cells (Kobayashi et al., 2001). In Gram-negative bacteria, the HlyB and MacB ABC pumps are well studied. The HlyB, exporter forms a tripartite complex with HlyD and TolC, to export the haemolysin, HlyA (Greene et al., 2018). In 2001, the MacB transporter was the first ABC transporter to be identified in Gram-negative bacteria, which forms a tripartite complex with the periplasmic subunit, MacA, and TolC in *E. coli* (Kobayashi et al., 2001). It is dependent on the outer membrane protein channel, TolC, to function and is involved in the export of macrolides, and its deletion from a cell leads to increased susceptibility to macrolides (Horiyama et al., 2010). It has been suggested that substrate export is via the periplasm rather than the IM (Greene et al., 2018). MacAB-TolC is the only drug ABC transporter in *S.* Typhimurium. In *S.* Typhimurium, *macAB* deletion has been implicated in reduced virulence, as well as increased resistance to macrolides, and has been found to be relevant to survival in macrophages which is important for *Salmonella* infection (Nishino et al., 2006, Bogomolnaya et al., 2013). MacAB homologs have also been identified in *Stenotrophomonas maltophila, Pseudomonas aeruginosa, Acinetobacter baumanii* and *Vibrio cholerae* (Greene et al., 2018). In 2020, an inhibitor to the MacAB-TolC pump was successfully identified (Yamagishi et al., 2020), which may be critical in the future when considering macrolide resistant infections.

1.6.4 Proteobacterial antimicrobial compound efflux (PACE) pumps

The most recent family of efflux pumps discovered are the PACE pumps. Transcriptomic analysis of *Acinetobacter baumanii* in the presence of chlorhexidine led to the identification of AceI (*Acinetobacter* chlorhexidine efflux protein) (Hassan et al., 2015, Hassan et al., 2013). It is predicted that the pump functions as an oligomer and that it contains four transmembrane α-helices that forms a two-tandem transmembrane pair domain (Hassan et al., 2018, Finn et al., 2016). Regulation of *aceI* in the presence of chlorhexidine is by the adjacent LysR-type transcriptional regulator (LTTR) family regulator, AceR (Liu et al., 2018). PACE pumps share high sequence similarity and are found in a number of pathogens including *Salmonella*, *Klebsiella*, *Pseudomonas*, *Enterobacter* and *Burkholderia* (Hassan et al., 2018). The physiological substrates of this family have been identified as polyamines (Hassan et al., 2019). Short chain diamines (e.g. cadaverine) were found to strongly induce the expression of *aceI*, and long chain polyamines (e.g. spermidine) had weaker induction (Hassan et al., 2019). Naturally occurring polyamines are substrates of the pumps, along with the structurally similar biocide, chlorhexidine (Hassan et al., 2019, Hassan et al., 2015, Hassan et al., 2013).

1.6.5 Resistance Nodulation Division (RND) pumps

RND efflux pumps are common amongst Gram-negative organisms. They span both membranes allowing export of compounds from periplasm to the extracellular environment. Like some ABC pumps, RND pumps are formed of three components, classifying them as tripartite pumps (Daury et al., 2016). Outer membrane proteins

(OMPs) form the component located on the OM, joined to the pump protein in the IM by periplasmic adaptor proteins (PAPs). The most studied systems are the AcrAB-TolC pump in *E. coli* and the MexAB-OprM system in *Pseudomonas aeruginosa* (Li et al., 1995). AcrAB-TolC in *S.* Typhimurium is highly homologous to the AcrAB-TolC pump in *E. coli* (Piddock et al., 2000).

Five RND systems have been described in *S.* Typhimurium, differing from *E. coli* (six systems) (Anes et al., 2015) and *Pseudomonas aeruginosa* (12 systems in PA01) (Lister et al., 2009). In *S.* Typhimurium, TolC is the common OMP for seven efflux pumps in total, including MacAB (ABC transporter) and EmrAB (MFS transporter) (Horiyama et al., 2010). The RND pumps are AcrAB-TolC, AcrAD-TolC, AcrEF-TolC, MdtABC-TolC and MdsABC (**Figure 1-8**) (Blair et al., 2015a). AcrA is the PAP required for both the AcrB and AcrD pumps, meaning there are only 4 PAPs present in *S.* Typhimurium (Yamasaki et al., 2011). RND efflux pumps are important in the development of multidrug resistance and are the class of pump most commonly found to be overexpressed in MDR clinical isolates. Each pump has a distinct substrate profile however common substrates include multiple classes of antibiotics e.g. fluoroquinolones, aminoglycosides and β-lactams but also disinfectants, detergents, dyes and virulence factors (Blair et al., 2015a).

Figure 1-8 The 5 RND efflux systems of *S. enterica* serovar Typhimurium

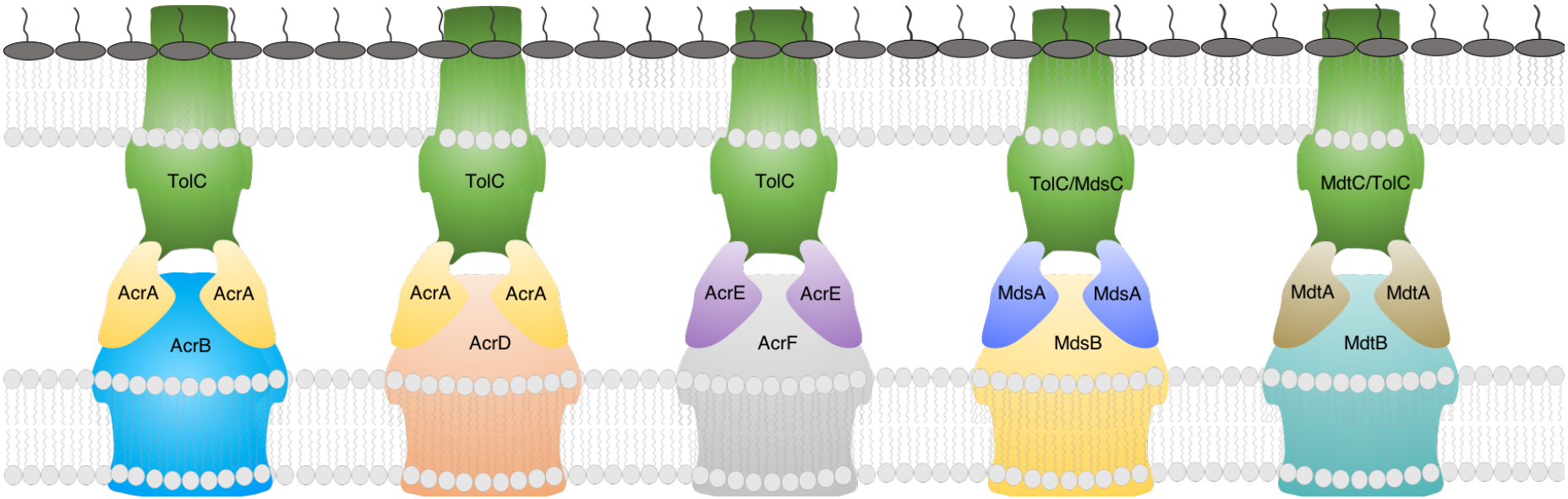

This schematic shows the AcrAB-TolC, AcrAD-TolC, AcrEF-TolC, MdsABC/TolC and MdtABC/TolC efflux systems. Figure adapted but produced by the author of this thesis for publication (Colclough et al., 2020)

1.7 AcrAB-TolC

AcrAB-TolC is the major RND efflux pump system that has been implicated in the development of AMR (Webber and Piddock, 2001). For this reason, it is important that the AcrAB-TolC system is well understood so that there are ways to prevent its export of antibiotics and its contribution to AMR in infections.

1.7.1 Structure and mechanism of transport

AcrAB-TolC is a tripartite complex that spans the IM, the periplasmic space and the OM (**Figure 1-9A**) (Symmons et al., 2009).

The OMP, TolC, can form tripartite complexes with other proteins, not just AcrAB (Paulsen et al., 1997). TolC, formed of three identical protomers, acts as a channel. The β-barrel is located in the OM with an α-helical bundle which protrudes into the periplasm (Koronakis et al., 2000). TolC remains in a closed formation when not in contact with AcrAB, preventing access of compounds from the extracellular environment (Shi et al., 2019). The α-helical domain of TolC interacts with the α-hairpin of the PAP protein AcrA, and both interact with peptidoglycan (Shi et al., 2019). AcrA is composed of three domains: the lipoyl, β-barrel and the membrane proximal domains (Mikolosko et al., 2006).

Figure 1-9 Structure of AcrAB-TolC and the mechanism of drug export.

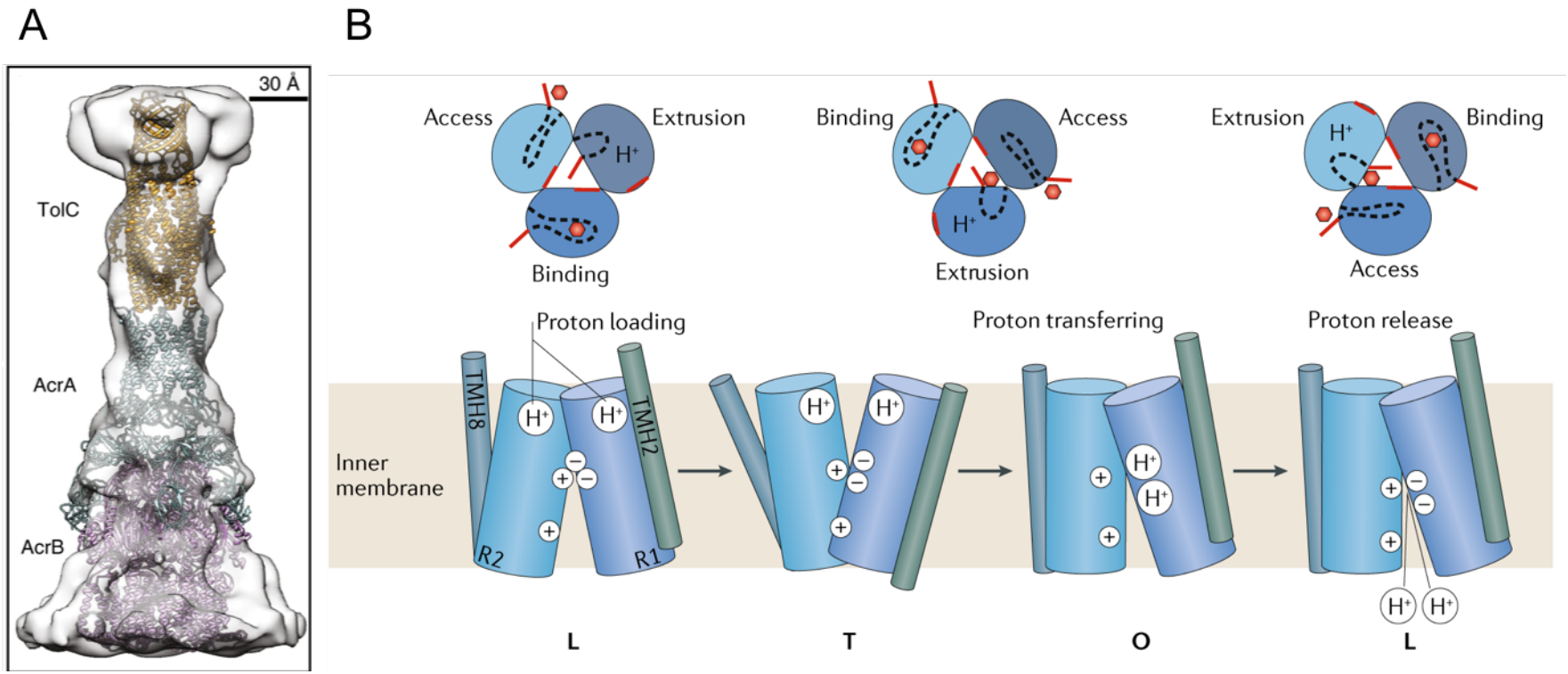

(**A**) shows the tripartite complex of AcrAB-TolC. Pink shows the AcrB protein, interacting with AcrA (green) which interacts with TolC (red and yellow). Figure from Shi et al. (2019).(**B**) Top panel depicts the conformational changes of AcrB from L, T and O states in the presence of drug. Entrance to the binding pocket (dashed lines) and opening and closing of pockets (red lines) are shown. The bottom panel shows how the conformation of AcrB changes due to the PMF interaction with the transmembrane domain. Figure reproduced from Du et al. (2018).

The inner membrane pump protein, AcrB, is formed of three identical protomers and each protomer is comprised of twelve transmembrane α-helices and two large hydrophilic loops which protrude into the periplasm (Murakami et al., 2006). AcrB has three domains: the docking, pore and transmembrane domains. For AcrB to export drugs from the periplasm, the structure goes through three conformational changes powered by the PMF (Du et al., 2018, Takatsuka and Nikaido, 2009). Drug binding occurs in the pore domain of the AcrB protomer, comprising three channels for drug entry and two channels for drug binding. Drug export through RND efflux pumps is via a functionally rotating mechanism (Murakami et al., 2006), and is shown in **Figure 1-9B**. When drugs gain entrance to the protomer binding pocket, the structure is in a loose (L) conformation. This L state then undergoes a conformational change to a tight (T) state as the drug moves further into the binding pocket. At this point, drugs can be extruded into the docking domain of AcrB for further export of the drug, and this is known as the open (O) conformation (Murakami et al., 2006, Du et al., 2018).

Shi et al. (2019) showed that AcrA and AcrB form a stable bipartite complex using electron cryo-tomography (Cryo-ET), with the α-hairpin of AcrA associating with the peptidoglycan to form a stable structure. It was suggested that this bipartite structure may move along the membrane until it comes into contact with TolC (Shi et al., 2019). This complex then changes conformation in the presence of antibiotics, and recruits a ‘closed’ TolC protein which then opens to expel antibiotics. Tripartite structures were obtained by Cryo-ET in the closed state in the presence of antibiotics, and in the open state in the presence of the AcrB inhibitor, MBX3132 (Shi et al., 2019). Prior to this in situ study, protein structure was limited to single components of the

AcrAB-TolC pumps, but now this study suggests the overall stoichiometry of an assembled pump is 3 TolC: 6 AcrA: 3 AcrB (Shi et al., 2019).

1.7.2 Regulation of AcrAB-TolC

The contribution of AcrAB-TolC to AMR is commonly due to overexpression of the pump, leading to increased export of antimicrobials (Yasufuku et al., 2011, Keeney et al., 2008, Swick et al., 2011). For this reason, understanding the global regulation of the AcrAB-TolC pump is key to targeting its activity. Transcriptional regulation of AcrAB-TolC is complex, with local and global regulation (**Figure 1-10**), but less is known about post-transcriptional and translational control of AcrAB-TolC.

1.7.2.1 Local regulation

The AcrAB pump is locally regulated by the TetR family transcriptional regulator, AcrR (Ramos et al., 2005). The *acrR* gene is situated upstream of the *acrAB* operon and acts to repress the operon to prevent overexpression of the efflux pump (Ma et al., 1996). As well as being present in *S.* Typhimurium (Olliver et al., 2004), AcrR is present in *E. coli* (Ma et al., 1996). In *E. coli*, the local repressor of the RND efflux pump gene AcrEF, EnvR, has also been shown to repress the *acrAB* operon (Hirakawa et al., 2008).

Mutations in AcrR have been described in clinical and veterinary isolates causing overexpression of AcrAB-TolC (Weston et al., 2018, Webber et al., 2005, Ma et al., 1996).

Figure 1-10 The local and global regulation of *acrAB*

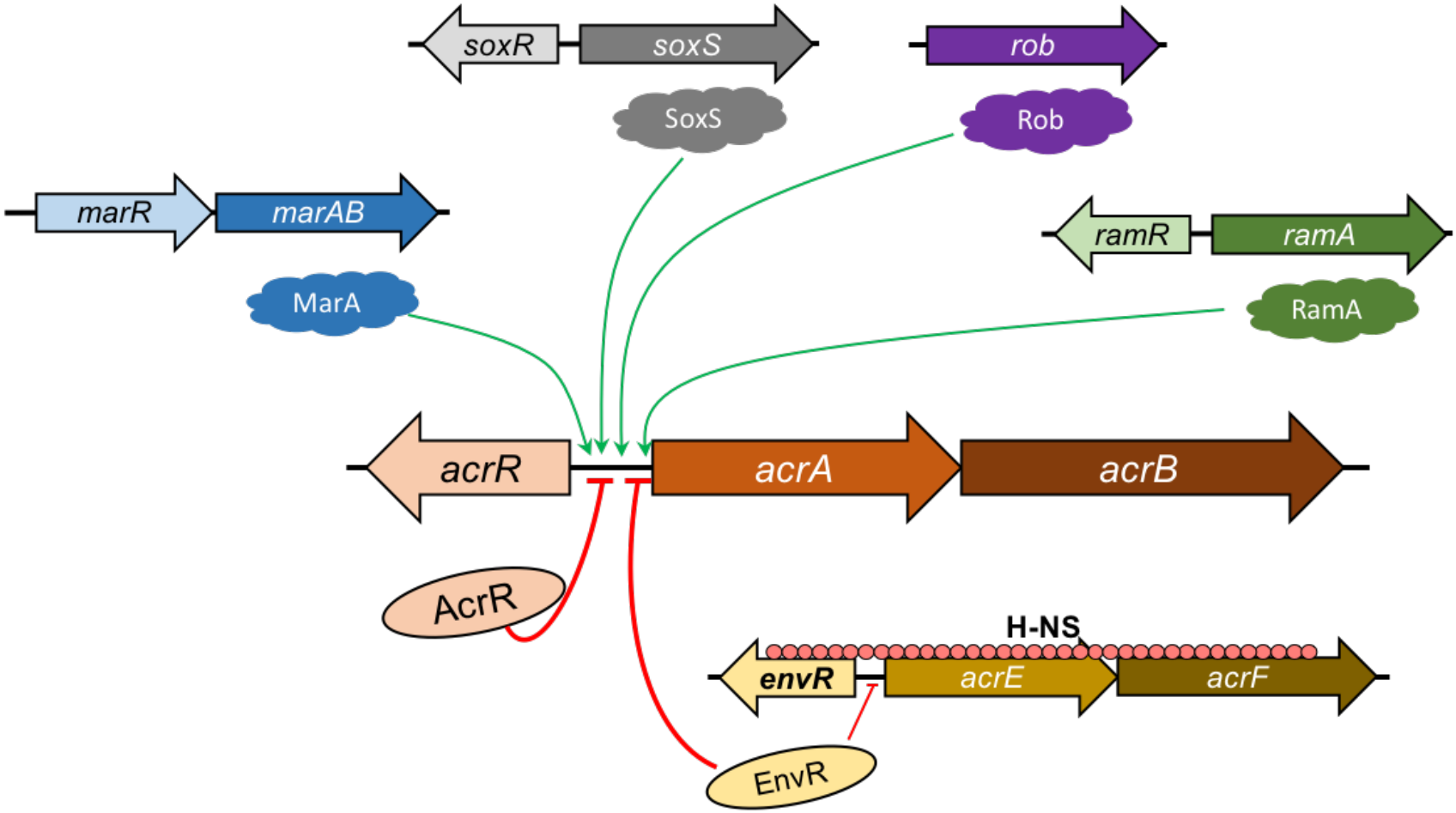

AcrR is the local repressor of the *acrAB* operon. The repressor of the *acrEF* operon, EnvR, can also repress *acrAB*. The increased transcription of global regulators RamA, MarA, SoxS and Rob lead to the upregulation of efflux pump expression.

1.7.2.2 Global regulators of AcrAB-TolC

Global regulators are defined as regulators or activators that are not fixed to regulation within their own operon. They can control multiple genes or operons that are within other metabolic pathways, contributing to multiple regulatory networks (Duval and Lister, 2013). Several regulators of the AraC-XylS family have been shown to activate expression of efflux pumps including AcrAB-TolC. In *E. coli,* these activators include MarA, Rob and SoxS (McMurry et al., 1998, White et al., 1997) and an additional RamA regulator can be found in *Salmonella sp.* and *Klebsiella pneumoniae* (van der Straaten et al., 2004, George et al., 1995, Bailey et al., 2010). The AraC-XylS family regulate genes through the binding of their helix-turn-helix motifs to sequences of DNA (Rhee et al., 1998, Sharma et al., 2017). In the case of MarA, Rob, SoxS and RamA, they bind to DNA sequences named 'marboxes', found in the promoters of genes to allow for activation (Sharma et al., 2019).

MarA is locally repressed by its local regulator MarR which inhibits transcription of *marA* (Alekshun and Levy, 1997). This repression is relieved in response to an environmental signal such as the presence of antibiotics or if mutation of MarR stops the repressor binding (Seoane and Levy, 1995, Maneewannakul and Levy, 1996). Increased expression of *marA* leads to increased expression of *acrAB* and *tolC* (Okusu et al., 1996). SoxS is upregulated by oxidative stress (Hidalgo et al., 1998) and Rob by antibiotics and organic solvents (Nakajima et al., 1995). RamR represses *ramA* expression and is released by the presence of environmental signals, like MarA, and is able to activate the expression of *acrAB-tolC* (Abouzeed et al., 2008, Ricci and Piddock, 2009, Weston et al., 2018).

1.7.2.3 Post-transcriptional regulation of AcrAB-TolC

Regulation of AcrAB-TolC also occurs at the post-transcriptional level. Carbon storage regulator A, CsrA, is an RNA binding protein that is able to bind to the *acrAB* mRNA transcript and controls translation of the gene by preventing the ribosome accessing the 5'-UTR of the transcript (**Figure 1-11A**). CsrA consequently contributes to controlling the level of AcrAB-TolC efflux pump in a cell (Ricci et al., 2017).

Another RNA binding protein, Hfq has also been described as playing a role in the translational control of AcrB (Yamada et al., 2010). The main role of Hfq is to act as a chaperone protein, and facilitate the interactions of small regulatory RNAs (sRNAs) to mRNAs (Vogel and Luisi, 2011). Hfq can facilitate the function of sRNAs therefore preventing access of the ribosome to the transcript (Yamada et al., 2010, Vogel and Luisi, 2011). One sRNA which has been identified as a post-transcriptional control of AcrAB-TolC is SdsR. Parker and Gottesman (2016) used AcrA, AcrB and TolC translational fusions to study expression in the presence of overexpressed Hfq-dependent sRNAs. Only SdsR was found to repress *tolC* translation by binding upstream of the ribosomal binding site. No sRNA was found to modulate expression of *acrAB* (**Figure 1-11B**) (Parker and Gottesman, 2016).

Figure 1-11 Post-transcriptional regulation of AcrAB-TolC.

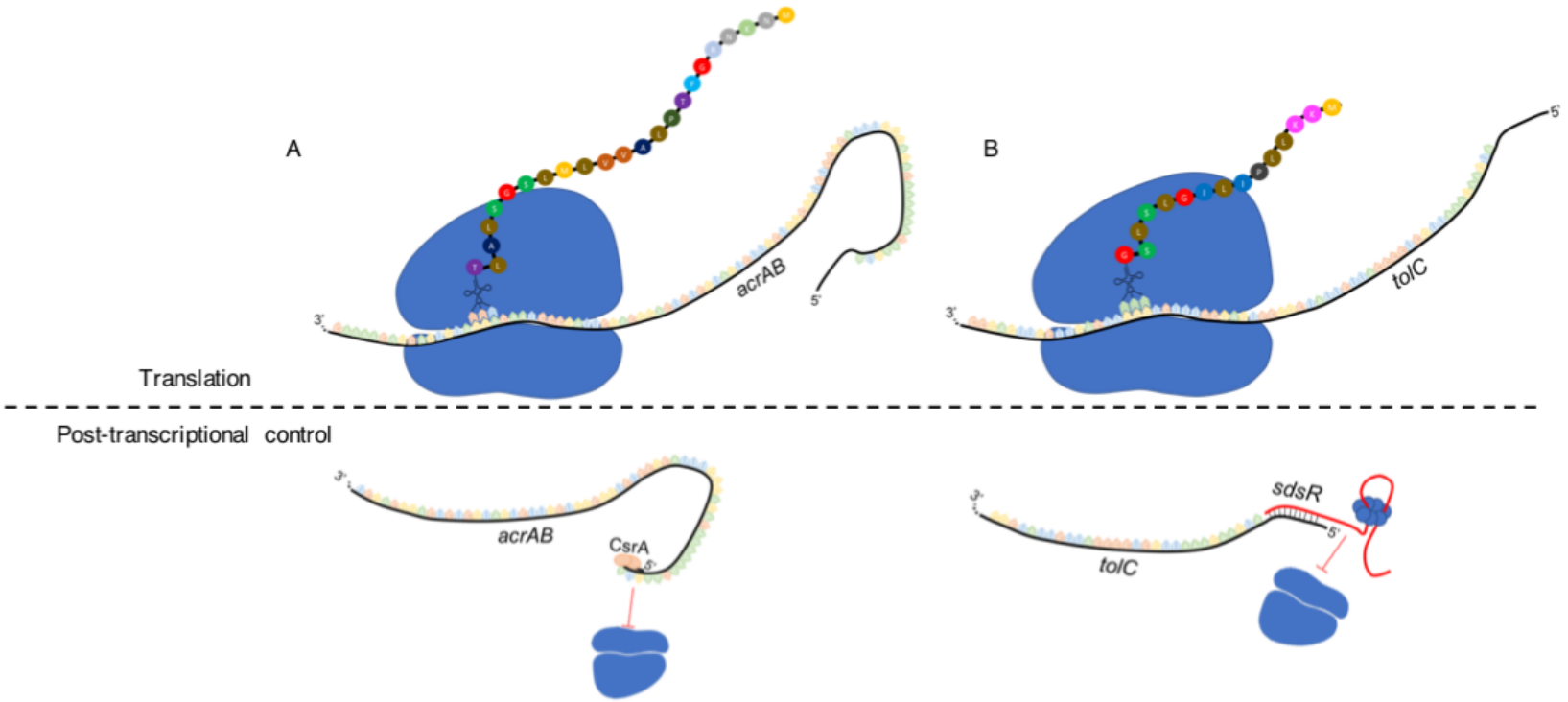

(**A**) The translation of *acrAB* transcripts is controlled by the CsrA protein. CsrA binds the 5' end of mRNA, stabilising it and preventing entry of the ribosome and in turn controlling translation. (**B**) The translation of *acrAB* transcripts is controlled by the binding of regulatory RNA, SdsR, to the 5' untranslated region of the *tolC* transcript and is directed to the transcript with the aid of the Hfq chaperone protein. This in turn, prevents the access to the ribosome. Figure was made by E. Whittle for Colclough et al. (2020).

It has been shown that the Lon protease is involved in degrading RamA (Ricci et al., 2014), which activates transcription of *acrAB* (Ricci et al., 2014, Bailey et al., 2008, Nikaido et al., 2008, Ruzin et al., 2005). Lon is also important for unfolding misfolded proteins (Van Melderen and Aertsen, 2009). If Lon degrades RamA, it is then unable to activate the transcription of *acrAB.* Recognition of the N-terminus of RamA by Lon, aids protein degradation.

1.7.3 AcrAB-TolC and AMR

As previously discussed in **Section 1.2.5**, overexpression of efflux pumps can lead to increased AMR. A number of studies suggest that removal of AcrAB-TolC from *S.* Typhimurium or *E. coli* leads to increased susceptibility to antibiotic treatment (Nishino et al., 2006, Blair et al., 2009). It has also been shown that cells lacking *acrB* lead to an increase in *ompF* expression, in turn, decreasing cellular permeability (Webber et al., 2009).

Overexpression of AcrAB-TolC in clinical isolates leads to ineffective treatment due to increased export of antibiotics. A large-scale study of fluoroquinolone-resistant clinical and veterinary isolates of *E. coli* from Spain and Argentina showed that most mutations leading to overexpression of AcrAB-TolC were found in the regulators (Webber and Piddock, 2001). In around 50% of the isolates, the local repressor AcrR had a single point mutation (Arg45Cys) leading to reduced repression of *acrAB* (Webber and Piddock, 2001). Mutations were also found in global regulators *marR* and *soxR* (Webber and Piddock, 2001). Similarly, the Arg45Cys mutation in AcrR was also found in MDR *E. coli* isolated from urinary tract infections (UTIs) (Chowdhury et al., 2019). Mutations in *acrR* and *ramA* overexpression in clinical

isolates of *Klebsiella pneumoniae* have been described, leading to overexpression of *acrB* and increased resistance to fluoroquinolones (Schneiders et al., 2003). Increased expression of *acrB* has been linked to a decrease in *mutS* expression (El Meouche and Dunlop, 2018). The *mutS* gene encodes a DNA mismatch repair protein, and decreased expression of this leads to an increase in mutations (El Meouche and Dunlop, 2018), possibly to accumulate more mutations that are beneficial for resistance during antibiotic treatment.

AcrAB-TolC overexpression in MDR clinical isolates is present and a driver of further development of resistance and therefore it is important to understand the mechanism of AcrAB-TolC to target it and reduce AMR.

1.7.4 Physiological roles of AcrAB-TolC

The presence of bacterial efflux pumps in bacteria precedes the clinical introduction of antibiotics. For this reason, it is well known that the intrinsic role of AcrAB-TolC and other RND pumps is not the extrusion of antibiotics or the contribution to AMR (Colclough et al., 2020).

A number of studies have shown the involvement of AcrAB-TolC in the formation of biofilms and motility. *S*. Typhimurium was shown to have impaired biofilm formation (Baugh et al., 2012), either by lacking a number of efflux pumps or by inhibiting efflux function. Impaired biofilm formation was linked to the repression of genes involved in curli biogenesis (Baugh et al., 2014). Curli are proteins present in the extracellular matrix and are involved in cell adhesion, and are therefore important in the development of biofilms (Barnhart and Chapman, 2006). Removal of AcrAB-TolC and

other efflux pumps in *E. coli* reduces biofilm formation (Kvist et al., 2008). It was shown that in *S.* Typhimurium *acrB::aph*, there was decreased expression of genes involved in motility and chemotaxis (Webber et al., 2009). More recently, in *S.* Typhimurium and *E. coli*, strains lacking *acrB* protein or function increases expression of genes involved in flagella biosynthesis, and strains lacking pump function can swim and are more motile (Wang-Kan et al., 2017, Ruiz and Levy, 2014).

In *S.* Typhimurium, AcrAB-TolC has been identified as important in invasion (Blair et al., 2009, Wang-Kan et al., 2017, Virlogeux-Payant et al., 2008), colonisation (Buckley et al., 2006) and for virulence in mice and in *Galleria mellonella* (Nishino et al., 2006, Wang-Kan et al., 2017, McNeil et al., 2019).

A number of studies highlight the importance of AcrAB-TolC in surviving sublethal concentrations of bile salts, therefore suggesting bile salts are a substrate of the pump (Nishino et al., 2009b, Lacroix et al., 1996, Urdaneta and Casadesus, 2018). In *S.* Typhimurium, bile salts activate the expression of *ramA*, therefore increasing expression of *acrAB* (Baucheron et al., 2014). The survival of *S. enterica* in high bile salts allows for colonisation and biofilm formation in the gallbladder (Crawford et al., 2010). Bile salts and fatty acids also induce the activator Rob, therefore increasing the expression of *acrAB* (Rosenberg et al., 2003). Bile salts and fatty acids are also substrates of AcrAB-TolC and promote survival of *E. coli* in the intestinal tract (Rosenberg et al., 2003).

Inactivated or overexpressed AcrAB-TolC in *E. coli* significantly changes the tricarboxylic (TCA) cycle suggesting that the pump plays a physiological role in metabolism. Roles in amino acid metabolism, the export of lysine, as well as fatty

acid and carbohydrate metabolism have also been highlighted (Cauilan et al., 2019, Colclough et al., 2020).

Enterobactin is a siderophore with affinity to iron. Enterobactin is also considered a substrate of AcrAB-TolC. Previously, it was suggested that only TolC was required for Enterobactin secretion (Bleuel et al., 2005), but more recently, RND pumps such as AcrAB have been implicated in its export (Horiyama and Nishino, 2014). Siderophores such as enterobactin have been proposed as important for colonisation of *E. coli* and *S.* Typhimurium in the intestinal tract (Pi et al., 2012) and macrophages (Saha et al., 2019), respectively.

1.7.5 RND efflux inhibitors

Overexpression of efflux pumps confers AMR, and is fundamental for biofilm formation and virulence, so inhibition of these systems is an attractive strategy for treating drug resistant infections. By inhibiting the pumps, the intracellular accumulation of antibiotics is increased, and activity of already prescribed antibiotics may be potentiated. A few inhibitors have already been identified that can potentiate existing antibiotics, but none have been approved for use clinically.

The peptidomimetic, phenylalanyl arginyl β-naphthylamide (PAβN) was identified (Renau et al., 1999), and found to have inhibitory activity against the MexAB pump in *Pseudomonas aeruginosa*, potentiating the activity of fluoroquinolones. This compound was also found to have some activity against AcrAB (Lomovskaya et al., 2001) but not with the same level of potency as it does in *Pseudomonas aeruginosa.*

In 2006, the RND pump inhibitor 1-(1-Naphthylmethyl)-Piperazine (NMP) was identified in *E. coli* (Kern et al., 2006). It was not a successful inhibitor but was identified to potentiate levofloxacin, similar to PAβN (Opperman and Nguyen, 2015).

The class, pyranopyridines, namely MBX2319 (Opperman et al., 2014) were discovered to have potency against AcrAB in *E. coli*. Using a high throughput inhibitor screen, MBX2319 was found to potentiate the activity of ciprofloxacin. The activity of other fluoroquinolones and β-lactams were also potentiated by the presence of MBX2319 (Opperman and Nguyen, 2015).

Repurposing already clinically used drugs, with efflux inhibiting properties, has also been studied. Phenothiazines are used to treat psychological conditions, however these compounds such as chlorpromazine and amitriptyline, have also been shown to act as efflux inhibitors of the AcrAB-TolC efflux pump in *Salmonella sp.* and *E. coli*, potentiating the activity of antibiotics (Grimsey and Piddock, 2019, Grimsey et al., 2020).

Recently, eleven novel efflux inhibitors have been identified using a high-throughput assay measuring *ramA* expression (Marshall et al., 2020). These inhibitors were shown to potentiate the activity of some antibiotics in at least one of the following species: *E. coli, S.* Typhimurium, *Pseudomonas aeruginosa* and *Acinetobacter baumanii*, without bactericidal activity themselves These inhibitors were identified from already existing Prestwick and Roche chemical compound libraries and shows the importance of assessing already available compounds for efflux inhibitory properties (Marshall et al., 2020).

Efflux pump inhibition is widely researched; however, toxicity is often an issue and may explain why inhibitors have not been approved for use clinically (Tegos et al., 2011, Sharma et al., 2019). This has not prevented ongoing efforts to find efflux inhibitors to help to overcome AMR. As *S.* Typhimurium has 5 different RND systems and *E. coli* has 6 RND systems, inhibitors should be designed to have broad spectrum activity against all RND pumps to potentiate existing antibiotics.

1.8 Bacterial Growth

To study micro-organisms in a laboratory under controlled conditions, methods of batch culture or continuous cultures are most commonly used. However, bacterial growth during infection is complex, not only due to environmental conditions compared to laboratory medium, but also the fact that the environment changes during an infection due to the inflammatory response, and infection in new host sites (Smith, 1998). Changes in environment will also lead to a change in the growth rate. In terms of infection, actively growing cells may be found during initial mucosal interactions, tissue invasion and acute infection to produce a large population with the ability to overcome the host immune response (Smith, 1998). Slow bacterial growth and non-growing bacteria (stationary phase) is archetypal to chronic bacterial infection (Smith, 1998), which is more resistant to antimicrobial treatment (Eng et al., 1991).

1.8.1 Continuous culture

The concept of continuous culture is that bacteria grows at a constant rate with controlled concentration of nutrients, pH and metabolic waste products (Herbert et

al., 1956, Hoskisson and Hobbs, 2005). For this growth in a laboratory, a chemostat is used which can maintain the conditions required for constant bacterial growth (Hoskisson and Hobbs, 2005).

1.8.2 Batch culture

The most common method of bacterial growth in a laboratory is batch culture, which involves growth of a single colony of bacteria in a defined volume of nutrient media. There are different growth phases during batch culture growth with physiological changes due to environment and nutrient supply depletion (**Figure 1-12A**).

1.8.2.1 Lag phase

The earliest stage of bacterial growth in batch culture is lag phase. This phase of growth is poorly understood due to the low concentration of cells present (Rolfe et al., 2012). It represents bacterial cells that are inoculated in fresh media and it has been assumed that cells are physiologically adapting to fresh culture conditions (Madigan, 2000, Rolfe et al., 2012). Entrance into lag phase leads to a drastic change in transcriptome of *S.* Typhimurium, with 1119 gene expression changes within 4 minutes of sub-culturing into fresh medium (Rolfe et al., 2012, Bertrand, 2019). It has also been assumed that the process involves repair of damage from stationary phase cultures (Dukan and Nystrom, 1998), as well as the expression of genes and the synthesis of proteins required for growth. Lag phase cells are metabolically active (Martin, 1932) and precedes the exponential doubling of cells in culture. An extended lag phase period has also been linked to the development of tolerance to antibiotics (Li et al., 2016, Bertrand, 2019, Fridman et al., 2014).

Figure 1-12 Bacterial growth phases.

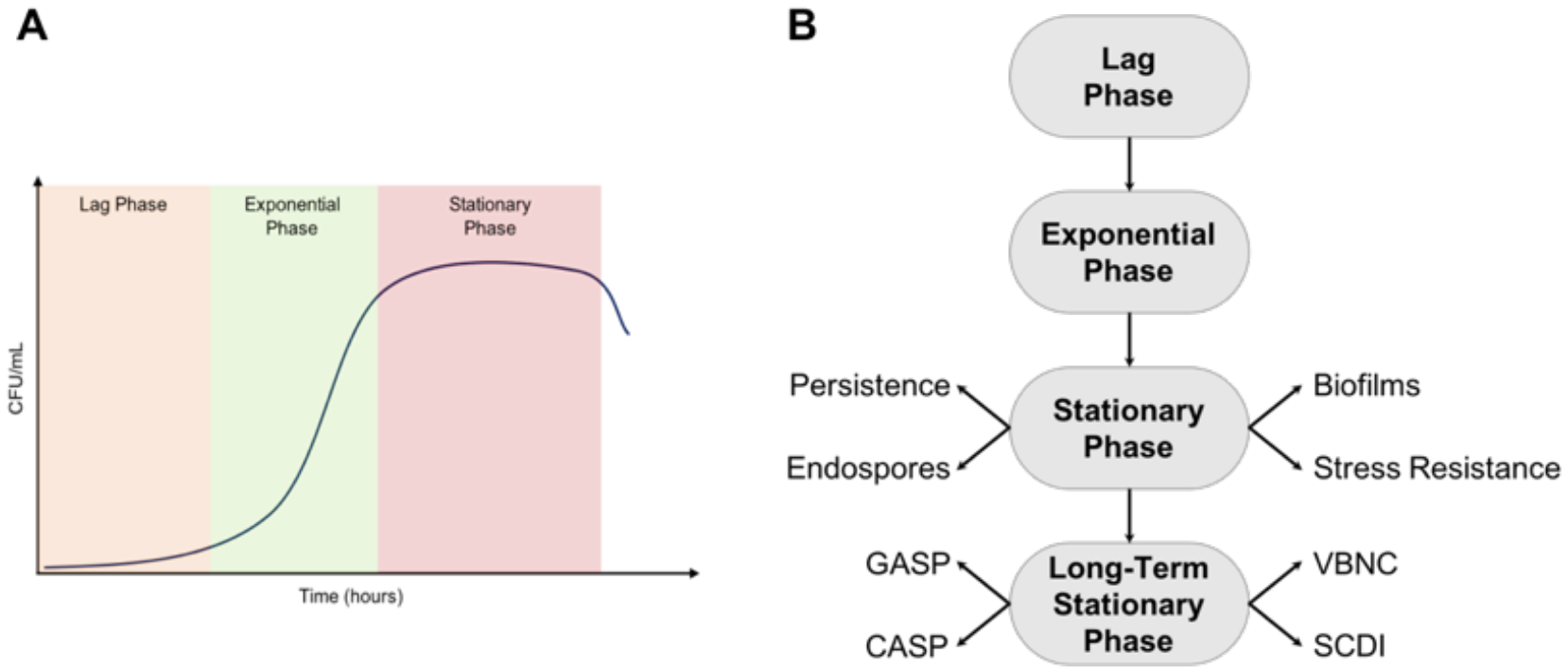

(**A**) shows a standard growth curve for bacteria in batch culture with an initial lag phase, cell division in exponential phase and stationary phase. This figure has been adapted from Maier (2009). (**B**) highlights the different phenotypes that can result from stationary phase and 'Long term stationary phase'. This figure was adapted from Jaishankar and Srivastava (2017).

1.8.2.2 Exponential phase

During exponential phase, cells divide by binary fission resulting in exponential growth. The doubling time of cells in batch culture during exponential phase varies but typically *E. coli* and *S.* Typhimurium take around 20 minutes to divide in rich media at 37°C. Doubling time is dependent on environment and availability of nutrients as well as the organism.

1.8.2.3 Stationary phase

In batch culture, there are points where cells cease to divide and grow (Kolter et al., 1993). The entrance into this phase, stationary phase, is a tightly regulated process (Navarro Llorens et al., 2010). Stationary phase signifies the reduction in growth rate (and a constant optical density (Gefen et al., 2014)), however cells are still metabolically active (Jaishankar and Srivastava, 2017). This stage is entered due to a reduction in nutrients, therefore leading to nutrient deprivation, accumulation of toxic metabolites and cell response to stress such as pH and temperature (Jaishankar and Srivastava, 2017). Stationary phase is not limited to a batch culture phenomenon. Bacterial populations, in soil, air, and water are almost entirely in a non-growing metabolically active state due to constant nutrient deprivation (Gefen et al., 2014).

In early stationary phase, survival under stress can be achieved in several ways. In Gram-positive cells, sporulation to endospores is a key way to survive nutrient deprivation and stress (Abel-Santos, 2015). Activation of the stringent response is common under nutrient deprivation such as stationary phase, leading to the formation of persister cell populations, and cells that can survive large amounts of stress

(Jaishankar and Srivastava, 2017). Although not strictly a phenotype of stationary phase, biofilms composed of bacterial cells and exopolysaccharide are largely non-growing and survive stressful environments and nutrient deprivation (Donlan, 2002). All these non-growing bacterial cell phenotypes add to the difficulty of antibiotic treatment due to their high tolerance and intrinsic resistance to toxic compounds and antimicrobials (Jaishankar and Srivastava, 2017).

Bacterial cells can be maintained in stationary phase for an extremely long period of time in the environment to survive harsh conditions. This becomes 'long term stationary phase' and 4 different adaptations for survival have been described due to prolonged starvation: viable non-culturable state (VNBC), growth advantage in stationary phase (GASP), constant activity at stationary phase (CASP) and Stationary Phase Contact Dependent Inhibition (SCDI) (**Figure 1-12B)**.

The VNBC state defines cells that are dormant and alive, however cannot be cultured (Jaishankar and Srivastava, 2017). These cells are considered metabolically active (Navarro Llorens et al., 2010) and this state was identified as an adaptation of starvation, as cells can regrow with the addition of pyruvate or catalase (Na et al., 2006, Mizunoe et al., 1999). This state is of concern in chronic human infection but also in food, as contamination may go undetected (Navarro Llorens et al., 2010, Jaishankar and Srivastava, 2017). Bacteria that have been shown to do this include but are not limited to *E. coli* (O157:H7 on lettuce) (Tyagi et al., 2019), *S.* Typhimurium (Rocard et al., 2018) and *Campylobacter jejuni* (Jones et al., 1991, Ferro et al., 2018). Cells in this state also remain resistant to antibiotic treatment (Hu and Coates, 2012).

The GASP state is defined as a phenotype where old stationary phase cells outcompete younger stationary phase cells (Navarro Llorens et al., 2010). This state involves mutations in genes important in stationary phase, giving bacterial cells an advantage to nutrient limited environments. Mutations of the GASP phenotype include stationary phase sigma factor *rpoS* (Zambrano et al., 1993), followed by the leucine responsive regulator, *lrp* (Zinser and Kolter, 2000), both identified in *E. coli*. Other bacteria such as *Salmonella, Shigella* (Martinez-Garcia et al., 2003) and *Pseudomonas* sp as well as some Gram-positive bacteria (Navarro Llorens et al., 2010).

In liquid culture, it has been shown that bacteria can acquire mutations in stationary phase which allow for the killing or inhibition of growth of their parental strains and is dependent on the physical contact between cells named SCDI (Lemonnier et al., 2008). In this state, bacteria that were outcompeting parent cells were found to overproduce glycogen due to mutations in *glgC,* a gene required for glycogen biosynthesis (Lemonnier et al., 2008).

CASP state is the most recent stationary phase phenotype to be described (Gefen et al., 2014). It is a state in which bacteria can maintain constant protein expression for 60 hours of stationary phase and starvation, therefore constant activity of ribosomes and RNA polymerase. This state is likely to end due to the requirement for energy conservation (Gefen et al., 2014).

1.9 Changes that occur in stationary phase cells

1.9.1 Regulation

1.9.1.1 The stationary phase sigma Factor, RpoS

RNA polymerase (RNAP) is required for transcription. The RNAP enzyme consists of 5 subunits ($\beta\beta'\alpha_2\omega$) and a further subunit called sigma (σ) which associates with the RNAP and is involved in promoter recognition and transcription of specific genes (Paget and Helmann, 2003).

In stationary phase, *rpoS* encodes the RpoS sigma factor or σ^S (σ^{38}), described as the stationary phase or stress sigma factor (Lange and Hengge-Aronis, 1991b). Although expressed in exponential phase, it is upregulated at the onset of stationary phase (Lange and Hengge-Aronis, 1994, Navarro Llorens et al., 2010). Upregulated expression of σ^S has also been described in unfavourable conditions such as nutrient starvation, high osmolarity, low pH and heat- and cold- shock (Jaishankar and Srivastava, 2017). These environmental signals guide σ^S-dependent transcription of genes involved in morphological changes (Lange and Hengge-Aronis, 1991a), cell envelope changes (Mitchell et al., 2017) and for survival in starvation (Navarro Llorens et al., 2010).

RpoS translation is, in part, controlled by small non-coding RNAs (sRNAs). sRNAs control translation and stabilise mRNA, often in the presence of a chaperone such as Hfq (Vogel and Luisi, 2011). sRNAs DsrA, RprA and ArcZ are activators and unfold mRNA allowing access of the ribosome for translation (Mandin and Gottesman, 2010). CyaR sRNA has been shown to repress RpoS translation, but binds to ArcZ

(Kim and Lee, 2020). The binding to ArcZ signals for CyaR degradation therefore activating RpoS translation (Kim and Lee, 2020). RpoS has also been shown to transcribe an sRNA, SraL, in *S.* Typhimurium (Silva et al., 2013). This sRNA is highly expressed in stationary phase and interacts with Rho mRNA, the transcription terminator (Silva et al., 2019).

1.9.1.2 Leucine responsive regulator protein (Lrp)

The leucine responsive regulator protein (Lrp) in *E. coli* is a well-studied example of a global transcriptional regulator of the Lrp family (Brinkman et al., 2003). Expression level of this regulator is inversely related to growth rate (Landgraf et al., 1996) and can be negatively or positively regulated in response to leucine (Calvo and Matthews, 1994) but also methionine and alanine (Hart and Blumenthal, 2011). Lrp has been found to control expression of 10% of genes in *E. coli*, the majority of these genes are transcribed on entrance to stationary phase (Tani et al., 2002), but also indirectly regulates genes (Kroner et al., 2019). Lrp plays vital roles in metabolism namely the anabolism of amino acids and reduction of catabolism during starvation (Calvo and Matthews, 1994, Navarro Llorens et al., 2010), and is upregulated by ppGpp (Calvo and Matthews, 1994), an inducer of the stringent response.

1.9.1.3 Nucleoid compaction via Dps and IHF

DNA protection during starvation (Dps) protein compacts the bacterial cell nucleoid protecting the cells from stress (Janissen et al., 2018). It is the most abundant protein in the nucleoid in stationary phase (Azam and Ishihama, 1999). Dps has been shown not to play a global role in transcription (Janissen et al., 2018). By condensing the nucleoid in stationary phase, it prevents external environmental stresses from killing

the cell (Janissen et al., 2018). Stresses include carbon and nitrogen starvation as well as oxidative stress (De Martino et al., 2016). In *S.* Typhimurium, Dps was shown to protect bacterial cells from oxidative stress, therefore surviving in a murine macrophage and accounting for an increase in virulence (Halsey et al., 2004).

It has been shown that increasing pH switches Dps from binding to DNA to another DNA binding protein abundant in stationary phase, IHF (Lee et al., 2015). IHF (Integration Host Factor) affects gene expression of stationary phase genes (Navarro Llorens et al., 2010). IHF binds to DNA and bends it, contributing to the condensation of the nucleoid as well as contributing to gene expression (Lee et al., 2015). As with Dps, in *S.* Typhimurium, IHF is important in the expression of virulence genes (Mangan et al., 2006).

1.9.1.4 The Stringent Response

Gram-negative bacteria can survive amino acid starvation due to the stringent response. The transcription of rRNA and tRNAs are stopped and instead expression turns in favour of amino acid biosynthesis (Traxler et al., 2008, Navarro Llorens et al., 2010). The stringent response is regulated by the accumulation of guanosine 5',3' bispyrophosphate (ppGpp), described as an alarmone (Traxler et al., 2008). ppGpp is synthesised by RelA in response to amino acid starvation (Traxler et al., 2008, Gentry and Cashel, 1996) and the turnover of ppGpp is also controlled by SpoT (Gentry and Cashel, 1996) in carbon starvation as well as decreased concentrations of fatty acids (Seyfzadeh et al., 1993). ppGpp signals not only the shutdown of RNA synthesis but also the upregulation of RpoS and stress proteins at the entrance to stationary phase (Gentry et al., 1993, Navarro Llorens et al., 2010).

1.9.2 Physiological changes

1.9.2.1 Morphological changes

In stationary phase, bacterial cells change from bacilli to coccoid in shape, combined with a reduction in size (Nystrom, 2004). Cells shrink in stationary phase as a result of nutrient starvation, known as 'dwarfing'. Cell size reduces through the degradation of cell material such as protein (Reeve et al., 1984), however the OM is not degraded in *E. coli* and *S.* Typhimurium, therefore increasing the volume of the periplasmic space (Nystrom, 2004).

The RpoS-dependent, *bolA*, is responsible for the overall coccoid shape of bacterial cells in stationary phase (Lange and Hengge-Aronis, 1991a). BolA is a transcriptional regulator which controls genes encoding for PBP4 and PBP5, and *ampC*, which contribute to the change in cell shape (Santos et al., 2002). Coccoid cells through expression of BolA, are also produced in nutrient deprived conditions (Santos et al., 1999). BolA also plays a vital role in reduced expression of motility (Dressaire et al., 2015) and increased production of biofilms in *E. coli* (Vieira et al., 2004, Moreira et al., 2017), virulence in *S.* Typhimurium (Mil-Homens et al., 2018), and decreasing the permeability of the OM (Freire et al., 2006).

1.9.2.2 Protein Synthesis

With the onset of starvation and stationary phase, there is an 80% reduction in the rate of protein synthesis (Reeve et al., 1984). As previously mentioned, the stringent response plays a role in survival in starvation because empty ribosome acceptor sites are bound by uncharged tRNAs promoting the synthesis of ppGpp and the shut down

in transcription of ribosomes (Traxler et al., 2008). tRNAs also differ in abundance depending on growth rate (Huisman et al., 1996). As described above, there is a phenotype of stationary phase (CASP) in which bacteria can maintain constant protein expression for 60 hours of stationary phase and starvation (Gefen et al., 2014). New protein can also be synthesised in stationary phase by utilising amino acids from degraded proteins of exponential phase (Reeve et al., 1984). Although protein synthesis rate decreases, already synthesised proteins can prolong their activity into stationary phase, this is true of AcrB which has a 6-day half-life (Chai et al., 2016).

1.9.2.3 Metabolism

The entrance into stationary signals the conservation of energy. The PMF decreases in stationary phase (Kashket, 1981) and the cytochrome oxidases of the electron transport chain change from cytochrome o, to cytochrome *d* and cytochrome *bd* complexes (Huisman et al., 1996).

As bacteria such as *E. coli* grow in glucose rich conditions, they do not utilise it all, but instead conserve glucose in the form of acetate (Luli and Strohl, 1990). Acetate is excreted from the cell in large amounts but re-enters the cell on its entrance to stationary phase (Luli and Strohl, 1990, Huisman et al., 1996). In stationary phase, a variation of the TCA cycle, called the glyoxylate shunt is upregulated (Huisman et al., 1996). Shown in **Figure 1-13**, the glyoxylate pathway is similar to the TCA cycle but circumvents the CO_2 producing step in the TCA cycle (Ahn et al., 2016). The glyoxylate shunt can then use acetate or fatty acids to synthesise glucose in carbon limited stationary phase (Ahn et al., 2016, Huisman et al., 1996). This cycle has also

been shown to be upregulated in oxidative stress (Ahn et al., 2016). It has also been found that pyruvate oxidase, *poxB*, converts pyruvate to acetyl-CoA, via acetate synthesis in cultures with low growth rate (Abdel-Hamid et al., 2001).

Figure 1-13 The TCA cycle and the Glyoxylate Shunt.

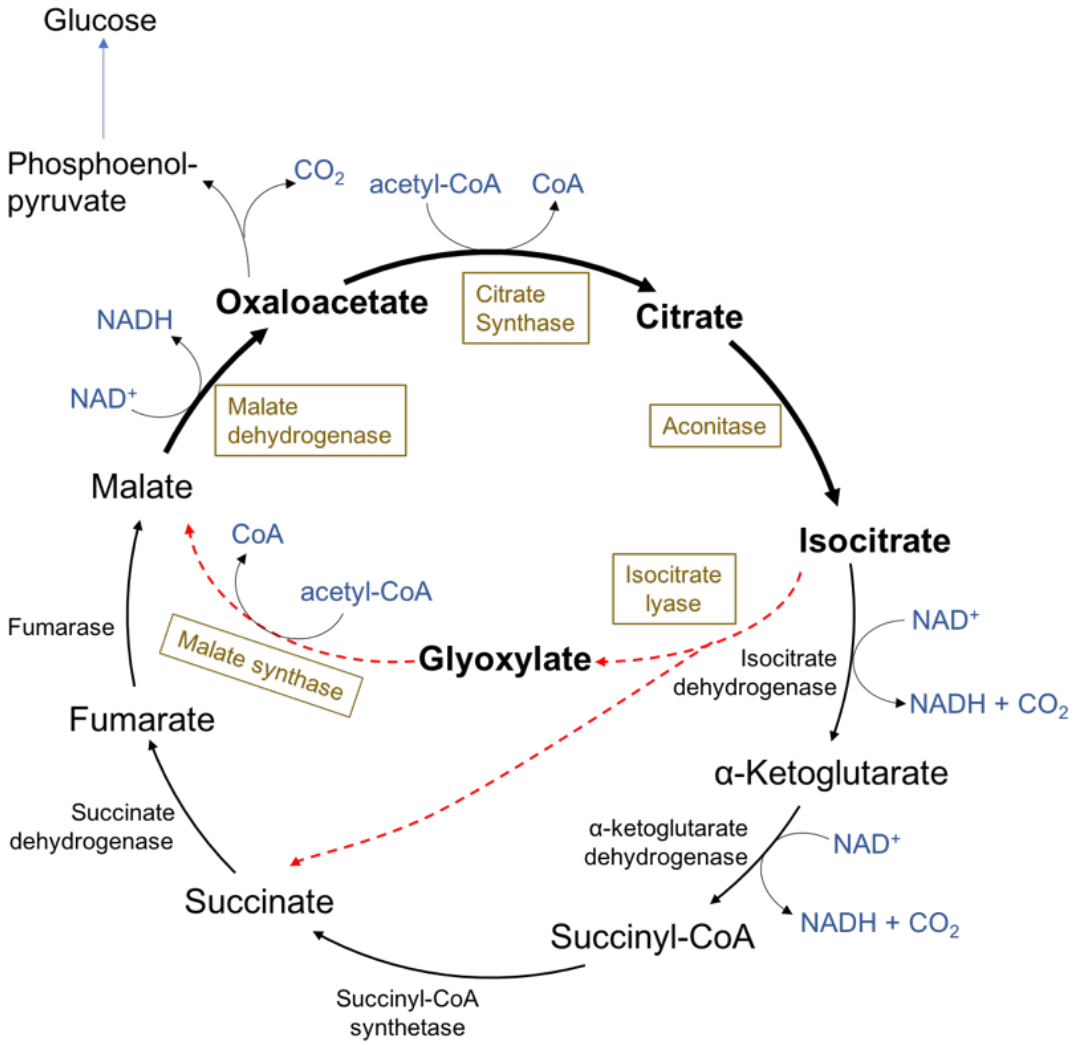

Above shows the TCA cycle and the glyoxylate cycle. The TCA cycle is shown but in stationary phase, the cell converts isocitrate to glyoxylate and succinate rather than using a step that wastes carbon as CO_2. Glyoxylate feeds back into the citric acid cycle. Figure has been adapted from Dunn et al. (2009).

Another metabolic pathway essential for survival in carbon limiting conditions is the accumulation and storage of glycogen, which is synthesised from glucose (Wilson et al., 2010). Glycogen synthesis can be controlled by an number of stationary phase signals such as ppGpp (Romeo and Preiss, 1989) and the upregulation of RpoS dependent genes (Hengge-Aronis and Fischer, 1992). The cell also scavenges for sugar by upregulating sugar transport systems (Huisman et al., 1996) and as previously stated, degrades protein to scavenge for amino acids (Reeve et al., 1984).

1.9.2.4 Membrane changes

During stationary phase, the inner and outer membranes of Gram-negative cells, and the peptidoglycan layer undergoes extensive changes.

In the OM, the concentration of LPS increases (Huisman et al., 1996). The increase in LPS increases the overall negative charge on the bacterial cell membrane. It is possible that this may reduce the susceptibility of the cell to membrane acting agents (Agrawal et al., 2019). The concentration of OMPs are reduced (Allen and Scott, 1979), however there is an increase in some proteins including those involved in curli biogenesis. The *csg* operon involved in curli biogenesis is directly regulated by RpoS which is bound by Crl, directing transcription (Arnqvist et al., 1994, Barnhart and Chapman, 2006). Other OMPs upregulated include flagellin and pili (Huisman et al., 1996). There is also an increased concentration of murein lipoprotein, which increases the connection between the OM and the peptidoglycan layer in stationary phase (Wensink et al., 1982, Pisabarro et al., 1985).

The peptidoglycan layer adjusts in both thickness and composition in stationary phase. In actively growing cells in rich media, the peptidoglycan accounts for 0.7% –

0.8% of the dry weight of the bacterial cell, but this increases during stationary to a dry weight of 1.4% to 1.9% of the bacterial cell (Mengin-Lecreulx and van Heijenoort, 1985). The transition from exponential to stationary phase also comes with gradual modification of the peptidoglycan, in which glycan chains become shorter but with increased crosslinks between peptides (Pisabarro et al., 1985). Although most cell wall components do not change significantly, there has been shown to be an increase in PBP6 in stationary phase cells, helping to stabilise the peptidoglycan in non-growing cells (Buchanan and Sowell, 1982, Huisman et al., 1996). The disaccharide, trehalose, has been shown to accumulate within the periplasm (Huisman et al., 1996). The *otsAB* genes involved in its biosynthesis are regulated osmotically but also by RpoS on entrance to stationary phase (Hengge-Aronis et al., 1991). Trehalose has been shown to be important in carbon stress (Moruno Algara et al., 2019) and osmotic stress (Giaever et al., 1988, Purvis et al., 2005), and increases tolerance to temperature in stationary phase (Hengge-Aronis et al., 1991, Kandror et al., 2002).

The IM undergoes drastic changes to its composition in stationary phase (Huisman et al., 1996). Within the IM of Gram-negative bacteria such as *E. coli* and *S.* Typhimurium, monounsaturated fatty acids comprise the majority of fatty acids within the IM (Huisman et al., 1996). With the onset of starvation and stationary phase, the concentration of monounsaturated fatty acids reduce (El-Khani and Stretton, 1981). Cyclopropane fatty acid concentration increases and accounts for 50% of the fatty acids within the IM in stationary phase (Cronan, 1968, Huisman et al., 1996). Cyclopropane fatty acid biosynthesis from unsaturated fatty acids is aided by the RpoS regulated synthase, *cfa* (Wang et al., 1992, Charoenwong et al., 2011). The

increase in these fatty acids has been linked to acid resistance in *E. coli* (Chang and Cronan, 1999) and *S.* Typhimurium (Kim et al., 2005). Along with cyclopropane fatty acids, cardiolipin increases in stationary phase (Cronan, 1968). All these changes to the membrane contribute to survival during starvation as well as osmotic stress, oxidative stress and tolerance to pH and temperature.

As it is known that the membrane is important for antibiotic entry and it is known that both the membrane and efflux expression changes through growth, the initial aim of this work was to see whether bacterial growth phase altered drug accumulation, and the importance of the interplay between influx and efflux in different growth phases.

1.10 Aims

1. Develop a method to measure drug accumulation in single cells using flow cytometry.
2. Measure ethidium bromide accumulation capacity of *S.* Typhimurium WT and a Δ*acrB* strain over a batch culture growth curve to assess accumulation in different growth phases.
3. To analyse the importance of efflux pumps for drug accumulation in exponential and stationary phase bacteria.
4. To determine the role of decreased outer membrane permeability in stationary phase, and whether this phenotype means that stationary phase accumulation is efflux-dependent.
5. Use RNAseq to distinguish changes in the transcriptome of a WT and a Δ*acrB* strain in different growth phases to explain the accumulation patterns seen.

Chapter 2- Materials and Methods

2.1 Bacterial strains, growth and storage

For the majority of this study, *Salmonella enterica* serovar Typhimurium SL1344 was used as the wild-type (WT) strain (Wray and Sojka, 1978). A complete list of strains, including those previously made or constructed for this study are shown in **Table 2-1**. All *S.* Typhimurium strains were stored using protect beads (Technical Services Consultants (TSC)) at -20 ˚C. *Escherichia coli* MG1655, *Klebsiella pneumoniae* ecl8 and *Pseudomonas aeruginosa* PA01 were stored using protect beads at -80 ˚C (**Table 2-1**).

When these bacterial strains were required, protect beads were spread on Luria Bertani (Lennox) (LB) agar plates and incubated at 37˚C overnight. These agar plates were then stored at 4˚C for up to a week. When the strains were required for experiments, they were grown in 5 mL LB broth at 37˚C overnight, unless otherwise stated. A list of the media types used is shown in **Table 2-2**. Some experiments used filter sterilised MOPs minimal media (Teknova) for which the composition is shown in **Table 2-2**. SL1344 is a histidine auxotroph therefore L-histidine was added to MOPs minimal media to give a final concentration of 0.4 mg/mL. For minimum inhibitory concentration (MIC) assays, a semi-defined iso-sensitest agar/broth was required and some phenotypic assays required salt-free media. All are shown in **Table 2-2**.

Table 2-1. *S.* Typhimurium Strain list

Laboratory Code	Genotype	Resistance	Reference
SE01	*S. enterica* Serovar Typhimurium SL1344		Wray and Sojka (1978)
SE44	*S.* Typhimurium 14082s		ATCC
EC19	*E. coli* Colindale NCTC 10418 MIC control strain		NCTC
SE02	SL1344 Δ*acrB*		Eaves et al. (2004b)
SE365	SL1344 Δ*tolC*		Buckley et al. (2006)
SE10	SL1344 Δ*acrA* Δ*acrE* Δ*mdsA* Δ*mdtA*		McNeil et al. (2019)
EC07	*E. coli* MG1655		Blattner et al. (1997)
EC29	MG1655 Δ*acrB*		Wang-Kan et al. (2017)
KP02	*Klebsiella pneumoniae* ecl8		Forage and Lin (1982)
KP03	Ecl8 *acrB::Gm*		Whittle et al. (2019)
PA19	*Pseudomonas aeruginosa* PA01		Held et al. (2012)
PA20	PA01 Δ*mexA*		Held et al. (2012)
PA22	PA14		Liberati et al. (2006) (pa14.mgh.harvard.edu)
PA23	PA14 Δ*mexA*		Liberati et al. (2006) (pa14.mgh.harvard.edu)
SA01	*Staphylococcus aureus* ATCC29213		ATCC
EC10	*E. coli* BW1125 + pKD4	Amp^R, Kan^R	Datsenko and Wanner (2000)
SE160	SL1344 + pCP20	Amp^R	Datsenko and Wanner (2000); Cherepanov and Wackernagel (1995)
SE67	SL1344 + pSIM18	Hyg^R	Chan et al. (2007)
SE258	SL1344 Δ*acrB* + pSIM18	Hyg^R	This study
SE270	SL1344 *rpoS::aph*	Kan^R	This study
SE271	SL1344 Δ*acrB rpoS::aph*	Kan^R	This study
SE273	SL1344 Δ*rpoS*		This study
SE274	SL1344 Δ*acrB* Δ*rpoS*		This study
SE368	SL1344 *ompF::aph*	Kan^R	This study
SE369	SL1344 Δ*acrB ompF::aph*	Kan^R	This study
SE373	SL1344 Δ*ompF*		This study
SE374	SL1344 Δ*acrB* Δ*ompF*		This study
SE387	SL1344 *ompC::aph*	Kan^R	This study
SE388	SL1344 Δ*acrB ompC::aph*	Kan^R	This study
SE392	SL1344 Δ*ompC*		This study
SE393	SL1344 Δ*acrB* Δ*ompC*		This study
SE403	SL1344 Δ*ompC* + pSIM18	Hyg^R	This study
SE406	SL1344 Δ*ompC ompF::aph*		This study
SE408	SL1344 Δ*ompC* Δ*ompF*		This study
SE404	SL1344 Δ*acrB* Δ*ompC* + pSIM18	Hyg^R	This study
SE407	SL1344 Δ*acrB* Δ*ompC ompF::aph*		This study
SE409	SL1344 Δ*acrB* Δ*ompC* Δ*ompF*		This study

SE59	SL1344 + pMW82-*ramA*	Amp^R	Lawler et al. (2013)
SE205	SL1344 + pMW82-*acrA*	Amp^R	A gift from E. Trampari and M. Webber
SE206	SL1344 + pMW82-*acrE*	Amp^R	A gift from E. Trampari and M. Webber
SE207	SL1344 + pMW82-*acrD*	Amp^R	A gift from E. Trampari and M. Webber
SE208	SL1344 + pMW82-*mdsA*	Amp^R	A gift from E. Trampari and M. Webber
SE209	SL1344 + pMW82-*mdfA*	Amp^R	A gift from E. Trampari and M. Webber
SE210	SL1344 + pMW82-*mdtK*	Amp^R	A gift from E. Trampari and M. Webber
SE211	SL1344 + pMW82-*emrA*	Amp^R	A gift from E. Trampari and M. Webber
SE212	SL1344 + pMW82-*macA*	Amp^R	A gift from E. Trampari and M. Webber
SE213	SL1344 + pMW82-*mdtA*	Amp^R	A gift from E. Trampari and M. Webber
SE236	SL1344 + pMW82-*acrA*	Amp^R	A gift from E. Trampari and M. Webber
SE237	SL1344 Δ*acrB* + pMW82-*acrE*	Amp^R	This study
SE238	SL1344 Δ*acrB* + pMW82-*acrD*	Amp^R	This study
SE239	SL1344 Δ*acrB* + pMW82-*mdsA*	Amp^R	This study
SE240	SL1344 Δ*acrB* + pMW82-*mdfA*	Amp^R	This study
SE241	SL1344 Δ*acrB* + pMW82-*mdtK*	Amp^R	This study
SE242	SL1344 Δ*acrB* + pMW82-*emrA*	Amp^R	This study
SE243	SL1344 Δ*acrB* + pMW82-*macA*	Amp^R	This study
SE244	SL1344 Δ*acrB* + pMW82-*mdtA*	Amp^R	This study
EC85	*E. coli* DH5α + pET GFP LIC cloning vector (u-msfGFP)	Amp^R	A gift from Scott Gradia (Addgene plasmid # 29772)
EC90	NEB5α + pET LIC cloning vector (msfGFP + *aph*)	Amp^R, Kan^R	This study
SE342	SL1344 AcrB-GFP (*aph*)	Kan^R	This study
SE344	SL1344 AcrB-GFP		This study

Table 2-2 Growth media

Media	Components	Product code
LB (Lennox) broth (500 mL)	10 g LB (Lennox) powder	L3022; Sigma
LB (Lennox) agar (500 mL)	17.5 g LB agar powder	L2897; Sigma
MOPs minimal media (1 L)	100 mL of 10X MOPS	M2101; Teknova
	10 mL 0.132 M K_2HPO_4	M2102; Teknova
	10 mL 20% Glucose	G0520; Teknova
	400 mg L-histidine (98%)	10665602; Fisher
Salt Free LB broth (500 mL)	5 g Tryptone	10158962; Fisher
	2.5 g yeast extract	10108202; Fisher
	500 mL H_2O	
Salt Free LB agar (500 mL)	5 g Tryptone	10158962; Fisher
	2.5 g yeast extract	10108202; Fisher
	7.5 g agar	DS662; Beckton Dickinson
	500 mL H_2O	
Iso-sensitest agar (2 L)	31.4 g Iso-sensitest agar	10661475; Oxoid
Iso-sensitest broth (1 L)	23.4 g Iso-sensitest broth	10311053; oxoid

Table 2-3 Antibiotics used for cloning

Antibiotic	Stock concentration	Final concentration	Product code
Kanamycin	10,000 µg/mL (H_2O)	50 µg/mL	K1876; Sigma
Ampicillin	10,000 µg/mL ($NaHCO_3$)	50 µg/mL	A9393; Sigma
Hygromycin	10,000 µg/mL (H_2O)	150 µg/mL	H7772; Sigma

When SL1344 contained plasmids, it was grown with appropriate antibiotics supplemented in LB agar or LB broth. The plasmids, pKD4, pSIM18 and pCP20 (**Table 2-4**) used for homologous recombination and gene deletion, required kanamycin, hygromycin and ampicillin respectively. The final concentrations for these antibiotics are shown in **Table 2-3**. The pSIM18 and pCP20 plasmids were temperature sensitive, and therefore strains containing these were grown at 30˚C. Strains that contained pMW82 plasmids were grown on agar/broth containing ampicillin (**Table 2-1**).

Table 2-4 Plasmids

Plasmid	Description	Resistance	Reference
pKD4	Used to amplify a PCR product with homology to the KO gene of interest at the 5' and 3' end of the gene. *aph* is a FRT-flanked kanamycin resistance cassette.	Amp^R, Kan^R	Datsenko and Wanner (2000)
pSIM18	Encodes the λ red recombinase for homologous recombination of FRT sites (temperature sensitive: 30 °C)	Hyg^R	Chan et al. (2007)
pCP20	Encodes the FLP recombinase for removal of *aph* at the FRT sites (temperature sensitive: 30 °C)	Amp^R	Datsenko and Wanner (2000) Cherepanov and Wackernagel (1995)
pMW82	Contains GFP; Promoters can be fused to GFP to produce transcriptional reporters	Amp^R	Bumann and Valdivia (2007)
pET LIC vector (u-msfGFP)	This plasmid contains a GFP described by Pedelacq et al. (2006) with SNPs that enhance brightness and solubility and inhibits dimerisation		A gift from Scott Gradia (Addgene plasmid # 29772)
pET LIC vector (msfGFP + *aph*)	Insertion of the *aph* kanamycin resistance cassette into the pET LIC vector (u-msfGFP) downstream of GFP	Amp^R, Kan^R	This study

2.2 Measuring ethidium bromide accumulation using flow cytometry in mid-exponential phase

The method discussed was developed as part of this thesis and has been published (Whittle et al., 2019). For all flow cytometry assays, unless otherwise stated, 4 biological replicates have been analysed.

2.2.1 Set up of the flow cytometer

The Attune® NxT Acoustic Focusing Cytometer (Invitrogen) was calibrated according to the manufacturer's instructions using Attune® Performance Tracking Beads (4449754; Fisher) and Attune Focusing Fluid (448862; Fisher). The Yellow laser was set at 561 nm; channel YL1, 585/16 nm filter for fluorophore SYTO-84 Orange Fluorescent Nucleic Acid Stain (SYTO-84) (Lot no: 1890520; Invitrogen) which has excitation/emission maxima of 567 nm / 582 nm. The blue laser was set at 488 nm; channel BL3, 695/40 nm filter for ethidium bromide (EtBr) (excitation 482 nm emission 616 nm). The Sip Sanitize function with 4% bleach was used to clean the machine between samples and a deep clean was performed at the end of each experiment.

2.2.2 Measurement of EtBr accumulation in Gram-negative bacteria

Bacterial strains were grown in 5 mL LB broth at 37˚C, shaking overnight. Bacterial overnight cultures were used to re-inoculate fresh LB at 4 %, and grown for 1 hour at 37˚C. After 1 hour of growth, cells from 300 µL culture were harvested by

centrifugation. Cells were then re-suspended in 100 µL of 1 x HEPES buffered saline (HBS) (J61239.AK; Alfa Aesar). Phosphate buffered saline (PBS) could not be used because it is not compatible with SYTO-84.

The dyes, SYTO-84 and EtBr were added to 500 µL of 1 × HBS giving final concentrations of 10 µM and 100 µM respectively. The previously prepared 100 µL bacterial cell suspension was then added to the 1 × HBS and dyes, and incubated for 10 minutes at room temperature. Accumulation of EtBr could then be measured in each cell within a population using flow cytometry. Information about the dyes used in this method can be found in **Table 2-5.**

Using the gating strategy shown in **Figure 2-1**, EtBr accumulation was measured. Initially, cells emitting SYTO-84 fluorescence were visualised **(Figure 2-1A)** using a forward scatter-height (FSC-H) vs SYTO-84 emission plot. This dye was used to gate around cells and omit background cell debris. The SYTO-84 fluorescence emission was collected in the YL1-H channel. This channel collects 585/16 nm emissions using 561 nm yellow laser. Using the red gate **(Figure 2-1A)**, 10,000 SYTO-84 positive events could be counted. This population was then plotted on a logarithmic histogram, and EtBr fluorescence emission measured in the BL3-H channel. The blue gate **(Figure 2-1B)** showed EtBr accumulation by using the X-median value as relative fluorescent units (RFU). For this and following experiments, the PMT voltages were: FSC at 700, SSC at 500, YL1 at 500 and BL3 at 400.

Compensation corrected for spill-over in fluorescence. Spill-over is defined as an overlap in excitation or emission maxima. Based on the fluorescence excitation and emission of the SYTO-84 and EtBr **(Figure 2-2)**, compensation was configured.

Figure 2-1 Gating strategy to measure EtBr fluorescence/accumulation

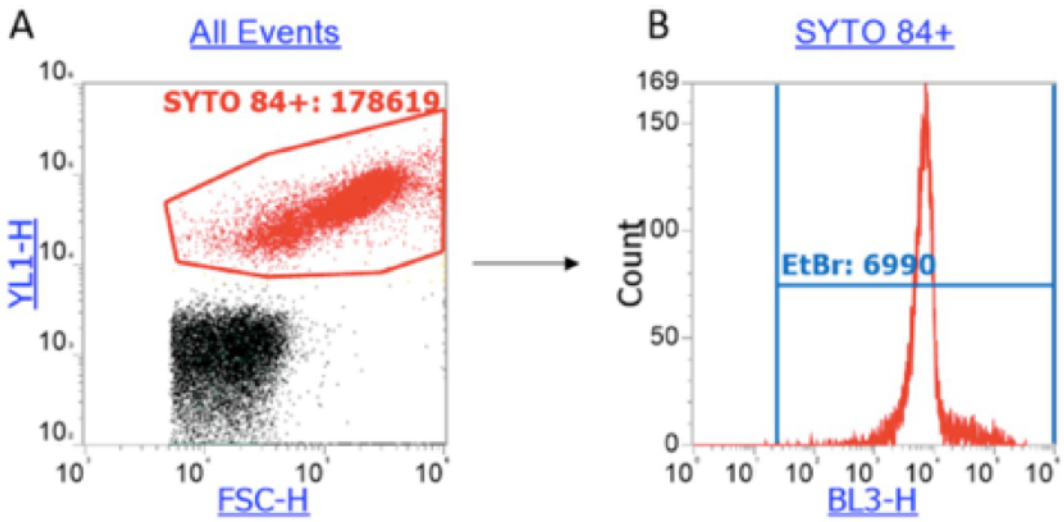

(**A**) SYTO-84 fluorescence is plotted vs FSC-H to separate fluorescence emission from background cell debris (black). 10,000 SYTO-84$^+$ events were collected within the red gate. (**B**) SYTO-84$^+$ events within the red gate were then plotted on a logarithmic histogram collecting fluorescence in the BL3-H filter for EtBr. The blue gate value was the X-median for fluorescence and was used as the measure of accumulation. This figure was produced by EE Whittle and previously published in Whittle et al. (2019).

Table 2-5 Dyes and fluorescent proteins used for flow cytometry

Dye/Fluorescent protein	Company	Ex/Em (nm)	Laser	Emission filter (nm)	Channel name
SYTO™ 84 Orange (SYTO-84)	Fisher	567/582	Yellow	585/16	YL1
SYTO™ 9 Green (SYTO-9)	Fisher	485/498	Blue	590/40	BL2
Ethidium bromide	95%, Fisher	482/616	Blue	695/40	BL3
Nile red	99%, Fisher	549/628 510/580	Yellow	585/16	YL1
GFP (pMW82)	A gift from Mark Webber	488/510	Blue	530/30	BL1
GFP (msfGFP)	Addgene plasmid # 29772	488/510	Blue	530/30	BL1

Figure 2-2 Excitation/Emission of SYTO-84 and EtBr.

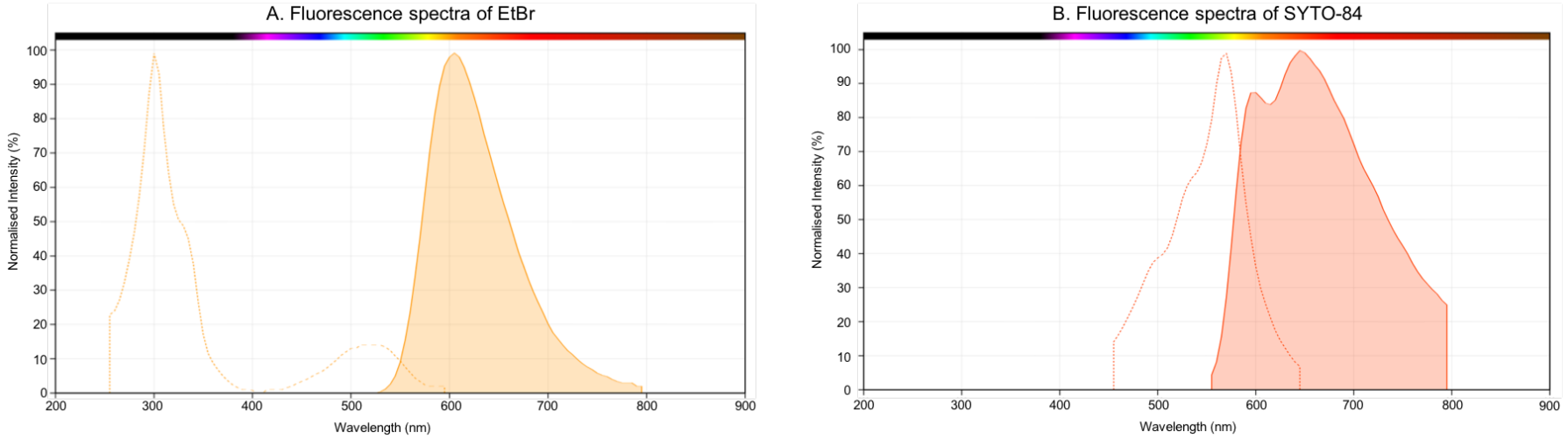

(**A**) represents the excitation (dashed line)/emission spectra (solid orange line) of EtBr. EtBr is excited by a blue laser (488 nm) and its emission is within the BL3 channel for emissions of 695/40 filter. (**B**) represents the excitation (dashed line)/emission spectra (solid red line) of SYTO-84. SYTO-84 dye is excited by the yellow laser (561 nm) and its emission is within the YL1 channel for an emission of 585/16 nm. This figure was created and adapted using ATT Bioquest's interactive Spectrum Viewer (https://www.aatbio.com/spectrum/).

Compensation of BL3-H and YL1-H channels was set using Attune NxT software. For this, an unstained control of 100 µL cells was added to 500 µL of filtered HBS. YL1-H compensation was set using 100uL cells with 10 µM SYTO-84 in 500 µL HBS and BL3-H by 100 µL cells with 100 µM EtBr. Compensation was set to ensure data quality but the SYTO-84 and EtBr were excited using differing channels so spill-over in fluorescence emission was minimal.

2.2.3 Measuring EtBr accumulation with GFP fluorescence

EtBr accumulation and GFP fluorescence were measured in parallel in the same cells. RamA is a transcriptional activator of the *acrAB-tolC* operon. Using SL1344 pMW82-*ramA*, the transcription of *ramA* was measured alongside EtBr accumulation. In this experiment, indole, an inducer of *ramA* was added to act as a control for the transcriptional reporter. Due to the presence of the pMW82 plasmid, cultures were initially grown for 2 hours at 37˚C in LB supplemented with ampicillin (final concentration shown in **Table 2-3**). After 2 hours of growth, cells from 200 µL of culture were harvested and then resuspended in 1 × HBS and then sample set up continued as previously described. For the samples which were induced, the 200 µL culture was incubated with a final concentration of 2 mM indole for 30 minutes. Cells were then harvested after 30 minutes and samples were set up as previously described.

To measure GFP, additional gating and compensation were required. An SL1344 negative control strain with no GFP fluorescence was used to identify when no GFP was expressed. It was then possible to correctly measure fluorescence of GFP in those cells where it was expressed. As previously shown, a gate was added to select

for SYTO-84$^+$ populations **(Figure 2-3A+D)** and then a further gate was added to measure EtBr accumulation in a SYTO-84$^+$ population using the BL3-H filter. SYTO-84$^+$ populations were also used to analyse GFP. Initially, GFP was identified using a BL1-H fluorescence (for GFP) vs YL1-H (for SYTO-84) dot plot. Comparing SL1344 to a GFP producing strain **(Figure 2-3B+E)**, a quadrant gate was added to the dot plot. Those cells emitting GFP were shown in the GFP$^+$ gate in **Figure 2-3E**. The population within the GFP$^+$ gate was then plotted on a logarithmic histogram and the X-median value was taken as GFP fluorescence. Compensation was set for the emission of each fluorophore against an unstained control using the Attune NxT software.

Figure 2-3 Gating strategy for the measurement of GFP.

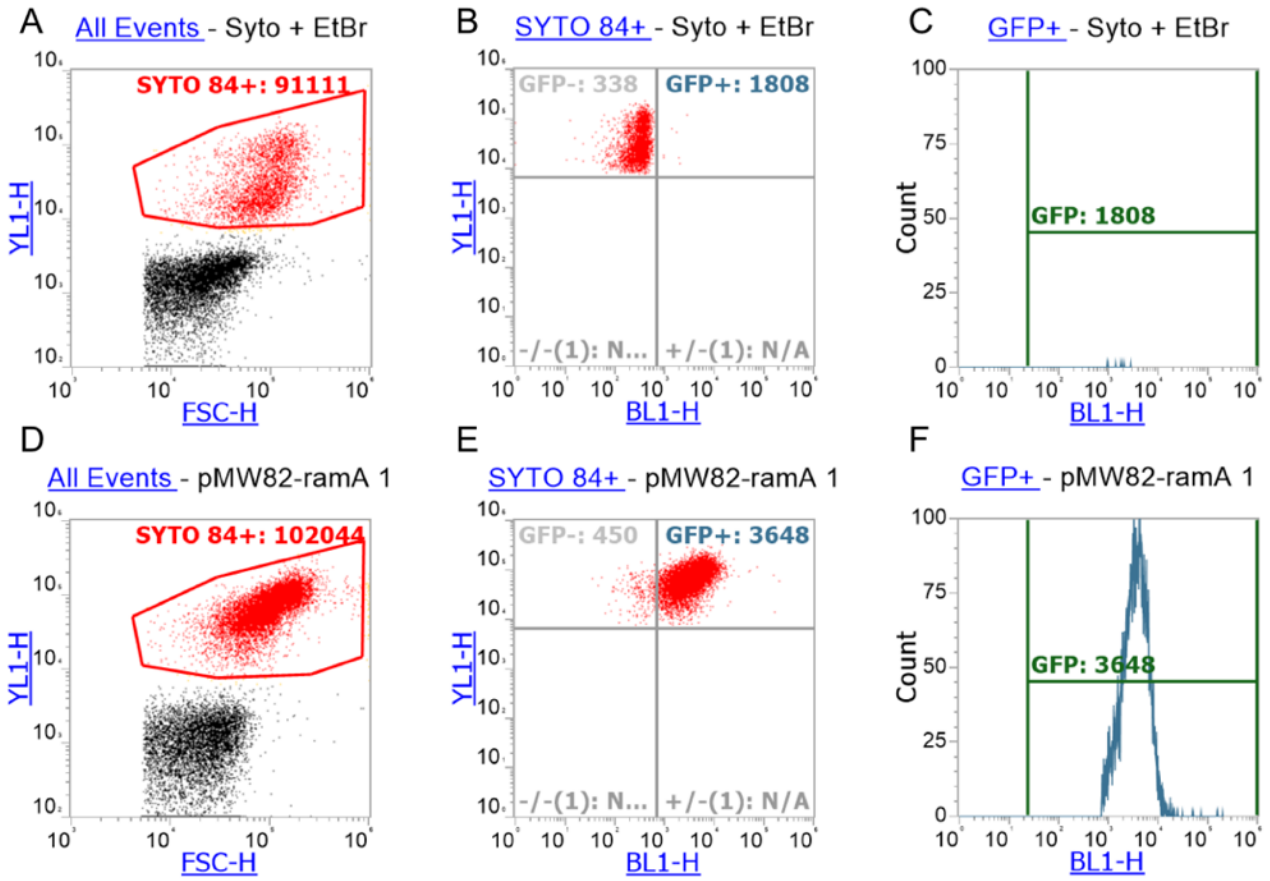

(**A-C**) shows SYTO-84 and GFP fluorescence in SL1344. (**D-F**) shows SYTO-84 and GFP fluorescence in SL1344 pMW82-ramA. (**A+D**) show initial collection of 10,000 SYTO-84^{+} events within the red gate. Using the red gated population, (**B+E**) shows GFP vs SYTO-84 fluorescence. (**B**) is the non-GFP control and therefore was considered GFP-. (**E**) using the quadrant gate, GFP+ cells were gated and the population appears red. (**C+F**) show the GFP+ populations on a logarithmic histogram using the BL1-H filter for GFP fluorescence. This figure was created by the author of this thesis but taken from Whittle et al., 2019.

2.2.4 Measuring Nile Red accumulation using flow cytometry

The method described above for measuring EtBr accumulation was adapted to measure accumulation of Nile Red. The final concentration of Nile Red used was 75 μM. SYTO-84 was replaced with SYTO-9 in these experiments because SYTO-84 fluorescence ex/em overlaps with the ex/em of nile red when it is staining both triglycerides and phospholipids (Greenspan and Fowler, 1985). SYTO-9 fluorescence was collected using the BL2-H channel for green fluorescence, in order to separate from background cell debris. Using the SYTO-9^{+} population, nile red emission was then measured using the YL1-H channel. In this case, compensation was again set using the Attune software.

2.2.5 Measuring EtBr accumulation in the presence of inhibitors

Using SL1344, this assay was optimised to measure accumulation of EtBr and Nile Red in the presence of compounds that inhibit efflux. The examples used were the PMF inhibitor, carbonyl cyanide 3-chlorophenylhydrazone (CCCP) and the RND inhibitor PaβN.

To analyse the effect that CCCP (Fisher) had on dye accumulation, CCCP was added to 500 μL of 1 × HBS to give a final concentration of 100 μM CCCP (Smith and Blair, 2014), followed by the addition of EtBr and SYTO-84. Cell suspension was added and samples were incubated for 10 minutes before analysing using flow cytometry.

With PaβN, EtBr was not used due to previous studies that suggest the inhibitor does not prevent EtBr export (Lomovskaya et al., 2001, Kern et al., 2006). Nile Red accumulation was used to study the effects of PaβN on substrate accumulation. The

set up followed that described in **Section 2.2.4**, where a final concentration of 50 µg/mL PaβN was added to 500 µL of 1 × HBS.

2.3 Measurement of Accumulation of EtBr over growth using Flow Cytometry

The method discussed below is an adaptation of the previously described method to allow measurement of accumulation in cells taken from different points in the growth curve. Unless otherwise stated, accumulation was measured in 4 biological replicates for these flow cytometry assays.

2.3.1 Accumulation assay in cells taken from different time points across the growth curve

Cultures were grown at 37°C overnight in 5 mL of LB. Strains were then sub-cultured using a 4 % inoculum in 25 mL of LB or MOPs in a 250 mL Duran bottle and grown for 6 hours at 37°C with aeration. At every hour for 6 hours (including time point 0), samples were taken (of different volumes), cells harvested, and resuspended in 1 × HBS at differing volumes stated in **Table 2-6**. Samples were set up, as previously stated in **Section 2.2.2**. Both SYTO-84 and EtBr were added to 500 µL of 1 × HBS and then the cell suspension was added. Cultures were grown in drug-free broth and dyes were only ever added to samples that were harvested, dyes were never added to the growing cultures.

The volume of culture that was removed was dependent on the time point, as diluted samples with a low cell count are required for flow cytometry **(Table 2-6)**. Initial

experiments using SL1344 compared to Δ*acrB,* Δ*acrAE,* Δ*tolC* and Δ4PAP took a 100 µL sample from cultures which were grown for 4 to 6 hours. However, cultures which were grown for longer than 4 hours contained far more cells and so the sample volume was reduced to 50 µL Samples were incubated with SYTO-84 and EtBr for 10 minutes at room temperature before analysis by flow cytometry.

Table 2-6 Sample collection from 0-6 hours

Sample time (h)	culture taken (µL)	HBS re-suspended in (µL)
0	400	100
1	300	100
2	200	200
3	200	1000
4	100	1000
5-6	50	1000

2.3.2 Gating strategy for measuring EtBr across the growth curve

A flow cytometric gating strategy for measuring EtBr accumulation was described in **Section 2.2.2**. However, in stationary phase cells, the SYTO-84$^+$ cells did not form a simple defined and separated population from background cell debris and became more difficult to gate. Therefore, an extra gating step was added to increase the reliability of the EtBr accumulation results. Briefly, the YL1-H channel detected the presence of SYTO-84 stain as previously mentioned. Gating via dot plot again allowed for separation of cells from background particles based on SYTO-84 fluorescence. A gate was added to collect the SYTO-84$^+$ population (gate name: SYTO 84+) on a YL1-H vs FSC-H plot **(Figure 2-4B)**. The SYTO-84$^+$ population was plotted on a dot plot showing forward scatter (FSC-H) and side scatter (SSC-H) based on size and granularity **(Figure 2-4C)**. This extra gate allowed EtBr accumulation to be correctly measured in stationary phase as size and granularity did not differ between time points. A new gate from this plot (Cells) was plotted on a logarithmic histogram for EtBr fluorescence. The final gate was added to measure the X-median fluorescence per cell ('EtBr' gate) using the BL3-H channel **(Figure 2-4D)**, confirm EtBr fluorescence and therefore accumulation.

The gating strategy described in this section was used for all experiments where accumulation of dyes was measured across the growth curve.

Figure 2-4 Gating Strategy for accumulation assay over time.

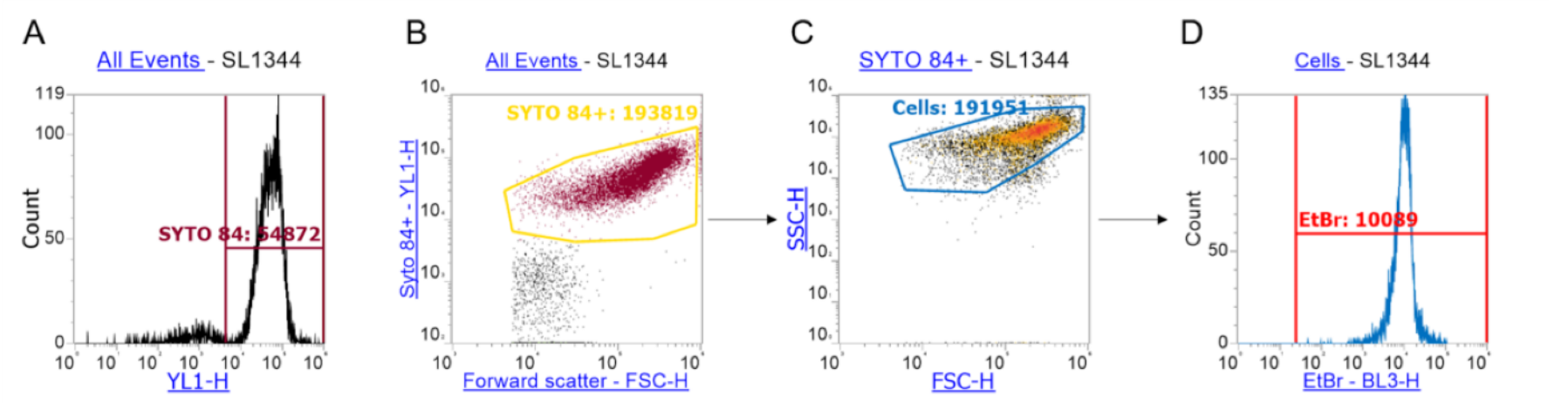

(**A**) Cells are gated in purple with the name 'SYTO 84' and appear purple on YL1-H vs count histogram plot. (**B**) Using a FSC-H vs YL1-H dot plot, SYTO 84^{+} cells were gated (yellow) to separate them from background cell debris. (**C**) The SYTO-84^{+} population was further gated (blue) on an FSC-H vs SSC-H dot plot for a single cell population. FSC vs SSC dot plot shows size vs granularity. (**D**) Cells are gated in red and the peak appears blue based on 'Cells" and gives the X-median value of EtBr fluorescence used as a measure of accumulation.

2.3.3 Adaptation of flow cytometry assay across growth curve to test other variables

The flow cytometry assay measuring EtBr across the growth curve described in **Section 2.3.1** was adapted for use with the Nile Red dye and also to test other hypotheses. The details are outlined below.

2.3.3.1 Nile Red

Nile Red accumulation was measured in *S.* Typhimurium across the growth curve in place of EtBr. Using a final concentration of 75 µM Nile Red and SYTO-9 in place of SYTO-84, as stated in **Section 2.2.4**, the method for accumulation across the growth curve **(2.3.1)** was repeated.

2.3.3.2 Addition of CCCP

Measuring EtBr accumulation in the presence of CCCP was described in **Section 2.2.5**. Samples of growing culture were taken every hour **(Table 2-6)**. A final concentration of 100 µM CCCP was added to 500 µL HBS, followed by EtBr and SYTO-84. Samples were incubated for 10 minutes and then analysed.

2.3.3.3 EtBr accumulation measured with GFP fluorescence

The promotor of *acrAB* has been cloned upstream of green fluorescent protein (*gfp*) on the pMW82 plasmid. This plasmid can report on the level of *acrAB* transcription as GFP is expressed when *acrAB* is transcribed (this pMW82 plasmid was a gift from Dr. Mark Webber (Webber et al., 2017)). SL1344 with the pMW82-*acrA* plasmid was used in this method. This strain was also grown for 6 hours in 25 mL LB, but was

supplemented with ampicillin due to the plasmid. The sample set up was carried out as in **Section 2.3.1**. However, GFP fluorescence using flow cytometry was measured as stated in **Section 0**.

2.3.3.4 Assay in the presence of EDTA to disrupt the membrane

This assay was carried out in a similar way to **Section 2.3.1**. However, samples were only taken at 1, 3 and 5 hours and only 3 biological replicates were carried out.

Cell pellets were resuspended in volumes of 1 × HBS (**Table 2-6**) with a final cell suspension of 500 µL. Then samples were treated with 0 µM, 1 µM, 10 µM, 100 µM, 200 µM or 500 µM of EDTA at pH 8. EtBr and SYTO-84 dyes were then added. The volume of these dyes was adjusted to maintain final concentration. Samples were then analysed by flow cytometry.

2.3.4 Measurement of cell viability

2.3.4.1 Cells grown in LB for 0-6 hours

The samples collected for flow cytometry **(section 2.3.1)** were serially diluted 1 in 10 to a final ratio of 1:100000 and 5 µL of each dilution was plated on LB agar in triplicate. Agar plates were incubated at 37°C overnight and colony forming units/mL (CFU/mL) were calculated the following day.

2.3.4.2 Cells incubated in the presence of EDTA for 10 minutes

To determine whether bacterial viability was affected by EDTA concentration, samples from the experiment described in **Section 2.3.3.4** were taken before SYTO-84 and EtBr were added. Following addition of EDTA, samples were incubated

for 10 minutes and then viable counts were performed as described in **Section 2.3.4.1**.

2.4 Statistical analysis of Flow Cytometry data

2.4.1 Statistical analysis of accumulation at a single time point

For data produced based on the methods that measure EtBr accumulation at only mid-exponential phase **(Section 2.2)**, all graphs were produced using Prism GraphPad software. To compare EtBr accumulation of SL1344 to Δ*acrB*, Δ*tolC*, Δ*acrAE*, and Δ4PAP (Δ*acrA*, Δ*acrE*, Δ*mdtA*, Δ*mdsA)* strains, a one-way ANOVA and Dunnett's multiple comparisons test was used. A one-way Analysis of Variance (ANOVA) was used in this case because EtBr accumulation was measured in more than two strains. For EtBr accumulation of *E. coli*, *K. pneumoniae* and *P. aeruginosa* compared to a single efflux mutant, unpaired T-tests were used for analysis. Unpaired T-tests were also used for the analysis of nile red accumulation, the fluorescence of GFP and the presence and absence of inhibitors.

Most graphs shown in this thesis, contain asterisks that relate to significant p-values and is shown in **Table 2-7**.

Table 2-7 How asterisks relate to p-value

P-value	Asterisk
>0.05	ns
0.01 - 0.05	*
0.001 - 0.01	**
0.0001 - 0.001	***
<0.0001	****

2.4.2 Statistical analysis of EtBr accumulation over time

The average EtBr fluorescence per cell collected in the BL3-H channel equated to EtBr fluorescence. The X-median was used as a statistic for the average accumulation of EtBr per cell. The events per µL statistic was used to calculate CFU/mL using the following equation.

$$^{1}cells\ per\ mL\ in\ culture = \left(events\ per\ \mu L * \ (z + 515)\right) * \left(\frac{y}{z}\right) * \left(\frac{1000}{x}\right)$$

[1] **x µL volume of culture taken; y µL HBS resuspended in; z µL added to the 515 µL sample.**

The median of EtBr accumulation and the number of cells were plotted using Prism software. When measuring EtBr accumulation at different timepoints in a single strain (SL1344), a one-way ANOVA and multiple comparisons test was used. A two-way ANOVA and multiple comparison tests were required when comparing EtBr accumulation between two strains at a number of different time points due to the number of variables. Statistical tests used are stated with each result in the proceeding chapters.

2.5 Disruption of genes in S. Typhimurium

The *rpoS*, *ompC* and *ompF* genes were disrupted in *S*. Typhimurium using the homologous recombination method described by Datsenko and Wanner (2000). The *rpoS* gene was deleted in SL1344 and SL1344 Δ*acrB* to produce a single and double knockout respectively **(Table 2-1)**. The major porin genes, *ompC* and *ompF,* were deleted from SL1344 and SL1344 Δ*acrB* to produce a single and double knockout respectively. The *ompF* gene was also deleted from SL1344 Δ*ompC* and SL1344

Δ*acrB* Δ*ompC* to produce a suite of porin deleted strains that can be found in **Table 2-1**.

2.5.1 Generation of PCR product for gene disruption

Oligonucleotides (**Table 2-8**) were designed with approximately 40 base pairs (bp) of homology upstream or downstream of the gene to be disrupted and approximately 20 bp homology to the *aph* (which encodes aminoglycoside phosphotransferase) cassette of the pKD4 plasmid. The template pKD4 plasmid was purified from *E. coli* strain BW1125 **(Table 2-1)** using a plasmid miniprep kit according to manufacturer's instructions (Qiagen). Oligonucleotides (Invitrogen) were reconstituted in Ultrapure H_2O to a concentration of 100 µM, and then diluted for use to 25 µM. Polymerase chain reaction (PCR) samples contained 12.5 µL MyTaq DNA polymerase (Bioline), 9.5 µL Ultrapure H_2O and 1 µL of both forward and reverse primers with 2 µL of pKD4 as a template. The cycling conditions for this and all PCR reactions can be found in **Table 2-9**. Agarose gel electrophoresis was used to separate 50 µL of PCR product, and DNA was then excised from the gel and purified using a Gel extraction kit (Qiagen). The concentration of DNA was measured using a nanodrop.

Agarose gels were made by making 1 % agarose (Sigma) in Tris-acetate EDTA (TAE) buffer (Sigma), and 10 µL Midori Green stain was added to aid visualisation. DNA was separated on agarose gels at 100 V for 1 hour, unless not well separated. Agarose gels were imaged with UV on an Amersham Imager 680.

Table 2-8 List of oligonucleotides

Code	Description	Sequence (5'-3')
82	*acrB* check (F)	GCTCAGCCCAGGTCTTAACTT
83	*acrB* check (R)	CTCACTGTTGATAAGGCCGC
36	K2; internal *aph* check (F)	CGGTGCCCTGAATGAACTGC
37	Kt; internal *aph* check (R)	GGATTCATCGACTGTGGCCG
191	(F) to knockout *rpoS* (*aph* insertion)	TTGCTAGTTCCGTCAAGGGATCACGGGTAGGAGCCACCTTGTGTAGGCTGGAGCTGCTTC
192	(R) to knockout *rpoS* (*aph* insertion)	GGACCATGGCTAATTCCCTAAGTACCCTTGTCAAAAAAAGGCCAGTCTGTCGACTGGC
193	*rpoS* check (F)	AGGGGAAATCCGTAAACCCG
194	*rpoS* check (R)	ATCGCGCCAGGTATACAGAC
242	(F) for inserting *aph* into msfGFP with upstream AscI site	TATATTGGCGCGCCGTGTAGGCTGGAGCTGCTTC
243	(R) for inserting *aph* into msfGFP with downstream KpnI site	AGGATATTCATATGGACCATGGCTAATTCCCATGGTACCCCGATA
246	*aph* insertion into msfGFP (F)	GTCCAAGCTGAGCAAAGACC
247	*aph* insertion into msfGFP (R)	TGAATGAACTGCAGGACGAG
261	(F) to insert msfGFP-*aph* downstream of *acrB*	GAGCATAGTCATTCGACAGAACATCGCGGTAGCGGTAACAAAGGTCAGGGCGTGAGCAAGGGCGAGGAGCTGTT
249	(R) for the insertion of msfGFP-*aph* downstream of *acrB*	GGACCATGGCTAATTCCCATTTTGCTCACTGTTGATAAGGCCGCGCAAGCGGCCTTTTTTACGCAAAAATCT
254	*acrB-gfp* check (F)	TGGTCTATCCCGTTCTCCGT
255	*acrB-gfp* check (R)	GGGCACAAGCTGGAGTACAA
260	(F) to insert a 6xHis tag + *aph* downstream of *acrB*	GAGCATAGTCATTCGACAGAACATCGCCATCACCATCACCATCACTAAGTGTAGGCTGGAGCTGCTTC
268	*ompC* check (F)	AATGGACTTGCCGACTGGTT
269	*ompC* check (R)	CCTCATCGCAGCCCATAAGT
270	*ompF* check (F)	TAGCACTTTCACGGTAGCGA
271	*ompF* check (R)	AAAGCCCGCCTGTTTTTGAA
272	(F) to knockout *ompF* (*aph* insertion)	GCAGGTGTCATATAAAAAAACCAATGAGGGTAATAAATAGTGTAGGCTGGAGCTGCTTC
273	(R) to knockout *ompF* (*aph* insertion)	ATGGCTAATTCCCATTGATCAGCAGACCCCTTTGTTTTATGCCTCAAAAACAGGA
307	(F) to knockout *ompC* (*aph* insertion)	AAAGCAATAAAGGCATATAACAGAGGGTTAATAACGTGTAGGCTGGAGCTGCTTC
308	(R) to knockout *ompC* (*aph* insertion)	ATGGCTAATTCCCTAATCAGCAAAAGATGTTGCTAAAGGGCCTGCGGGCCCTT

Table 2-9 PCR cycling times and temperatures

PCR cycle name	Initial Denaturation	Denaturation	Annealing	Extension	Final extension
		(x30 cycles)			
***rpoS* check**	95°C (1 min)	95°C (15s)	65°C (15s)	72°C (30s)	72°C (10 min)
***acrB* check**	95°C (1 min)	95°C (15s)	51°C (15s)	72°C (40s)	72°C (10 min)
AscI and KpnI insertion	98°C (30s)	98°C (10s)	65°C (15s)	72°C (30s)	72°C (10 min)
***acrB-gfp* check**	95°C (1 min)	95°C (15s)	60°C (15s)	72°C (30s)	72°C (10 min)
		(x35 cycles)			
***aph* product for KOs**	95°C (1 min)	95°C (30s)	50°C (30s)	72°C (40s)	72°C (10 min)
***gfp-aph* homologous recombination**	95°C (1 min)	95°C (15s)	61°C (15s)	72°C (3 mins)	72°C (10 min)
***gfp-aph* check**	95°C (1 min)	95°C (30s)	65°C (15s)	72°C (30s)	72°C (10 min)
***ompF* and *ompC* check**	95°C (1 min)	95°C (15s)	58°C (15s)	72°C (2 mins)	72°C (10 min)

2.5.2 Bacterial transformation

To transform recipient strains with the plasmids required for the gene disruption method (pSIM18 or pCP20 shown in **Table 2-4**), bacteria were made electro-competent. Overnight cultures were prepared as described in **Section 2.1** and 2 mL was used to inoculate 50 mL of LB broth in a 500 mL Duran bottle. The culture was grown at 37°C, with shaking until an OD_{600} of 0.6 was reached. Cells were transferred to a 50 mL falcon tube and chilled on ice for 10 minutes followed by centrifugation at 2250 x *g* for 10 minutes at 4°C. The supernatant was discarded and cells were resuspended in 25 mL of ice cold 15 % glycerol and harvested by centrifugation a further 3 times. Cells were resuspended in a final volume of 500 µL of 15 % glycerol. A maximum volume of 2 µL of plasmid DNA was added for final volume of 50 µL of competent cells in a chilled 0.2 cm electroporation cuvette. Electroporation was performed at 2.5 kV (25 µF, 200 Ω), then 950 µL of warm LB broth was immediately added to the cuvette and then cells were transferred to a universal tube and recovered at 30°C with shaking for 1 hour. Cells were then spread on LB agar plates with 150 µg/ml hygromycin to select for transformed strains and incubated overnight at 30°C.

2.5.3 Lambda red recombination

Strains containing pSIM18, were transformed with the PCR products made in **Section 2.5.1**. The pSIM18 encodes a λ red recombinase system which mediates homologous recombination (**Table 2-4**). As a result, the PCR product containing the *aph* cassette incorporates into the target gene and disrupts it.

Overnight cultures were prepared with 150 µg/mL of hygromycin, and incubated at 30°C. This was used to inoculate 50 mL of fresh LB at 4 %, and this culture was grown to OD_{600} nm of 0.3. Cells were transferred to a 50 mL falcon tube and heat shocked at 42°C for 15 minutes in a water bath, then cooled on ice for 10 minutes. Cells were made competent by washing 3 times in 15 % ice cold glycerol as described in **Section 2.5.2** and resuspended in a final volume of 200 µL. Electroporation was performed as described in **Section 2.5.2** using 45 µL of cells and 5 µL of PCR product. Cells were incubated for 2 hours at 37°C in universal tubes and then plated on LB agar with 50 µg/mL kanamycin to select for incorporation of the *aph* cassette by homologous recombination. The plates were incubated at 37°C overnight and successful transformants were streaked onto fresh LB agar with 50 µg/mL kanamycin. To cure pSIM18 from gene disruption candidates, they were grown in 5 mL of LB overnight at 37˚C and then streaked onto LB agar without antibiotics, and grown overnight at 37˚C. A colony from each candidate was then streaked onto kanamycin and hygromycin. Colonies which grew on kanamycin, but not hygromycin, confirmed the loss of pSIM18.

2.5.4 *aph* removal by pCP20

Knock-out strains containing *aph* were made competent as in **Section 2.5.2** and resuspended in 400 µL of glycerol followed by electroporation with 5 µL pCP20 plasmid (Datsenko and Wanner, 2000, Cherepanov and Wackernagel, 1995). Electroporated cells were recovered in 950 µL of LB broth and incubated at 30°C for 1 hour to recover. The cells are then spread on LB plates with 50 µg/mL ampicillin (**Table 2-3**) and incubated for 24-48 hours at 30°C. To cure the plasmid, candidate

colonies were inoculated in 10 mL of LB and grown overnight with aeration at 43°C. A loop of culture was then streaked onto LB and incubated overnight at 37°C. The loss of pCP20 was screened by plating colonies on LB only, LB with kanamycin and LB with ampicillin. The cells that lost both pCP20 and *aph* do not grow on ampicillin or kanamycin.

2.5.5 Verification of *aph* insertion and removal by PCR

Correct insertion and pCP20 removal of the *aph* gene into the recipient strain was confirmed by PCR. The correct size for all genes, knockouts and Δ strains are shown in **Table 2-10**.

Primers were created upstream and downstream of the gene of interested to confirm the size if *aph* was present or absent. Primers are shown in **Table 2-8**. Cycling conditions for PCRs are shown in **Table 2-9**. Successful insertions and pCP20 removals of *aph* into the recipient gene were confirmed by visualising 5 µL of the PCR products by agarose gel electrophoresis. These PCR products were then purified using the PCR purification kit protocol (Qiagen) and then the concentration measured by nanodrop.

Table 2-10 Sizes (bp) of PCR products

Gene	WT (bp)	+ *aph* (bp)	Δ (bp)
acrB	3214	1583	386
rpoS	1289	1793	400
ompF	1355	1762	367
ompC	1405	1765	300

2.5.6 Sequencing

All KO and Δ strain PCR products were sequenced using TubeSeq from the Eurofins genomics service (Sanger sequencing).

2.6 Chromosomal insertion of *gfp* downstream of *acrB*

To measure the protein level of AcrB in *S.* Typhimurium, a gene encoding a monomeric super-folder GFP (msfGFP) was inserted downstream of *acrB* on the chromosome to produce a AcrB-msfGFP fusion protein. Strain construction was based on the method used by Bergmiller et al. (2017) in *E. coli.* Using restriction and ligation, the *aph* gene was inserted into pET LIC vector (u-msfGFP), so that strains containing the plasmid could be selected for. Using this plasmid as template, *gfp* and *aph* were inserted into the chromosome downstream of *acrB* in SL1344 to produce a protein fusion strain.

2.6.1 Insertion of *aph* into pET LIC vector (u-msfGFP)

The restriction sites downstream of the *gfp* gene that enable cutting by AscI and KpnI-HF (NEB) restriction enzymes, were used to insert *aph* into the msfGFP encoding plasmid. The msfGFP plasmid was purified using the Qiagen plasmid prep kit protocol. Enough plasmid was purified for 1 µg DNA in the restriction digest reaction.

The *aph* gene was amplified from the pKD4 plasmid. Oligonucleotides **(Table 2-8)** were designed with homology to the *aph* gene. The forward oligonucleotide contained the AscI restriction site at the 5' end, where the KpnI restriction site was

present at the 5' end of the reverse oligonucleotide. This DNA product was amplified using PCR with Phusion polymerase (ThermoFisher). The mastermix for this reaction is in **Table 2-12** and the PCR cycle times in **Table 2-9**.The DNA was separated by agarose gel electrophoresis and the size of the DNA product was 1522 bp which was then purified using the Qiagen gel extraction kit protocol.

Restriction digest was carried out on the msfGFP plasmid and the *aph* DNA product using the enzymes stated above to produce overhangs of DNA for re-ligation. Both restriction enzymes had 100% activity in CutSmart® Buffer. The following restriction digest reactions were set up as in **Table 2-11**, with an uncut control, single cuts controls (AscI or KpnI-HF), double cut plasmid and *aph* product.

Table 2-11 Sample set up for restriction digest

	Uncut	**Single (AscI)**	**Single (KpnI-HF)**	**Double (GFP)**	**Double (*aph*)**
DNA	0.5 µg (14 µL)	0.5 µg (14 µL)	0.5 µg (14 µL)	1 µg (9.5 µL)	235 ng (15 µL)
10 x buffer	5 µL	5 µL	5 µL	5 µL	5 µL
AscI	0 µL	1 µL	0 µL	1 µL	1 µL
KpnI	0 µL	0 µL	1 µL	1 µL	1 µL
H_2O	31 µL	30 µL	30 µL	33.5 µL	0 µL

The samples were made as described in **Table 2-11** and then incubated at 37°C for 1 hour. After 1 hour, 1 µL of alkaline phosphatase (NEB) was added to the tubes containing double cut msfGFP plasmid to prevent re-ligation of the plasmid to itself. The samples were then incubated at 37°C for 1 hour. As the *aph* PCR product already had a low concentration of DNA, the sample was then purified using the PCR purification kit protocol (Qiagen) to prevent more loss of DNA by gel electrophoresis. The DNA from all other samples was separated by size using agarose gel electrophoresis with a 6 x loading buffer to visualise the DNA. The double cut plasmid was then purified using the gel extraction kit protocol (Qiagen).

For the ligation reaction, the following ratios were used for plasmid to PCR product: 1:1, 3:1 and 9:1 in order to optimise and obtain successfully ligated *aph* into the msfGFP plasmid. The ligation reactions were incubated overnight at 16°C. **Figure 2-5** shows the plasmid map for the msfGFP-*aph* plasmid.

The ligation reactions were then transformed in to NEB 5- α *E. coli* (C29871) using the NEB transformation protocol. Transformations were spread on LB agar plates containing kanamycin and incubated overnight at 37°C. Candidates were checked for correct insertion of *aph* using PCR and sequencing.

Figure 2-5 Plasmid map of msfGFP-*aph* plasmid.

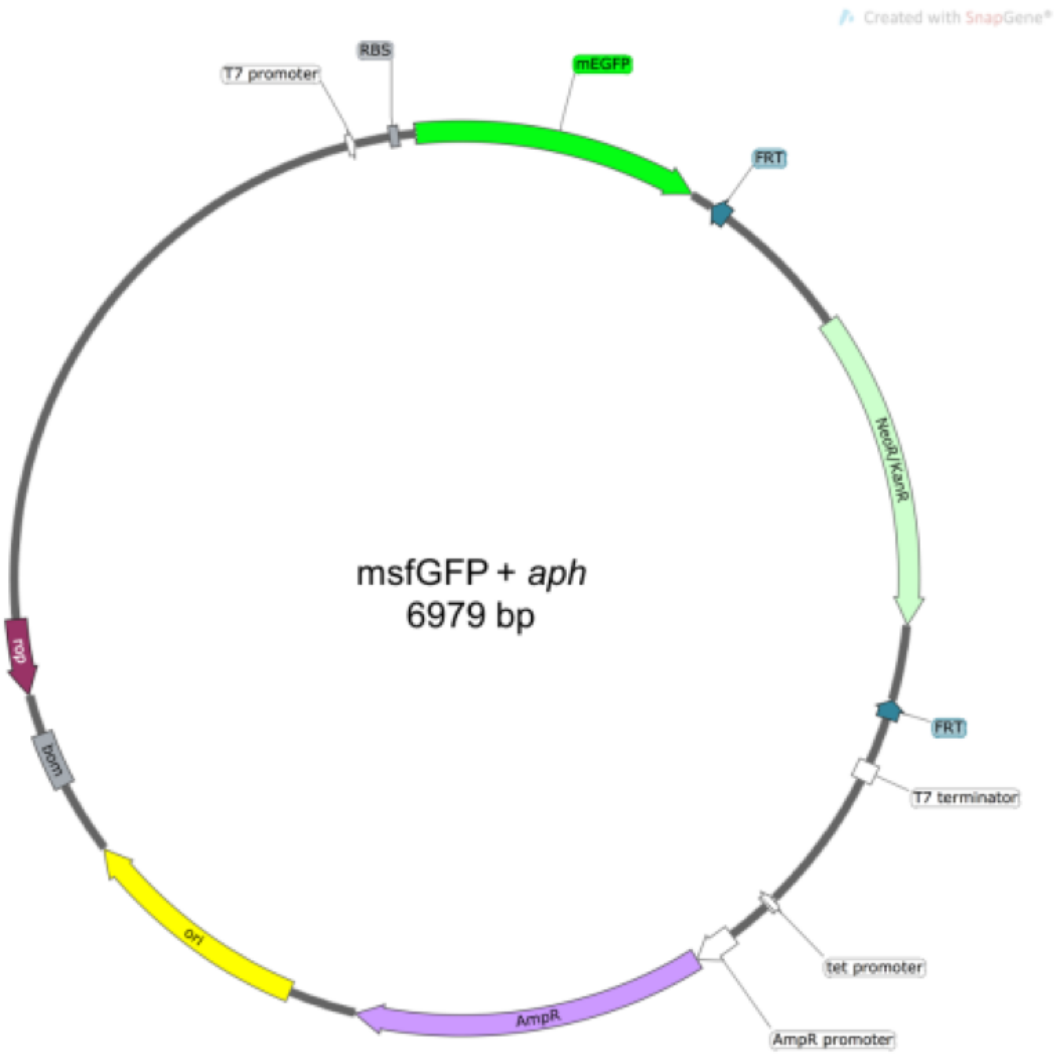

This plasmid had an Amp^R cassette. A Kan^R (*aph*) cassette was inserted into the plasmid using restriction-ligation downstream of msfGFP. Schematic made using Snapgene software.

2.6.2 PCR amplification of *gfp-aph*

The msfGFP + *aph* plasmid was purified using the Qiagen plasmid prep protocol.

Oligonucleotides were designed to amplify GFP and *aph* from the plasmid with homology to *acrB*. The forward oligonucleotide shown in **Table 2-8**, was designed to have homology to the 3' end of *acrB,* a codon optimised polylinker (GgtAgcGgtAacAaaGgtCagGgc) used by Bergmiller et al. (2017) and homology to the 5' of *gfp* (**Figure 2-6**).The reverse oligonucleotide had homology to the end of *aph* and a non-coding downstream region of *acrB*.

The DNA was amplified using PCR and Phusion polymerase (mastermix in **Table 2-12**) with a cycle time shown in **Table 2-9**. The correct band size was 2356 bp and the DNA was concentrated using gel extraction (Qiagen).

Table 2-12 Phusion polymerase mastermix set-up (50 µL)

Component	Volume (µL)
10 µM forward primer	2.5
10 µM reverse primer	2.5
DMSO	1.5
2x Phusion polymerase mastermix	25
Template	2
H_2O	16.5

Figure 2-6 Schematic of *gfp* inserted downstream of *acrB* on the chromosome.

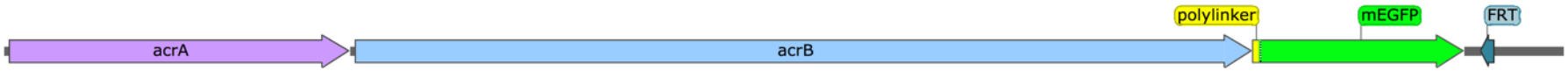

This schematic shows *acrA* (purple), *acrB* (blue) where the stop codon has been removed and a polylinker (yellow) and GFP (green) fused to it. Schematic produced using Snapgene software.

2.6.3 Homologous recombination

Insertion of *gfp* and *aph* downstream of *acrB* was done using homologous recombination, and the method used was previously described in **Section 2.5.3**. PCR and sequencing confirmed correct fusion of *gfp* to *acrB* and then *aph* was removed using pCP20 described in **Section 2.5.4**.

2.6.4 Confirmation of construction of SL1344 AcrB-GFP

Successful candidates were checked by amplification using oligonucleotides within *acrB*, *gfp* and *aph.* Amplification of a product containing part of *acrB,* the polylinker and *gfp* was done using primers p254 and p255 for a 920 bp product. The oligonucleotides and cycling times can be found in **Table 2-8** and **Table 2-9** respectively. Sequencing confirmed the removal of *aph* and correct construction of SL1344 AcrB-GFP.

2.7 Phenotypic characterisation of mutant strains

2.7.1 Growth kinetics

Overnight cultures of strains were grown in 5 mL of LB at 37°C. Strains were diluted 1:10000 in either LB or MOPs minimal media and this was then diluted 1:10. Cultures were added to a flat bottomed, clear 96-well plate with lid (Greiner), with 200 µL per well and 3 technical replicates of each. LB or MOPs alone were added as blanks. The plate was then covered with a 'BreatheEasy' membrane (Diversified Biotech) to prevent evaporation. Absorbance was measured at 600 nm using a FLUOstar Omega at 37°C. Absorbance was taken using well-scan mode and shaking of the

plate occurred between readings. Absorbance readings were taken every 20 minutes for 12 hours. There were three biological replicates for each strain where growth kinetics was measured. Generation times were calculated for each biological replicate and a one-way ANOVA and Tukey's multiple comparison test was used for statistical analysis.

2.7.2 Antimicrobial susceptibility

The Minimum Inhibitory Concentrations (MICs) of a number of antibiotics and dyes were established by the agar dilution method of Clinical and Laboratory Standards Institute (CLSI, 2018). Antibiotic and dye stocks were freshly made and used to supplement Iso-sensitest agar. The list of antibiotics and dyes used are shown in **Table 2-13**.The MIC data was the modal value of 3 biological replicates. A control strain, *E. coli* Colindale NCTC 10418 (**Table 2-1**), with defined MIC values was used to confirm consistency of MICs data.

Table 2-13 Antibiotics and dyes used for MICs

Compound	Company	Solvent	Concentration
Ampicillin	Sigma; A0166	$NaHCO_3$	0.008 µg/mL – 8 µg/mL
Ciprofloxacin	Fisher; 13531640	Acetic acid + H_2O	0.008 µg/mL – 8 µg/mL
Crystal violet	Fisher; AC447570500	H_2O	1 µg/mL – 1024 µg/mL
Erythromycin	Fisher; AC227330050	70 % ethanol	1 µg/mL – 1024 µg/mL
EtBr	Fisher; 10042120	H_2O	1 µg/mL – 1024 µg/mL
Fusidic acid	Sigma: F0881	H_2O	1 µg/mL – 1024 µg/mL
Norfloxacin	Alfa Aesar; J6265203	Acetic acid + H_2O	0.008 µg/mL – 8 µg/mL
Rhodamine 6G	Fisher; AC419010050	H_2O	1 µg/mL – 1024 µg/mL
Rifampicin	Sigma; R3501	H_2O	1 µg/mL – 1024 µg/mL
SDS	Fisher; 10593355	H_2O	1 µg/mL – 1024 µg/mL
Vancomycin	Alfa Aesar; J62790.06	H_2O	1 µg/mL – 1024 µg/mL

2.7.3 Broth microdilution MICs

Fresh antibiotic and dye stocks were prepared. Overnight cultures were grown at 37°C with aeration. *E. coli* NCTC 10418 was included as a control strain. The overnight cultures were then diluted 1:100 and then again 1:20 to give ~5 x 10^5 cfu/mL for inoculation into a 96-well plate. Bacteria are incubated with no antibiotic and 11 different concentrations of the antibiotic MIC being measured. To measure the MIC, 12 wells in a 96-well plate (1 row) were used. 50 µL iso-sensitest broth was added to wells 2-12. Antibiotic was diluted in iso-sensitest broth to the twice the required top concentration for measurement. 50 µL of this dilution is added to well 1 and well 2. Well 2 containing 100 µL of broth + antibiotic is the starting point for a serial dilution where 50 µL is removed and added to the next well until well 11, where the 50 µL is removed. No antibiotic is added to well 12. 50 µL bacterial suspension is then added to each of the 12 wells. This process is repeated for each antibiotic and each strain where the MIC is measured. The 96-well plate is then incubated at 37°C overnight. The MIC value is then taken and is the first well where bacterial growth is not observed. Results were only accepted if the observed MIC of *E. coli* NCTC 10418 was within 1 doubling dilution of the expected result as defined by Andrews and Testing (2006). The MIC data was the modal value of 3 biological replicates.

2.7.4 Broth microdilution MIC from 3 different time points of growth

Briefly, the assay is carried out as above in **Section 2.7.3**, except that MIC value is not based on the dilution of an overnight culture. Antibiotics used were ciprofloxacin,

EtBr, SDS and vancomycin. Overnights are sub-cultured at a 4% inoculum and grown for 5 hours. After 1,3 and 5 hours of growth, samples were taken and MIC 96-well plates set up from these cultures. At each hour, the bacterial culture was diluted to ~5 x 10^5 cfu/mL, so that MICs could be compared to the standard MIC of an overnight. CFU/mL for each time was based on CFU/mL result from flow cytometry assays.

2.7.5 Direct efflux assay

As well as measuring EtBr accumulation, efflux activity can also be measured using EtBr. In this method, the efflux substrate EtBr accumulates within bacterial cells in the presence of an efflux inhibitor, and then when efflux pumps are re-energised with glucose, fluorescence of EtBr can be measured as it is exported from cells.

Overnight cultures were sub-cultured in 10 mL fresh LB and grown shaking at 37°C until an OD_{600} nm of 0.4. Cells were harvested at 3000 x *g* for 10 minutes at 23°C. Pellets were resuspended in 10 mL of PPB buffer (50 mL 0.1 M potassium phosphate buffer; 200 mL H_2O; 250 µL $MgCl_2$) and OD_{600} nm was adjusted to 0.15 in 10 mL. Then, 100 µM CCCP and 50 µg/mL EtBr were added to 10 mL suspension which was then incubated shaking at 23°C for 1 hour. Cells were then harvested again as above and resuspended in fresh PPB buffer + 5% glucose. Then, 200 µL was added to a black bottomed 96-well plate and fluorescence intensity was measured using a FLUOstar Omega. EtBr fluorescence gain was set to 1460.

For all efflux assays, results for each strain were based on three biological replicates. For each biological replicate, 3 technical replicates were averaged and then the data was normalised such that the first fluorescence value at time point 0 was equal to 1.

From this, the time taken for a 10%, 25% and 50% drop in fluorescence was measured. Unpaired T-tests were used to measure statistical differences between drops in fluorescence.

2.7.6 Adaptation of efflux assay to three time points

Briefly, overnight cultures of SL1344 and SL1344 Δ*acrB* were sub-cultured into 100 mL fresh LB and then grown for 5 hours at 37 °C. At the 1, 3 and 5-hour time points, 10 mL of culture was taken and the OD_{600} nm measured. The harvested cell pellet was then resuspended in PPB buffer and OD_{600} nm adjusted to 0.15 in 10 mL. From this point, efflux assays were carried out as previously described as above (Smith and Blair, 2014, Paixao et al., 2009). Data and statistical analysis were carried out as in **Section 2.7.5.**

2.7.7 Membrane leakage

To measure membrane leakage, the above efflux assay **(Section 2.7.6)** was repeated. However, at the point where EtBr and CCCP are washed in fresh buffer with glucose, glucose was not added. This means that cells were not re-energised and any decrease in fluorescence shows what has leaked out of the cell membrane.

2.7.8 Crystal violet biofilm quantification

Biofilm formation by bacteria can be measured after 48 hours of growth using the dye, crystal violet. Overnight cultures of strains were grown in 5 mL of LB without salt at 37°C. The positive control strain 14082s which produces a high level of biofilm was included. Overnight cultures were then sub-cultured into 25 mL LB (4% inoculum)

and samples were then taken at 1, 3 and 5 hours. Overnight cultures were diluted 1:10 in fresh salt free broth and OD_{600} nm adjusted to 0.1. 200 µl of diluted cell suspension was added to a clear 96-well plate. For each strain, three biological replicates were included. Each biological replicate was based on the averaged values of three technical replicates.

After 1, 3 and 5 hours of growth, samples were adjusted to an OD_{600} nm of 0.1 and added to the 96-well plate. The 96-well plate was then incubated at 30°C for 48 hours with gentle shaking. After 48 hours, the biofilms were washed with water to remove unattached cells. Then, 200 µl of 0.1 % crystal violet was added to the wells with biofilms and incubated for 15 minutes at room temperature. Crystal violet was then removed from the plate by washing the wells with water. The biofilm was then resolubilised in 200 µl of 70% ethanol. The remaining crystal violet equated to the biofilm that was present. The OD_{600} nm was measured using the FLUOstar OMEGA (BMG labtech).

2.7.9 Curli biogenesis

Using congo red supplemented agar, the biogenesis of curli can be visualised based on colony morphology and colour. Cultures of strains were grown in 5 mL of LB overnight at 37°C. Salt-free agar was cooled to 50°C and congo red (B24310; Alfa Aesar) added to make a final concentration of 40 µg/ml and poured into petri dishes. Overnight cultures were diluted 1:10 and the OD_{600} nm then adjusted to 0.1. Cultures were then spotted onto plates at a volume of 5 µL and incubated at 30°C for 48 hours. Plates were then imaged using a SMZ1000 zoom stereomicroscope (Nikon) at 1x

magnification. Red, dry and rough colonies indicated the production of curli and cellulose. Pink colonies indicated strains that produced cellulose but no curli.

This assay was adapted to measure curli production at 1, 3 and 5 hours. 25 mL of SL1344 and SL1344 Δ*acrB* was grown and at each of the above time points, the culture was OD_{600} nm adjusted to 0.1 in salt free media and then plated onto congo red agar plates.

2.7.10 Measuring transcription using pMW82 reporters in a whole population

The transcription levels of each efflux pump in SL1344 could be measured using the pMW82 plasmid. The promoter of each efflux pump (*acrA, acrD, acrE, mdsA, mdtA, macA, emrA, mdfA* and *mdtK*) was fused upstream of *gfp* on the pMW82 plasmid (these plasmid constructs were a gift from E. Trampari and M. Webber). These pMW82 plasmids, which were efflux transcriptional reporters were transformed into SL1344 and SL1344 Δ*acrB*. In both strains, GFP fluorescence could be measured across the growth curve and this equated to the level of transcription of each pump.

When measuring transcription, overnight cultures containing pMW82 transcriptional reporter plasmids (SE205-213 and SE236-244) were diluted 1:10000 in minimal media, supplemented with 50 μg/ml ampicillin. Then, 200 μL of each strain was added to a 96-well plate and incubated at 37˚C. OD_{600} nm and GFP fluorescence were measured every 20 minutes for 12 hours using a FLUOstar Omega. OD_{600} nm and GFP fluorescence were then analysed, with a background blank minimal media control subtracted from the data. For GFP fluorescence, SL1344 fluorescence was

subtracted from the pMW82 strains to remove background autofluorescence of the strain. GFP divided by OD_{600} nm was calculated to account cell density across growth. The transcription data is based on 3 biological replicates for each strain.

2.7.11 Whole population measurement of GFP from SL1344 AcrB-GFP

As in **Section 2.7.10,** overnight cultures were grown in LB and then diluted 1:10000 in MOPs minimal media. SL1344 AcrB-GFP was analysed in this experiment, and SL1344 was used as a control to account for *Salmonella* autofluorescence. Then, 200 µL of each strain was added to a 96-well plate and incubated at 37˚C. OD_{600} nm and GFP fluorescence were measured every 20 minutes for 16 hours using a FLUOstar Omega. The gain for GFP measurement was increased to 2260. Gain adjustment is the control of voltage, therefore increasing the signal, as this variant of GFP was found to have low signal. Gain was chosen based on the auto-gain adjustment. OD_{600} nm and GFP fluorescence were then analysed, with a background blank minimal media control subtracted from the data.

2.8 Microscopy

Overnights of SL1344 and SL1344 AcrB-GFP were grown shaking at 37°C and sub-cultured at 4% inoculum into 25 mL of fresh LB. Cultures were grown for 5 hours. After 1 hour (1 mL), 3 hours (500 µL) and 5 hours (100 µL) of growth, samples were taken and cells harvested at 14,000 x *g* for 5 minutes. The supernatant was removed and the pellet re-suspended in 300 µL 4 % PFA, which was then incubated on ice for 30 minutes. Cells were then harvested at 14,000 x *g* for 1 minute and PFA removed

followed by 3 x wash steps in 500 µL 1x PBS. Microscope slides were prepared by adding 5 µL of bacterial suspension onto a glass slide, adding 1 drop ProLong® Gold antifade reagent (Molecular probes; Life Technologies) then placing a 1.8 mm square glass coverslip on top. The coverslip was sealed in place with nail varnish. Cells were imaged using the Zeiss Axio Observer widefield microscope using the 100x oil objective. Phase contrast DIC images were taken for images of bacterial cells. GFP fluorescence images were taken using LED illumination at 488 nm with a 10 second exposure time. Figure images were made using Fiji/ImageJ.

To measure cell length using ImageJ, a line equalling 10 microns was drawn on microscope images as a calibration. Lines were then drawn across each bacterial cell and compared to the 10 micron calibrated line to calculate length of each cell. From this, 100 cells were measured in each time point. Cells considered in the process of cell division were not measured.

2.9 RNAseq

2.9.1 Production of samples

To analyse and compare the transcriptome of SL1344 and SL1344 Δ*acrB* at different time points (1, 3 and 5 hours), samples were prepared for next generation RNA sequencing. There were 4 biological replicates of each strain. The method described here was developed to produce cell pellets at different time points, but RNA extraction, rRNA depletion, sequencing and bioinformatics analysis was done by GENEWIZ Inc. GENEWIZ Inc recommend $1x10^8$ cells for micro-organisms and the

volume of culture taken at each time point was optimised to reflect the number of cells required.

Briefly, 150 ml of MOPS minimal media was inoculated (4 % inoculum) with overnight cultures in 500 ml bottles. The cultures were then incubated at 37°C, shaking for 5 hours. After 1 hour of growth, 5 ml of culture was added to a universal tube and then centrifuged at 3500 x *g* for 5 minutes at room temperature to harvest the cells. The supernatant was removed and the pellet was re-suspended in a further 1 ml of 1 hour culture, transferred to a 1.5 ml Eppendorf tube and re-harvested at 14000 x *g* for 1 minute. The supernatant was removed and the pellet was snap frozen. At the 3 and 5- hour time points, only 1 ml of culture was harvested and snap frozen.

2.9.2 RNA extraction, rRNA depletion, and RNA sequencing

GENEWIZ Inc. carried out the RNA extraction, quality control, library preparation, sequencing and bioinformatic analysis. Total RNA was extracted from *S.* Typhimurium cell pellets using RNeasy Plus Universal kit (Qiagen), following the manufacturer's instructions. RNA quality control was carried out using Qubit 2.0 Fluorometer to measure total RNA concentration and Agilent TapeStation (an automated electrophoresis system) to produce an RNA integrity number (RIN) and a DV_{200} score for the quantity of RNA fragments >200 nucleotides. To remove rRNA, the ribozero Removal Kit was used (Illumina). The NEBNext Ultra II RNA Library Prep Kit (Illumina) was used for library preparation, following the manufacturer's protocol. For library preparation, cDNA was synthesised, end repaired and adenylated at the 3' ends. Universal adapters were ligated to cDNA and library enrichment was carried out using limited cycle PCR. Quality control was again carried out using Qubit 2.0

and TapeStation but also using the KAPA qPCR assay (KAPA). Sequencing was carried out using Illumina HiSeq 4000. The workflow that followed for analysis was: evaluate sequence quality, trim reads, map reads to the genome, generate hit counts for genes, compare gene hit counts and analyse gene ontology. The reference genome used was SL1344 reference FQ312003 found on NCBI (https://www.ncbi.nlm.nih.gov/nuccore/FQ312003). Genewiz Ltd then provided the raw data files, aligned data and differential gene expression (DGE) results. The ArrayExpress database was used to store the raw data from this experiment (Accession code: E-MTAB-9679).

2.9.3 Data analysis

Using the DGE results provided as a .csv file, the FQ312003 reference genome was used to identify gene annotations based on SL1344 RS codes. Scatter plots were made using Microsoft excel. Pathway tools software (Karp et al., 2016) was used to analyse metabolic pathways that were changed at different time points. RS codes from SL1344 were not recognised when using the cellular overview, therefore in this case, *S.* Typhimurium strain LT2 was used as a reference.

Chapter 3- Flow cytometry can be used to measure intracellular accumulation in bacteria

All the data presented in this chapter has been published as a methods article: Whittle EE, Legood SW, Alav I, Dulyayangkul P, Overton TW, Blair JMA. Flow Cytometric Analysis of Efflux by Dye Accumulation. *Front Microbiol*. 2019;10:2319.

The experiments and data from this publication that are presented in this chapter were carried out by the author of this thesis, unless otherwise indicated in this chapter. The publication was also written by the author of this thesis (Whittle et al., 2019).

3.1 Background

For many antibiotics, successful and effective treatment of bacterial infections relies upon high level accumulation within cells. Antibiotic accumulation is dependent on the influx and efflux of antibiotics from cells. Measuring accumulation of antibiotics and dyes is well-established in bacterial cells, with various methods previously described (Blair and Piddock, 2016).

One common approach is to measure intracellular accumulation of fluorescent dyes that are differentially fluorescent when inside or outside bacterial cells. For example, the DNA intercalating dye, EtBr (Olmsted and Kearns, 1977), which fluoresces when bound to DNA, is commonly used to measure accumulation level within the entire population of bacterial cells. AcrAB-TolC along with other RND pumps have been

shown to export EtBr (Nishino and Yamaguchi, 2001). Another DNA intercalating dye, Hoechst 33342 has also been used (Coldham et al., 2010). These dyes are used as they are well characterised substrates of major efflux systems. The fluorescence of cells is measured prior to the addition of the fluorescent dye, and then subsequently measured as the dye accumulates within the cells of a bacterial population (Blair and Piddock, 2016, Coldham et al., 2010).

An alternative approach is to directly measure rate of efflux using dyes including EtBr, Nile Red (Bohnert et al., 2010) and 1,2-DNA (Bohnert et al., 2011). Cells are pre-loaded with the fluorescent dye in the presence of the PMF inhibitor, CCCP, followed by re-energising the pumps with glucose and then measuring the reduction in fluorescence. This correlates with the fluorescent dye being removed by efflux pumps.

Fluoroquinolones are naturally fluorescing antibiotics and this class includes several clinically relevant drugs such as ciprofloxacin. It is more difficult to measure accumulation of drugs such as these because cellular localisation does not change the fluorescent properties (Piddock et al., 1999, Blair and Piddock, 2016). To overcome this, accumulation cannot be measured in live cells but can be measured from lysed cells (Asuquo and Piddock, 1993).

Bacterial populations are heterogeneous. Therefore, it may be considered that dye/antibiotic accumulation within bacterial populations is also heterogeneous. Heterogeneous accumulation of antibiotics within cells, specifically some cells that accumulate antibiotics to a low level, would drive the acquisition of mutations and therefore drive AMR. For this reason, it is important to use experimental methods

which measure accumulation of drugs at the single cell level. Flow cytometry has previously been used to measure accumulation in single cells (Blair and Piddock, 2016, Sanchez-Romero and Casadesus, 2014, Hassan et al., 2016, Haynes et al., 2018), however a detailed method to measure and quantitatively compare accumulation using EtBr has not been produced.

Other than EtBr, Fluorescein diacetate (FDA) has been shown to be effective in dye accumulation assays to the single cell level (Haynes et al., 2018). Intracellular accumulation of Nile Red and rhodamine 6G has also been measured in *Saccharomyces cerevisiae* and *Candida albicans* (Ivnitski-Steele et al., 2009). Further to this, the natural fluorescent properties of fluoroquinolones have also been used to measure accumulation in single cells (Kascakova et al., 2012), but not by flow cytometry. Intracellular accumulation using deep ultraviolet microscopy with a synchrotron beamline was used to analyse single cell accumulation levels of fleroxacin, a fluoroquinolone (Kascakova et al., 2012). Accumulation of drugs, tetracycline and ampicillin, to a sub-cellular single cell level has also been shown using mass spectrometry, specifically 3D imaging cluster Time-of-Flight secondary ion mass spectrometry (ToF-SIMS) (Tian et al., 2017).

3.2 Hypotheses

1. Flow Cytometry can be used to measure accumulation of fluorescent compounds within single cells
2. This method can be used to show that efflux mutants accumulate significantly more of compounds that are substrates of the pump than WT cells.

3.3 Aims

1. Develop a robust assay to measure EtBr accumulation in single cells using flow cytometry
2. Develop this assay to work with different dyes, species and in combination with efflux pump inhibitors
3. Develop this assay to measure EtBr accumulation and GFP fluorescence (gene transcription) concurrently.

3.4 Assay Development

To measure the level of EtBr in single cells, we developed a novel method using flow cytometry. This method was developed using the Gram-negative bacterium *Salmonella enterica* serovar Typhimurium, a model organism which has commonly been used in whole population accumulation assays. Briefly, the assay is carried out as follows:

1. Cultures were grown for one hour in LB broth, to reach early-mid exponential phase, approximately the time point commonly used in other studies.
2. To distinguish cells from background cell debris, the fluorescent cell marker SYTO-84, which emits orange fluorescence when intercalated with DNA, was used. SYTO-84 was a good candidate to use alongside EtBr as there is no overlap in excitation and emission of these two dyes.
3. Accumulation of EtBr was then measured in 10,000 individual cells (SYTO-84$^+$ events) in a population based on fluorescence intensity.

3.4.1 Optimisation of dye concentrations

To find the optimum concentration of SYTO-84, the following range of concentrations was tested: 0.1 µM, 0.5 µM, 1 µM, 5 µM and 10 µM. The final concentration of SYTO-84 that gave a distinct cell population with the best separation from the background was 10 µM (**Figure 3-1A**).

The concentration of EtBr that gave the highest mean fluorescence in SL1344 was 100 µM. Scatter plots showing the optimum concentration of EtBr are shown in **Figure 3-1B**. These dye concentrations were then used for this assay throughout.

Figure 3-1 Concentrations of SYTO-84 and EtBr used in this assay.

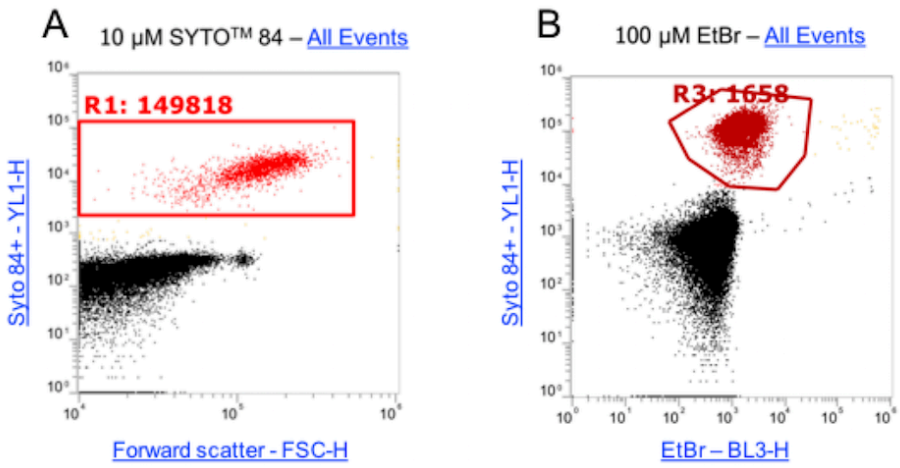

Example flow cytometry plots showing optimum concentrations of dyes used in the assay. (**A**) Staining of cells with SYTO-84. 10 µM SYTO-84 fluorescence was measured and displayed as a dot plot. Orange fluorescence (YL1-H) was plotted against forward FSC-H and a SYTO-84^{+} population was gated (R1). (**B**) Cells stained with SYTO-84 and EtBr. EtBr fluorescence (100 µM) was measured and plotted on dot plot showing YL1-H (SYTO-84) against BL3-H (EtBr). These plots are also published in Whittle et al. (2019).

3.5 EtBr accumulation can be measured in *S*. Typhimurium

In order to accurately measure EtBr fluorescence inside cells, a gating strategy (shown in **Figure 2-1** and in **Figure 3-2A-D**) was used to analyse EtBr fluorescence. Briefly, SYTO-84 fluorescence was plotted against FSC-H on a dot plot **(Figure 3-2A+C)** and SYTO-84$^+$ population was then gated collecting 10,000 events within the gate (gate name: SYTO 84+). The EtBr fluorescence of the SYTO-84$^+$ population was then plotted on a logarithmic histogram for EtBr fluorescence intensity (**Figure 3-2B + E**). The median EtBr fluorescence intensity was taken as the level of EtBr accumulating within each cell. The median is considered the most appropriate value to take as a value of mean fluorescence intensity (MFI) on a logarithmic histogram (Illingworth; website accessed 2020).

To show that the optimised assay worked to quantify intracellular accumulation of EtBr in different *Salmonella* strains, EtBr accumulation was measured in SL1344 and various previously studied efflux mutants. The strains used were isogenic mutants of SL1344 denoted as Δ*acrB* (Eaves et al., 2004b), Δ*tolC* (Buckley et al., 2006) and Δ4PAP, a strain which lacks the 4 PAPs in SL1344 (McNeil et al., 2019). As previously shown, strains that lack efflux pumps accumulated significantly more EtBr that WT.

Data was summarised in graphs as shown in **Figure 3-2E**. For the remainder of this thesis, data will be presented like this, rather than using dot plots.

Figure 3-2 Flow cytometry plots of SL1344 and strains lacking components of efflux pumps.

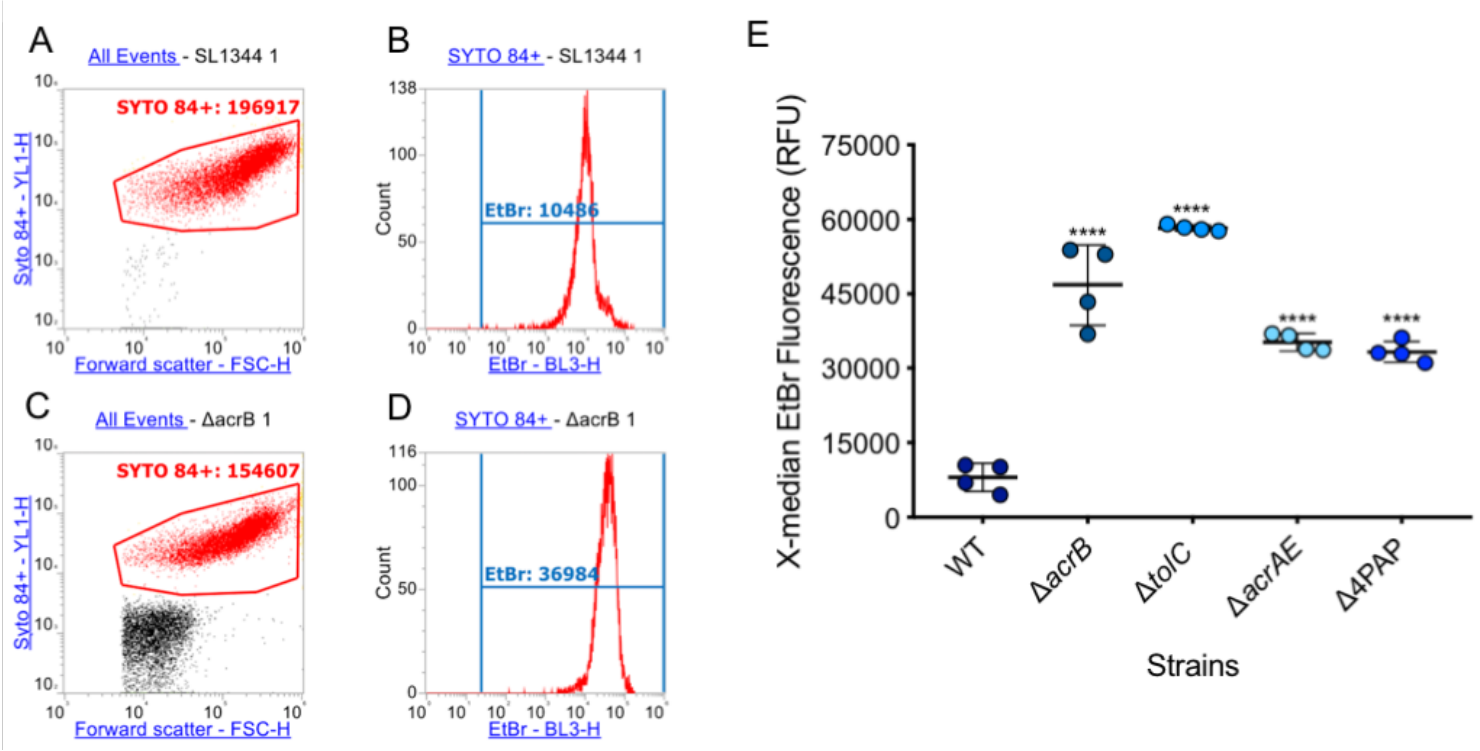

(A+B) shows plots of SL1344 and **(C+D)** SL1344 Δ*acrB*. **(A+C)** Cells were separated from background cell debris using channels YL1-H vs. FSC-H. A SYTO-84^{+} population of 10,000 events was gated (red). SYTO 84^{+} cells were then analysed in **(B+D)** plots (red peak represents red gate from previous plot) where the BL3-H channel measured the EtBr fluorescence median from an EtBr gate (blue). **(E)** Single circles represent the median of EtBr fluorescence from a SYTO 84^{+} population of cells within a biological replicate. There are 4 biological replicates for each strain. For each strain, the black bar represents the mean of the 4 biological replicates +/- standard error of the mean (SEM). The average RFUs were 8024 (WT), 46824 (Δ*acrB*), 58321 (Δ*tolC*) and 33359 (Δ4PAP). A one-way ANOVA and Dunnett's multiple comparison test were used to produce p-values. All p-values compared to WT were < 0.0001(represented by **** on the graph). Data also published in Whittle et al. (2019)

3.6 Adaptation to measure accumulation of Nile Red

EtBr is not the only dye that has been used to measure accumulation or efflux. Hoescht 33342 (Blair and Piddock, 2016) along with Nile Red (Bohnert et al., 2010), 1,2-DNA (Bohnert et al., 2011) and rhodamine 6G (Ivnitski-Steele et al., 2009) all have fluorescent properties inside cells which have been harnessed for these assays.

The flow cytometry assay was adapted to measure the fluorescence of Nile Red in place of EtBr showing that this assay is not limited to EtBr accumulation.

The fluorescence spectra of Nile Red and SYTO-84 overlap so this assay used SYTO-9 to separate cells from background debris. Nile Red was used at a concentration of 75 μM. The RFU of Nile Red was much lower than values produced when measuring EtBr. SL1344 accumulated a low level of Nile Red (744 RFU) but accumulation was 2-fold higher in Δ*acrB* and 13-fold higher in the absence of TolC function (**Figure 3-3**). These data confirmed that Nile Red is a substrate of the AcrAB-TolC pump and its accumulation can be measured using flow cytometry.

Figure 3-3 Accumulation of Nile Red in WT, Δ*acrB* and *tolC::aph* in *S*. Typhimurium

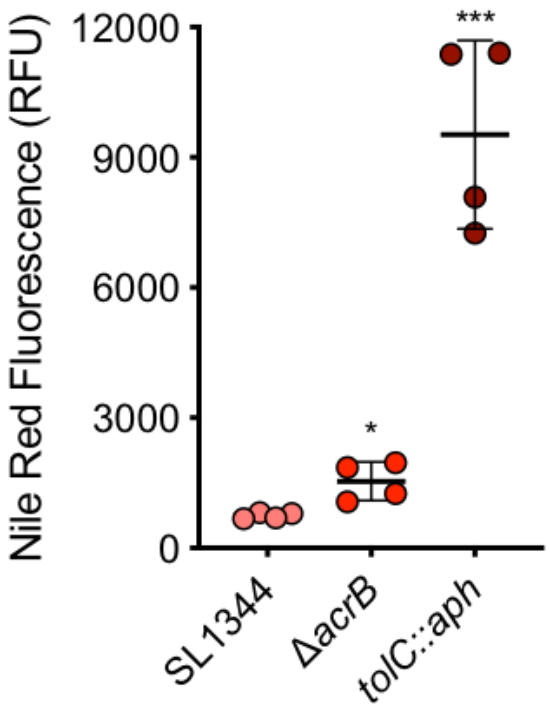

Single circles represent the median RFU value of nile red fluorescence from 10,000 cells in a SYTO 9+ population within a biological replicate. Accumulation in WT (pink), Δ*acrB* (red) and *tolC::aph* (dark red) was measured. There are 4 biological replicates for each strain, with a long bar to show the mean and SEM error bars. Significance values were based on an unpaired T-test comparing the efflux deficient strain to WT. Data taken from (Whittle et al., 2019).

3.7 The effects of efflux inhibitors on accumulation can be measured by flow cytometry

This assay was also adapted to measure EtBr accumulation in the presence of compounds which inhibit efflux, as opposed to disrupting genes coding for efflux proteins.

EtBr accumulation was measured in the presence of the PMF inhibitor, CCCP (Mahamoud et al., 2007). RND, MFS, SMR and MATE pumps all rely on the PMF for export of substrates. To inhibit efflux without damaging the cells, a sub-inhibitory concentration of 100 μM CCCP was incubated with the cells and then SYTO-84 and EtBr were added as before. In the presence of CCCP, there was a significant 6-fold increase in EtBr fluorescence, from 3936 RFU to 22596 RFU (**Figure 3-4**). As previously shown, this shows that efflux pumps were inhibited and that EtBr could not be exported. Importantly, this shows that this assay can be used to detect the inhibition of efflux.

The specific RND efflux pump inhibitor PAβN, was also tested. It has previously been shown that PAβN does not significantly change the MIC of or alter the level of EtBr accumulation (Lomovskaya et al., 2001, Kern et al., 2006, Viveiros et al., 2008) and preliminary experiments using our assay supported this. Therefore, to show that this flow cytometry assay could be used with PAβN, it was tested in combination with Nile Red. The inhibitor was incubated at 50 μg/mL in SL1344, with the addition of Nile Red. The concentration of PAβN did not kill bacterial cells. In the presence of PAβN,

there was a 7-fold increase in substrate accumulation because RND pumps were unable to export Nile Red.

Results for CCCP and PAβN show that this assay can be used to show inhibition of efflux and therefore, could be adapted for high throughput screening for efflux inhibitors.

Figure 3-4 Accumulation of EtBr in SL1344 in the absence and presence of 100 μM CCCP and 50 μg/mL of PAβN.

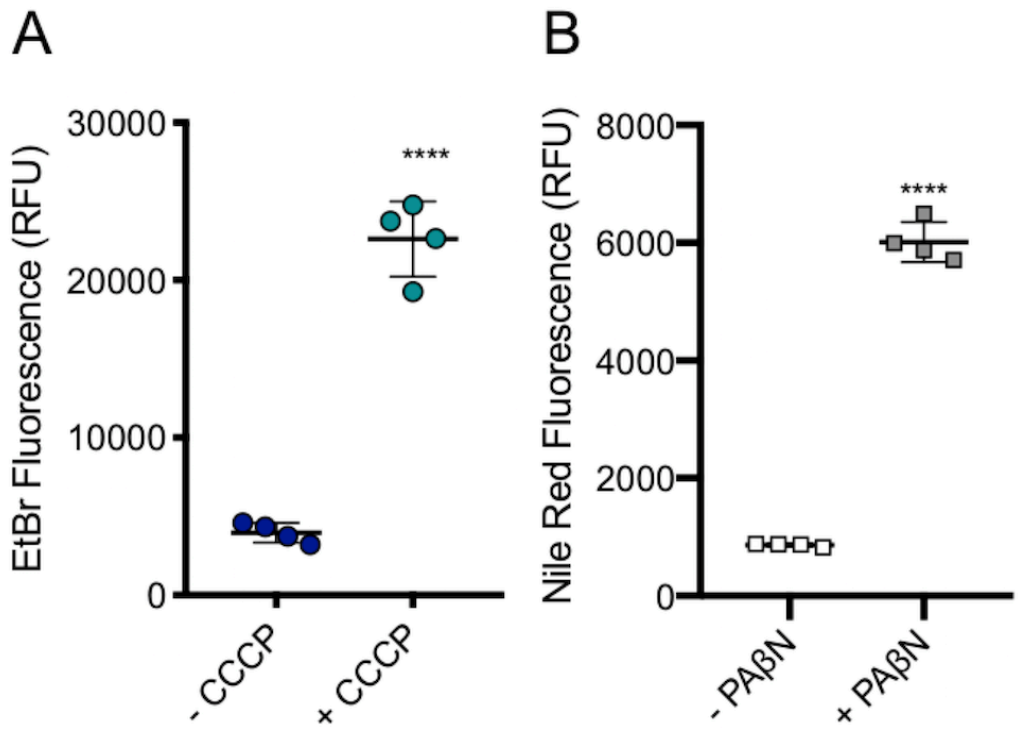

(A) SL1344 dots (-CCCP) are in blue and are green in the presence of CCCP (+CCCP). Single dots represent the median of EtBr from 10,000 SYTO 84$^+$ events within a biological replicate. There are 4 biological replicates for each strain. The horizontal bar shows the mean +/- standard error of the mean (SEM). **(B)** SL1344 squares (-PaβN) are in white and are grey in the presence of PaβN (+PaβN). Single squares represent the median value of nile red fluorescence in the presence and absence of PAβN, from 10,000 SYTO 84$^+$ events within a biological replicate. 4 biological replicates for each condition are shown, with a long bar to show the mean and SEM error bars. In **(A)** and **(B)** an unpaired T-test produced p-values. The p-values were < 0.0001 which was represented by **** in this figure. Data also published in Whittle et al. (2019).

3.8 Measuring GFP fluorescence and EtBr accumulation in parallel in single cells

GFP fluorescence is used for many molecular biology applications such as measuring expression of specific genes. The ability to measure GFP and EtBr accumulation in the same cell would be a powerful tool for linking gene expression to drug accumulation phenotypes. Therefore, the assay was developed to measure GFP and EtBr in parallel. In this case, a GFP transcriptional reporter was used to report on the transcription of a specific gene.

EtBr and GFP use the same excitation wavelength, 488 nm, but emission wavelengths differ significantly **(Figure 3-5A)**. Compensation can be set in this assay to avoid the spill-over in emissions from both fluorophores. The gating strategy for measuring fluorescence of the GFP and EtBr can be found in **Chapter 2** (**Figure 2-3**).

In order to show that EtBr and GFP could be measured concurrently, *ramA* transcription in *S.* Typhimurium was measured in parallel with EtBr accumulation in 10,000 SYTO-84^{+} cells. RamA is a transcriptional regulator involved in the regulation of *acrAB* in *S.* Typhimurium and indole is a known inducer of *ramA* transcription (Nikaido et al., 2008, Lawler et al., 2013). Transcription of *ramA* was measured using a transcriptional reporter plasmid where the *ramA* promoter was fused to *gfp* (pMW82-*ramA*).

Figure 3-5 Accumulation of EtBr and fluorescence of GFP.

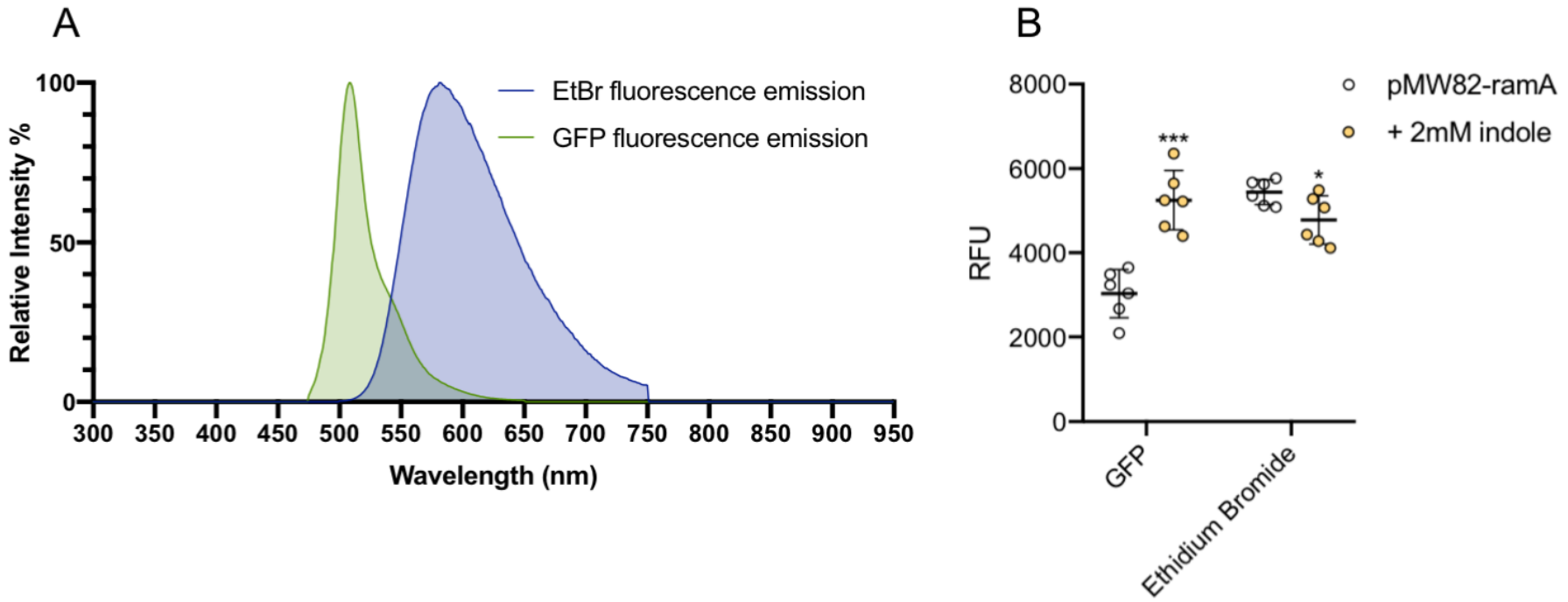

(A) The fluorescence emission spectra for EtBr (blue) and GFP (green). The area where there is an overlap in emission peaks is spillover and adds the requirement for compensation. Emission values were taken from ThermoFisher SpectraViewer. **(B)** The median RFU for GFP and EtBr is shown without indole (white) and with 2mM indole (orange) from 10,000 SYTO 84^{+} events using SL1344 + pMW82-*ramA*. There were 6 biological replicates with and without indole. The long bar represents the mean and error bars represent standard error of the mean (SEM). Unpaired T-tests compared fluorescence of GFP and EtBr with and without indole. The p-values were 0.0001 and 0.0315 for GFP and EtBr respectively. This graph is also published in Whittle et al. (2019).

Incubation of cells with indole caused a 2-fold increase in GFP fluorescence, showing increased *ramA* transcription and significantly lower accumulation of EtBr **(Figure 3-5B)**. This was probably because increased *ramA* transcription leads to increased transcription of *acrAB* allowing more EtBr to be removed from the cell by efflux (Nikaido et al., 2008). This shows that the assay is capable of measuring GFP and EtBr fluorescence in parallel.

3.9 EtBr accumulation in Gram-negative and Gram-positive bacteria

The flow cytometry accumulation assay was initially developed to work with *Salmonella* however, to assess its versatility it was tested with other bacterial species. Gram-negative bacteria heavily populate the WHO priority pathogen list and from this *Escherichia coli*, *Klebsiella pneumoniae* and *Pseudomonas aeruginosa* were selected. The assay was performed as before; EtBr was added to parental WT strains of each species (*E. coli* MG1655 (Blattner et al., 1997), *K. pneumoniae* ecl8 (Forage and Lin, 1982), *P. aeruginosa* PA14 (Liberati et al., 2006, pa14.mgh.harvard.edu)) and isogenic efflux mutants (MG1655 Δ*acrB* (Wang-Kan et al., 2017), ecl8 *acrB*::Gm (Whittle et al., 2019), PA14 Δ*mexA* (Liberati et al., 2006, pa14.mgh.harvard.edu)) and accumulation was measured. In all three species, the accumulation level was significantly higher (4-fold,14-fold and 3-fold respectively) in the absence of efflux pump components **(Figure 3-6A)**, comparable to the result shown in *S.* Typhimurium. It has also previously been shown that removing AcrAB-TolC in *E. coli* leads to an increase in EtBr accumulation (Paixao et al., 2009).

This shows that this assay works to assess substrate accumulation in a number of Gram-negative pathogens.

It was also important to show that this assay could be used to assess accumulation in Gram-positive bacteria, adding to the versatility of the assay that has already been shown. EtBr accumulation was measured in Gram-positive *Staphylococcus aureus*. Efflux mutants of this species were not available, so CCCP was used to inhibit the pumps that require PMF in *S. aureus*. Accumulation in *S. aureus* was low, but in the presence of CCCP, there was a significant increase in the level of EtBr accumulation **(Figure 3-6B)**.

This assay has proved versatile when measuring substrate accumulation in both Gram-negative and Gram-positive pathogens.

3.10 Discussion

The data presented in this chapter shows the development of a novel flow cytometry assay to measure accumulation of fluorescent dyes in single bacterial cells. Previous studies where EtBr or Hoechst H33342 accumulation has been measured in a bacterial population as a whole (rather than single cells) reports on average a 2-3 fold increase in *Salmonella* Δ*acrB* strains compared to parent strains (Blair et al., 2009, Coldham et al., 2010, Smith and Blair, 2014, Wang-Kan et al., 2017). With a 4.5-fold increase in EtBr accumulation in SL1344 Δ*acrB* compared to SL1344 here (**Figure 3-2**), the results when using flow cytometry are comparable to previous results that measure accumulation in a population. Bacteria with inhibited efflux pumps accumulate more EtBr because they are no longer able to export it.

Figure 3-6 Accumulation of EtBr in WT and efflux mutants of *E. coli*, *K. pneumoniae*, and *P. aeruginosa*, and in *Staphylococcus aureus* with CCCP.

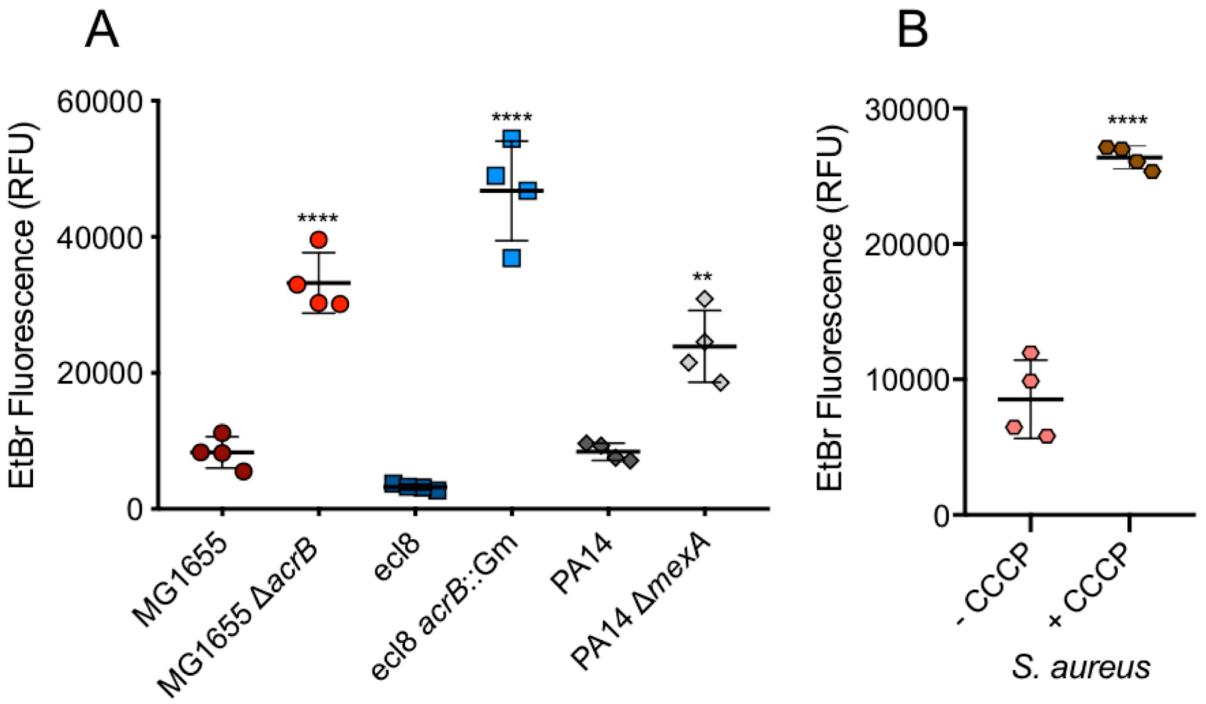

All EtBr data points are based on the EtBr median fluorescence from 10,000 SYTO 84$^+$ events. (**A**) *E. coli* MG1655 are shown as dark red circles with MG1655 Δ*acrB* shown as red circles. *Klebsiella pneumoniae* ecl8 was shown as dark blue squares and the inactivated *acrB*::Gm strain as light blue squares. *P. aeruginosa* strain PA14 EtBr fluorescence was shown as dark grey diamonds with Δ*mexA* shown as light grey diamonds. **(B)** *S. aureus* EtBr accumulation was measured in the absence (pink) and presence (brown) of CCCP. 4 biological replicates for each strain are shown. The mean was shown with a long bar and error bars showed +/- SEM. Statistical tests were unpaired T-tests between individual WT and efflux deficient strain. Results were considered significantly different if p-value ≤ 0.05. Figure is also published in Whittle et al. (2019)

Previously developed assays which measure accumulation or efflux have been important in investigating efflux pumps and possible efflux inhibitors which may be used clinically. However, these assays are limited by only measuring accumulation capacity of a whole population. The limitation with whole population studies is that bacterial cell populations are not homogeneous in phenotype. Stochastic gene expression is responsible for heterogeneous bacterial cell populations and studies have shown the importance of measuring accumulation at the single cell level for this reason (Sanchez-Romero and Casadesus, 2014, Davis and Isberg, 2016). Initial data using the flow cytometry assay presented in this chapter has shown that there is heterogeneity within populations. SL1344 appeared to have a subpopulation which accumulates more EtBr, whereas SL1344 Δ4PAP appeared to have a subpopulation that accumulates less EtBr **(Figure 3-7)**. This phenomenon was not investigated further in this thesis but is a subject of further work.

For the future development of efflux inhibitors to be used as therapeutics, single cell analysis is essential. For example, if a new efflux inhibitor was used in the presence of an antibiotic, a population of cells may have their efflux pump inhibited and therefore lead to high accumulation of antibiotics. If in the presence of an inhibitor, a sub-population developed where antibiotic accumulation was low, it may lead to the selection of compensatory mutations, survival of the subpopulation and further development of AMR. The assay described in this chapter can therefore also be used as a tool to investigate heterogeneity.

Figure 3-7 Heterogeneity in EtBr accumulation in SL1344 and SL1344 ∆4PAP

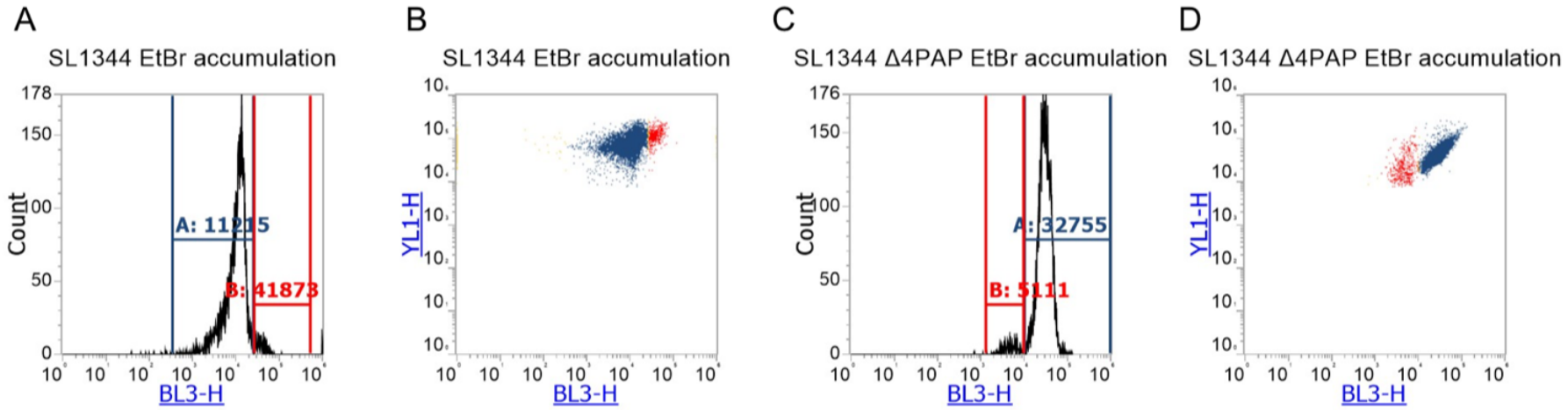

The plots shown here only show EtBr accumulation, however the populations shown in **A + C** represent 10,000 events with a SYTO 84^{+} gate. (**A**) The peak (black) shows EtBr accumulation in SL1344. On this histogram, there are 2 gates: A – represents the main population (blue) and B – a sub-population (red). The A gate shows median EtBr fluorescence at 11215 RFU, but the B gate shows the EtBr accumulation of the sub-population 4-fold higher at 41873 RFU in the same strain. (**B**) shows both gated populations as a dot plot highlighting that they are separate populations. (**C**) The peak (black) shows EtBr accumulation in SL1344 ∆4PAP. The population and sub-population gates are represented the same. The A gate shows median EtBr fluorescence at 32755 RFU, but the B gate shows the EtBr accumulation of the sub-population 6.5-fold lower at 5111 RFU in the same strain. (**B+D**) shows both gated populations as a dot plot highlighting that they are separate populations.

Further work and an area for exploration would be identifying the importance of heterogeneity and sub-populations when measuring drug accumulation and why and how they develop. There are a few possible reasons including transient expression, antibiotic tolerance or potentially the upregulation of other efflux pumps in the presence of selective pressure. By unpicking whether sub-populations develop via mutation or expression changes, environmentally or in the presence of inhibitors, would further advance knowledge of how bacterial infections should be treated. It is also unknown whether these sub-populations would present during an infection, so it is possible that this could be explored further using *in vivo* experiments.

The data here shows that this assay can be used to measure accumulation in a range of Gram-negative bacteria and the Gram-positive species *S. aureus*. It was unexpected that this assay would work so well for *Pseudomonas aeruginosa*. Not only does *P. aeruginosa* have 14 RND efflux pump systems, but also has an intrinsically impermeable membrane (Hancock, 1998, Breidenstein et al., 2011), so may have proved more difficult to measure accumulation in the presence of efflux inhibitors. However, this assay showed promise for measuring EtBr accumulation and therefore this assay may also be adapted for analysis of the intrinsically impermeable priority pathogen, *Acinetobacter baumanii*.

As previously mentioned, AcrAB-TolC along with other RND pumps have been shown to export EtBr as well as a large range of other substrates (Nishino and Yamaguchi, 2001). In *E. coli*, another pump, MdtEF-TolC also exports EtBr (Nishino and Yamaguchi, 2001, Kobayashi et al., 2006). However, efflux pumps can export a number of substrates with different chemical structures, different localisations within

the cells and different modes of action. For this reason, it was important to confirm that this assay could be adapted for other fluorescent substrates. In this case, Nile Red accumulation could also be measured in *S.* Typhimurium. Rhodamine 6G can also be measured, however, there was shown to be no significant difference between SL1344 and Δ*acrB* (Whittle et al., 2019). The intracellular accumulation of both these substrates has previously been measured in whole population assays (Bohnert et al., 2010, Ivnitski-Steele et al., 2009). This shows that this assay could be further adapted to measure other substrates of specific efflux pumps or identify new specific substrates of the pumps.

In summary, this chapter describes the development of a novel flow cytometry assay to measure the intracellular accumulation of various fluorescent dyes. The work in this chapter was published in the following article: Whittle et al., 2019. Flow Cytometric Analysis of Efflux by Dye Accumulation. This assay is an important tool for furthering our understanding of efflux and drug accumulation in single cells and will be used throughout this thesis with further adaptation to answer novel questions.

3.11 Key Findings:

- Flow cytometry can be used to measure efflux substrate accumulation in single cells (EtBr and Nile Red).
- Efflux mutants accumulate more dye than parental strains.
- Transcription of genes can be measured using GFP transcriptional reporters.
- This assay can be optimised for testing efflux inhibitors and for both Gram-negative and Gram-positive bacteria.

Chapter 4- The impact of growth phase on the capacity of *S.* Typhimurium to accumulate EtBr

4.1 Background

The efflux pump, AcrAB-TolC, can export many structurally varied antibiotics, detergents and dyes (Nishino et al., 2006). The RND family exports compounds from the periplasmic space to the extracellular environment, decreasing the intracellular concentration of these chemicals inside cells. This allows bacteria to survive at higher concentrations of drug. Intracellular accumulation is not simply a measure of efflux, but is in fact dependent on both how much drug gets into a cell, via influx, and how much is removed from a cell, by efflux.

In almost all published studies, assessment of efflux activity and accumulation is based on a mid-exponential phase bacterial culture (e.g. Richmond et al., 2013, Bohnert et al., 2010, Coldham et al., 2010, Wang-Kan et al., 2017). However, bacterial physiology, and specifically the expression of *acrAB,* are known to vary across the growth curve. A peak in *acrAB* expression occurs in mid-exponential phase (Bailey et al., 2006). However, it is not known how this affects the level of efflux and accumulation across the growth curve.

The flow cytometry assay described in **Chapter 3** (Whittle et al., 2019), was adapted to measure the capacity of cells from different growth stages to accumulate EtBr. In this thesis, the phrase “capacity to accumulate EtBr” is used to describe the relative

level of EtBr accumulated by a given sample of cells, taken from different points during growth.

4.2 Hypotheses

- Accumulation of EtBr in SL1344 will be growth phase dependent and will change with *acrAB-tolC* expression.
- Accumulation of EtBr in SL1344 Δ*acrB* will be high across growth due to the absence of efflux pump function.

4.3 Aims

1. To adapt the flow cytometry assay to measure EtBr accumulation from samples taken during different growth phases.
2. To measure the accumulation of EtBr in samples of *S*. Typhimurium SL1344 taken from across the growth curve and to measure whether it correlates to *acrAB* transcription.
3. To measure the accumulation of EtBr in samples of *S*. Typhimurium SL1344 Δ*acrB* taken from across the growth curve.
4. To determine whether the accumulation phenotype is the same in other bacterial species and whether it is dependent on experimental conditions.
5. To identify other bacterial phenotypes that may vary based on growth phase.

4.4 Optimisation of flow cytometry accumulation assay to measure accumulation in different growth phases

The flow cytometry method used to measure EtBr accumulation described in **Chapter 3** was initially set up to use exponential phase bacteria as most other studies in the literature have done. In this chapter, the assay was adapted to analyse EtBr accumulation in samples taken from lag phase through to stationary phase. At every hour, from 0-6 hours, samples from a growing bacterial culture were taken and EtBr accumulation capacity measured every hour. At each time point, the volume of culture that was taken was adjusted so that approximately the same cell number was in each sample regardless of time point of growth.

Figure 4-1 shows the experimental set-up where, at each time point, samples were removed from a growing culture and then dyes were added to assess the accumulation of dye within cells at each time point.

Figure 4-1 Schematic of optimised flow cytometry assay to measure EtBr accumulation at different time points of the growth curve.

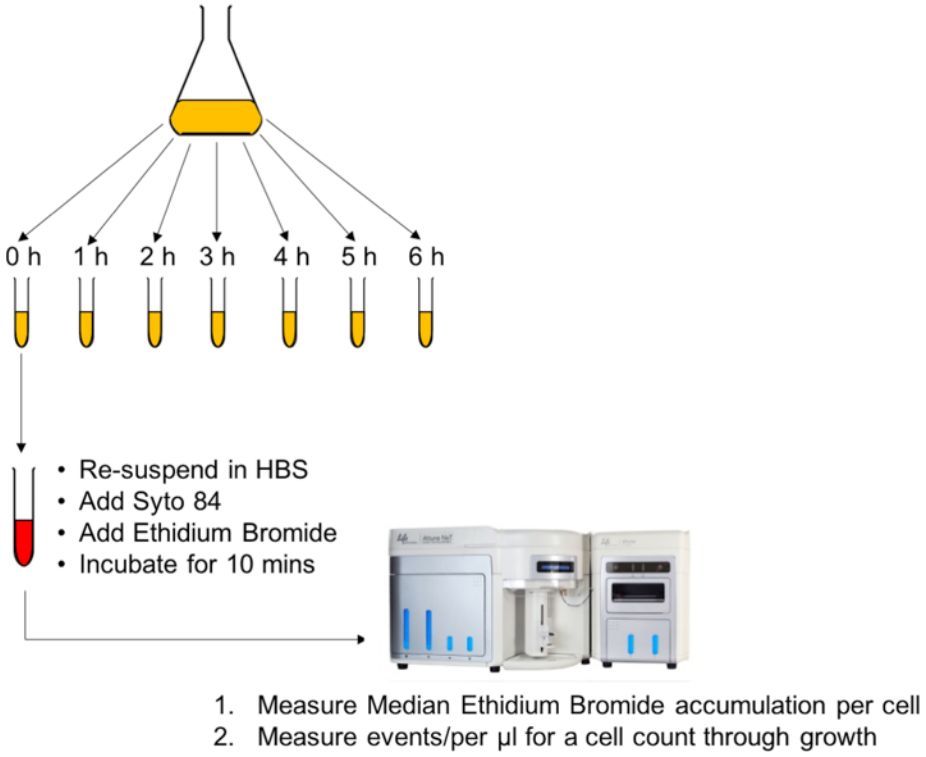

A culture of bacteria was grown for 6 hours. At each time point, a sample was removed, cells harvested and added to HBS buffer. At this point, EtBr and SYTO-84 was added to the sample. EtBr accumulation in each sample was then measured using flow cytometry. Growing cultures were never incubated or grown with EtBr removing the risk of adaptation or developing mutations.

As in **Chapter 3**, these experiments measured the capacity of cells to accumulate EtBr so cultures were not grown in the presence of EtBr, and the dyes were only added to the removed sample of cells. This means that any changes seen are not the result of mutations or adaptation to EtBr.

It was important that the cell number in each sample was also measured so that entrance into different growth phases could be determined. On each histogram used to measure median EtBr fluorescence, events per μL was also measured. Using this measurement, the cells per mL in the culture were calculated. The equation is shown in **Section 2.4.2**.

4.5 Low EtBr accumulation in SL1344 is continuous over the bacterial growth curve

To determine whether the accumulation of EtBr was growth phase dependent, the optimised flow cytometry assay was first used to measure EtBr accumulation in *S*. Typhimurium SL1344. SL1344 was grown for 6 hours in LB broth, with samples taken every hour and EtBr added to the sample.

As shown previously, accumulation of EtBr was low in SL1344. The time course experiment showed that this low level was unchanged across the growth curve (**Figure 4-2**). EtBr accumulation at every hour was compared to the 0 hour time point, and there were no significant difference in average EtBr accumulation per cell when comparing any other time point (**Table 4-1**). Cell number was also measured in the same sample and showed that cell number increased and showed normal growth in LB with stationary phase beginning at around 3 hours.

Figure 4-2 EtBr accumulation levels in SL1344 from 0-6 hours

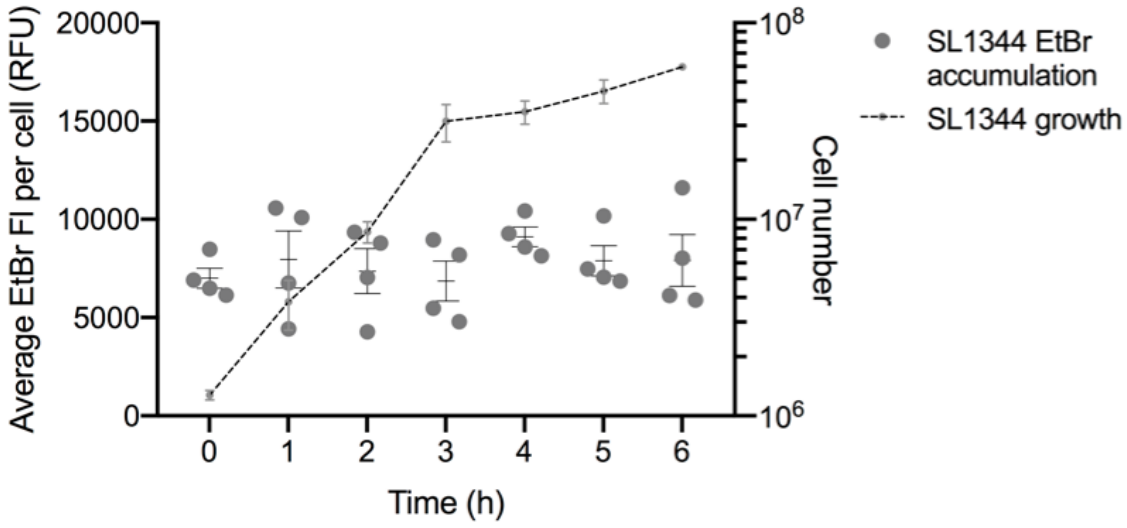

Single grey circles represent the X-median value of EtBr fluorescence per cell (from 10,000 SYTO-84$^+$ cell events) within a biological replicate. 4 biological replicates for each strain are shown, with a short mean bar and SEM error bars. Grey circle values are plotted on the left Y-axis. Calculated averaged cell number values were plotted on the right Y-axis with SEM error bars. EtBr fluorescence was measured every hour between 0 and 6 hours. This was based on a one-way ANOVA and Tukey's multiple comparison test to compare the differences between every hour. P-values for comparisons to 0 hour are shown in **Table 4-1**.

Table 4-1 Statistical analysis of SL1344 at each time point compared to T0

Comparison	P-value	Significance
T0 v T1	>0.9999	ns
T0 v T2	>0.9999	ns
T0 v T3	>0.9999	ns
T0 v T4	0.9991	ns
T0 v T5	>0.9999	ns
T0 v T6	>0.9999	ns

4.6 EtBr accumulation in SL1344 does not correlate with *acrAB* transcription level

AcrAB expression level has been shown to correlate with the level of drug or dye accumulation. In **Section 3.8**, indole induced *ramA* and this led to a significant decrease in EtBr accumulation, presumably through the induction of *acrAB* (Whittle et al., 2019). Overexpression of *acrAB* in clinical isolates through regulatory mutations, is also linked to decreased antibiotic susceptibility (Webber and Piddock, 2001, Schneiders et al., 2003, Chowdhury et al., 2019). Therefore, it was hypothesised that the capacity of a growing culture of *S*. Typhimurium to accumulate EtBr would correlate with *acrAB* transcription. Initial observations in **Figure 4-2** showed that EtBr accumulation remained low, and did not significantly differ between time points. A reasonable theory would be that EtBr accumulation would correlate to *acrAB* transcription, e.g. as transcription of *acrAB* increases, less EtBr would accumulate due to the presence of more efflux pumps. To further test this, the flow cytometry assay which was previously adapted to measure GFP and EtBr in the same cells was utilised. A strain of SL1344 containing pMW82-*acrA* (a transcriptional reporter plasmid on which the *acrAB* promoter is fused to GFP) was grown for 6 hours in LB containing ampicillin, and at each hour, samples were taken, and the EtBr accumulation and GFP fluorescence were measured. The median values for both GFP and EtBr were analysed.

As with the previous result, in SL1344 + pMW82-*acrA*, EtBr accumulation remained low across the growth curve. At no time point was there a significantly different level of EtBr accumulation (**Figure 4-3**), based on a one-way ANOVA and Tukey's multiple

comparison test. Using the cell number, which is plotted on the right Y-axis (black line) in **Figure 4-3**, it was shown that *acrAB* transcription peaked at approximately mid-exponential phase (2 hours of growth) based on GFP fluorescence (**Figure 4-3**). Dunnett's multiple comparison test compared GFP fluorescence at each time point to the peak at 2 hours, and all time points had significantly lower fluorescence, except for at 3 hours. Transcription of *acrAB* decreased as the culture entered stationary phase.

This shows that the levels of EtBr accumulation did not correlate with *acrAB* transcription.

Figure 4-3 EtBr accumulation and *acrAB* transcription measured in the same cells

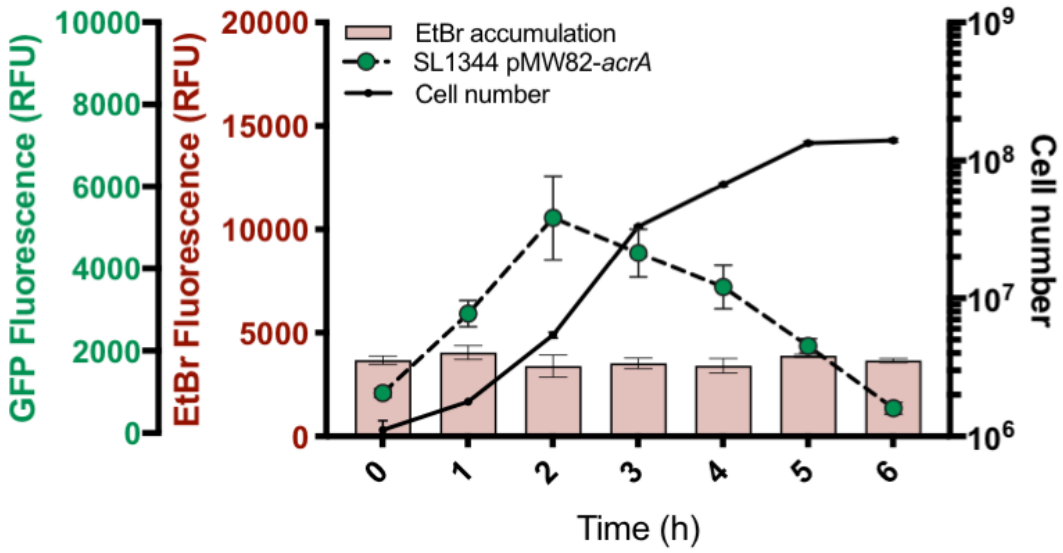

EtBr accumulation, *acrAB* transcription (GFP fluorescence) and cell numbers were measured in 10,000 SYTO-84^{+} events. Pink bars represent EtBr accumulation of SL1344 pMW82-*acrA* at each time point from 0-6 hours. Bars are based on 4 biological replicates representing the mean +/- SEM. These EtBr accumulation bars are plotted on the 1st left X-axis where the axis label 'EtBr fluorescence (RFU)' is coloured in red. Green dots represent GFP fluorescence and therefore *acrAB* transcription from each time point from 0-6 hours, based on the same 4 replicates with SEM error bars. The dashed connecting line connects transcription across the growth curve. GFP RFU is plotted on the left Y-axis ('GFP Fluorescence (RFU)' labelled in green. The solid black line represents the cell number and therefore growth curve of SL1344 pMW82-*acrA* and is plotted on the right X-axis.

4.7 EtBr accumulation in SL1344 Δ*acrB* was growth phase dependent

As *acrAB* transcription and EtBr accumulation did not correlate, the next step was to study the importance of the AcrAB-TolC efflux pump in accumulation of EtBr across growth. Using SL1344 as a control, EtBr accumulation in SL1344 Δ*acrB* was measured from samples taken following 0-6 hours of growth (**Figure 4-4**).

After 1 hour of growth, the accumulation was a mean value of 46299 RFU, 6-fold greater than SL1344 EtBr accumulation and significantly different. This result was comparable to previous mid-log data (Smith and Blair, 2014, Wang-Kan et al., 2017). At 2 hours, accumulation of EtBr started to drop with only a 3.5-fold difference to SL1344 at 2 hours. By hours 4, 5 and 6, EtBr accumulation in SL1344 Δ*acrB* was not significantly different to accumulation in SL1344 (**Table 4-2**).

Cell numbers compared (**Figure 4-4**) to SL1344 were also assessed to check for potential differences in growth between the strains but there was no significant difference. Previous studies show that the deletion of *acrB* does not lead to a growth defect *in vitro* (Wang-Kan et al., 2017). Based on **Figure 4-4**, it was deduced that entrance to stationary phase began at around 3 hours of growth.

Figure 4-4 EtBr accumulation in SL1344 and Δ*acrB* from 0-6 hours

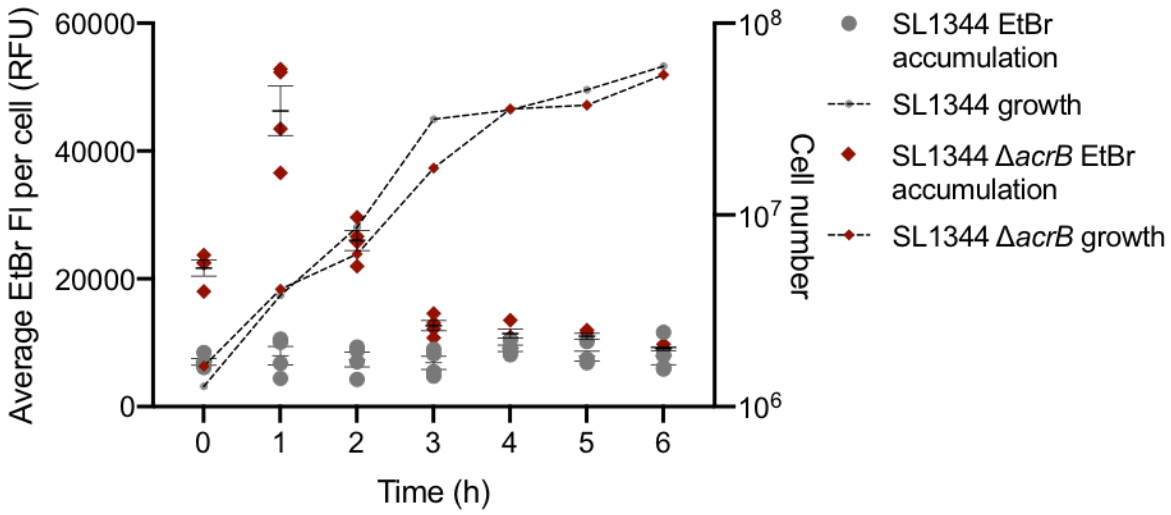

Median EtBr fluorescence per cell in 10,000 SYTO-84$^+$ events was measured every hour between 0 and 6 hours. Individual grey circles represent the X-median value of EtBr fluorescence in SL1344 (WT) (from 10,000 SYTO-84$^+$ cell events) within a biological replicate. Individual red diamonds represent the X-median value of EtBr fluorescence in SL1344 Δ*acrB* (from 10,000 SYTO-84$^+$ cell events) within a biological replicate. 4 biological replicates for each strain are shown, with a short mean bar and SEM error bars. EtBr accumulation is plotted on the left Y-axis. Calculated cell number values were plotted on the right Y-axis with corresponding symbols equating to strain and a dashed line to show growth of the culture. Cell numbers were based on the mean of the same biological replicates and the same gated population that EtBr fluorescence was measured from. Two-way ANOVA and Sidak's multiple comparison test were carried out for statistical analysis.

Table 4-2 Statistical analysis of SL1344 vs Δ*acrB* at each time point

Comparison	Fold Change (vs WT)	P-value	Significance
T0	3-fold	<0.0001	****
T1	6-fold	<0.0001	****
T2	4-fold	<0.0001	****
T3	2-fold	0.0402	*
T4	NA	0.8675	ns
T5	NA	0.6112	ns
T6	NA	0.9971	ns

It is well documented that substrate accumulation in efflux mutants is higher than corresponding WT strains in mid-exponential phase (Wang-Kan et al., 2017, Smith and Blair, 2014, Paixao et al., 2009). SL1344 Δ*acrB* showed this high level of EtBr accumulation after 1 hour of growth. However, EtBr accumulation levels decreasing in stationary phase has not been previously shown and was unexpected. It was assumed that the absence of AcrB would lead to consistently high EtBr accumulation regardless of growth phase. This result suggests that the capacity of cells to accumulate EtBr in stationary phase is reduced in an AcrB-independent manner.

4.8 Non-functional AcrB conferred the same phenotypic effect as total AcrB deletion

In SL1344 Δ*acrB*, it is possible that decreased EtBr accumulation in stationary phase is due to the increased expression of homologous RND pumps, as has previously been shown to happen in the absence of AcrB (Blair et al., 2015a). This will be explored in **Chapter 5.**

Another hypothesis to explain the unexpected accumulation pattern was that the absence of a large inner membrane protein, AcrB, could have made the membrane more permeable, and prone to EtBr leakage from the cell. This may explain the low accumulation in stationary phase. To test this hypothesis, SL1344 Δ*acrB* EtBr accumulation was compared to EtBr accumulation in a strain in which AcrB was present but inactivated by a mutation within the region required for PMF utilisation (SL1344 AcrB-D408A) (Wang-Kan et al., 2017).

Consistent with previous results, EtBr accumulation in SL1344 Δ*acrB* peaked after 1 hour of growth, and dropped on entry into stationary phase (**Figure 4-5**). In the AcrB-D408A mutant, results were consistent with SL1344 Δ*acrB*. EtBr accumulation peaked at 1 hour and dropped as cells entered stationary phase. There was no significant difference in accumulation between these strains. Cell number was also measured and there was no difference in growth between the two strains, as has been previously described (Wang-Kan et al., 2017).

Figure 4-5 EtBr accumulation in SL1344 Δ*acrB* compared to SL1344 AcrB-D408A

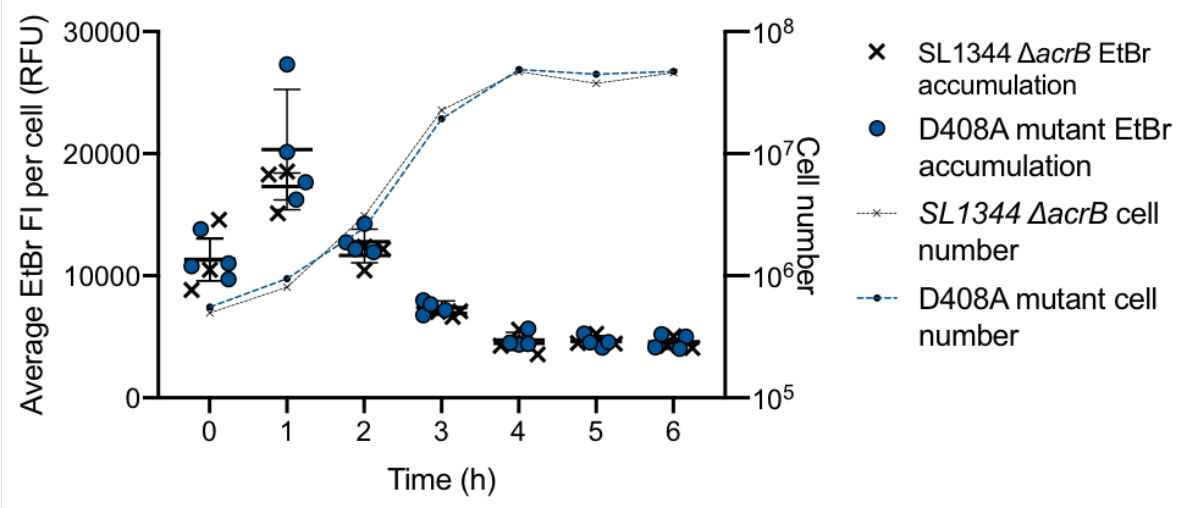

Median EtBr fluorescence per cell in 10,000 SYTO-84$^+$ events was measured every hour between 0 and 6 hours. Individual black X's represent the X-median value of EtBr fluorescence in SL1344 Δ*acrB* within a biological replicate. Individual blue circles represent the X-median value of EtBr fluorescence in SL1344 AcrB-D408A (within a biological replicate. 4 biological replicates for each strain are shown, with a short mean bar +/- SEM error bars. EtBr accumulation is plotted on the left Y-axis. Calculated cell number values were plotted on the right Y-axis with corresponding symbols equating to strain and a dashed line to show growth of the culture. Cell numbers were based on the mean of the same biological replicates and the same gated population that EtBr fluorescence was measured from. Two-way ANOVA and Sidak's multiple comparison test were used for statistical analysis of EtBr accumulation.

This data disproves the hypothesis that the EtBr accumulation phenotype in SL1344 Δ*acrB* is due to the loss of the protein causing membrane damage and in fact suggests that the EtBr accumulation phenotype in stationary phase is independent of AcrB protein and activity.

4.9 Cell viability is unchanged throughout the assay

Another possible explanation for the reduction in EtBr accumulation in stationary phase is that bacterial cells were dying during growth. In the flow cytometry assay, SYTO-84 is the dye used to gate for a population of cells, and the cell number at each time point is then calculated. As it only fluoresces when intercalated with DNA, gating SYTO-84$^+$ events does not mean that all cells in this population are alive at each time point and could not completely confirm growth. Cell death during batch culture has not been previously described for an *acrB* mutant and seemed unlikely because bacterial cultures were grown in drug-free LB. It has previously been shown that the growth kinetics of SL1344 Δ*acrB* are not significantly different from SL1344 also (Wang-Kan et al., 2017). However, further controls were introduced to exclude this possibility.

Initially, commonly used viability stains such as propidium iodide and 5-Carboxyfluorescein Diacetate, Acetoxymethyl Ester (CFDA-AM) were considered so that cell viability could be measured by flow cytometry. However, it would have been difficult to determine the viability of SL1344 Δ*acrB* because most dyes such as these are substrates of the AcrB efflux pump which may confound results.

For this reason, cell viability was assessed by viable cell counts at each time point. **Table 4-3** showed that SL1344 and the *acrB* mutant are still alive at each time point and confirms that the same number of cells were being measured in each sample by flow cytometry. Therefore, the accumulation phenotype was not as a result of cell death.

Table 4-3 Viable counts and CFU/mL

Time point	SL1344 – CFU/mL in FC sample	SL1344 Δ*acrB* – CFU/mL in FC sample
0	3.20E+06	2.60E+06
1	2.40E+07	1.60E+07
2	2.40E+07	2.40E+07
3	2.20E+07	2.20E+07
4	3.80E+07	3.00E+07
5	2.20E+07	1.80E+07
6	3.00E+07	1.60E+07

4.10 The pattern of EtBr accumulation is not changed by media type

Many aspects of bacterial physiology are altered by the type of media in which bacteria are grown (Blair et al., 2013). In order to confirm the accumulation pattern was not a result of the limitations of LB medium (Nikaido, 2009) the experiments were repeated in MOPs minimal media (supplemented with histidine) (Hoiseth and Stocker, 1981, Neidhardt et al., 1974).

The pattern of EtBr accumulation was broadly the same in MOPs minimal media as in LB. For SL1344, EtBr accumulation level remained low and did not significantly differ between time points. For, SL1344 Δ*acrB,* as in LB, accumulation peaked at 1 hour of growth (~6-fold different to WT with a p-value of <0.0001) and then dropped significantly at later time points (**Figure 4-6**). However, unlike LB, EtBr accumulation remained significantly different from SL1344 between 2-6 hours of growth, although it was clear that EtBr accumulation dropped with only a 1.4-fold difference at 6 hours. Cell number in SL1344 and Δ*acrB* was not significantly different and time point for entry into different growth phases did not differ.

Although EtBr accumulation was significantly different in stationary phase, the overall EtBr accumulation pattern remained the same as growth in LB. This confirmed that the pattern was not just as an effect of the limitations of LB (Nikaido, 2009) and that the EtBr accumulation pattern for both SL1344 and Δ*acrB* is independent of growth medium.

Figure 4-6 EtBr accumulation in SL1344 and Δ*acrB*, grown in MOPs minimal media for 6 hours.

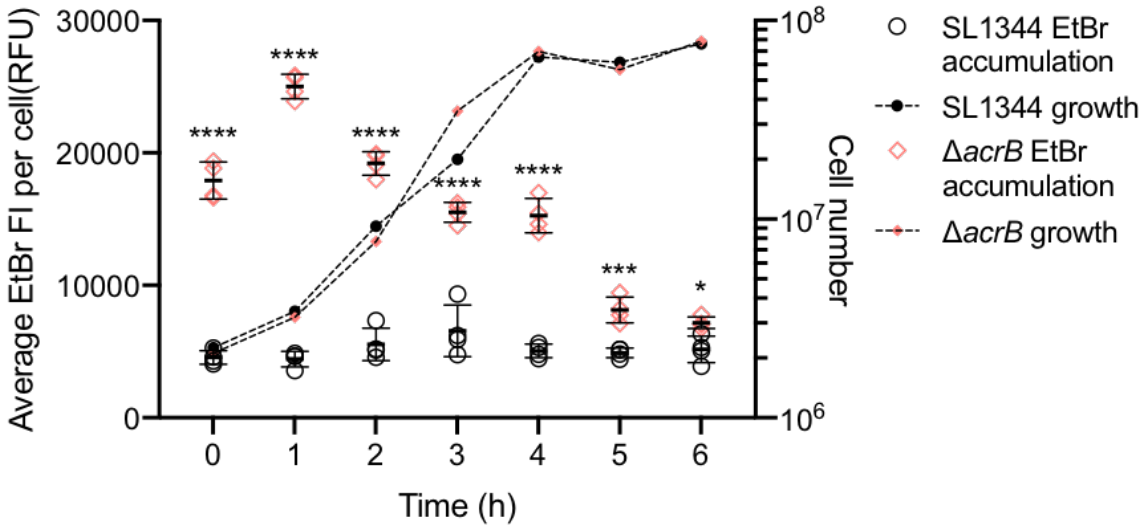

Median EtBr fluorescence per cell in 10,000 SYTO-84$^+$ flow cytometry events was measured every hour between 0 and 6 hours. Individual black circles represent the X-median value of EtBr fluorescence in SL1344 (WT) (from 10,000 SYTO-84$^+$ cell events) within a biological replicate, therefore the average accumulation of ethidium per cell. Individual pink diamonds represent the X-median value of EtBr fluorescence in SL1344 Δ*acrB* (from 10,000 SYTO-84$^+$ cell events) within a biological replicate. 4 biological replicates for each strain are shown, with a short mean bar and SEM error bars. EtBr accumulation is plotted on the left Y-axis. Calculated cell number values were plotted on the right Y-axis with corresponding symbols equating to strain and a dashed line to show growth of the culture. Cell numbers were based on the mean of the same biological replicates and the same gated population that EtBr fluorescence was measured from. Two-way ANOVA and Sidak's multiple comparison test were carried out for statistical analysis.

4.11 Accumulation of the lipophilic dye, Nile Red, produced the same pattern

To confirm that the accumulation pattern observed was not an artefact of using EtBr as a substrate, a dye with a different localisation and mechanism of action was used. The fluorescent dye Nile Red was selected because it localises in the membrane rather than in the cytoplasm and is a known substrate of AcrB (Bohnert et al., 2010). The method for measuring Nile Red accumulation has already been described in the preceding chapter (Whittle et al., 2019) and was adapted here to be measured across growth. As shown in **Section 3.6**, this assay is less sensitive than using EtBr and even at 1 hour of growth, only a slight difference could be detected in Nile Red accumulation between Δ*acrB* and SL1344. However, it was possible to measure a difference in Nile Red accumulation between SL1344 and Δ*tolC* (Whittle et al., 2019) so Δ*tolC* was compared to SL1344 in this case (data in **Chapter 5** shows that a *tolC* mutant produced a similar pattern of accumulation for EtBr to an *acrB* mutant).

Nile Red accumulation was measured in SL1344 Δ*tolC* compared to SL1344 across 6 hours of growth. As with previous data, the cell number at each hour was calculated and, in this case, showed that deleting TolC did not lead to a growth defect and that different growth phases were entered at the same time in both strains (**Figure 4-7**).

Importantly, the alternative dye produced very similar patterns to EtBr. In SL1344, Nile Red accumulation remained low at each time point during growth, not reaching above 1000 RFU. In SL1344 Δ*tolC,* Nile Red fluorescence peaked at 1 hour with an 8-fold difference to WT and then dropped significantly after 2 hours. From 3-6 hours,

accumulation levelled off at an average of 2500 RFU at each time point. However, this showed that accumulation of Nile Red was still significantly different to SL1344 in stationary phase, differing from EtBr.

The broadly equivalent pattern of Nile Red accumulation in the efflux mutant was equivalent to that for EtBr showing the effect was not an artefact of the dye used and remained true for other substrates of AcrB.

Figure 4-7 Nile red accumulation in SL1344 and SL1344 Δ*tolC* from 0-6 hours

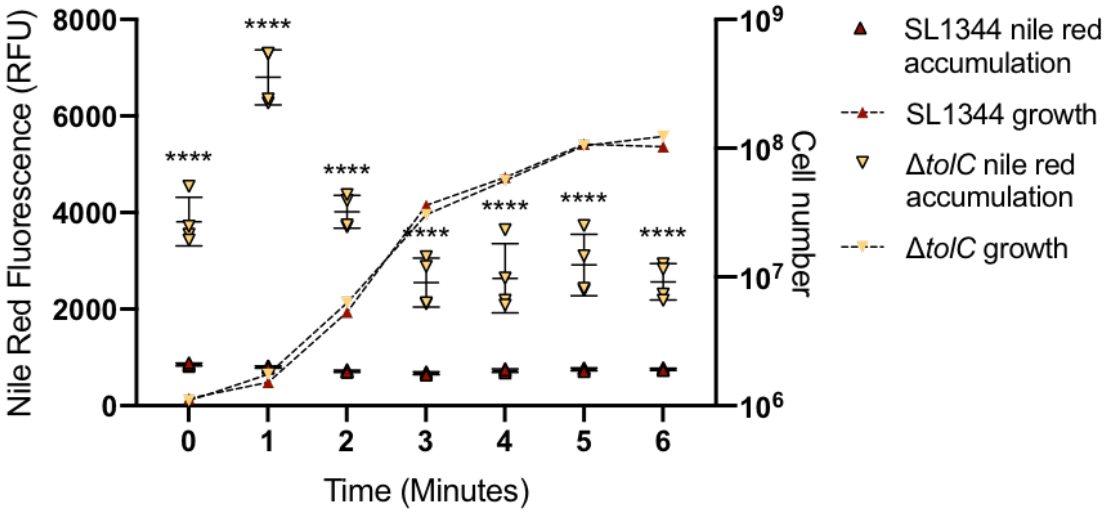

Median Nile Red fluorescence per cell in 10,000 SYTO-9$^+$ flow cytometry events was measured every hour between 1 and 6 hours. 0 hour time points were not included as SYTO-9$^+$ populations could not be gated. Single red triangles represent the X-median value of nile red fluorescence in SL1344 (WT) (from 10,000 SYTO-9$^+$ cell events) within a biological replicate. Individual orange triangles represent the X-median nile red fluorescence in Δ*tolC* (from 10,000 SYTO-9$^+$ cell events) within a biological replicate. 4 biological replicates for each strain are shown, with a short mean bar and SEM error bars. Nile red accumulation is plotted on the left Y-axis. Calculated cell number values were plotted on the right Y-axis with corresponding symbols equating to strain and a dashed line to show growth of the culture. Cell numbers were based on the mean of the same biological replicates and the same gated population that nile red fluorescence was measured from. Two-way ANOVA and Sidak's multiple comparison test were carried out for statistical analysis and '****' related to P <0.0001.

4.12 The pattern of EtBr accumulation is not specific to *S.* Typhimurium

To investigate whether the accumulation phenotype described was a *S.* Typhimurium phenomenon or whether it is more broadly relevant to other Gram-negative organisms, three other Gram-negative species, *E. coli, Klebsiella pneumoniae* and *Pseudomonas aeruginosa* were also tested along with isogenic efflux mutants.

EtBr accumulation was measured in *E coli* MG1655 compared to MG1655 Δ*acrB* (Eaves et al., 2004b). For MG1655, EtBr fluorescence remained low across the growth curve (0-6 hours) and this was consistent with the SL1344 pattern (**Figure 4-8A**). The pattern of MG1655 Δ*acrB* was comparable to SL1344 Δ*acrB.* MG1655 Δ*acrB* EtBr accumulation peaking at 1 hour, with a 6-fold difference to MG1655 and from hour 3 to 6, there is no significant difference between strains.

EtBr accumulation was measured in *K. pneumoniae* ecl8 compared to ecl8 *acrB::*Gm, which has an interruption in the *acrB* gene using a gentamicin cassette (Whittle et al., 2019). As with previous WT strains with fully functioning efflux pumps, in ecl8, EtBr accumulation remained low across growth. However, ecl8 *acrB::*Gm showed the same pattern of all efflux mutants (**Figure 4-8B**). At 1 hour of growth, EtBr accumulation peaked with a 14-fold difference to ecl8. At 2 hours and 3 hours of growth, EtBr accumulation dropped, but was significantly different from ecl8 (7-fold and 6-fold difference respectively). At 4,5 and 6 hours, accumulation of EtBr was low, similar to ecl8, but there is still a significant difference in accumulation at 4 and 5 hours of growth compared to ecl8.

Figure 4-8 EtBr accumulation in *E. coli* and *K. pneumoniae* and their related efflux mutants

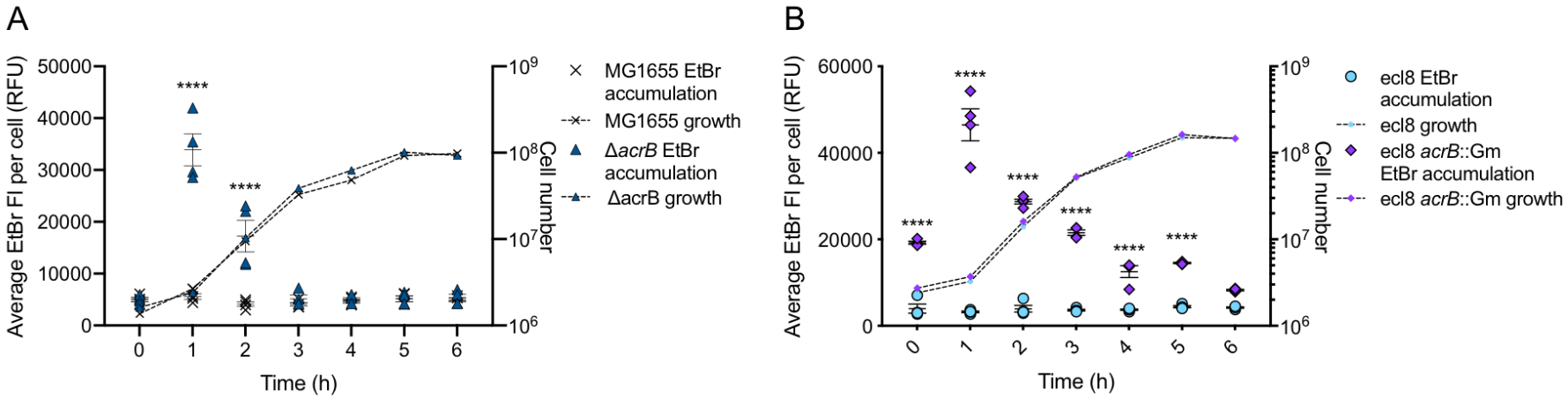

(A) shows *E. coli* MG1655 and Δ*acrB***.** Median EtBr fluorescence per cell in 10,000 SYTO-84$^+$ flow cytometry events was measured every hour between 0 and 6 hours. Individual black Xs (WT) and individual blue triangles (Δ*acrB*) represent the median value of EtBr fluorescence within a biological replicate. **(B)** shows *K. pneumoniae* ecl8 and ecl8 *acrB::Gm.* Median EtBr fluorescence per cell in 10,000 SYTO-84$^+$ flow cytometry events were measured every hour between 0 and 6 hours. Individual blue circles (WT) and individual purple diamonds (*acrB::*Gm) represent the median value of EtBr fluorescence within a biological replicate. 4 biological replicates for each strain are shown, with a short mean bar and SEM error bars. EtBr accumulation is plotted on the left Y-axis. Calculated cell number values were plotted on the right Y-axis with corresponding symbols equating to strain and a dashed line to show growth of the culture. Cell numbers were based on the mean of the same biological replicates and the same gated population that EtBr fluorescence was measured from. Two-way ANOVA and Sidak's multiple comparison test were carried out for statistical analysis.

Pseudomonas aeruginosa PA01 has 14 RND efflux pump systems. The major pump related to AMR, MexAB-OprM was chosen with the periplasmic adaptor protein component, MexA, deleted from the cell. EtBr is a known substrate of the MexAB-OprM pump (Li et al., 2003). A 0 hour data point has not been added to this growth curve as it was not possible to reliably separate cells from background in the flow cytometer, but it was not known why this happened. Cell number was measured again however, compared to previous organisms, the cell number at 1 hour was lower. Mid-exponential phase was reached at 2 hours which is comparable to previous data. PA01 EtBr accumulation across growth was low and therefore was similar to previous data suggesting that EtBr is exported from the cell at each timepoint **(Figure 4-9)**. PA01 Δ*mexA* reached a peak of EtBr accumulation at 2 hours with a 4-fold difference to WT. This was different to previous data where the accumulation peak was at 1 hour, where in this case there was only a 3-fold difference. This may due to cell number. From 3 hours, the EtBr accumulation level started to drop as cells entered stationary phase. At 4 and 6 hours, the capacity to accumulate EtBr was not significantly different to PA01, but there was a significant different at 5 hours **(Figure 4-9)**.

The results presented in this section show that the EtBr accumulation pattern of SL1344 and Δ*acrB* is a robust phenotype consistent across a number of Gram-negative species.

Figure 4-9 EtBr accumulation in *P. aeruginosa* PA01 and Δ*mexA*

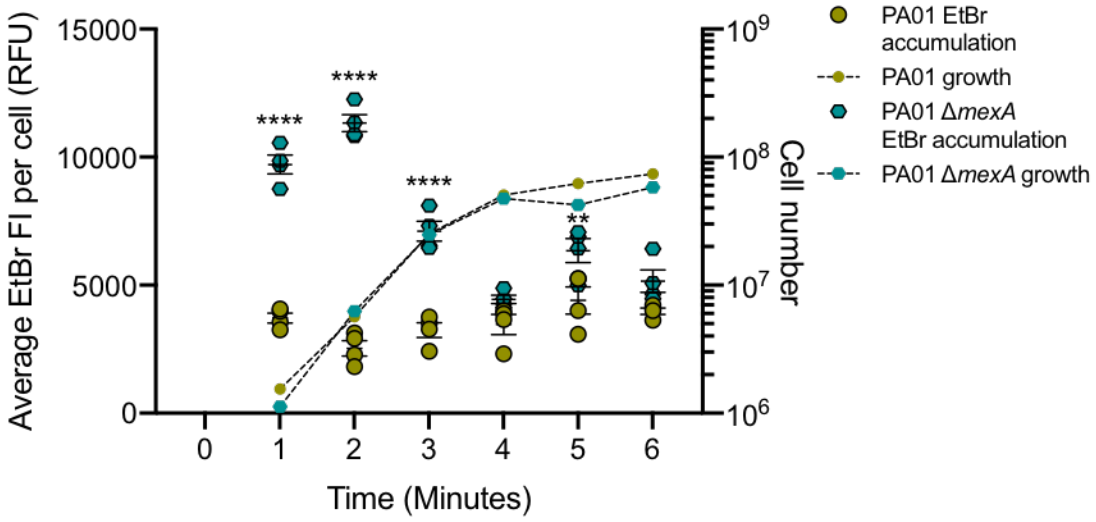

Median EtBr fluorescence per cell in 10,000 SYTO-84$^+$ flow cytometry events was measured every hour between 0 and 6 hours. Individual green circles (WT) and individual blue hexagons (Δ*mexA*) represent the median value of EtBr fluorescence within a biological replicate.4 biological replicates for each strain are shown, with a short mean bar and SEM error bars. EtBr accumulation is plotted on the left Y-axis. Calculated cell number values were plotted on the right Y-axis with corresponding symbols equating to strain and a dashed line to show growth of the culture. Cell numbers were based on the mean of the same biological replicates and the same gated population that EtBr fluorescence was measured from.

4.13 Do other phenotypes reflect accumulation pattern?

To understand what the differences in EtBr accumulation at different points during growth might mean, other phenotypes related to efflux were studied. Antimicrobial susceptibility, biofilm formation, curli biogenesis, and cell shape were all studied after 1, 3 and 5 hours of growth. This was to identify if any changes were occurring when EtBr accumulation peaks (1 hour), in early exponential phase, compared to late exponential (3 hour) and early stationary phase (5 hours).

4.13.1 Antimicrobial susceptibility across growth

Previous published data shows that in SL1344 strains where efflux pump components are removed, there is increased susceptibility to antimicrobials (Blair et al., 2015a). MICs were measured to see whether the pattern of accumulation seen across growth correlated or altered antimicrobial susceptibility. Susceptibility to four different efflux substrates (EtBr, SDS, vancomycin and ciprofloxacin) were measured using cultures taken from 3 different time points of growth.

The MIC values of EtBr were measured to draw a direct comparison to flow cytometry accumulation data. In SL1344, the MIC of an overnight culture was 1024 μg/mL. The MIC for cultures grown for 1, 3 and 5 hours remained the same regardless of timepoint. The MIC of EtBr in SL1344 Δ*acrB* is 64 μg/mL, 5-fold lower than SL1344. A large difference in EtBr MIC in these strains has been described previously (Blair et al., 2015a). The absence of the efflux pump increases the accumulation of the dye meaning the concentration required to kill the bacteria is lower. Using a culture of SL1344 Δ*acrB* grown for 1 hour, the MIC increased 4-fold to 256 μg/mL, which

suggests there was decreased susceptibility to EtBr in actively growing cells (**Table 4-4**). At 3 and 5 hours of growth of the initial culture, comparable to the overnight, the MIC was 64 μg/mL.

Sodium dodecyl sulphate (SDS) is a detergent that kills bacterial cells by permeabilising its membranes (Shafa and Salton, 1960) and susceptibility has previously been shown to be growth phase dependent (Mitchell et al., 2017). In SL1344, regardless of time point, the MIC was >1024 μg/mL. The MIC of SDS in Δ*acrB* was 256 μg/mL, apart from after 3 hours of growth of the initial culture, where the value was 512 μg/mL. It was a 2-fold or greater difference between WT and Δ*acrB,* however there is no difference in MIC at different time points between strains (**Table 4-4**).

Table 4-4 Susceptibility profiles of SL1344 and Δ*acrB* at 1, 3 and 5 hours

Strain	Time	MIC (μg/mL)			
		EtBr	SDS	Vanc	Cip
SL1344	Overnight	1024	>1024	1024	0.06
	1	>1024	>1024	1024	0.06
	3	1024	>1024	1024	0.06
	5	1024	1024	>1024	0.25
Δ*acrB*	Overnight	64	256	1024	0.008
	1	256	256	1024	0.03
	3	64	512	1024	0.03
	5	64	256	1024	0.015

EtBr: Ethidium bromide; SDS: Sodium dodecyl sulphate; Vanc: Vancomycin; Cip: Ciprofloxacin

Vancomycin is a large glycopeptide antibiotic, mainly used to treat Gram-positive infections. Vancomycin is too large to enter through the Gram-negative OM (Fernandes et al., 2017). It was important to assess whether this was the same at all time points, as the membrane may be weaker and allow the entrance of more compounds at certain timepoints. However, the MIC of vancomycin in both strains at each timepoint was consistently 1024 μg/mL (**Table 4-4**). This showed that vancomycin was unable to kill Gram-negative cells at the range of concentrations used, regardless of growth phase.

The fluoroquinolone, ciprofloxacin, inhibits bacterial growth by accumulating DNA double stranded breaks via binding DNA gyrase (LeBel, 1988). At high concentrations, ciprofloxacin is bactericidal. The MIC of ciprofloxacin in SL1344 was 0.06 μg/mL. This did not change when the initial culture was grown for 1 or 3 hours but at 5 hours the MIC increased to 0.25 μg/mL (2-fold). In SL1344 Δ*acrB,* the MIC was 0.008 μg/mL, 3-fold different to the overnight growth of SL1344. At 1 and 3 hours, the MIC values of ciprofloxacin in Δ*acrB* strains was 0.03 μg/mL, 2-fold different to the overnight control, and at 5 hours was 1-fold different to the overnight control (0.015 μg/mL). These results at different timepoints were not considered significant (**Table 4-4**).

4.13.2 Curli biosynthesis

Curli are proteins present on the surface of *Enterobacteriaceae* including *S.* Typhimurium. They are important when considering clinical infection as they have been implicated in not only cell adhesion and invasion, but also in inducing the host

inflammatory response and in the formation of biofilms (Barnhart and Chapman, 2006). Curli biogenesis was tested in this case as it is already known that curli biogenesis is altered in the absence of efflux (Baugh et al., 2012).

Curli producing *S.* Typhimurium can be stained red when grown on LB supplemented with the dye, congo red, and grown for 48 hours. The production of red, dry and rough colonies indicated the production of curli and cellulose. Strains that formed pink colonies produce cellulose but no do not biosynthesise curli, and white colonies represent strains that cannot produce curli or cellulose. This assay was performed to determine whether curli biogenesis was different at different time points.

Figure 4-10A shows the control strain 14028s grown from an overnight culture. This colony is red and rough showing its production of curli and cellulose. SL1344 overnight control showed a red rough colony (**Figure 4-10B**). Inoculation of plates with SL1344 grown for 1, 3 or 5 hours produced red smooth colonies, possibly suggesting curli formation but to a lesser extent than the overnight control (**Figure 4-10C-E**). There was no difference in curli production at 1, 3 and 5 hours in SL1344 Δ*acrB* (**Figure 4-10F-I**), and there was no substantial difference in the colony appearance to SL1344.

Figure 4-10 Curli biogenesis of 14028s, SL1344 and SL1344 Δ*acrB* stained with congo red

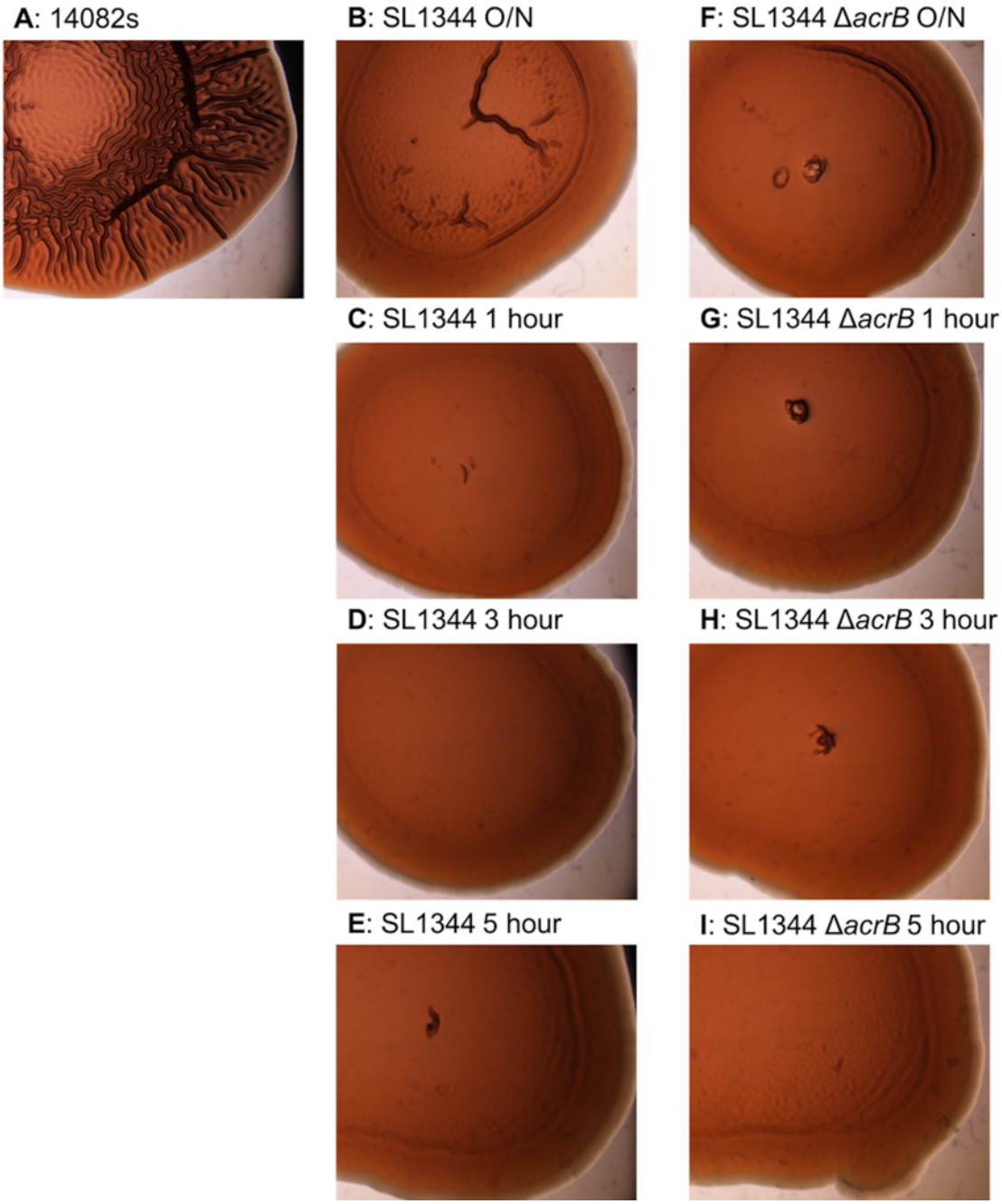

(A) shows the control strain 14028s diluted and regrown on congo red plates from an overnight culture. **(B-E)** represent SL1344 diluted from an overnight **(B)**, 1 hour **(C)**, 3 hour **(D)** and 5 hour **(E)** timepoints. **(F-I)** represent SL1344 Δ*acrB* diluted from an overnight **(F)**, 1 hour **(G)**, 3 hour **(H)** and 5 hour **(I)** time points. Red, dry and rough colonies indicate the production of curli and cellulose. Pink colonies represent strains that produce cellulose but are not producing curli fibres. White colonies are strains that are not producing curli or cellulose in their extracellular matrix.

4.13.3 Biofilms

As with curli biogenesis, biofilm production has been shown to be changed in the absence of efflux (Baugh et al., 2012). Biofilm formation can be measured using a well described crystal violet method (O'Toole, 2011, Jackson et al., 2002). The strong biofilm producing strain 14028s was used as a control.

This assay, as with MICs and curli is usually analysed based on an overnight culture. For this reason, SL1344 and Δ*acrB* biofilm formation from an overnight were also analysed and compared to 14028s. The average OD_{600} for biofilms formed from overnight cultures was 1.75 in 14028s. There was a significant difference between 14028s and the SL1344 strains, with an almost 4-fold increase in OD_{600} in 14028s, equating to large production of biofilm. However, there was no significant difference between SL1344 and Δ*acrB* and the OD_{600} values did not get past 0.5 for either strain. There were also no significant differences between cultures that had grown for 1, 3 or 5 hours in both strains showing, along with curli data, that SL1344 is not a good producer of biofilms (**Figure 4-11**).

Using this assay, samples taken after 1, 3 and 5 hours of growth of the initial culture were adjusted based on cell number, and then re-grown for 48 hours. For this reason, it is likely that these assays are not sensitive enough to show any differences in biofilm production that may occur in different growth phases.

Figure 4-11 Biofilm formation by crystal violet staining in *S.* Typhimurium at 1, 3 and 5 hours.

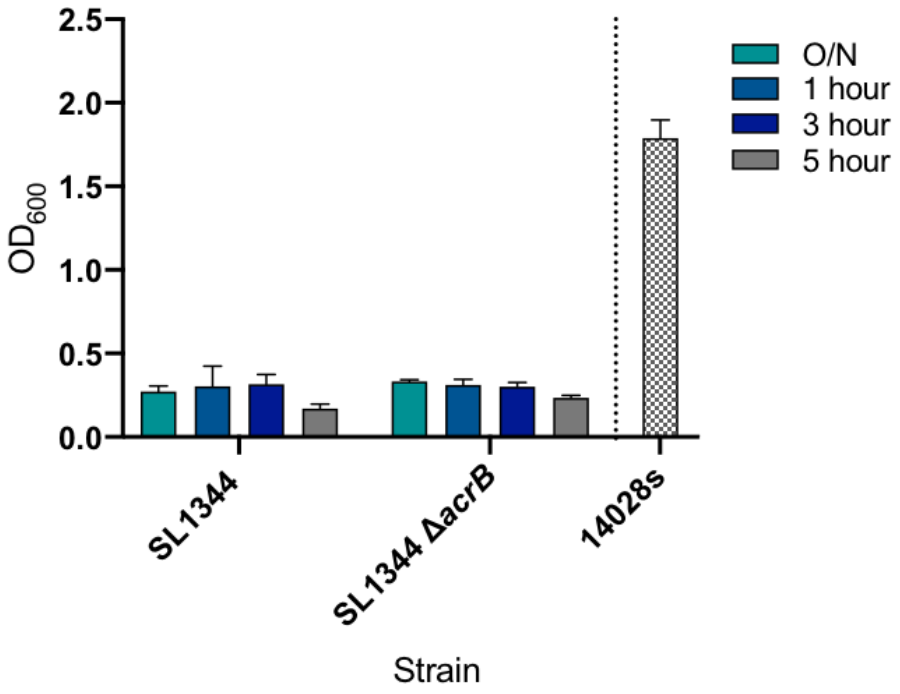

Crystal violet biofilm formation is based on 3 biological replicates. Columns represent the OD_{600} presented on the Y-axis and error bars represent +/- SEM. 14028s is used in the control. SL1344 is grouped to the left with 4 bars and ∆*acrB* is grouped to the right with 4 bars. Grouped data presented on the graph shows formation from an original overnight culture (green), 1 hour growth (light blue), 3 hour growth (dark blue) and 5 hour growth (grey) points.

4.13.4 Cell morphology

Previous results in **Section 4.13** did not produce any significant changes in phenotype between exponentially and stationary phase cells. Changes in morphology of Gram-negative bacilli in stationary phase have been previously described (Navarro Llorens et al., 2010).

SL1344 grown for 1, 3 and 5 hours was visualised by microscopy. After 1 hour of growth, representing early exponential phase and 3 hours, representing late exponential phase, SL1344 were still considered bacilli in shape (**Figure 4-12A** and **B**). By stationary phase, bacilli change morphology to a shorter coccoid shape (**Figure 4-12C**).

At 1 hour, the mean cell length was 6.14 μm, and was significantly different to both 3 and 5 hours according to unpaired T-tests, with p-values of <0.0001. The average length at 3 hours was 4.30 μm and 3.02 μm at 5 hours, and cell length was significantly different at these time points (p-value <0.0001) (**Figure 4-13**). This result confirms that a change in morphology in SL1344 here is consistent with a well described phenotype of stationary phase.

.

Figure 4-12 Representative image of cell morphology of SL1344 at 1, 3 and 5 hours.

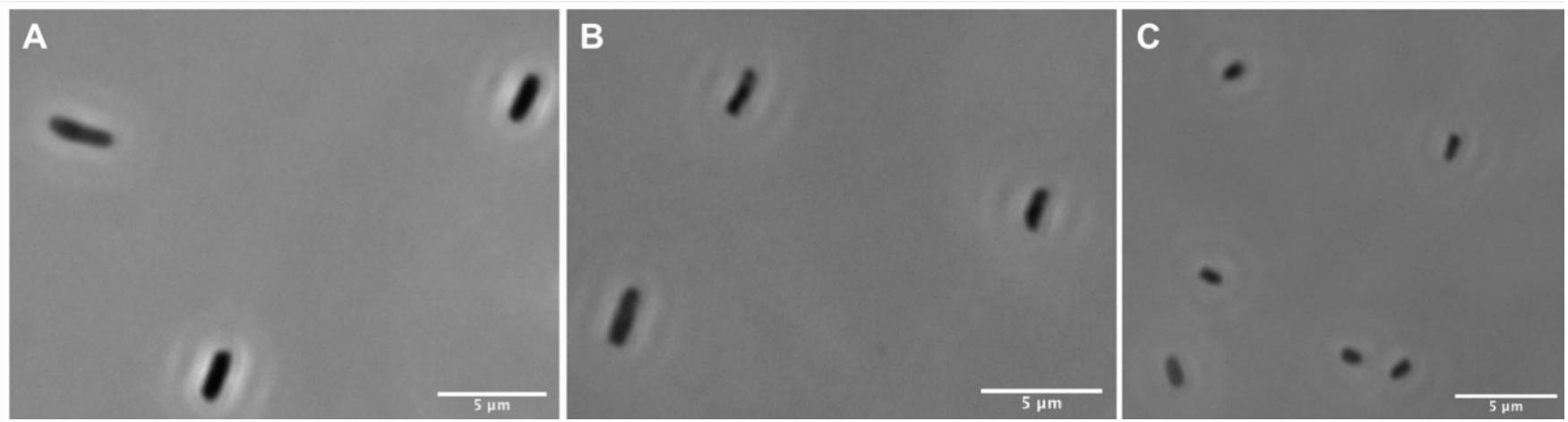

(A) shows a differential interference contrast (DIC) image of SL1344 at 1 hour. **(B)** shows a DIC image of SL1344 at 3 hours of growth. **(C)** shows a DIC image of SL1344 at 5 hours of growth. The scale bar in the bottom right shows 5 μm. Microscopy images were taken of fixed cells at each time point using the Nikon AxioObserver with a 100x oil objective.

Figure 4-13 Cell length of SL1344 at 1, 3 and 5 hours.

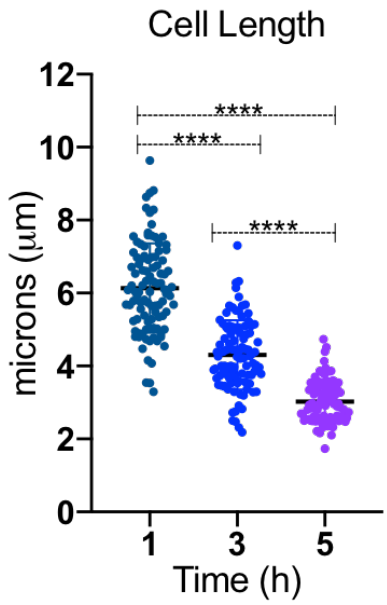

A sample of 100 SL1344 cells were measured at each time point, using ImageJ and microscopy images. Length was measured in μm. 1 hour (dark blue), 3 hour (light blue) and 5 hour (purple) were the statistically analysed by multiple unpaired T-tests. All were significantly different from each other with a p-value of <0.0001. The **** represents this p-value.

4.14 Discussion

The data presented in this chapter challenges the commonly accepted notion that deleting efflux pumps in Gram-negative bacteria simply causes an increase in the accumulation of antibiotics and dyes. In fact, this concept only appears to be true in actively growing cells, implying that intracellular accumulation of drugs is growth phase dependent.

The capacity of SL1344 to accumulate EtBr accumulation remained low in every growth phase. The data for EtBr accumulation was slightly unexpected as studies have already shown that transcription of efflux pumps, namely *acrAB* transcription, does alter with growth phase and rate (Rand et al., 2002, Bailey et al., 2006). Studies

into *acrAB* transcription have previously drawn different conclusions. In 2002, it was shown that *acrAB* transcription is regulated as a function of growth rate (Rand et al., 2002). Slow growing *E. coli* may upregulate the expression of *acrAB*, which was linked to the idea that increased expression increases drug resistance (Rand et al., 2002). It has also been suggested that *acrAB* transcription is quite stable across growth phases in *E. coli* (Kobayashi et al., 2006). In contrast, in 2006, it was shown that in *Salmonella* grown in LB medium, *acrAB* transcription peaked in early exponential phase and dropped in late exponential phase (Bailey et al., 2006). Kroger et al. (2013) created an interactive online browser called 'SalCom' for RNAseq based transcriptomic data of *S.* Typhimurium. This *S.* Typhimurium SalCom data showed that *acrAB* expression in *S.* Typhimurium is highest in early exponential phase with decreased expression in late exponential and stationary phase cells (Kroger et al., 2013).

Following the studies that show growth phase dependent expression of *acrAB*, it was hypothesised that *acrAB* transcription peaks in early-mid exponential phase, and increased transcription would lead to increased efflux activity, therefore lower EtBr accumulation. The data in this chapter confirmed that transcription peaked at early-mid exponential phase, however, interestingly, transcription and EtBr accumulation did not correlate. This may suggest normal transcriptional changes of growth do not lead to an increase in efflux activity. It is possible that expression in different growth phases is lower than in clinical isolates, where described overexpression of pumps leads to AMR (Webber and Piddock, 2001).

The low accumulation phenotype across growth may be explained by protein level and activity rather than transcription. The half-life of AcrAB is considered long with one study suggesting it can be present in stationary phase cells for up to 6 days (Chai et al., 2016). In 2017, it was suggested that AcrB protein undergoes biased partitioning, in which AcrB protein is localised to an old cell pole during cell division, and a new daughter cell needs to make new protein (Bergmiller et al., 2017). One hypothesis is that *acrAB-tolC* transcription peaks in mid-exponential phase because cell division rates are high so there are many new daughter cells that require new protein to be synthesised. However, accumulation level may not change because this doesn't represent more protein per cell. This hypothesis will be studied further in **Chapter 5**.

To further investigate the link between efflux expression and EtBr accumulation, the growth phase experiment was repeated in a strain lacking AcrB. Previous data in many Gram-negative species has shown high accumulation of substrates molecules in efflux mutants due to an inability to export the compounds (Blair et al., 2015a, Smith and Blair, 2014, Wang-Kan et al., 2017, Paixao et al., 2009, Richmond et al., 2013). However, these studies were all carried out with mid-exponential phase or in actively growing cells. When measuring the EtBr accumulation of SL1344 Δ*acrB* across the growth curve, the result showed growth phase dependence. As shown previously, accumulation of EtBr was significantly higher in the *acrB* mutant than in the WT background strain suggesting that low accumulation in exponential phase is dependent on AcrAB-TolC (Wang-Kan et al., 2017, Blair et al., 2009, Smith and Blair, 2014). However, the decrease in EtBr accumulation seen in stationary phase has not

previously been shown in SL1344 Δ*acrB.* Importantly, this suggests that the EtBr accumulation level in stationary phase may not be efflux dependent.

In 2015, Blair et al., used RT-PCR to show that in an *acrB* mutant*, acrD* and *acrF* are upregulated, partially counteracting the loss of AcrAB-TolC function (Blair et al., 2015a). It is therefore plausible that low accumulation in SL1344 Δ*acrB* in stationary phase may be due to other efflux pump systems such as AcrAD-TolC and AcrEF-TolC being upregulated to counteract the loss of AcrAB-TolC and this hypothesis will be addressed in the next chapter of this thesis.

It is important to note that accumulation of EtBr is not just the measure of efflux but is influenced by the rate of influx of EtBr as well as efflux. Data presented in this chapter suggests that efflux is less important to the level of accumulation in stationary phase, and possibly, how much dye gets into the cell is a more important factor. In 2016, it was shown that AcrAB-TolC is only important in surviving the pressure of SDS in actively growing cells (Mitchell et al., 2017). The study showed that in nitrogen and carbon starved environments, the absence of efflux made no difference to survival, and RpoS, the stationary phase sigma factor was suggested to be important in activating genes that strengthened the outer membrane barrier. Results presented here also suggest that efflux is not important to the level of substrate accumulation in stationary phase. This result could suggest that the likelihood of bacteria developing efflux-mediated resistance may differ depending on the type of infections and its growth state. This result is also important when considering the potential treatment of slow- or non-growing infections with efflux inhibitors, as efflux may not be the true driver of low drug accumulation in some infections. Therefore, efflux

inhibition may prove ineffective in potentiating the activity of antibiotics in some infections.

In *Salmonella* SL1344, the EtBr accumulation across growth was constant. However, this work shows that efflux is only important to accumulation during exponential, but not stationary, growth phase. One hypothesis to explain this is that in stationary phase, decreased permeability of the OM prevents accumulation of EtBr, explaining why accumulation level seems to be efflux independent at this stage. This hypothesis will be investigated further in **Chapter 6**.

The EtBr accumulation phenotype in SL1344 Δ*acrB* is especially important due to its robustness in other conditions. EtBr accumulation consistently peaks in early exponential phase and drops in stationary phase in MOPs media (more nutrient limited), with a differently localised substrate (Nile Red) and with a range of clinically relevant Gram-negative bacteria.

Nile Red is a lipophilic dye which stains triglycerides and phospholipids. It was important to show that the accumulation phenotype using EtBr was not just an artefact of that particular dye. Measuring efflux using Nile Red has been used previously in *E. coli* (Bohnert et al., 2010). Bohnert et al., 2010, showed that in the absence of *acrAB*, Nile Red efflux was diminished. Data presented in **Chapter 3** showed little difference in Nile Red accumulation in SL1344 compared to Δ*acrB* (Whittle et al., 2019). It is not known why Nile Red is a less sensitive substrate in this assay when used with *Salmonella* rather than *E. coli* but to get around this problem, a mutant lacking the outer membrane channel TolC was used in these experiments as the difference in accumulation was greater. The peak in Nile Red fluorescence in

exponential phase in SL1344 Δ*tolC* shows the necessity of TolC for export of this dye. TolC as the outer membrane component, can form tripartite pumps in a number of other systems and may suggest Nile Red is the substrate of another pump. Nile Red accumulation does drop as stationary phase is entered, and this may suggest that outer membrane permeability does play a role preventing access to drugs in stationary phase (Bohnert et al., 2010). However, Nile Red accumulation is always significantly different to SL1344 regardless of growth phase, suggesting that either efflux pumps export Nile Red in stationary phase, or that low EtBr accumulation in stationary phase may rely more on the permeability of the IM. It is also possible that the mechanism for export for both these dyes is different.

Other common substrates for measuring accumulation include Hoechst 33342 and 1,2-DNA (Blair and Piddock, 2016, Bohnert et al., 2011). However, it was not possible to test these here as the flow cytometer was not fitted with a violet laser. Future work would include optimising this assay for other dyes, and possibly fluorescent antibiotics (Stone et al., 2020) to be able to assess the true clinical relevance of this accumulation phenotype.

Apart from drug accumulation, other phenotypes have been described when AcrB is deleted from cells, and so these phenotypes were investigated in different growth phases. It is well known that cell shape and length change from exponential to stationary phase in Gram-negative bacilli (Navarro Llorens et al., 2010). This was confirmed in *Salmonella* SL1344 in this chapter. For many other efflux related phenotypes there was no phenotypic difference between cells from different growth phases but this may be due to sensitivity issues associated with the way these assays

were performed. The phenotypic assays were adapted to measure the potential phenotypes at certain points in growth. For MIC, curli and biofilm assays, the assays were set up using cultures grown for different lengths of time (1, 3 or 5 hours) but then the assays require incubation for 24-48 hours. This makes these assays insensitive so it was unlikely that any difference in phenotype would be identified. Further work on this would include optimising these assays to increase sensitivity. Assessing antibiotic sensitivity could be measured at different time points if cultures were treated with antibiotic in different growth phases and assessed for survival.

4.15 Key Findings

- Levels of EtBr accumulation in exponential phase were dependent on the presence of AcrAB-TolC.
- EtBr accumulation in stationary phase in an efflux mutant is low, regardless of growth medium, organism and dye, and therefore appears to be a consistent phenotype.
- Low accumulation may be due to the activity of other efflux pumps or reduced by outer membrane permeability changes and both these hypotheses will be considered in more detail

Chapter 5- Low accumulation in stationary phase is efflux independent

5.1 Background

In the previous chapter, a novel accumulation phenotype was identified in wild type Gram-negative bacteria and in their respective efflux mutant strains, when in different growth phases.

In Gram-negative bacteria, EtBr accumulation remained low regardless of growth phase. One obvious hypothesis was that accumulation remains low due to the presence of the major efflux pump AcrAB-TolC. However, changing *acrAB* transcription levels across growth had no impact on the level of accumulation. It was hypothesised that AcrAB protein level is the key factor in determining the level of efflux and therefore maintaining low accumulation.

There is limited information of the amount of AcrB protein present in the cell and how it relates to transcription. It is well known that *acrAB* is highly and tightly regulated at the local and global transcriptional level. The transcription of *marA* and *soxS* is expressed to a greater extent in early to mid-exponential phase, comparable to transcription of *acrAB* (Bailey et al., 2006).

Less well understood is the importance of post-transcriptional and translational control of AcrAB-TolC. The importance of CsrA and sRNAs has been discussed (**Chapter 1**). Briefly, they direct or prevent translation of *acrAB* transcripts (Ricci et al., 2017, Parker and Gottesman, 2016, Yamada et al., 2010). However, it is not

understood how the control of AcrB level differs in different growth phases. It has been shown that AcrB has a long half-life and could explain why low EtBr accumulation capacity is maintained across growth. This hypothesis will be studied further here.

The hypothesis regarding the levels of AcrB protein may be disproved by the EtBr accumulation phenotype of SL1344 Δ*acrB*. The peak in EtBr accumulation after 1 hour of growth confirms substrate accumulation is dependent on efflux in actively growing cells. However, EtBr accumulation in SL1344 Δ*acrB* is the same as SL1344 in stationary phase. This suggests that EtBr accumulation is independent of AcrB in stationary phase. One possible explanation for the decrease in accumulation in stationary phase is that other efflux pumps could function or indeed have increased expression during later growth phases which would ameliorate the effects of losing AcrB on accumulation. There are 4 other RND pumps in *S.* Typhimurium: AcrEF-TolC, AcrAD-TolC, MdsABC/TolC and MdtABC/TolC, which may be involved in the export of EtBr in stationary phase as well as 4 other MDR pumps from different efflux pump classes. Their importance in the EtBr accumulation phenotype will be explored here.

5.2 Hypotheses

- AcrB protein level and therefore efflux activity remains constant over growth
- Efflux pumps other than AcrAB, are responsible for the drop in EtBr accumulation in stationary phase.

5.3 Aims:

1. To determine whether efflux activity varies across the growth curve
2. To measure AcrB protein level and study the importance of protein level on EtBr accumulation
3. To investigate whether efflux pumps other than AcrAB are responsible for the drop in EtBr accumulation in stationary phase
4. To measure transcription of all MDR efflux pumps to determine their importance in different growth phases

5.4 Accumulation is low in stationary phase in the absence of *acrB* but efflux capability is constant across growth phases

In the previous chapter, it was shown that low EtBr accumulation in actively growing cells was dependent on the presence of AcrAB-TolC, but this was not the case in stationary phase cells. To determine whether efflux activity in SL1344 cells varied in different growth phases and could contribute to changing levels of EtBr accumulation, the level of efflux activity was measured at different time points during growth. The following assay does not directly measure the activity of AcrAB-TolC, but the efflux capacity of the cell based on the activity of all efflux pumps that are able to transport EtBr in SL1344.

This assay works by maximally preloading cells with EtBr in the presence of an efflux inhibitor, CCCP, which dissipates the PMF. Glucose is then added to restore the PMF and re-start efflux. The decrease in fluorescence as EtBr is actively pumped out of the cells is then measured.

Figure 5-1A shows the drop in EtBr fluorescence in SL1344 grown for 1,3 or 5 hours, for the 60 minutes that followed re-energisation by the introduction of glucose. Based on this data, it appeared that the levels of EtBr from cells grown for 3 and 5 hours began to drop at the same time following addition of glucose. In cells grown for 1 hour, there is a lag (3.74 and 4.55 minutes later than a culture grown for 3 and 5 hours respectively) before EtBr starts being exported from the cell.

To statistically analyse this data, the maximum EtBr fluorescence value was taken for each biological replicate at each time point and from this value, the time (minutes) for fluorescence to drop by 10%, 25% and 50% was calculated **(Figure 5-1B)**. There were three biological replicates for each condition. There was no significant difference in the time taken for the fluorescence to drop between cells grown for 1, 3 or 5 hours. This suggests that regardless of time point, efflux pumps are present and still have the capacity to function.

Taken together, the low EtBr accumulation across time in SL1344 and the data presented here, suggests that although *acrAB* transcription peaks in mid-exponential phase, the AcrAB-TolC activity level is constant. It is possible that efflux capacity is constant due to the long half-life of AcrAB (Chai et al., 2016) and may explain why EtBr accumulation remains low in stationary phase. AcrAB protein level will be explored further in **Section 5.5**.

Figure 5-1 Efflux capacity of SL1344 after 1, 3 and 5 hours of growth.

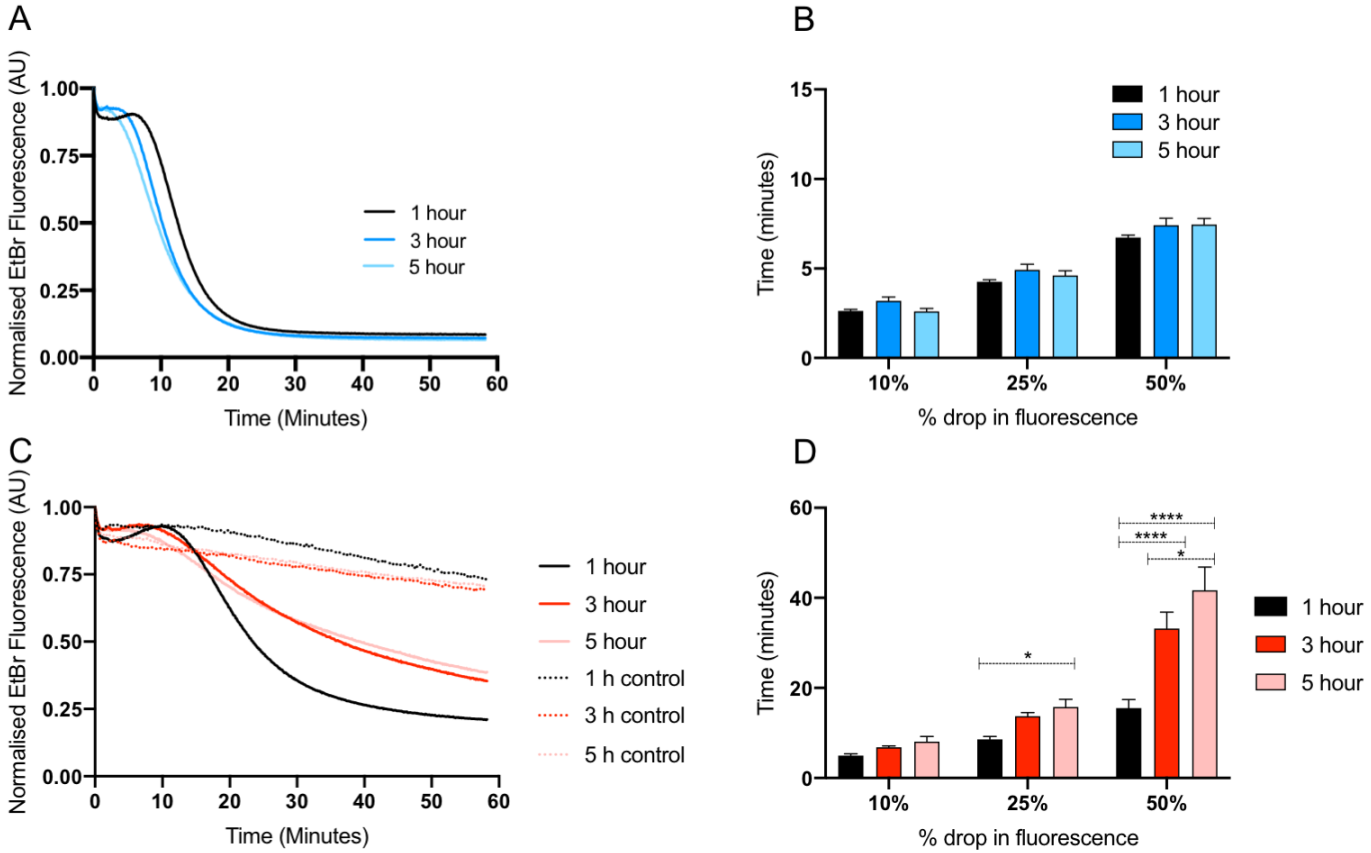

SL1344 (**A + B**) and SL1344 Δ*acrB* (**C + D**) were loaded with EtBr and CCCP after growing for 1, 3 and 5 hours. (**A + C**) shows the EtBr fluorescence over 60 minutes. 0 minutes is the time point where glucose is added to the cells to re-energise. The lines represent fluorescence of EtBr as it is being pumped out of the cells. The figure legend is shown in in each panel. Starting fluorescence at 0 minutes was normalised to 1. In (**C**), controls were added, where no glucose had been added to Δ*acrB* therefore efflux was not re-energised (**B + D**) Bars represent the time taken for EtBr fluorescence to drop by the stated %. There were biological 3 replicates for each condition and error bars of +/- SEM.

The assay was repeated for SL1344 Δ*acrB* grown for 1, 3 or 5 hours. Previously, it was shown that the EtBr accumulation in Δ*acrB* peaked at 1 hour of growth and then dropped into stationary phase. To understand how efflux activity and the EtBr accumulation pattern may relate, the efflux assay described previously was repeated with SL1344 Δ*acrB.* It was clear that efflux activity was reduced compared to SL1344 for each of the hours where samples were taken. In SL1344 Δ*acrB* cultures grown for 1 hour, there appeared to be more efflux activity than cultures grown for 3 and 5 hours **(Figure 5-1C)**. There was a significant increase in the time taken for a 25% drop in fluorescence after 5 hours of growth compared to 1 hour of growth. Both at 3 and 5 hours of growth, there was a significant increase in the time taken for 50% drop compared to 1 hour ($p < 0.0001$) **(Figure 5-1D)**. Using controls where SL1344 Δ*acrB* was not re-energised with glucose confirmed that these cells can still efflux in the absence of AcrAB-TolC but to a lesser extent than SL1344. In *S*. Typhimurium, AcrEF and MdsABC export EtBr (Nishino et al., 2006), and in *E. coli*, MdfA was also shown to export EtBr (Nishino and Yamaguchi, 2001), and it is possible that these pumps are involved in EtBr export after 1 hour of growth. The clear difference in time taken for fluorescence to drop between 1 and 3/5 hours, may suggest that a cell has higher efflux activity in actively growing cells.

The data presented in **Figure 5-1C + D** is complex but it could be hypothesised that in Δ*acrB*, other efflux pumps still function to maintain low EtBr accumulation and circumvent the requirement for AcrAB-TolC in stationary phase. This hypothesis will be explored in this chapter.

5.5 Does AcrB protein level stay constant across growth contributing to low EtBr accumulation in SL1344?

It is apparent that efflux pumps are functional in every growth phase in SL1344. Constant efflux capacity suggests levels of AcrAB-TolC protein level remains constant within the cell. To explore this further, it was important to investigate the levels of AcrB within a cell at different growth phases and to identify its role in maintaining low EtBr accumulation in stationary phase in SL1344.

A chromosomal fusion of GFP to the C-terminal end of AcrB with a codon optimised poly-linker, has previously been described in *E. coli* (Bergmiller et al., 2017). To measure AcrB protein in single cells by flow cytometry here, a GFP-tagged AcrB protein was used. To construct SL1344 AcrB-GFP, the same basic protocol was used as presented previously for *E. coli* by Bergmiller et al. (2017), except that a GFP plasmid was optimised by inserting *aph* directly downstream of msfGFP for use as a selectable marker for correct insertion.

5.5.1 Construction of SL1344 AcrB-GFP strain

5.5.1.1 Restriction and ligation to produce a *gfp* + *aph* plasmid

To produce a strain with GFP fused to AcrB on the chromosome, first the pET GFP LIC cloning vector (u-msfGFP) plasmid was modified by insertion of *aph,* a kanamycin resistance cassette, downstream of *gfp*. To insert *aph,* two restriction sites downstream of *gfp* were chosen. The first cutting site enzyme was AscI, followed by KpnI, providing targeted directionality of the *aph* insert gene (**Figure 5-2**).

Figure 5-2 Cloning strategy to construct the modified GFP plasmid.

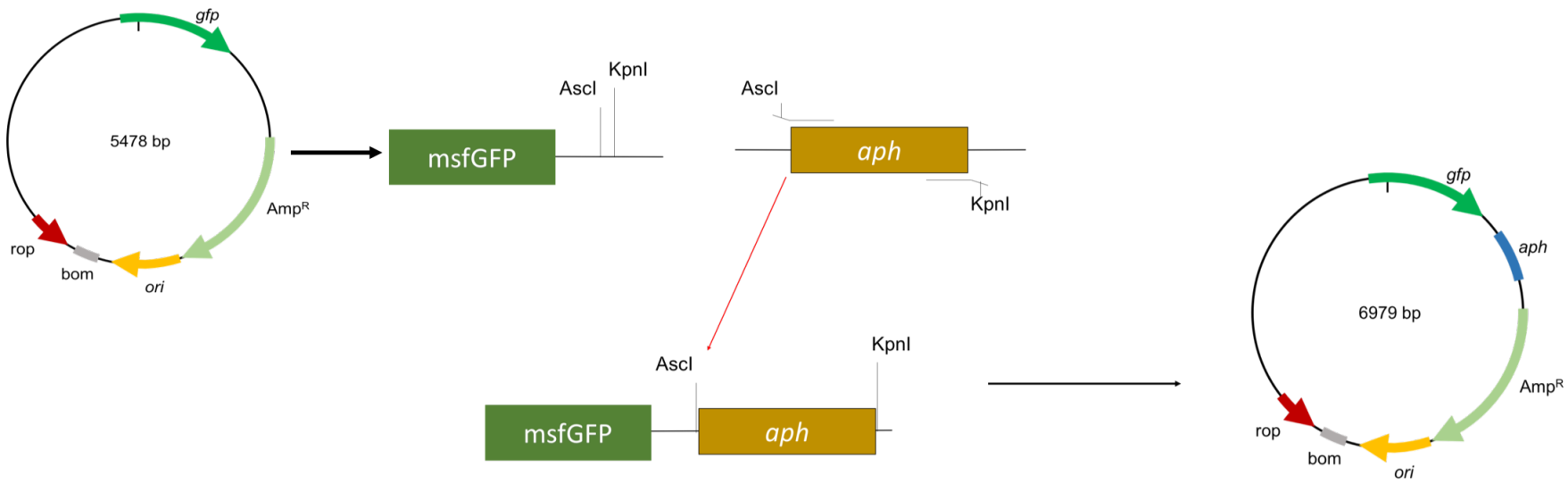

This schematic shows a plasmid map of the original pET-LIC (u-msfGFP) plasmid which was 5478 bp. Downstream of msfGFP was a multiple cloning site where 2 restriction sites (AscI and KpnI) were chosen for the ligation of *aph* downstream of *gfp*. The final constructed plasmid was 6979 bp.

To confirm correct cutting, the plasmid was separated by gel electrophoresis. An uncut plasmid was used as a control, followed by cuts with a single restriction enzyme to confirm each enzyme was linearizing the plasmid. **Figure 5-3** showed that both single cut plasmids and plasmids '1' and '2' (two candidates cut with both enzymes), had slower passage of DNA through the gel than uncut plasmid and confirmed successful cutting.

Figure 5-3 Agarose gel electrophoresis image to identify successful restriction digest of pET-LIC (u-msfGFP) plasmid

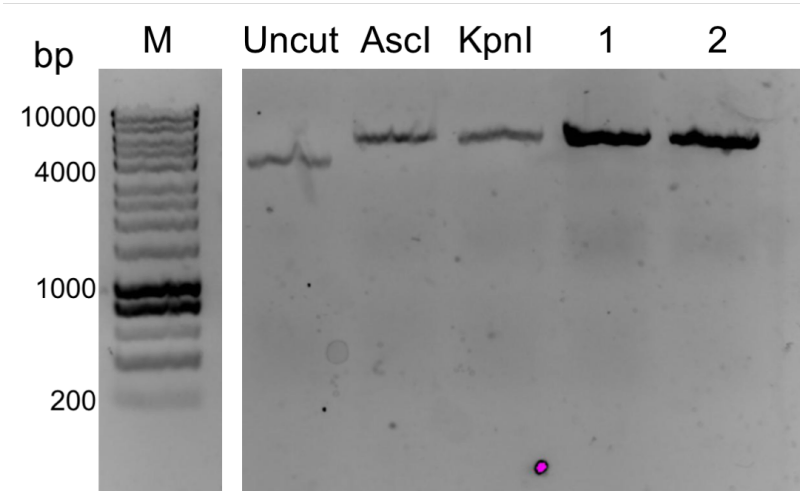

M represents the marker with size of bands in bp labelled. Uncut represents the 5478 bp plasmid that has not been digested. All plasmid that has been successfully digested is represented as a larger band on the agarose gel. AscI represents a single cut control and KpnI represents a single cut control. 1, 2 represent samples that have been digested with both restriction enzymes.

Oligonucleotides were designed (**Table 2-8**) that would amplify the *aph* gene from the pKD4 plasmid with an AscI restriction site on the forward primer, and a KpnI restriction site on the reverse primer. Amplified *aph* was then also digested with both restriction enzymes to produce sticky ends that were then ligated into the pET GFP LIC plasmid. This new plasmid was successfully transformed into NEB 5-alpha cells and grown on LB supplemented with kanamycin. One successful transformant of this plasmid was purified and used in the next steps to produce this strain.

5.5.1.2 Homologous recombination to insert GFP and *aph* downstream of AcrB

Using the plasmid produced in **5.5.1.1**, GFP and the *aph* cassette could be amplified from the plasmid using PCR, and the product recombined downstream of AcrB.

The forward oligonucleotide was designed such that the first 27 nucleotides had homology to AcrB with the stop codon removed, then the codon optimised poly-linker and 23 nucleotides of homology to GFP. The reverse oligonucleotide was designed with homology to the 3' end of the *aph* cassette and the non-coding region downstream of AcrB. GFP and *aph* were successfully amplified from the plasmid and confirmed by agarose gel electrophoresis (data not shown). The purified PCR product was then inserted chromosomally into SL1344 by homologous recombination. Successful insertion of GFP and *aph* was confirmed by growth on agar supplemented with kanamycin and 5 candidates were screened for insertion using PCR **(Figure 5-4)**. A DNA product was amplified using oligonucleotides with homology to *acrB* (forward) and *gfp* (reverse). Successful insertion of GFP downstream of *acrB* was shown in all 5 candidates which produced a 920 bp product.

All these products were then sequenced for further confirmation and the full sequence alignment for candidate 3 is shown in **Appendix III** . **Figure 5-5** shows the sequencing alignment to confirm that the codon-optimised poly-linker was successfully inserted. Amplification of a PCR product containing *gfp* and *aph* also further confirmed correct insertion.

One candidate (AcrB-GFP '3' with *aph*) was transformed with pCP20 for successful removal of the *aph* cassette which was confirmed by the inability of the strain to grow on kanamycin.

Figure 5-4 Agarose gel electrophoresis images to confirm successful insertion of GFP downstream of *acrB*

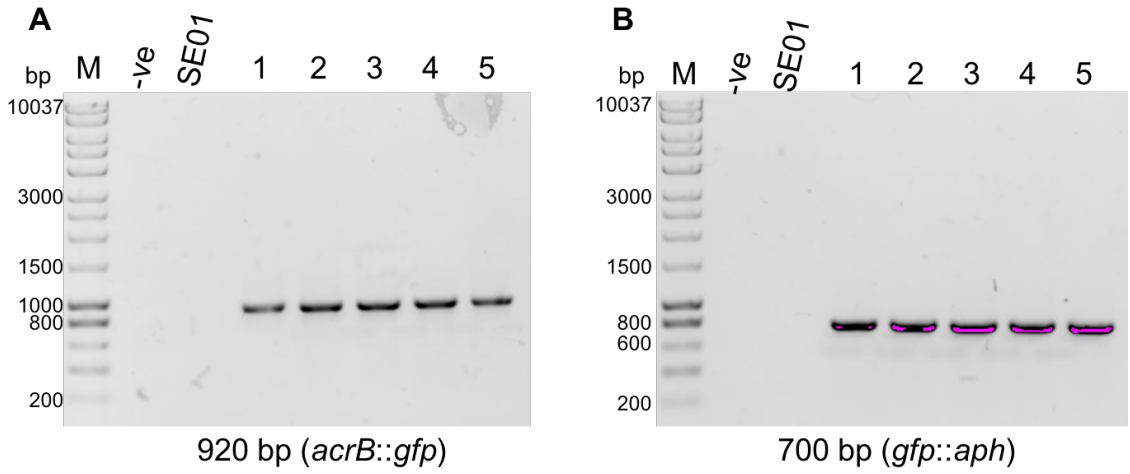

Both **(A)** and **(B)** was a negative control (-ve) where no DNA template was added and an SL1344 control (SE01) which should no amplify any DNA with the oligonucleotides used. **(A)** shows 920 bp bands for transductant strains 1-5 that amplified *acrB*, the polylinker and GFP. **(B)** shows 700 bp bands to confirm *aph* was successfully inserted into SL1344 along with GFP.

Figure 5-5 Gene alignment to show nucleotide sequence of the SL1344 AcrB-GFP candidate strain compared to SL1344

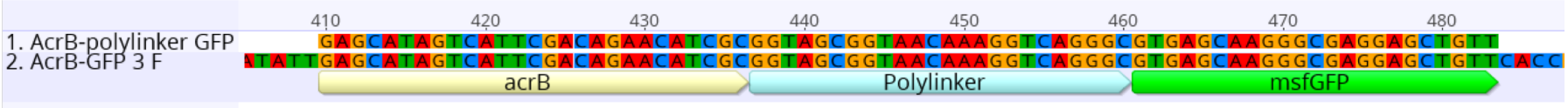

(1) labelled AcrB-polylinker-GFP is the reference strain based on the expected sequence with the correct codon optimised poly-linker. **(2)** labelled AcrB-GFP 3 F shows the 5' – 3' sequencing based on PCR amplification shown in **Figure 5-4.**The strain sequenced was candidate 3. This image was created using Geneious software.

5.5.2 C-terminal attachment of GFP to chromosomal AcrB does not affect the phenotype of SL1344

To confirm that this strain could be used to study the AcrB protein, it was first necessary to check that the insertion of GFP did not lead to a growth defect or that its attachment to AcrB did not interfere with efflux activity.

5.5.2.1 C-terminal GFP does not affect growth rate

To confirm that the GFP fusion did not affect the growth rate of SL1344, cultures were grown and the OD_{600} was measured every 20 minutes for 12 hours in LB **(Figure 5-6)**.

The generation times based on cell division were calculated for each strain and unpaired T-tests compared SL1344 to both SL1344 AcrB-GFP and SL1344 Δ*acrB* **(Table 5-1)**. SL1344 Δ*acrB* was used as a control as previously published data shows Δ*acrB* does not lead to a growth defect (Wang-Kan et al., 2017). None of the generation times were over 30 minutes nor were they significantly different from each other.

This shows that fusing GFP to the C-terminal end of AcrB does not confer a detectable growth defect.

Figure 5-6 Growth kinetics curve of SL1344, SL1344 Δ*acrB* and SL1344 AcrB-GFP.

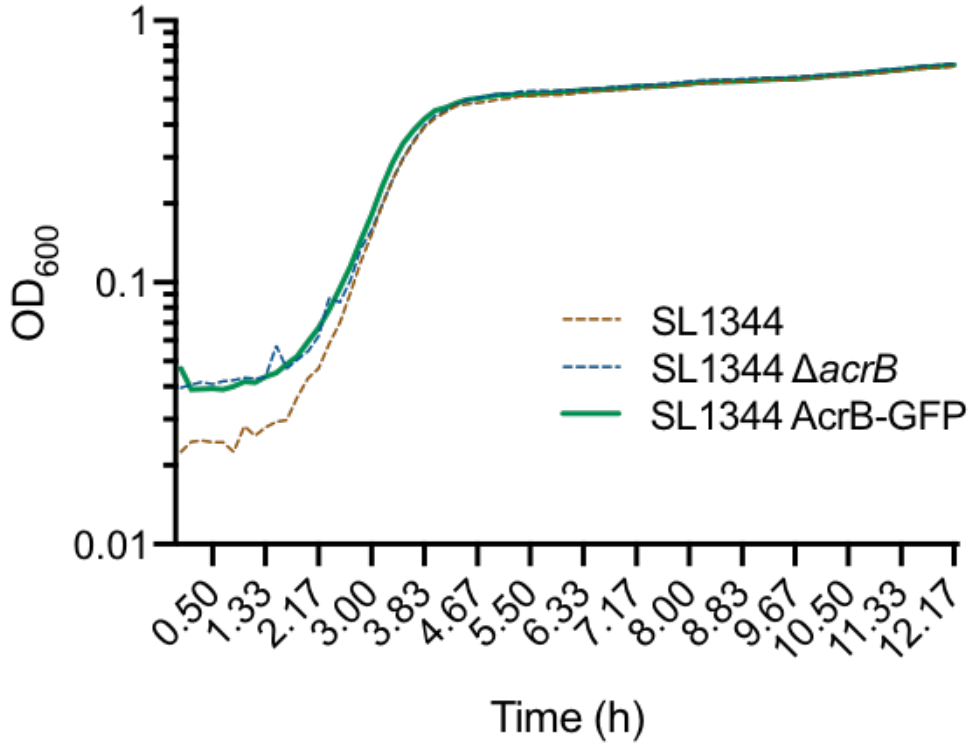

SL1344 (brown dashed), SL1344 Δ*acrB* (blue dashed) and SL1344 AcrB-GFP (green) were grown for 12 hours in LB. The OD_{600} value was measured every 30 minutes and plotted against time. These OD_{600} values were blank corrected by removing the OD_{600} values of LB from each strain. The data is the mean of 3 biological replicates for each strain and presented on a $\log_{10}$ scale.

Table 5-1 Generation times for SL1344, SL1344 Δ*acrB* and SL1344 AcrB-GFP in LB medium

Strain	Generation Time (minutes) (mean ± SD)	Significance (P-value) compared to SL1344
SL1344	27.347 ± 2.14	
SL1344 AcrB-GFP	30.047± 3.24	ns (0.4393)
SL1344 Δ*acrB*	28.507 ± 0.95	ns (0.2955)

5.5.2.2 C-terminal GFP does not impede efflux activity

It was also important to confirm that a protein fusion at the C-terminal end of AcrB did not interact or impede the function of export. This is because this strain would be used to study efflux and, inhibiting efflux by the positioning of GFP would confound any results and conclusions that could be made.

To analyse the effect on efflux, the efflux assay used previously was repeated, except this assay was done at a single growth time (mid-log). Like in **Section 5.4**, the time taken for EtBr fluorescence to drop 10%, 25% and 50% was measured. As shown in **Figure 5-7** and **Table 5-2**, SL1344 Δ*acrB* EtBr fluorescence takes significantly longer to decrease, when compared to SL1344. However, for each % drop in fluorescence, there was no significant difference in time taken for both SL1344 and SL1344 AcrB-GFP. This shows that the fusion of GFP to the C-terminus of AcrB does not alter efflux activity and could be used for further study.

Figure 5-7 Efflux capacity of SL1344, SL1344 Δ*acrB* and SL1344 AcrB-GFP in mid-exponential phase.

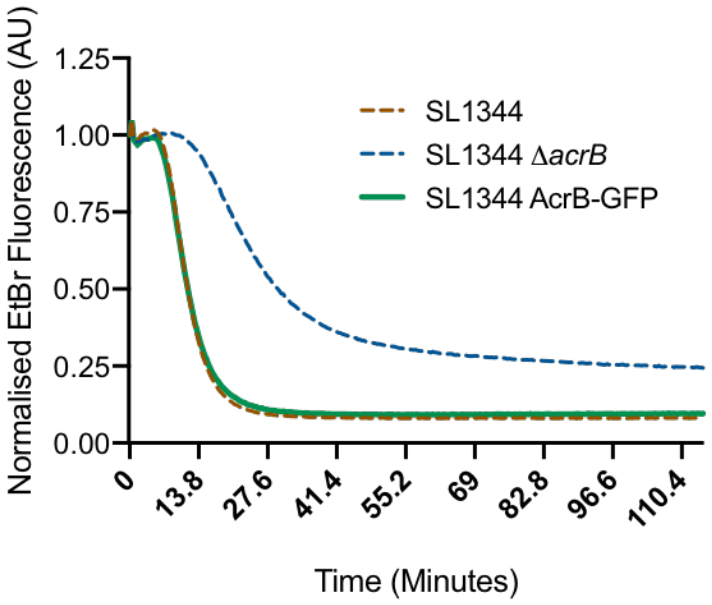

EtBr fluorescence was constantly measured for 114 minutes in SL1344 (brown dashed), SL1344 Δ*acrB* (blue dashed) and SL1344 AcrB-GFP (green). EtBr fluorescence values were normalised so that the first value read equaled 1. Data is based on 3 biological replicates for each strain.

Table 5-2 Statistical analysis of time taken for a drop in EtBr fluorescence

	Strain	Time for fluorescence drop (mean ± SD)	Significance (P-value) compared to SL1344
10% drop	SL1344	3.07 ± 0.38	
	SL1344 AcrB-GFP	2.69 ± 0.38	ns (0.2895)
	SL1344 Δ*acrB*	7.79 ± 1.90	Significant (0.0134)
25% drop	SL1344	4.73 ± 0.61	
	SL1344 AcrB-GFP	4.35 ± 0.22	ns (0.3596)
	SL1344 Δ*acrB*	11.75 ± 0.59	Significant (0.0001)
50% drop	SL1344	6.91 ± 0.69	
	SL1344 AcrB-GFP	6.77 ± 0.58	ns (0.8118)
	SL1344 Δ*acrB*	20.81 ± 1.25	Significant (<0.0001)

5.5.3 AcrB protein level remains constant across the growth curve

SL1344 AcrB-GFP was constructed to measure the level of AcrB present in a cell or population across growth. It was hypothesised that the level of protein within a cell would not increase in line with the increase in *acrAB* transcription at mid-exponential phase, but instead remain constant resulting in constant capacity to efflux EtBr and maintain low EtBr accumulation (**Section 5.4**).

5.5.3.1 Measuring the levels of GFP using flow cytometry and microscopy

Initially, the aim was to measure AcrB level using SL1344 AcrB-GFP in single cells by flow cytometry. However, the GFP signal from this *gfp* variant turned out to be too low to measure. It was not possible to collect GFP fluorescence using SYTO-84 to gate cells and measure GFP from this, using original flow cytometry settings that had previously been used to measure GFP, as described in **Section 2.3.3.3**. For this reason, the voltage through the BL1-H channel (for GFP) was increased, but GFP could still not be measured from this strain.

Another approach attempted was to measure AcrB levels in single cells using microscopy. Initially, confocal microscopy was used on live samples. However, in order see any GFP from cells required a 10 second exposure time. This meant that using a confocal laser photobleached cells beyond the field of view, making it difficult to consistently measure GFP fluorescence. A new approach was taken, namely to fix cells in formaldehyde after growth for 1, 3 and 5 hours, and take images to measure fluorescence using LED to achieve a GFP fluorescence emission. The

fluorescence signal was low and results too inconsistent to be considered quantitative.

To measure AcrB level using this strain at the single cell level would require a more powerful flow cytometer than the Attune NxT and a more powerful microscope than 100x LED phase microscopes, which were not available at the time.

5.5.3.2 Measuring AcrB protein level across the growth phase of an entire population of cells

As it had proved difficult to measure AcrB-GFP in single cells due to the GFP signal, AcrB-GFP was measured in a whole population of cells grown in MOPs minimal media, using a 96-well plate reader. For this assay, SL1344 autofluorescence was also measured and this was subtracted from the GFP fluorescence measured in SL1344 AcrB-GFP. The gain for GFP was set to account for the low signal.

Figure 5-8 shows the GFP fluorescence/OD_{600} over 16 hours of growth, with measurements recorded every 20 minutes. The GFP/OD_{600} value was used to correct for increase in cell density. It was clear that for the first 220 minutes of growth, GFP/OD_{600} was highly variable and spiked inconsistently (**Appendix IV**). However, until around 380 minutes, SL1344 AcrB-GFP was in lag phase in MOPs minimal media and therefore was not a reflection of AcrB level across the growth curve. Therefore, GFP/OD_{600} was then plotted starting from 300 minutes to remove the spikes at the beginning of lag, and the OD_{600} was also plotted to compare growth to the pattern of GFP/OD_{600}. From 300 to 500 minutes, the GFP/OD_{600} decreased, however +/- SEM was large. From around 600 minutes to the final 16 hours of growth, GFP/OD_{600} level remained constant.

The results here show that GFP level and therefore AcrB level is more varied in early exponential phase than stationary phase. The fluorescence decreased around 2-fold from 300 to 500 minutes, and it is possible that when cells are growing and dividing at their highest rate, new AcrB protein production in daughter cells may be at its lowest rate. However, AcrB protein level was relatively constant within a cell population across the growth curve, and does not correlate to the pattern of *acrAB* transcription. It may suggest that in an entire population of cells, AcrB level remains constant across growth and that a peak in transcription in mid-exponential phase is as a result of making new proteins in dividing cells so that protein level always does remain constant.

Figure 5-8 GFP/OD_{600} from SL1344 AcrB-GFP over 16 hours of growth in MOPs minimal media.

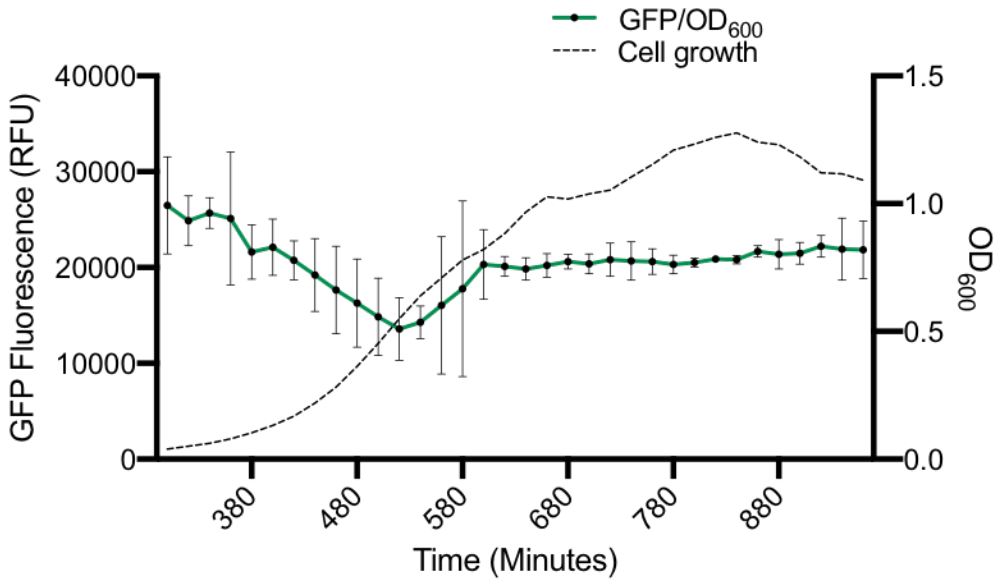

This graph shows GFP/OD_{600} from AcrB-GFP at the end of lag phase (300 minutes) until the last time point at 16 hours. The dashed black line shows the OD_{600} whereas the green line error bars +/- SEM shows GFP fluorescence. SL1344 autofluorescence was subtracted from this data.

5.5.4 Biased partitioning of AcrB to old cells poles could not be shown

The data above suggests that the average level of AcrB protein per cell remains relatively stable across growth and this leads to a constant ability to efflux substrates from the cell regardless of growth phase in WT.

One study described that the AcrAB-TolC protein had a strong partitioning bias for mother cell poles during cell division (Bergmiller et al., 2017). It is possible that transcription peaks in mid-exponential phase only due to requirement of new daughter cells to make new AcrAB protein. The study used a microfluidics channel to show AcrB biased partitioning (Bergmiller et al., 2017). To reproduce this finding and confirm this as the case for AcrB in *S.* Typhimurium, images of fixed cells undergoing binary fission were taken using microscopy **(Figure 5-9)**.

A dividing cell of SL1344 was shown to compare the difference between autofluorescence and AcrB-GFP. The dividing SL1344 cell in **Figure 5-9B** shows limited GFP fluorescence after 10 seconds of exposure. In both examples provided for SL1344 AcrB-GFP, it appears that GFP signal is strongest at the cell membrane and that fluorescence is not localised to one pole of the dividing cell. This result is qualitative, and higher resolution microscopy is required to confirm this result however it may suggest that AcrB does not localise at old cell poles in these conditions. It is possible that the previous result could be an artefact of the microfluidic system and AcrB may in fact be spread across the cell.

Figure 5-9 Representative microscope images of dividing SL1344 and SL1344 AcrB-GFP cells.

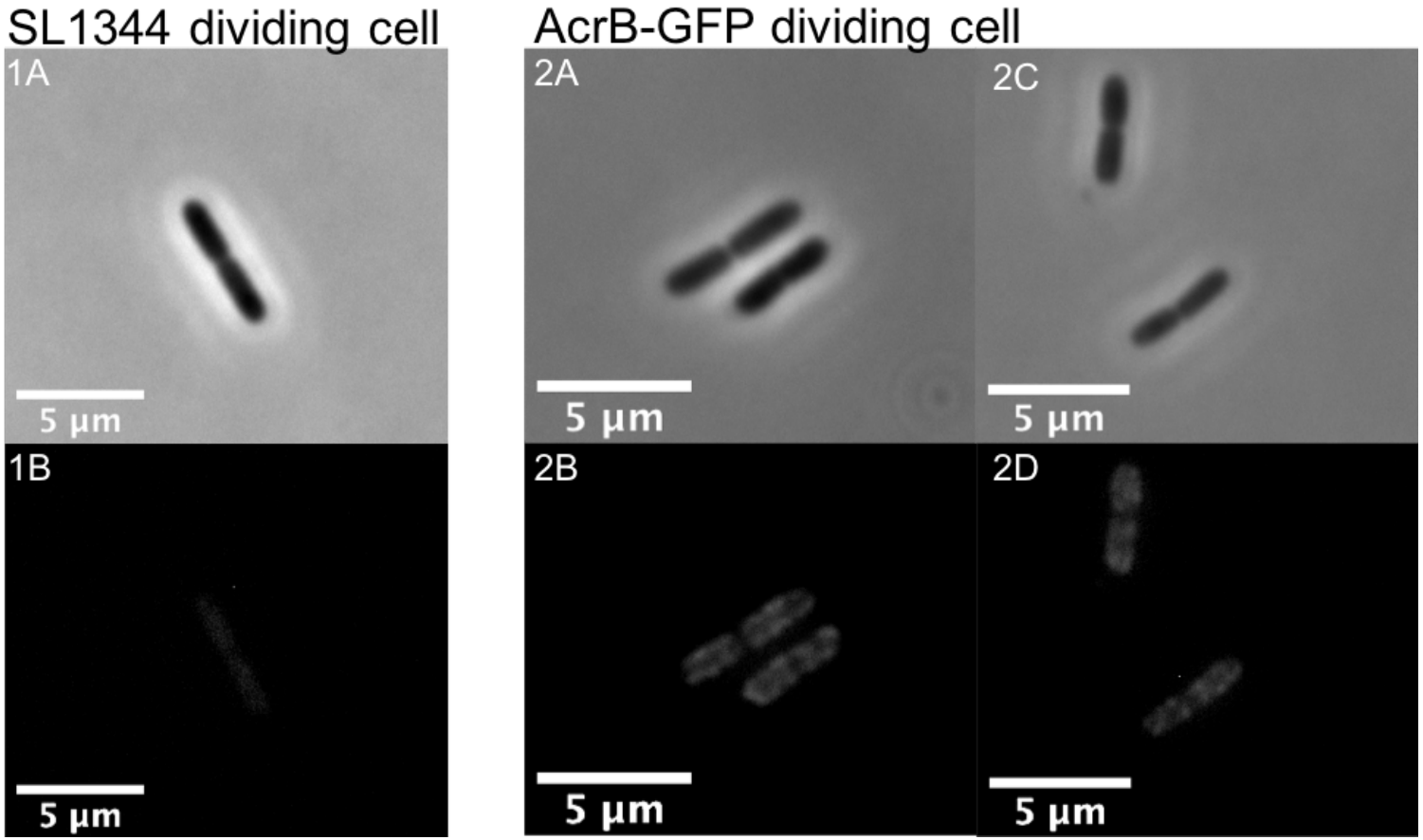

(**1**) show SL1344 producing no GFP, and were used as a control. (**2**) shows AcrB-GFP of which there are 2 representative examples. (1A,2A and 2C) show standard light DIC images of both strains. (1B,2B and 2D) show GFP fluorescence of the dividing cells of each strain. Images were taken with the Nikon AxioObserver and 100x oil objective.

5.6 Low accumulation in stationary phase is not due to the activity of other efflux pumps

In SL1344 Δ*acrB,* EtBr accumulation peaked at 1 hour as expected due to the loss of the pump, but in stationary phase, EtBr accumulation was as low as in SL1344. This suggests that the stationary phase phenotype is not as a result of AcrB protein. One hypothesis to explain this is that other efflux pumps may export EtBr in the absence of AcrB.

5.6.1 The removal of other efflux components maintains the same accumulation pattern as SL1344 Δ*acrB*

If other efflux pumps play a role in exporting EtBr from cells in stationary phase, then measuring EtBr accumulation in different efflux mutant strains should show an altered accumulation pattern.

The EtBr accumulation assay was repeated with SL1344 Δ*tolC,* a deletion that inhibits the efflux function of all RND pumps, and the ABC pump, MacAB-TolC. SL1344 was used as a control. **Figure 5-10A** shows that EtBr accumulation in SL1344 remained low as previously shown. In SL1344 Δ*tolC*, accumulation followed a similar pattern to that seen for the *acrB* mutant; EtBr accumulation peaked after 1 hour of growth and from 4 – 6 hours the EtBr accumulation level was not significantly different to SL1344. This suggests that the low EtBr accumulation in stationary phase is not due to any of the pumps that require TolC to function.

Figure 5-10 EtBr accumulation in SL1344 Δ*tolC* and Δ4PAP across growth.

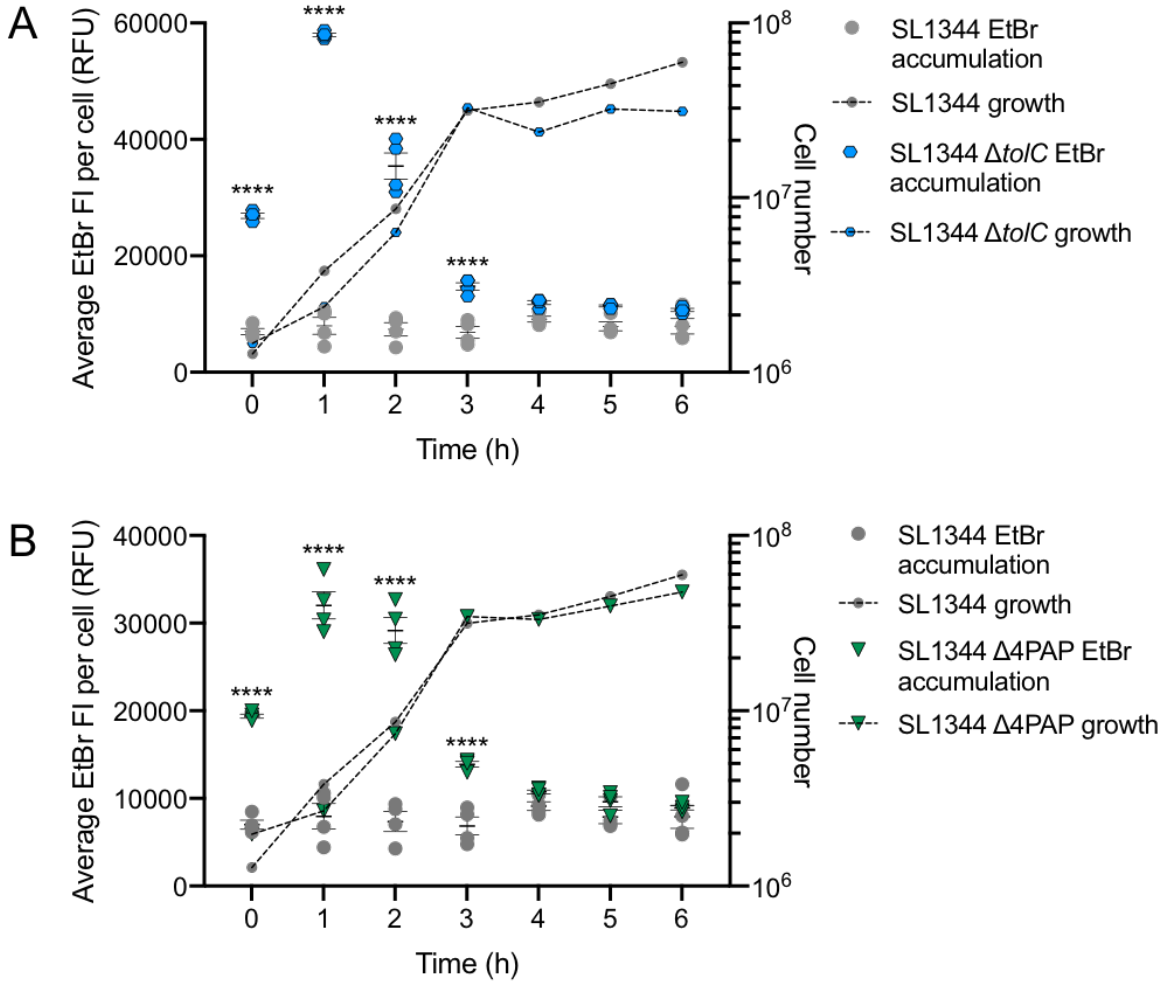

(A) shows SL1344 vs Δ*tolC*. Median EtBr fluorescence per cell in 10,000 SYTO-84$^+$ flow cytometry events was measured every hour between 0 and 6 hours. Individual grey circles (WT) and individual blue hexagons (Δ*tolC*) represent the median value of EtBr fluorescence within a biological replicate. **(B)** shows SL1344 vs Δ4PAP. Median EtBr fluorescence per cell in 10,000 SYTO-84$^+$ flow cytometry events was measured every hour between 0 and 6 hours. Individual grey circles (WT) and individual green triangles (Δ4PAP) represent the median value of EtBr fluorescence within a biological replicate. 4 biological replicates for each strain are shown, with a short mean bar and SEM error bars. EtBr accumulation is plotted on the left Y-axis. Calculated cell number values were plotted on the right Y-axis with corresponding symbols equating to strain and a dashed line to show growth of the culture. Cell numbers were based on the mean of the same biological replicates and the same gated population that EtBr fluorescence was measured from. Two-way ANOVA and Sidak's multiple comparisons test were used for statistical analysis.

To further confirm that no other RND pumps were causing low EtBr accumulation in stationary phase, EtBr accumulation was measured in an SL1344 strain that had all the RND PAPs removed, named ∆4PAP, meaning the 5 RND pumps do not function. EtBr accumulation peaked at 1 hour, and had high accumulation at 2 hours of growth **(Figure 5-10B)**. After 3 hours of growth, EtBr accumulation started to drop and by 4 to 6 hours, the EtBr accumulation level was not significantly different from SL1344. This shows that other RND pumps are not responsible for the export of EtBr in stationary phase, either in SL1344 or in the absence of AcrB.

Together, these results show that RND pumps and the ABC pump, MacAB-TolC, do not contribute to low EtBr accumulation in stationary phase. If they did, EtBr accumulation would have been high in the absence of the pump function.

5.6.2 Inhibiting efflux with CCCP leads to a decrease in EtBr accumulation in stationary phase

The EtBr accumulation patterns in the efflux mutants described in **Section 5.6.1** could not rule out that members of the MFS and MATE pumps, EmrA, MdtK or MdfA, were exporting EtBr. These remaining pumps, like RND pumps, use the PMF as an energy source for the export of substrates. Every pump, with the exception of the ABC pump, MacAB-TolC, are inhibited by the addition of PMF inhibitor, CCCP.

To investigate the role of all PMF-dependent efflux pumps on EtBr accumulation, EtBr accumulation was measured at each time point in SL1344 and ∆*acrB*, when CCCP had been added to samples. CCCP was not added to growing culture, only to samples being prepared for flow cytometric analysis. **Figure 5-11A** shows that, as

previously, SL1344 EtBr accumulation remained low across growth. When samples were incubated with 100 μM CCCP, the EtBr accumulation pattern changed. Addition of CCCP to the SL1344 samples gave a broadly similar pattern to deletion of AcrB. In the presence of CCCP, EtBr accumulation peaked at 1 hour with a 9-fold increase ($p < 0.0001$). These data points can initially be compared to previous EtBr accumulation patterns shown in all efflux mutants. The EtBr accumulation decreased after 2 hours, into stationary phase, showing a similar pattern that had previously been shown in the absence of AcrB. It was unexpected that EtBr accumulation, although lower, remained significantly different from SL1344. This might suggest that the remaining efflux pumps not tested in the previous section may play a minor role in EtBr export in stationary phase. However, the remaining efflux pumps clearly are not the major factor responsible for the low EtBr, as the accumulation level did not dramatically change to the levels shown at 1 hour.

The experiment with the addition of CCCP was repeated in SL1344 Δa*crB*. It was shown that there was no significant difference in EtBr accumulation in the absence or presence of CCCP in culture after it had been grown for 1 hour (**Figure 5-11)**. This suggests that in early exponential phase, AcrB is fundamental for the level of EtBr accumulation. As previously shown, EtBr accumulation in SL1344 Δa*crB* drops to SL1344 levels in stationary phase, and this was also shown in the presence of CCCP. The combined effect of inactivating efflux and inhibiting the PMF did not did not massively alter the accumulation phenotype of SL1344 Δa*crB.* However, EtBr accumulation was significantly different from SL1344 Δa*crB*, as with SL1344. Although unlikely, this result may also suggest that other efflux pumps that require the PMF, may export EtBr in stationary phase.

Figure 5-11 EtBr accumulation of SL1344 and SL1344 Δ*acrB* in the presence of CCCP over 6 time points.

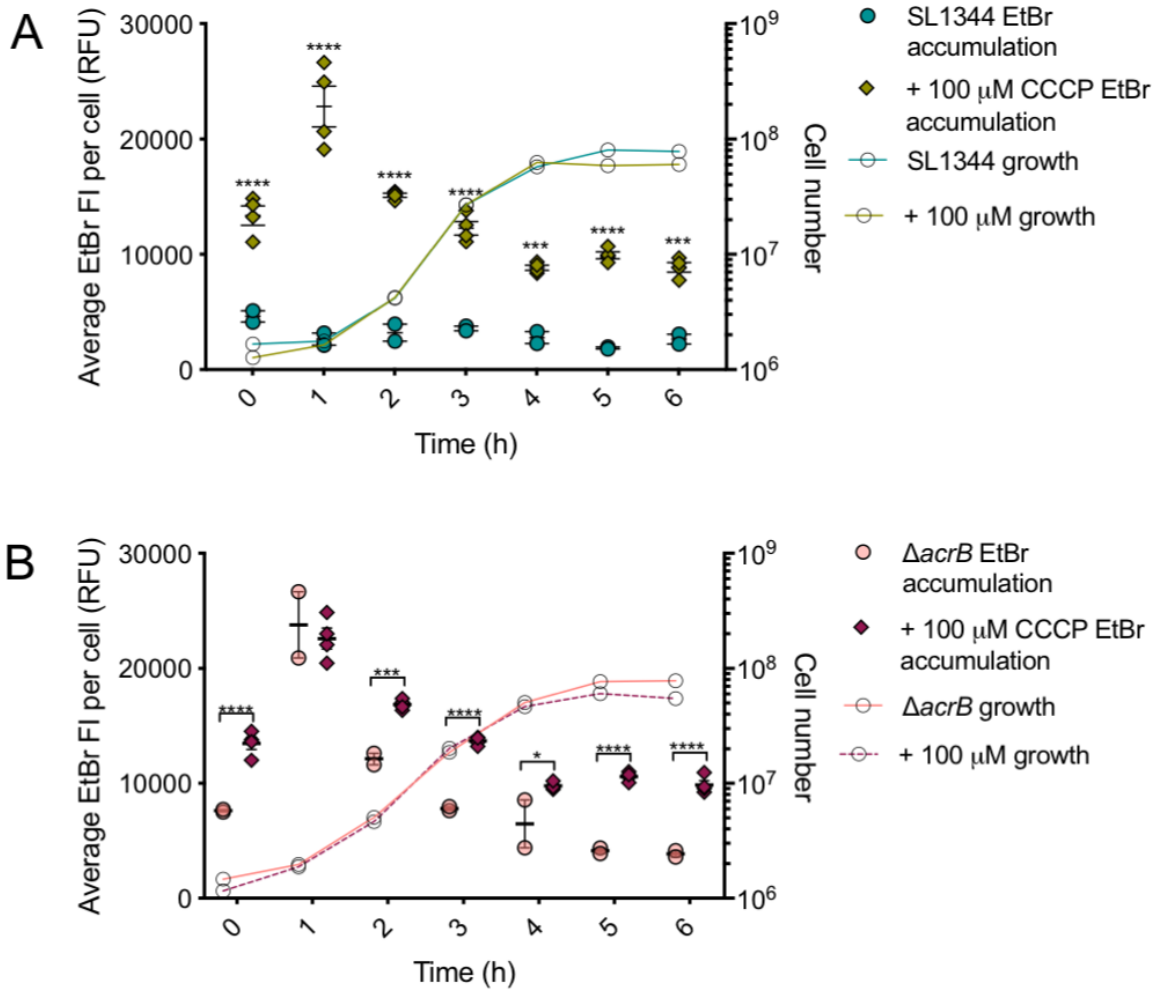

(A) shows SL1344 vs SL1344 + 100 μM CCCP**.** Median EtBr fluorescence per cell in 10,000 SYTO-84$^+$ flow cytometry events was measured every hour between 0 and 6 hours. Individual green circles (WT) and individual green diamonds (+ CCCP) represent the median value of EtBr fluorescence within a biological replicate. **(B)** shows SL1344 Δ*acrB* vs Δ*acrB* + CCCP. Median EtBr fluorescence per cell in 10,000 SYTO-84$^+$ flow cytometry events was measured every hour between 0 and 6 hours. Individual pink circles (Δ*acrB*) and individual red diamonds (Δ*acrB* + CCCP) represent the median value of EtBr fluorescence within a biological replicate. 2 biological replicates for the control strains are shown, and 4 replicates for those with CCCP, with a short mean bar and SEM error bars. EtBr accumulation is plotted on the left Y-axis. Calculated cell number values were plotted on the right Y-axis with corresponding symbols equating to strain and a dashed line to show growth of the culture. Cell numbers were based on the mean of the same biological replicates and the same gated population that EtBr fluorescence was measured from. Two-way ANOVA and Sidak's multiple comparisons test were used for statistical analysis.

This data suggests that high EtBr accumulation in SL1344 Δ*acrB* at 1 hour, is due to the loss of the pump. It can be hypothesised that low EtBr accumulation in actively growing cells is dependent of the activity of efflux pumps. It is also clear that inhibiting the PMF has less of an effect on EtBr accumulation in stationary phase cells, since the accumulation level decreases, and is similar to the SL1344 EtBr accumulation level. However, this result could not completely rule out the activity of PMF driven pumps in stationary phase due to the significant difference in EtBr accumulation in stationary phase, with the addition of CCCP. By measuring transcription in the preceding section, it will show the importance of the other efflux pumps in stationary phase.

5.6.3 Transcription levels suggest accumulation levels are efflux-dependent in stationary phase.

Although tightly regulated, *acrAB* expression is high when grown in laboratory media, as previously shown in **Figure 4-3**. Expression of other efflux pumps is tightly regulated, and often requires specific inducers for expression when grown in laboratory medium. For example, *acrEF* expression has been shown in *S.* Typhimurium when H-NS is deleted in a Δ*acrAB* strain (Nishino et al., 2009a).

If other pumps are partially responsible for accumulation patterns seen in stationary phase, then expression of these pumps would need to increase. Therefore, transcription of these pumps was measured across growth.

Transcription was measured using pMW82 plasmids, where the promoter of each efflux pump was fused to GFP. Therefore, the efflux gene promoter activity was

driving the transcription and production of GFP protein. The OD_{600} and GFP fluorescence were measured for 12 hours in MOPs minimal media for 18 strains, both SL1344 and SL1344 Δ*acrB* containing pMW82-*acrA,* pMW82-*acrE,* pMW82-*acrD,* pMW82-*mdsA,* pMW82-*mdtA,* pMW82-*mdfA,* pMW82-*mdtK,* pMW82-*emrA* and pMW82-*macA. Salmonella* autofluorescence was measured and subtracted from the fluorescence produced from each strain.

Figure 5-12A shows that transcription of *acrAB* peaks in mid-exponential phase. This matches the pattern produced by the flow cytometry assay shown in **Figure 4-3**. The other RND pumps in SL1344, *acrE, acrD, mdsA* and *mdtA* were not transcribed during the 12 hours of growth. In this experiment, the deletion of *acrB* did not lead to compensatory transcription of the other RND pumps **(Figure 5-12B-E)**. This may explain why inhibiting the activity of the other RND pumps with CCCP or through gene deletion in SL1344 had no effect on EtBr accumulation. These RND pumps are tightly regulated and may not be transcribed in normal growth medium, but rather under specific environmental conditions.

Figure 5-12 Transcription profiles of each efflux pump in SL1344 over 12 hours of growth.

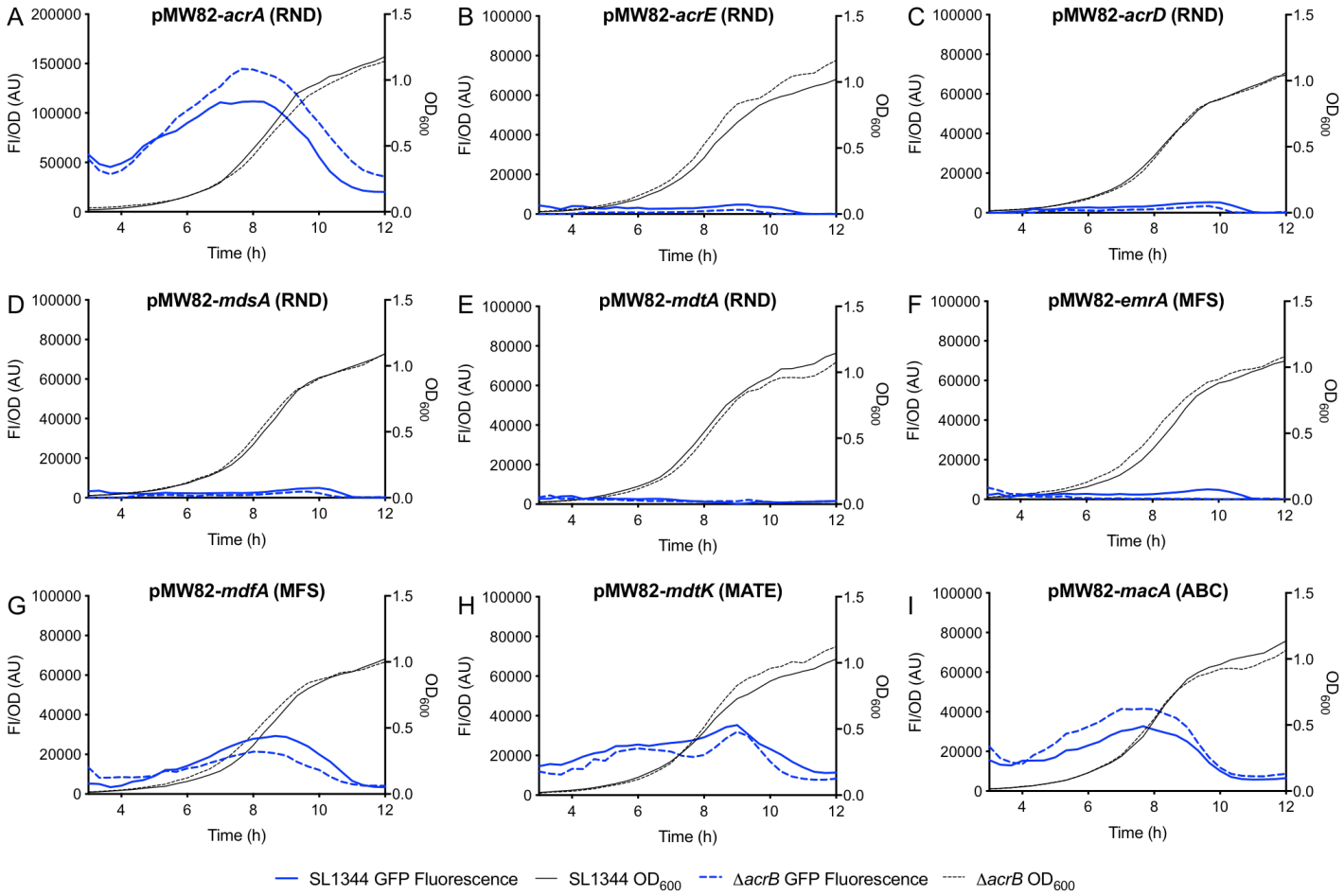

In the following graphs **A-I**, the GFP/OD_{600} and therefore transcription of each pump is represented as a solid blue line (SL1344) or a dashed blue line (Δ*acrB*). The OD_{600} was also plotted and shown as a solid black line (SL1344) or a dashed black line (Δ*acrB*). Each graph represents the fluorescence of a different transcriptional reporter: (**A**) *acrA*, (**B**) *acrE*, (**C**) *acrD*, (**E**) *mdsA*, (**D**) *mdtA*, (**F**) *emrA*, (**G**) *mdfA*, (**H**) *mdtK* and (**I**) *macA*.

EmrA and MdfA are MFS efflux pumps in SL1344. Here, it was shown that there was no transcription of *emrA* under these growth conditions therefore showing that low EtBr accumulation in stationary phase is not EmrA dependent **(Figure 5-12F)**. The MFS pump, *mdfA* did however show GFP fluorescence with a peak equivalent to mid-exponential phase **(Figure 5-12G)**. A similar transcription result was seen with *mdtK* (MATE) with a peak at 9 hours and *macA* with a peak at 8 hours **(Figure 5-12H-I)**. Therefore, each of the pumps that are transcribed in normal growth media peak in mid-exponential phase. It was also important to note that the GFP/OD_{600} for *acrAB* transcription peaked at around 100,000 whereas the other 3 pumps have peaked at GFP/OD_{600} values around 30,000. This shows that although transcribed, they are less abundant than AcrAB-TolC and it is unlikely they play a large role in EtBr accumulation in stationary phase.

This suggests that other pumps are not involved in EtBr accumulation in stationary phase, and it can be hypothesised that low EtBr accumulation in SL1344 in stationary phase is efflux independent.

5.7 Discussion

In the previous chapter, it was shown that *acrAB* transcription in SL1344 peaks in mid-exponential phase and did not correlate to EtBr accumulation. It was previously hypothesised that an increase in transcription in mid-exponential phase, would lead to an increase in AcrB protein in the same phase and therefore increased efflux capacity. However as this was disproved, it was then hypothesised that efflux activity in stationary phase relates to level of protein.

Here, it was shown that efflux could function regardless of growth phase, which may explain why, in SL1344, EtBr accumulation remains low across growth. In 2016, it was shown that AcrA and AcrB have a long half-life, about 6/7 days (Chai et al., 2016). This data suggests that AcrAB-TolC is present within cells in stationary phase and can export EtBr in all growth phases. It was also found that stability of the AcrAB protein did not depend on efflux activity but instead, on the presence of AcrA (Chai et al., 2016). It can be hypothesised that AcrAB is constantly anchored within the IM regardless of growth phase, and does not become degraded if not used. This would explain why EtBr may be exported from cells in all growth phases, but does not explain why EtBr accumulation remains low in stationary phase in the absence of AcrB.

Using SL1344 AcrB-GFP, it was shown that AcrB protein level remains constant in stationary phase, under normal growth conditions. Measuring AcrB protein level by western blot (using a strain of SL1344 where AcrB is his tagged) is part of further work to confirm that the result produced by the GFP strain is consistent. The question remained why transcription of *acrAB* peaks in mid-exponential phase if protein remains constant across growth. In 2017, it was shown that AcrB protein undergoes biased partitioning in which AcrB accumulates at old cell poles during binary fission and therefore is only present in the parent rather than the daughter cell (Bergmiller et al., 2017). This information led to the development of the hypothesis that the peak in *acrAB* transcription in mid-exponential phase is due to the need to produce new AcrB protein in new daughter cells that have not inherited existing AcrB protein. Transcription drops in stationary phase as each cell within the population has AcrB protein with a long half-life. In this chapter, it was not possible to show AcrB localising

to old cell poles in free media using microscopy. It is possible that biased partitioning is as an effect of using a microfluidic device as differences to normal growth media conditions have been described (Yang et al., 2018). However, biased partitioning may not have been identified due to limitations in microscopy here. Future work would include optimising an assay to measure GFP more consistently using microscopy and identifying any localisation. The succinimidyl ester, Texas red, is a fluorescent membrane reagent which localises to the poles of cells (de Pedro et al., 2004). Using a pulse-chase experimental set-up (Zupan et al., 2013), bacteria may be stained with Texas Red, and cultures left to grow meaning that only old cell poles which had been originally stained would fluoresce with Texas Red. Used together with SL1344 AcrB-GFP, it may confirm that AcrB localises at old cell poles but also that new AcrB protein is made in daughter cells.

Although it can be hypothesised that AcrB is present across all growth phases to a constant level, this does not explain why EtBr accumulation in the absence of AcrB is low in stationary phase. It may suggest low EtBr accumulation depends on a mechanism other than efflux.

Measuring efflux activity of SL1344 Δ*acrB* after 1,3 and 5 hours of growth suggested there was still some efflux activity in the absence of AcrAB-TolC function and this was explored further. To completely rule out that efflux pumps were involved in low EtBr accumulation in stationary phase, EtBr flow cytometry assays were repeated using SL1344 Δ4PAP and SL1344 Δ*tolC*. The EtBr patterns still maintained low EtBr accumulation in stationary phase confirming that the RND pumps in SL1344 played no role in accumulation in stationary phase. Previously it has been shown that

AcrAB-TolC was the major efflux pump in *S.* Typhimurium, with deletion of AcrF and AcrD having little effect on MICs of clinically relevant drugs (Piddock, 2006). In a study where all RND pumps were removed in *S.* Typhimurium, it was also shown that by removing AcrB there was a reduction in MIC of EtBr, but no change of MIC when removing any other RND pump (Nishino et al., 2006). Transcription of these RND pumps under normal growth conditions using the pMW82 reporters was shown to be limited in all growth phases. Previous studies have shown that *S.* Typhimurium's suite of RND pumps are tightly regulated and are only expressed in the presence of specific inducers. AcrEF is H-NS silenced (Nishino et al., 2009a) but AcrAD and MdtABC is induced by indole, zinc or copper (Nishino et al., 2007) and MdsABC is induced in the presence of gold (Pontel et al., 2007, Song et al., 2015). Data presented here suggests that no RND pumps in *S.* Typhimurium significantly alter EtBr accumulation level in stationary phase.

The EtBr accumulation pattern in Δ*tolC* confirmed that the ABC, MacAB-TolC was also not responsible for the export of EtBr in stationary phase. This pump has only be shown to export macrolides (Kobayashi et al., 2001), enterotoxin (Yamanaka et al., 2008), protoporphyrin (Turlin et al., 2014) and linearised enterobactin (Bogomolnaya et al., 2020) and would explain why this pump plays no role in EtBr accumulation.

Using CCCP, EtBr accumulation in the absence MdfA, MdtK and EmrA function was also measured. Importantly, the EtBr accumulation pattern of SL1344 in the presence of CCCP remained similar to the pattern of SL1344 Δ*acrB*. This suggested that all efflux pumps in SL1344 were not the key drivers of low EtBr accumulation in

stationary phase, and that another mechanism contributes to low EtBr accumulation. However, the significant difference between SL1344 and SL1344 + CCCP in EtBr accumulation added to the complexity of this set of results. It is possible that other PMF dependent efflux pumps are important for maintaining low EtBr accumulation in stationary phase. The efflux pump, EmrAB, exports EtBr and CCCP (Lomovskaya et al., 1995). CCCP induces transcription of *emrAB* (Xiong et al., 2000), therefore It is possible that CCCP induces the activity the pump, however, with 10 minutes of incubation with CCCP, it is unlikely. It is also important to note that CCCP does not simply inhibit efflux. As it inhibits the PMF, it also inhibits more cell processes that require the PMF, such as motility, but also acts as an inhibitor of oxidative phosphorylation and ATP synthesis (Rottenberg and Steiner-Mordoch, 1986). Therefore, it is more unlikely that the small difference in EtBr accumulation is simply as a result of inhibiting efflux function. The transcription of *mdfA* and *mdtK* peaked at mid-exponential phase, like *acrAB*, but to a much lower extent and was therefore still difficult to confirm that they did not play a role in EtBr accumulation. MdfA has previously been shown to export EtBr in *E. coli* (Nishino and Yamaguchi, 2001). Further work here would include measuring EtBr accumulation in range of strains that contained a single knockout of each efflux pump or identifying specific inhibitors to each pump.

Taken together this data suggests that efflux is only important in maintaining low drug accumulation in actively growing cells.

5.8 Key Findings

- AcrB protein level and efflux activity are constant regardless of growth phase and do not correlate to *acrAB* transcription.
- *mdtK*, *mdfA* and *macAB* are the only other antibiotic exporting pumps in *S.* Typhimurium that have transcriptional activity in normal laboratory media.
- Deleting other efflux components or adding inhibitors does not change the overall accumulation pattern.
- Although AcrB protein level is constant, EtBr accumulation is still low in stationary phase and this is not caused by EtBr export from efflux pumps.

Chapter 6- Outer Membrane Permeability explains low accumulation in Stationary Phase

6.1 Background

Data from previous chapters suggest that across growth, EtBr accumulation levels do not correlate with *acrAB* transcription, and that low EtBr accumulation is dependent on AcrAB-TolC in actively growing cells only. Data presented in **Chapter 5** shows that in stationary phase, low EtBr accumulation is independent of efflux. One hypothesis to explain this is that the low accumulation in stationary phase may instead be due to decreased permeability of the OM.

Finding methods to measure permeability of *S.* Typhimurium to EtBr in this study was not straightforward. Some studies use EtBr as a probe for outer membrane permeability (Miki and Hardt, 2013), however, as EtBr is a substrate of the AcrAB-TolC pump (Paixao et al., 2009, Blair and Piddock, 2016), it cannot effectively be used as a probe when analysing strains lacking components of AcrAB-TolC. For this reason, the level of EtBr within the cell is based on how much gets into the cell, as well as how much is removed (i.e. accumulation) and does not measure permeability alone. Another dye commonly used to measure permeability is 1-N-phenylnaphthylamine (NPN) (Muheim et al., 2017). However, NPN is also an efflux pump substrate (Misra et al., 2015) and is not suitable for assessing the balance between influx and efflux in this study.

There is little information about how EtBr enters cells. Some studies suggest that EtBr cannot enter through intact Gram-negative cell membranes (Miki and Hardt, 2013, Aeschbacher et al., 1986), however it has been extensively studied and used as an efflux substrate without having to damage the cell envelope. It is more likely that EtBr can enter cells but that accumulation level is a balance between influx and efflux (Paixao et al., 2009). Porins are channels which allow entrance of several small hydrophilic compounds into the cell and it is possible that EtBr may enter through these protein channels. Porins in Gram-positive *Mycobacterium smegmatis* allow the entrance of EtBr into cells (Rodrigues et al., 2011). It has also been suggested that EtBr just enters cells through passive diffusion (Paixao et al., 2009). Permeabilising the cell with EDTA or polymyxin, which displaces divalent cations, also allows the entrance of compounds into the cell (Hancock and Bell, 1988).

There are a number of studies which describe changes in the cell envelope during stationary phase (previously described in **Chapter 1**), however, an integrated overview of how bacterial cell membranes change is lacking. Outer membrane changes include a decrease in the overall concentration of membrane proteins (Allen and Scott, 1979) and an increase in lipoprotein bound to peptidoglycan (Wensink et al., 1982) to strengthen the outer barrier. In the IM, the composition of fatty acids changes with a decrease in monounsaturated fatty acids (El-Khani and Stretton, 1981) and an increase in cyclopropane fatty acids, catalysed by *cfa* (Grogan and Cronan, 1997). Increased layers of peptidoglycan have also been described in stationary phase (Mengin-Lecreulx and van Heijenoort, 1985).

Mitchell et al. (2017) showed that the cell envelope was less permeable in stationary phase via RpoS-dependent mechanisms. Using the detergent, SDS, they showed that AcrAB-TolC was responsible for SDS resistance in actively growing cells, but not in stationary phase. However, in a carbon-limited environment, AcrAB-TolC had no impact on SDS resistance, but SDS resistance was dependent on *rpoS*. This study strengthens the hypothesis that low EtBr accumulation in stationary phase is due to a strengthening of the membrane barrier leading to reduced permeability.

6.2 Hypothesis

The hypothesis is that low EtBr accumulation in stationary phase is efflux-independent and due to decreased permeability.

6.3 Aims

1. To measure EtBr accumulation in porin mutants and show whether they play a role in EtBr accumulation and if EtBr enters cells through porins.
2. To determine whether the strength of the permeability barrier changes in stationary phase.
3. To measure EtBr accumulation in the absence of RpoS to analyse its importance in low accumulation.

6.4 EtBr does not enter Gram-negative bacteria through porins

There is no consensus in the literature concerning how EtBr enters Gram-negative bacterial cells. Porins are implicated in the development of AMR (Nikaido, 1989), and also a porin in *Mycobacterium* has been shown to import EtBr (Rodrigues et al., 2011). For this reason, it was hypothesised that downregulation of porins may play a role in membrane permeability for influx of EtBr in stationary phase. *S.* Typhimurium has a number of major and minor porins. The major porins, OmpC and OmpF were analysed due to their involvement in the development of AMR.

6.4.1 Removal of major porins in SL1344

Major porins, OmpC and OmpF were deleted from SL1344 and SL1344 Δ*acrB* using the homologous recombination method (Datsenko and Wanner, 2000). The following strains were made: SL1344 Δ*ompC,* SL1344 Δ*ompF,* SL1344 Δ*ompC* Δ*ompF,* SL1344 Δ*acrB* Δ*ompC,* SL1344 Δ*acrB* Δ*ompF* and SL1344 Δ*acrB* Δ*ompC* Δ*ompF*. An *aph* cassette was inserted into the *ompC* and *ompF* genes in each strain by homologous recombination using lambda red recombinase encoded on pSIM18 (Chan et al., 2007), as previously described. Presence of the *aph* cassette was confirmed by growth on kanamycin and PCR for the *aph* gene. Removal of the pSIM18 plasmid was confirmed by the inability to grow on hygromycin. PCR was used to amplify *ompC::aph* and *ompF::aph* and amplimers were sequenced to confirm correct insertion.

The *aph* cassette was removed with pCP20 and the loss confirmed by lack of growth on ampicillin and PCR amplification and sequencing to confirm gene deletion. Strains with *ompC* and *ompF* deleted produced 300 bp and 367 bp products respectively (**Figure 6-1**).

Figure 6-1 Agarose gel image to confirm deletion of porins from SL1344

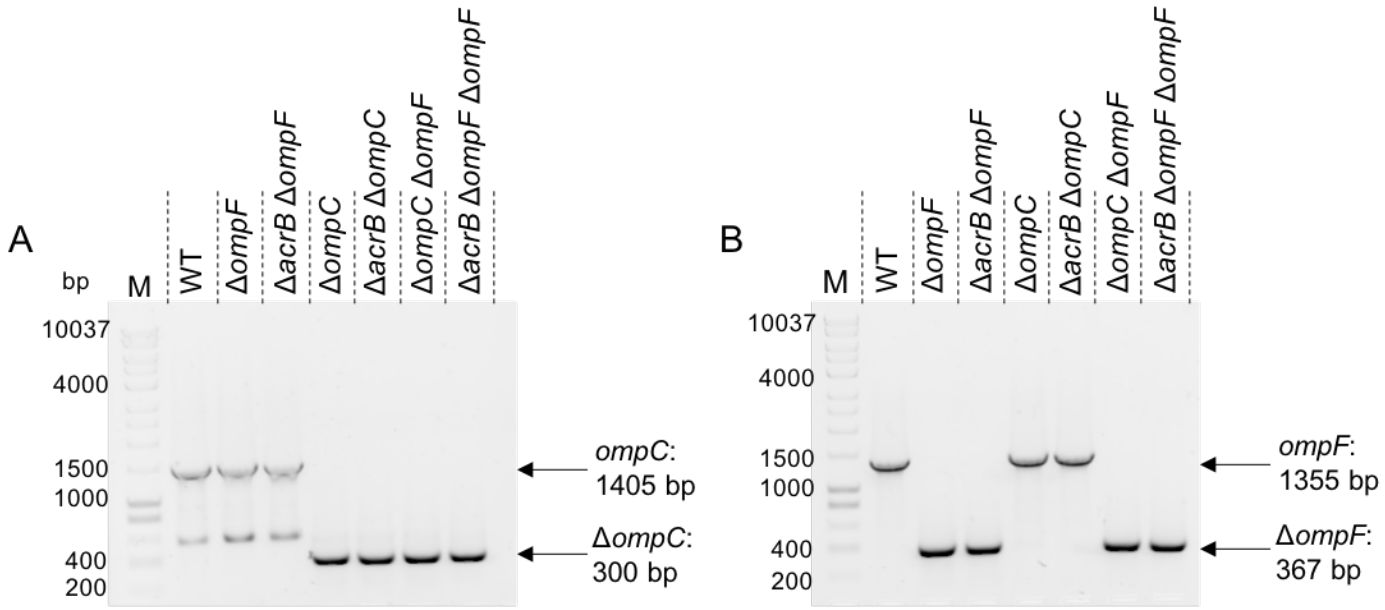

Both **A + B** show images from gel electrophoresis. PCR products have been separated and DNA bands shown for each strain. (**A**) using oligonucleotides with homology up and down stream of the *ompC* gene, DNA was separated to confirm the deletion of *ompC* in each strain. In those strains where *ompC* was not deleted, the product size was 1405bp. Strains containing Δ*ompC* had a product size of 300 bp. (**B**) using oligonucleotides with homology up and down stream of the *ompF* gene, DNA was separated to confirm the deletion of *ompF* in each strain. In those strains where *ompF* was not deleted, the product size was 1355bp. Strains with Δ*ompF* had a product size of 367 bp.

6.4.2 The deletion of porins does not alter the EtBr accumulation pattern

It was hypothesised that when the major porins of SL1344 were deleted, EtBr accumulation would decrease in stationary phase as the lack of porins would prevent access of the dye.

Alongside measuring EtBr accumulation, the cell numbers of each strain were analysed to show that there was no growth defect accompanied with the deletion of porins and growth phases are entered at the same time for each strain (**Figure 6-3**).

SL1344 was compared to Δ*ompC*, Δ*ompF* and Δ*ompC* Δ*ompF* **(Figure 6-2A)**. There was no significant difference in accumulation level between all strains at each time point. This suggested that EtBr does not enter bacterial cells through the major porins, OmpC or OmpF. These strains were also compared for EtBr accumulation when AcrB was deleted **(Figure 6-2B)**. As common to the phenotype, accumulation peaked at 1 hour and dropped as bacterial cells entered stationary phase. An increase in EtBr accumulation was seen in SL1344 Δ*acrB* Δ*ompC* Δ*ompF* and at 2 hours, EtBr accumulation was significantly higher than SL1344 Δ*acrB* with a p-value of 0.0226. In 2019, a study showed that deleting porins may in fact damage the membrane leading to increased permeability, and the data presented here would also suggest that (Choi and Lee, 2019).

Figure 6-2 EtBr accumulation in WT and Δ*acrB* compared to porin mutant strains

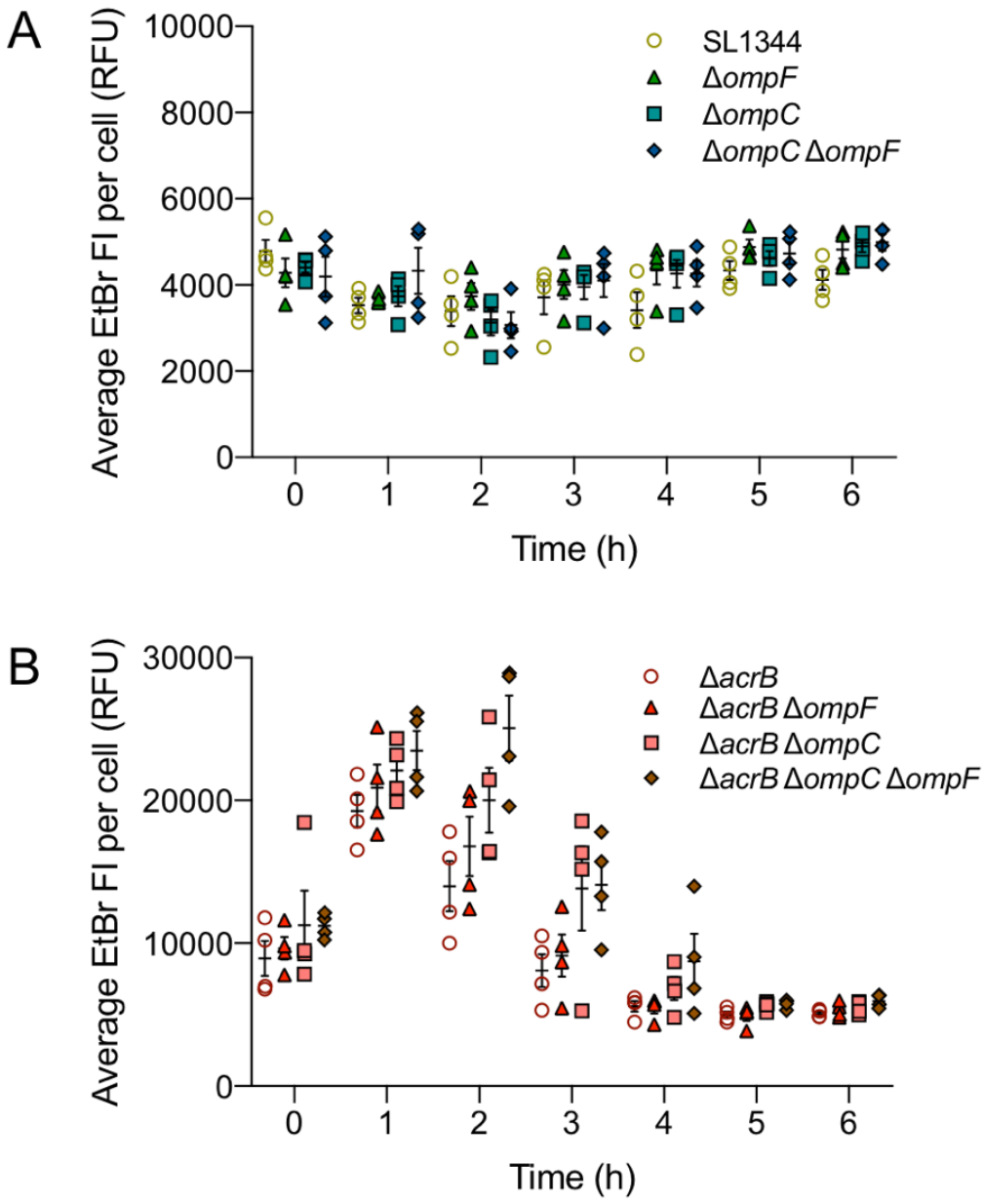

(A+B) 4 biological replicates for each strain are shown, with a short mean bar and SEM error bars. EtBr accumulation is plotted on the left Y-axis **(A)** shows SL1344 WT (individual green dots) vs Δ*ompF* (green triangles), Δ*ompC* (green square) and Δ*ompC* Δ*ompF* (blue diamonds)**.** Median EtBr fluorescence per cell in 10,000 SYTO-84^{+} flow cytometry events was measured every hour between 0 and 6 hours. Individual symbols represent the median value of EtBr fluorescence within a biological replicate. **(B)** shows SL1344 Δ*acrB* (red dots) vs Δ*acrB* Δ*ompF* (red triangles), Δ*acrB* Δ*ompC* (pink square) and Δ*acrB* Δ*ompC* Δ*ompF* (red diamonds)**.** Median EtBr fluorescence per cell in 10,000 SYTO-84^{+} flow cytometry events was measured every hour between 0 and 6 hours. Individual symbols represent the median value of EtBr fluorescence within a biological replicate. A two-way ANOVA and Dunnett's multiple comparison test were used for statistical analysis.

Figure 6-3 Growth curves for SL1344 compared to porin mutant strains

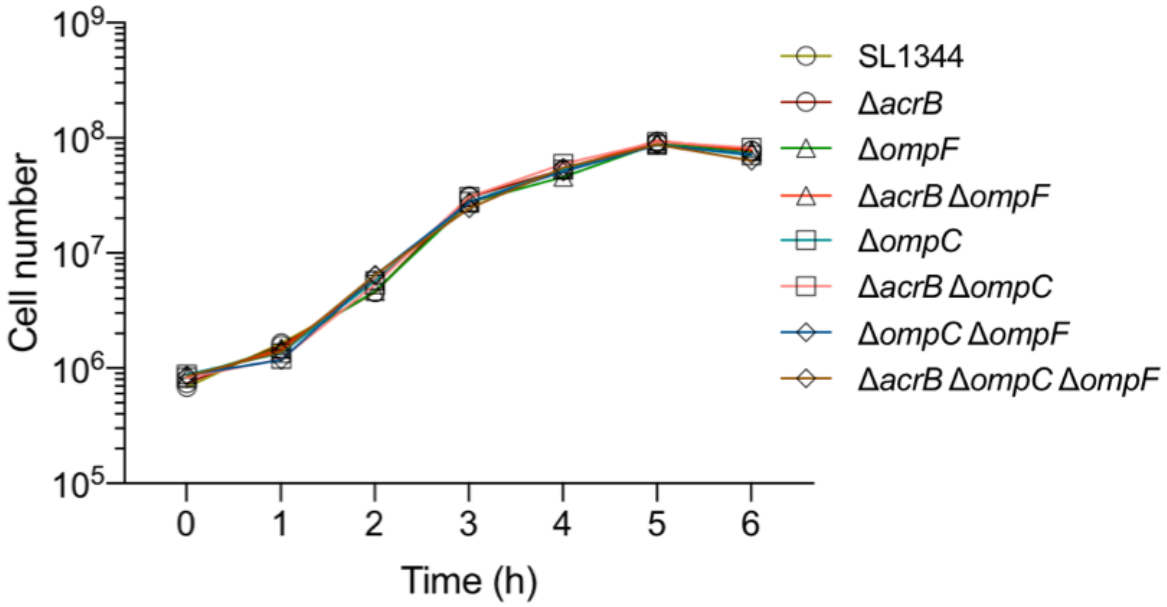

This graph shows the growth curve of all strains. Calculated cell number values were plotted on a logarithmic scale and strains shown in the legend. Cell numbers were based on the mean of the same biological replicates and the same gated population that EtBr fluorescence was measured from.

This data suggests that EtBr does not enter the cell through the porins OmpC and OmpF and that passive diffusion is a more likely mechanism (Paixao et al., 2009). Further work such as MICs could be used to determine whether susceptibility to EtBr changes in the absence of these porins.

6.5 Membrane permeability decreases in stationary phase

Having shown that EtBr does not enter Gram-negative cells through porins, the hypothesis that membrane permeability is reduced in stationary phase was explored. As previously discussed, probes that are utilised to measure membrane permeability are often efflux substrates. Therefore, membrane permeability was assessed based on membrane leakage, using SYTO-84 and using EDTA.

6.5.1 The level of EtBr leaking from cells was too inconsistent to assess membrane permeability

It was reasoned that the decreased permeability which leads to reduced influx in stationary phase, may also lead to less EtBr leakage through membranes into the extracellular environment, than in actively growing cells. To investigate this, the previously described efflux assay in **Section 5.4**, was adapted to measure how much EtBr leaks from a population of cells after 1, 3 and 5 hours of growth. To measure efflux, cells were pre-loaded with EtBr in the presence of CCCP to inhibit efflux, and cells are washed and re-energised with glucose. To measure EtBr leakage, glucose was not added, therefore the PMF was not re-energised and the levels of EtBr that leak out of cells independently of efflux could be measured.

Initial results appeared to suggest that more EtBr leaks out of cells at 1 hour of growth than at 3 and 5 hours of growth. This would have confirmed the hypothesis that actively growing cells have weaker membranes than in stationary phase. However, the error bars (not shown) from 6 biological repeats (1 hour) and 3 biological repeats (3 and 5 hours) for the data points in **Figure 6-4A** were large. Therefore, each replicate for each hour was plotted and the gradient of the line was calculated as a measure of the rate of EtBr leakage (**Figure 6-4B-D**). At 3 and 5 hours, the average rate was not significantly different based on an unpaired T-test, with a rate (m for gradient of line) of 0.0003. At 1 hour, 6 replicates were shown because the data from each replicate was inconsistent. The rates calculated greatly varied and for this reason, EtBr leakage was not significant regardless of time point and could not confirm our hypothesis that the membrane is less permeable in stationary phase.

Figure 6-4 Membrane EtBr leakage capacity in SL1344 at 1, 3 and 5 hours of growth.

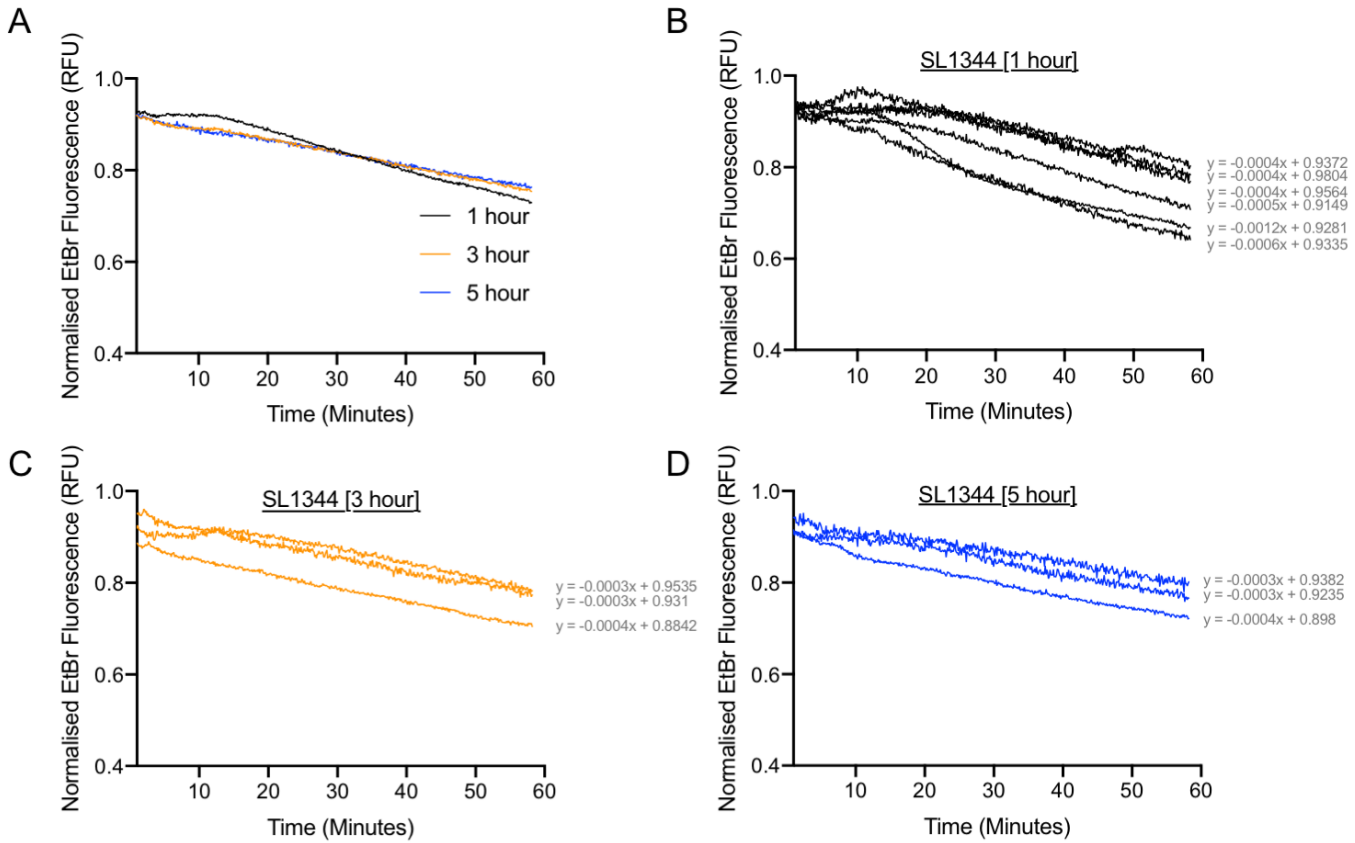

Each graph shows the time taken for EtBr to leak out of a population of cells that have not been re-energised with glucose after CCCP treatment. **(A)** shows a line graph of the rate at which EtBr leaks out of cells in SL1344 at 1 hour (black) based on 6 biological replicates, 3 hours (orange) and 5 hours (blue) based on 3 biological replicates. Error bars are not shown but were large. **(B)** shows the 6 replicates of EtBr leakage at 1 hour. **(C)** shows the 3 replicates of EtBr leakage at 3 hours. **(D)** shows the 3 replicates of EtBr leakage at 5 hours. The rate was determined by measuring the gradient of the line, and y=mx + c was shown next to the end of each line.

6.5.2 Bacterial cells become less permeable to SYTO-84 in stationary phase.

It has been previously suggested that EtBr enters cells though passive diffusion (Paixao et al., 2009). It was hypothesised that if permeability to EtBr is reduced in stationary phase, then this would also be the case for the non-efflux substrate SYTO-84. Our novel flow cytometry assay uses SYTO-84 dye as a probe for gating bacterial cells. Re-analysing data from **Figure 4-4,** the level of SYTO-84 fluorescence was measured to investigate whether bacterial cells become less permeable to this dye also.

There was no significant difference between the accumulation of SYTO-84 in SL1344 and SL1344Δ*acrB* with a peak in SYTO-84 fluorescence at 1 hour of growth (**Figure 6-5**). This would suggest that SYTO-84 is not an efflux substrate and shows the importance of efflux in maintaining low accumulation of drugs and dyes that are substrates in actively growing cells. However, SYTO-84 fluorescence decreases in both strains on entrance to stationary phase. This does suggest that a substrate that is not exported via efflux, is also less able to accumulate during stationary phase due to a strengthening of the permeability barrier. It is important to note that, although the SYTO-84 fluorescence does reduce around 2.5-fold, the lowest value is still over 45,000 RFU, and therefore can still be successfully used to gate cells for the measurement of EtBr using flow cytometry. However, as stated in the methods, extra gating was used for stationary phase samples to account for the shift in fluorescence values of SYTO-84.

Together this data suggests that accumulation levels of two DNA intercalating dyes in stationary phase are completely independent of efflux activity, and that passive diffusion into bacterial cells reduces in stationary phase, due to decreased membrane permeability.

Figure 6-5 SYTO-84 accumulation measured every hour for 6 hours in WT and Δ*acrB*.

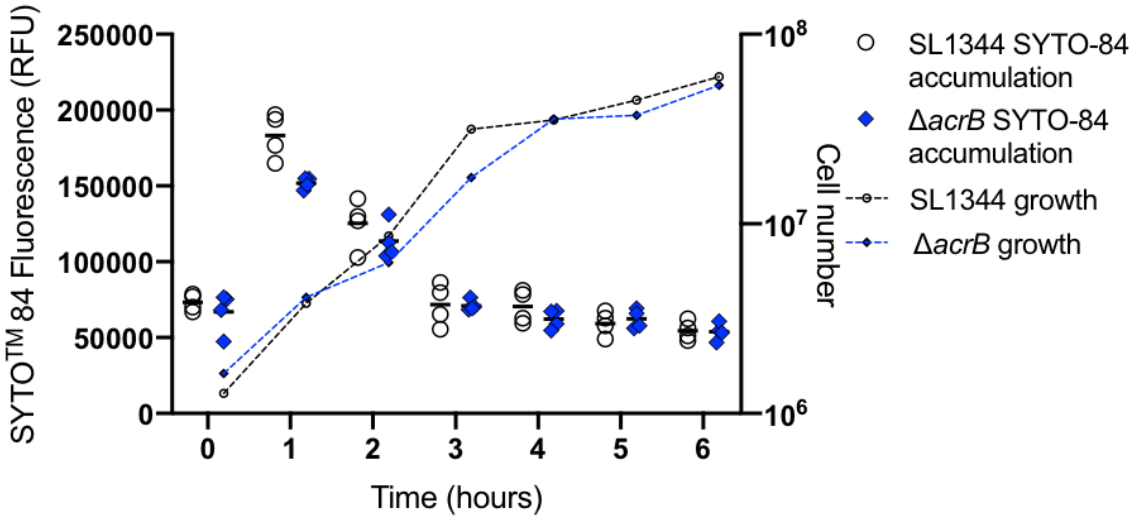

Median SYTO-84 fluorescence per cell in 10,000 flow cytometry events was measured every hour between 0 and 6 hours. Individual black dots represent the X-median value of SYTO-84^{+} accumulation in 10,000 events of SL1344 (WT) within a biological replicate. Individual blue triangles represent the X-median value of SYTO-84 accumulation in 10,000 events of Δ*acrB* within a biological replicate. 4 biological replicates for each strain are shown, with a short mean bar and SEM error bars. SYTO-84 accumulation is plotted on the left Y-axis. Calculated cell number values were plotted on the right Y-axis with corresponding symbols equating to strain and a dashed line to show growth of the culture. Cell numbers were based on the mean of the same biological replicates and the same gated population that EtBr fluorescence was measured from.

6.5.3 The outer membrane is more resistant to EDTA destabilisation in stationary phase

Thus far, results based on SYTO-84 accumulation support the hypothesis that membrane permeability decreases in stationary phase leading to low EtBr accumulation. It is possible that a 'strengthened' or impermeable membrane may be less susceptible to permeabilisation of compounds such as EDTA.

To increase the permeability of the OM, EDTA can be used as a 'permeabiliser'. EDTA displaces the divalent cations which crosslink LPS, making the membrane more fluid and more permeable to compounds that passively diffuse through cells, and to hydrophobic compounds that would usually not enter (Hancock and Bell, 1988). Using flow cytometry, EtBr accumulation was measured in bacterial cells at 1, 3 and 5 hours of growth after incubation with increasing concentrations of EDTA to permeabilise the membrane **(Figure 6-6A).**

As with previous results, EtBr accumulation in SL1344 at 1, 3 and 5 hours with no EDTA remained low with no significant difference in accumulation between the time points. When cells were incubated with 1 mM, 10 mM or 100 mM EDTA when sampled at each time point, there was no significant difference in accumulation compared to the no EDTA control. At 1 and 3 hours of growth, cells incubated with 200 mM or 500 mM EDTA accumulated significantly more EtBr than in the absence of EDTA. This suggests that EDTA at these high concentrations destabilises the OM, making cells more permeable to EtBr, in actively growing cells. At 5 hours of growth, there was no significant difference in EtBr accumulation with the addition of any concentration of EDTA, including 500 mM EDTA.

Figure 6-6 Accumulation of EtBr in SL1344 and Δ*acrB* in the presence of EDTA

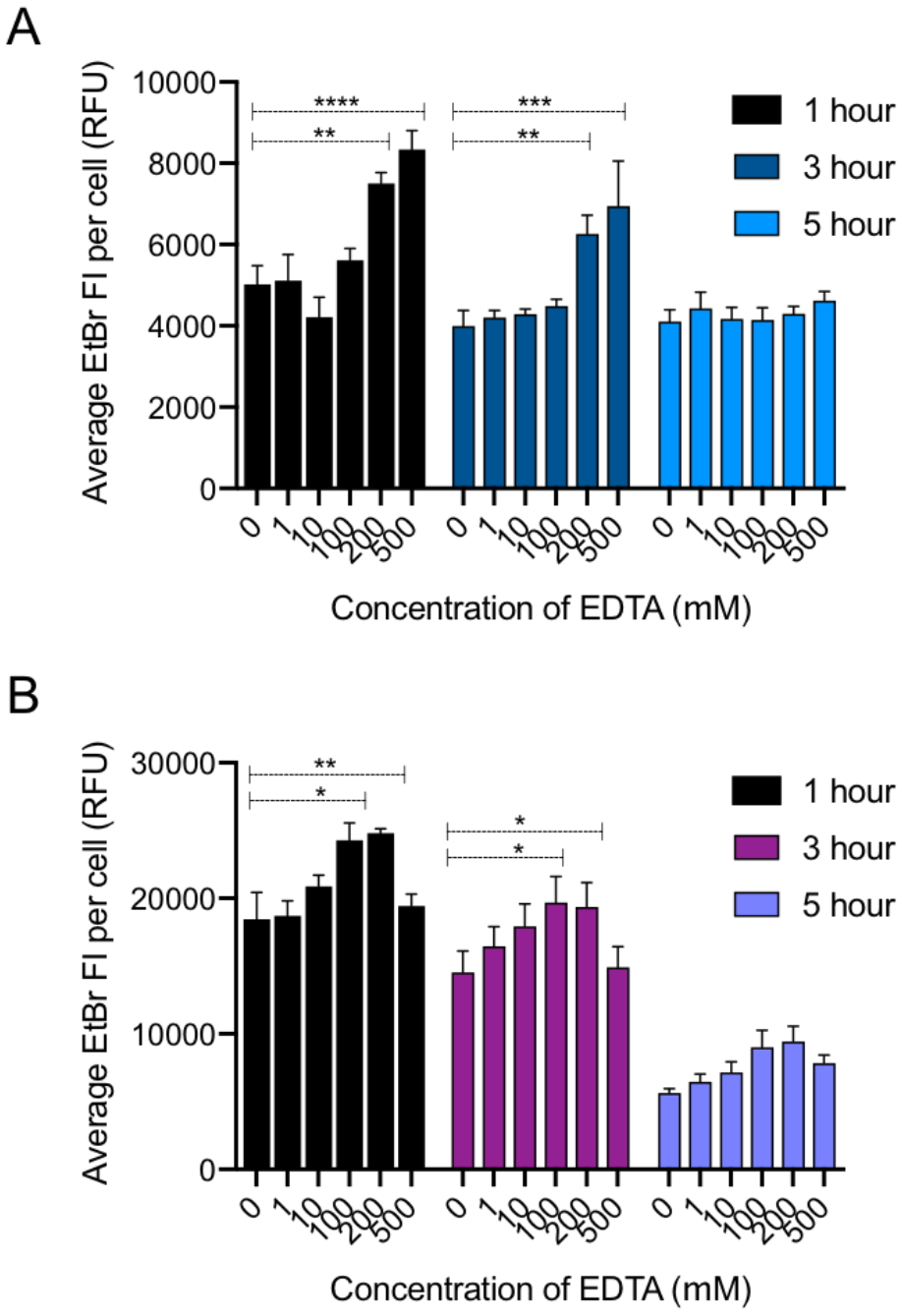

Bars represent EtBr accumulation in single cells per 10,000 SYTO-84^{+} events **(A)** EtBr accumulation in SL1344. EtBr accumulation was measured in the presence of increasing concentrations of EDTA (0, 1, 10, 100, 200 and 500 mM) from a culture grown for 1 hour (black), 3 hours (dark blue) and 5 hours (light blue). **(B)** EtBr accumulation in Δ*acrB*. EtBr accumulation was measured in the presence of increasing concentrations of EDTA (0, 1, 10, 100, 200 and 500 mM) from a culture grown for 1 hour (black), 3 hours (dark purple) and 5 hours (light purple). For both **(A)** and **(B)**, error bars show SEM from 3 biological replicates. Dashed lines above the bars with asterisks represent significance value when based on a T-test compared to no EDTA added.

The experiment was repeated for SL1344 Δ*acrB* **(Figure 6-6B)**. As with previous data, EtBr accumulation peaked at 1 hour of growth and decreased at 3 and 5 hours of growth. At 1 and 3 hours, there was no significant difference in EtBr accumulation with addition of 1 mM or 10 mM. EtBr accumulation significantly increased with 100 mM and 200 mM EDTA but with the addition of 500 mM accumulation was not significantly different. Based on viable counts, SL1344 Δ*acrB* did not die in the presence of 500 mM EDTA. Significant EtBr accumulation with 100 mM EDTA suggested that the OM of SL1344 Δ*acrB* might be slightly more permeable than SL1344. However, the important conclusion is that the OM in actively growing cells is weaker in both strains as it was more susceptible to disruption by EDTA. In SL1344 Δ*acrB* after 5 hours of growth, there was no significant difference in EtBr accumulation with the addition of any of the EDTA concentrations use, therefore suggesting increased strength of the permeability barrier in both strains in stationary phase.

This experiment was also attempted with SDS, a detergent which disrupts the inner and outer membrane and denatures membrane proteins at a range of concentrations. However, this was unsuccessful because either the SDS concentration added was too small to see a difference in EtBr accumulation or the concentration was too high that SYTO-84^{+} cells could not be successfully or consistently gated (data not shown).

To conclude, the data presented in this section is key to confirming the hypothesis that the membrane is more stable in stationary phase, causing cells to accumulate less dye.

6.6 The role of RpoS in strengthening the outer membrane barrier in stationary phase.

It has previously been shown that the OM of *E. coli* is 'strengthened' via RpoS-dependent mechanisms (Mitchell et al., 2017). Previous data in **Section 6.5**, confirms the hypothesis drawn that low EtBr accumulation in stationary phase is due to outer membrane permeability changes. It was therefore hypothesised that RpoS regulated the mechanisms required for reduced permeability to EtBr in stationary phase. To establish the importance of RpoS in the EtBr accumulation pattern in stationary phase RpoS was deleted from SL1344.

6.6.1 Removal of RpoS from SL1344 and SL1344 Δ*acrB*

The sigma factor gene *rpoS* was deleted from SL1344 and SL1344 Δ*acrB.*

An *aph* cassette was inserted into the *rpoS* gene in each strain by homologous recombination using the lambda red recombinase encoded on pSIM18 (Chan et al., 2007). Presence of the *aph* cassette was confirmed by growth on kanamycin and removal of the pSIM18 plasmid confirmed by the inability to grow on hygromycin. Successful *rpoS::aph* candidates produced a PCR product of 1289 bp. The *aph* cassette was removed from each strain and production of Δ*rpoS* strains was shown in **Figure 6-7** by the amplification of a 400 base pairs *rpoS* product.

Figure 6-7 Agarose gel image to confirm deletion of *rpoS* from SL1344 and Δ*acrB*

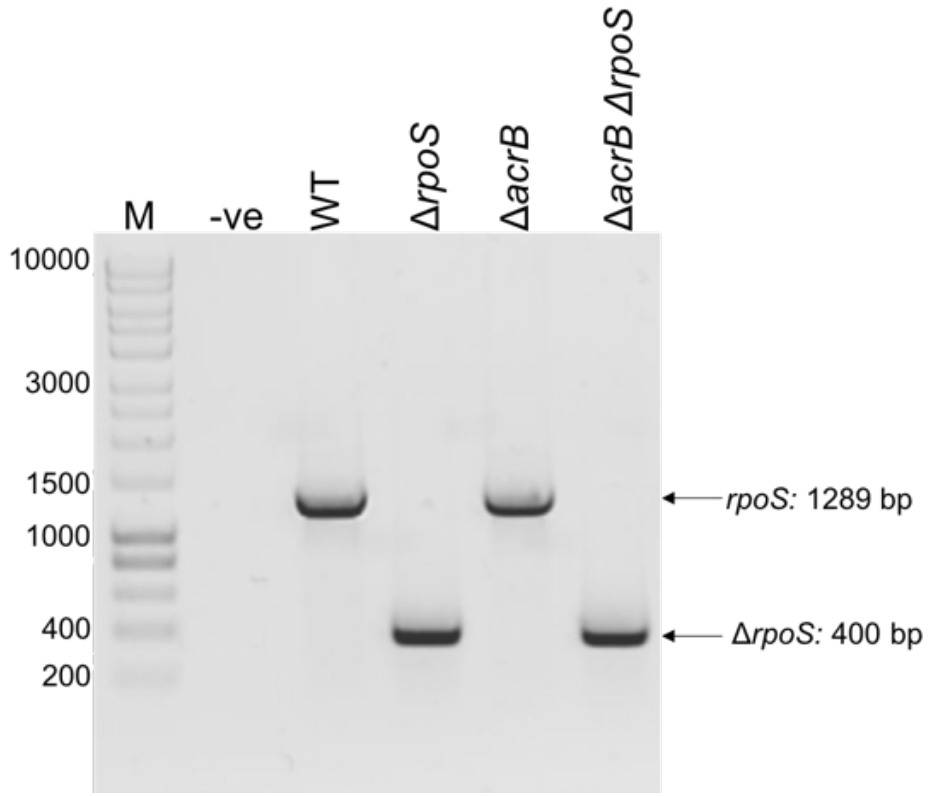

Gel image from agarose gel electrophoresis showing deletion of *rpoS* in SL1344 and Δ*acrB*. PCR products have been separated and DNA bands shown for each strain. In those strains where *rpoS* was not deleted, the product size was 1289 bp. Strains containing Δ*rpoS* had a product size of 400 bp.

6.6.2 Curli is not produced in the absence of RpoS

The curli operon *csgBAC* is highly expressed in stationary phase and its expression is regulated by RpoS. The sigma factor binding protein, Crl, interacts with RpoS, and facilitates RpoS attachment to the promoter region of *csgBAC* to drive transcription (Barnhart and Chapman, 2006). A congo red assay was carried out to assess curli and cellulose formation that contribute to the ability of bacteria to form biofilms (Jonas et al., 2007). This assay acted as a positive confirmation of the deletion of *rpoS* from strains.

S. Typhimurium 14028s is a control strain used when assessing curli biogenesis as it is a strong producer of biofilms. **Figure 6-8A** shows 14028s as a red, rough colony formation capable of producing curli and cellulose. SL1344 is not a strong biofilm producer however the colony appeared red with a rough surface therefore produced both curli and cellulose. Efflux deleted strains are known to be less able to form biofilms (Baugh et al., 2012). SL1344 Δ*acrB* still produced a red colony however it did not produce a rough colony therefore does not produce curli but did produce cellulose **(Figure 6-8C)**. Both strains with RpoS deleted produced white colonies meaning that they do not produce curli or cellulose and therefore are unable to form biofilms **(Figure 6-8D+E)**.

Figure 6-8 Curli biogenesis in S. Typhimurium 14028s, SL1344 and Δ*acrB* versus *rpoS* mutant strains.

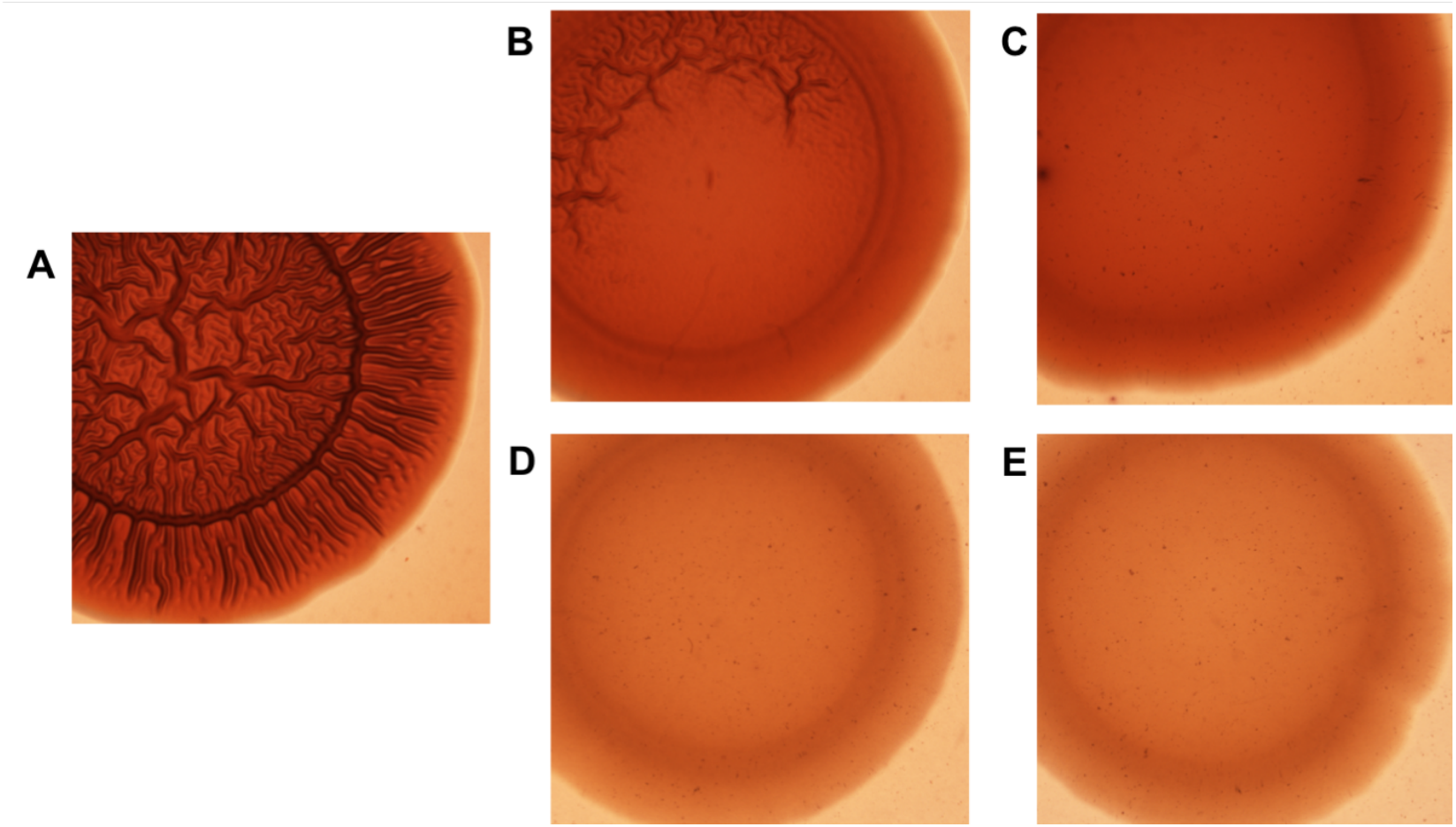

Data shows colonies of **(A)** 14028s, **(B)** SL1344, **(C)** SL1344 Δ*acrB*, **(D)** SL1344 Δ*rpoS*, **(E)** SL1344 Δ*acrB* Δ*rpoS* grown on congo red to distinguish curli biogenesis. Red rough colonies represent strains that can produce curli and cellulose, where white smooth colonies cannot produce curli or cellulose.

6.6.3 Removing RpoS does not come with a growth defect

To deduce whether the deletion of *rpoS* led to a growth defect, growth kinetics of the strains were measured in the absence of selective pressure, in both LB and MOPs minimal media. There was a significant difference in growth in LB compared to MOPs minimal media (All p-values <0.0001). In MOPs, there was a longer lag phase and exponential phase began at 5 hours.

The growth kinetics of SL1344 and SL1344 Δ*acrB* **(Figure 6-9A+B)** were measured to determine whether there was an effect of deleting efflux pumps on a strain's growth. Deleting efflux pumps made no significant difference to the generation times, all of which had generation times of between 20 and 26 minutes (P >0.05). There were no significant differences in generation times of SL1344 and SL1344 Δ*acrB* in MOPs minimal media (P >0.05) (**Table 6-1**).

Table 6-1 Generation times of each strain during cell division and significance based on unpaired T tests compared to parent strain

Strain	Generation time (LB)	Significance (vs parent)	Generation time (MOPs)	Significance (vs parent)
SL1344	21.37 ± 3.01		52.28 ± 7.22	
Δ*rpoS*	26.76 ± 2.08	ns (p 0.46)	50.90 ± 6.55	ns (p 0.83)
Δ*acrB*	19.23 ± 3.36		51.27 ± 2.38	
Δ*acrB* Δ*rpoS*	21.59 ± 4.86	ns (p 0.16)	52.09 ± 6.32	ns (p 0.83)

Figure 6-9 Growth kinetics of SL1344 and SL1344 Δ*acrB* and the effect of deleting *rpoS* on fitness cost.

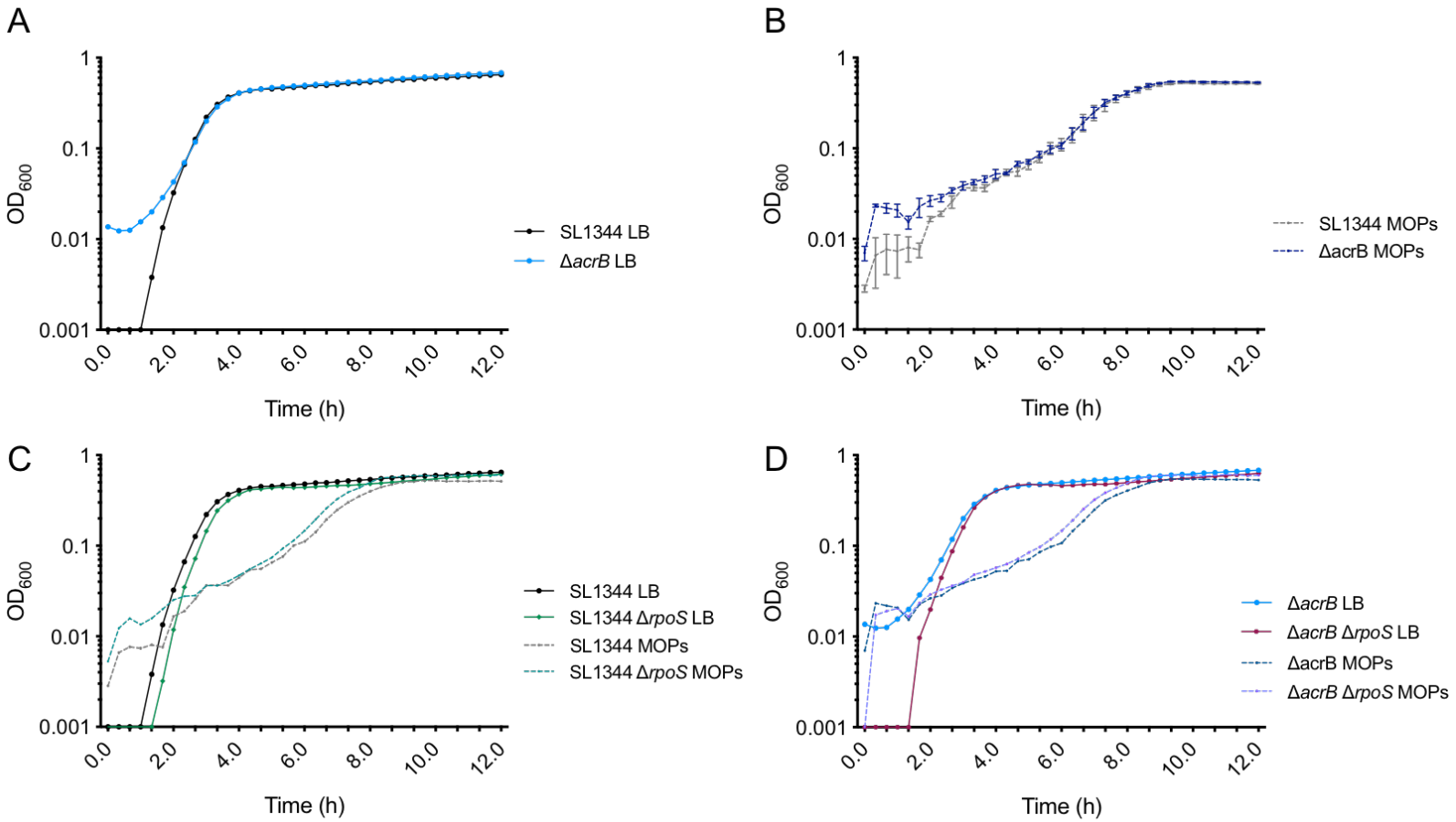

All above growth curves are based on 3 biological replicates (error bars are not shown). **(A)** compares the growth curves of SL1344 (black) and Δ*acrB* (blue) in LB. **(B)** compares SL1344 (grey) and Δ*acrB* (dark blue) in MOPs minimal media. **(C)** compares Δ*acrB* SL1344 in LB and MOPs (light blue; dark blue) to SL1344 Δ*acrB* Δ*rpoS* (dark purple; light purple. **(D)** compares SL1344 (black; grey) to SL1344 Δ*rpoS* (dark green; light green) in LB and MOPs minimal media.

For all *rpoS* mutants compared to their parent strains, there was no significant difference in generation time between them in LB (All P >0.05) **(Figure 6-9C)**. In MOPs minimal media, all Δ*rpoS* strains grew to a higher OD_{600} than their parent strain **(Figure 6-9D)**. However, the generation times do not differ significantly from Δ*rpoS* strains compared to their parental strain (All P >0.05).

6.6.4 RpoS deletion did not affect the antimicrobial susceptibility profile

Antimicrobial susceptibility was assessed by measuring the MICs of various antibiotics, dyes and detergents to SL1344, Δ*acrB*, SL1344 Δ*rpoS* and Δ*acrB* Δ*rpoS* strains. The agar dilution method was used to identify whether deleting RpoS increased the susceptibility to antibiotics. As previously described, the deletion of the pump component AcrB increased susceptibility of *S.* Typhimurium to a number of antibiotics **(Table 6-2)**. The MIC of all antibiotics for SL1344 Δ*acrB* were more than 2-fold different to SL1344, except rifampicin.

The MIC of antibiotics for Δ*rpoS* strains did not differ from the parent significantly (more than a 2-fold reduction in MIC), therefore RpoS does not contribute to the antimicrobial susceptibility of *S.* Typhimurium. Rifampicin was tested as it targets the RNA polymerase of a bacterial cell which may have interfered with the function of RpoS sigma factor. SDS detergent was also tested (Rami et al., 2005) as it has previously been described to have a reduced MIC to Δ*rpoS* strains in *E. coli,* however this result was not reproduced in this study.

Table 6-2 MICs of antibiotics in *rpoS* mutant strains

Strain	MIC (µg/ mL)									
	AMP	**CIP**	**CV**	**ERY**	**EtBr**	**FUS**	**NOR**	**RHO**	**RIF**	**SDS**
SL1344	4	0.03	64	64	>1024	1024	0.06	>1024	8	>1024
SL1344 Δ*acrB*	**0.12**	**<0.008**	**4**	**4**	**128**	**8**	**0.015**	**32**	8	**256**
SL1344 Δ*rpoS*	4	0.03	64	64	>1024	1024	0.03	>1024	8	>1024
SL1344 Δ*acrB* Δ*rpoS*	**0.12**	**<0.008**	**4**	**4**	**128**	**8**	**0.008**	**32**	8	**256**

Ampicillin (AMP); Ciprofloxacin (CIP); Crystal violet (CV); Ethidium bromide (EtBr); Fusidic acid (FUS); Norfloxacin (NOR); Rhodamine 6G (RHO); Rifampicin (RIF); Sodium dodecyl sulphate (SDS)

6.6.5 RpoS does not alter the levels of EtBr accumulation in stationary phase

Using the *rpoS* mutant strains, EtBr accumulation level was measured using flow cytometry. It was hypothesised that deletion of RpoS would reduce the gene expression of RpoS-dependent genes involved in strengthening the permeability barrier and therefore lead to an increase in EtBr accumulation in stationary phase.

SL1344 EtBr accumulation was compared to SL1344 Δ*rpoS* over 6 hours of growth. There was no significant difference in accumulation between these strains. **Figure 6-10A** shows that EtBr accumulation in both these strains was low at each time point and that EtBr fluorescence did not exceed 10000 RFU for any replicate at any time. This suggests that RpoS is not an important factor for EtBr accumulation in stationary phase.

To assess the importance of RpoS in the absence of efflux, SL1344 Δ*acrB* EtBr accumulation was compared to SL1344 Δ*acrB* Δ*rpoS* **(Figure 6-10B)**. As with previous data, EtBr accumulation peaked at 1 hour and the deletion of RpoS did not significantly alter the accumulation level. At the 3 hour time point, EtBr fluorescence remained significantly higher in SL1344 Δ*acrB* Δ*rpoS* compared to SL1344 Δ*acrB.* It could be hypothesised that in the efflux deficient strain, *rpoS* is involved in directing transcription of genes involved in outer membrane permeability, however accumulation level does still drop on entrance into stationary phase and is not significantly different to SL1344 Δ*acrB* from 4 to 6 hours of growth.

Figure 6-10 EtBr accumulation in strains lacking RpoS.

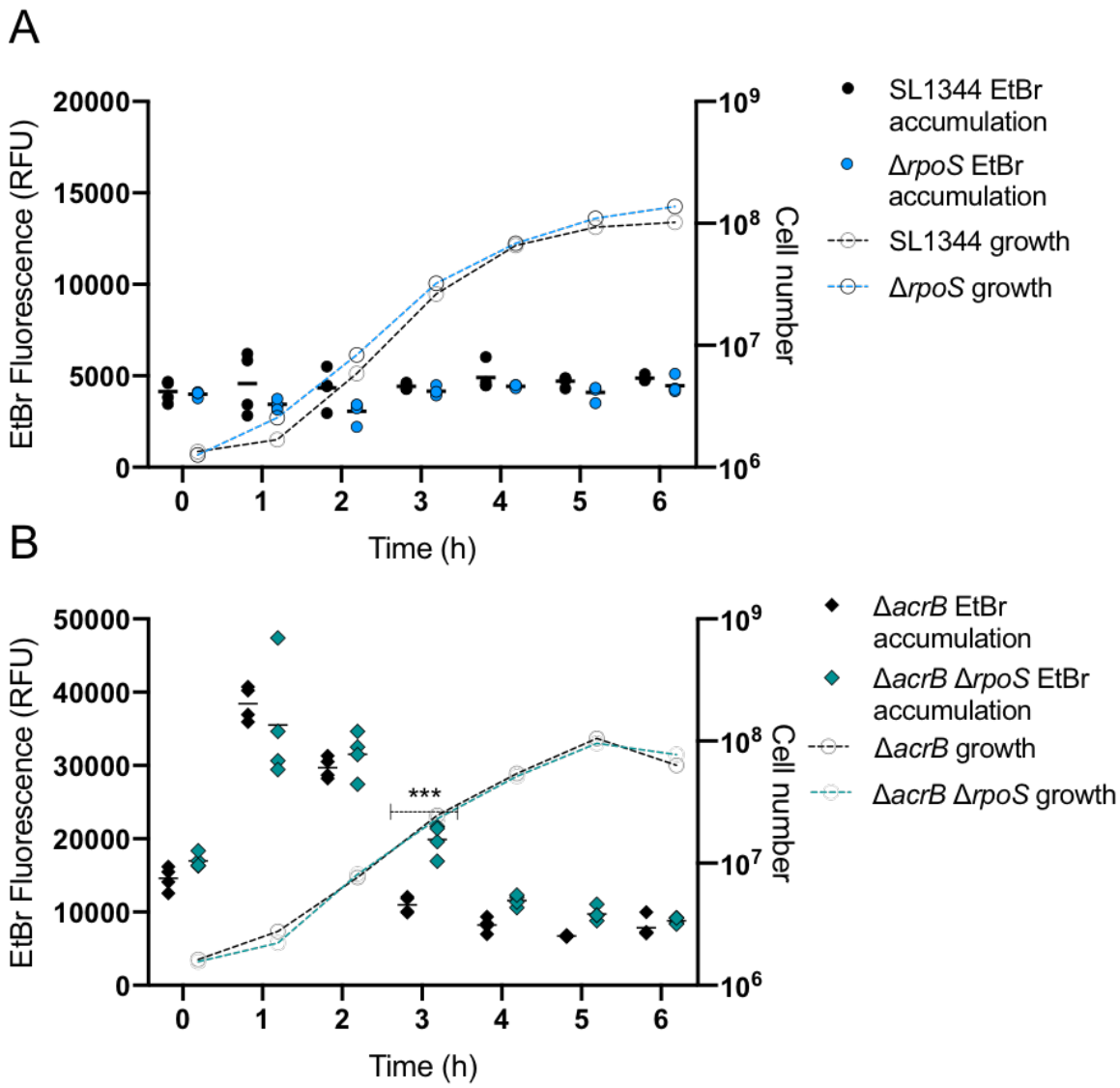

(A+B) 4 biological replicates for each strain are shown, with a short mean bar and SEM error bars. EtBr accumulation is plotted on the left Y-axis. Calculated cell number values were plotted on right Y-axis. Cell numbers were based on the mean of the same biological replicates and the same gated population that EtBr fluorescence was measured from. **(A)** shows SL1344 WT (individual black dots) vs Δ*rpoS* (blue dots). Median EtBr fluorescence per cell in 10,000 SYTO-84$^+$ flow cytometry events was measured every hour between 0 and 6 hours. Individual symbols represent the median value of EtBr fluorescence within a biological replicate. **(B)** shows SL1344 Δ*acrB* (black diamonds) vs Δ*acrB* Δ*rpoS* (green diamonds)**.** Median EtBr fluorescence per cell in 10,000 SYTO-84$^+$ flow cytometry events was measured every hour between 0 and 6 hours. Individual symbols represent the median value of EtBr fluorescence within a biological replicate. Significant differences to parent strain were measured by a two-way ANOVA and Sidak's multiple comparison test.

As previously shown in **Figure 6-9**, deletion of RpoS does not impact growth rate, and so is not responsible for any significant changes in EtBr accumulation at each time point.

6.7 Discussion

Data presented in this chapter supports the hypothesis that EtBr enters cells via passive diffusion in actively growing cells, but with increasing strength of the membrane barrier in stationary phase, less EtBr can enter cells.

The deletion of porins made no significant difference to EtBr accumulation regardless of growth phase. From this it can be hypothesised that the data is in agreement with previous data that shows EtBr enters Gram-negative bacterial cells via passive diffusion (Paixao et al., 2009). This study also showed that once inside cells, EtBr does not leak from cells and supports the result that showed there was no significant difference in EtBr leakage based on time points. The rates were so low that it could also be suggested that EtBr does not leak through cells, but can only be exported by efflux (Paixao et al., 2009).

Although difficult to directly measure membrane permeability, results presented here show that the OM of *Salmonella enterica* serovar Typhimurium has reduced permeability in stationary phase compared to actively growing cells. The addition of EDTA had no effect on EtBr accumulation in stationary phase. A similar result has been described by Alakomi et al. (2003) but this work concluded that the susceptibility of cells to EDTA in actively growing cells was independent of LPS release (Alakomi et al., 2003). Similar conclusions about colistin resistance have been made for the

Gram-negative *Acinetobacter baumanii* where resistance to colistin has been shown to increase in stationary phase (Soon et al., 2011b). Studies show an increased negative charge on the cell surface of colistin-resistant strains in stationary phase which could contribute to this resistance (Soon et al., 2011a). The antimicrobial peptide (AMP), cecropin A permeabilises the outer and inner membrane at low concentrations by penetrating LPS. It has been shown that a 10-fold higher concentration of cecropin A is required to permeabilise *E. coli* cells in stationary phase compared to exponential phase cells (Agrawal et al., 2019). The data presented in this chapter confirms that membrane permeability decreases in stationary phase, and that this in turn decreases the level of accumulation to EtBr in an efflux independent manner.

It was hypothesised that the reduction in passive diffusion of EtBr was due to RpoS dependent strengthening of the permeability barrier. Although RpoS has previously been implicated in the strengthening the permeability barrier in stationary phase (Mitchell et al., 2017), EtBr accumulation in SL1344 Δ*rpoS* was not significantly different to WT in stationary phase. As RpoS is a sigma factor that directs transcription of stationary phase genes, it is possible that this assay was not sensitive enough to identify changes in EtBr accumulation based on a single deletion of a sigma factor, possibly due to the activity of another sigma factors. This assay may have provided more insight if genes directly regulated by RpoS and involved in membrane permeability had been deleted.

There have been a few studies which aimed to identify RpoS dependent genes involved in membrane integrity, but these are not extensive. In carbon-limited

conditions, three RpoS-dependent genes have been identified which are involved in the strengthening the outer membrane barrier and increased resistance to SDS (Mitchell et al., 2017). This study was followed up with a detailed study into one of the genes, *yhdP*. Deletion of this gene led to increased susceptibility to vancomycin and detergents and was hypothesised to be due to cyclic ECA (enterobacterial common antigen). The hypothesis was that cyclic ECA damages the membrane in the absence of YhdP leading to increased permeability to the cell (Mitchell et al., 2018). A more recent study has shown that membrane permeability changes may be linked to interconnectivity between ECA and LPS (Klobucar et al., 2020). Further to this, RpoS-dependent genes such as *cfa* and *osmB* have been shown to be involved in resistance to pressure in stationary phase cells further proposing that RpoS plays a fundamental role in strengthening the permeability barrier in stationary phase cells (Charoenwong et al., 2011). The alternative sigma factor, RpoE, for protection of envelope stress, is upregulated on entrance into stationary phase but has also been implicated in membrane damage if high activity is too high (Nicoloff et al., 2017).

Further work would include following up by making RpoS-dependent gene deletions in SL1344 and then studying the effects of these deletions on EtBr accumulation in stationary phase. RpoS is not the only sigma factor important in stationary phase.

The membrane is strengthened in stationary phase cells and is more resistant to membrane permeabilising agents than in actively growing cells. Specific genes have not been identified that cause a direct effect on EtBr accumulation, but RNAseq data in the proceeding chapter will identify specific genes and biosynthetic pathways that may be responsible for this conclusion.

The data presented thus far shows that EtBr accumulation in stationary phase is independent of efflux and is low due to decreased membrane permeability. This conclusion calls into question the importance of efflux inhibitors in clinical infections where bacteria may be slow-growing or non-growing, especially if accumulation is independent of efflux. Data presented here does not dispute the importance of the development of efflux inhibitors to combat AMR but does provide further insight into when and how these inhibitors could be used effectively.

6.8 Key Findings

- EtBr does not enter *S.* Typhimurium through the major porins, OmpC or OmpF.
- SYTO-84, which is not an efflux substrate, showed high accumulation in both SL1344 and SL1344 Δ*acrB*, but low accumulation in stationary phase due to decreased permeability.
- High concentrations EDTA effectively destabilises the outer membrane in actively growing cells, increasing EtBr accumulation, but cannot destabilise the membrane in stationary phase.
- In this study, RpoS and decreased permeability in stationary phase could not be linked.

Chapter 7 - Genes involved in membrane changes are identified by RNAseq

7.1 Background

The balance between influx and efflux have been shown to change across bacterial growth. The hypotheses are that (i) during active growth the membrane is permeable and therefore efflux is a critical factor in the control of drug accumulation and (ii) accumulation of EtBr in stationary phase is independent of efflux pumps, and has been shown to be caused by decreased membrane permeability, thus reducing influx.

As previously discussed in **Chapter 1**, there are some known changes in physiology of the Gram-negative cell envelope that are well described, such as the accumulation of cyclopropane fatty acids, the increased thickness of the peptidoglycan layer and an overall decrease in the concentration of membrane proteins. However, these studies all describe individual aspects of stationary phase, and a more integrated review of cell envelope changes in stationary phase is required to understand its importance in dictating antibiotic accumulation.

To better understand the complex phenotypes uncovered in previous chapters, RNAseq analysis was performed for both WT SL1344 and the *acrB* mutant after 1, 3 or 5 hours growth in MOPs minimal media. In this chapter, the RNAseq data is presented to identify genes or metabolic pathways whose expression is changed and particular attention was given to those that may be involved in the stationary phase strengthening of the membrane barrier. A supplementary chapter (**Appendix V**)

showing well studied changes in stationary phase, including ribosomal and regulatory changes, carbon metabolism and anaerobic metabolism, confirms the validity of this dataset.

7.2 Hypothesis

Genes involved in controlling the strength of the Gram-negative bacterial membrane change in stationary phase. The strength of the membrane leads to reduced influx and accumulation of compounds, circumventing the requirement for efflux.

7.3 Aims

1. Perform RNAseq analysis on SL1344 and Δ*acrB* after growth in MOPs minimal media for 1, 3 and 5 hours.
2. Assess the literature for well-studied gene expression changes in stationary phase and compare this to the data-set produced
3. Identify expression changes in genes and pathways that may result in altering of the permeability barrier
4. Compare expression at different growth phases in WT against Δ*acrB*

7.4 Results and Discussion

To fully explore results from this data and derive hypotheses, results and discussion have been combined in this chapter.

7.4.1 RNAseq analysis of SL1344 elucidates changes in transcription on entrance into stationary phase

RNAseq analysis was used to identify genes and pathways that may be involved in changes to Gram-negative cells as they enter stationary phase. Briefly, growing cultures of SL1344 were sampled after 1 hour, 3 hours and 5 hours of growth. Cells from these time points were harvested and samples were snap frozen. GENEWIZ Inc. carried out RNA extraction, rRNA depletion, quality control, library preparation and sequencing, followed by bioinformatic analysis.

SL1344 cultures at 1 hour were used as the control group and compared to cultures grown for 3 hours (late exponential/preparation to stationary phase) and 5 hours (stationary phase). From these comparisons, genes with expression that was increased (log2fold >1) or decreased (log2fold <-1) at 3 or 5 hours compared to 1 hour, were considered to be significantly changed. For all other analysis, fold changes were calculated and used in place of log2fold change with fold change >2-fold being considered to have significantly increased expression and <0.5-fold being significantly decreased expression.

The percentage of differentially expressed genes (DEGs) within the genome was calculated for both 3 and 5 hours and is shown in **Figure 7-1**. Each differentially expressed gene was then assigned a COG code (Clusters of Orthologous Genes) for an overall identification of function. Comparing SL1344 at 1 hour compared to 3 hours of growth showed that 26% of genes were differentially expressed (**Figure 7-1**). Of this 26%, 37% of DEGs were involved in metabolism, 17% were involved in information storage and processing (transcription/translation), 19% were involved in

cellular processes and signaling and 17% were categorised as poorly characterised (**Figure 7-1**). At 5 hours of growth, 47% of the genes in the genome were differentially expressed. At 5 hours, changes in gene expression involved in metabolism were again the highest in percentage. However, this analysis has some limitations. Several genes were not assigned COGs and a large percentage of genes had unknown functions. For this reason, this analysis could only be a guide to show that the largest number of genes that had significantly changed expression was after 5 hours of growth, and that most changes were involved in metabolism, as may be expected for cells transitioning from exponential to stationary phase.

Figure 7-1 Percentage of genes differentially expressed at 3 and 5 hours of growth and COG characterisation

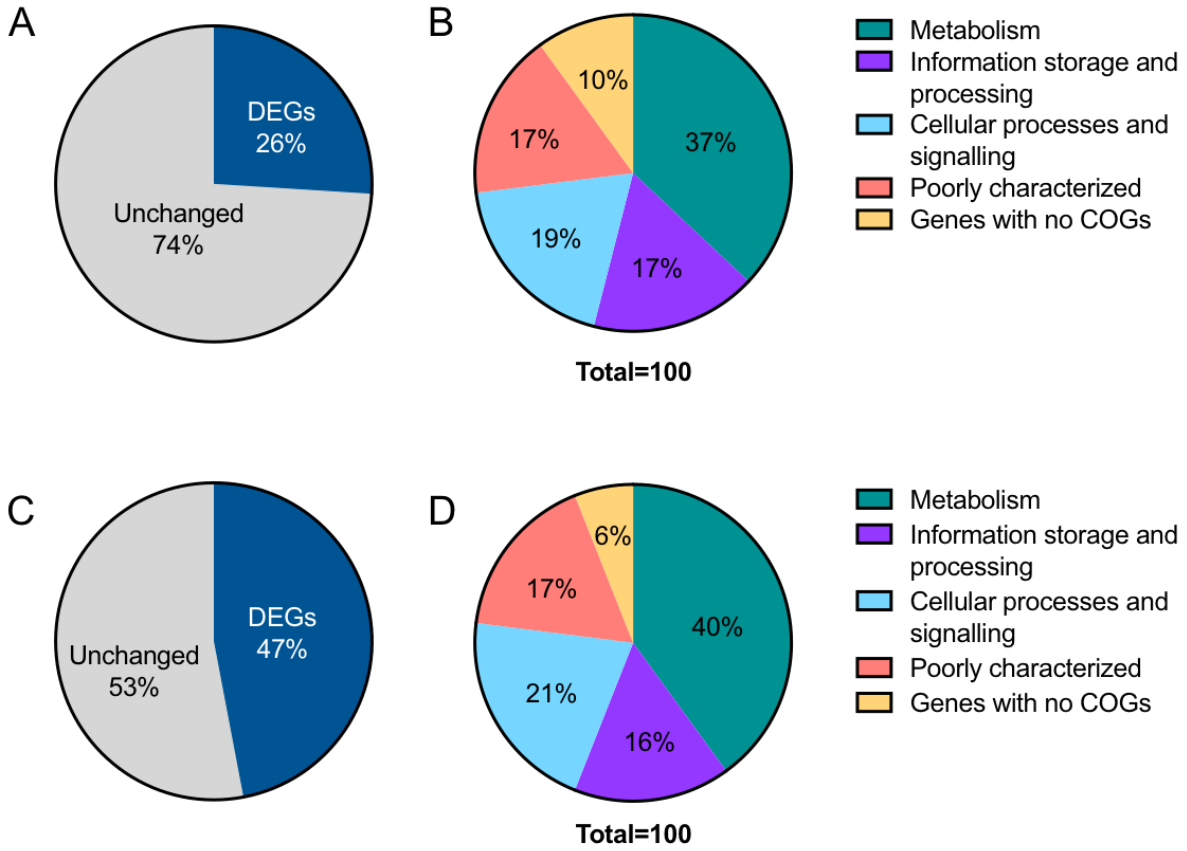

(**A**) shows the % of DEGs at 3 hours compared to 1 hour of growth in SL1344. Of the 26% of DEGs at 3 hours, genes were then allocated a COG code based on overall function (**B**). (**C**) shows the % of DEGs at 5 hours compared to 1 hour of growth in SL1344. Of the 47% of DEGs at 5 hours, genes were then allocated a COG code based on overall function (**D**).

Scatter plots were created to visualise the genes for each comparison with the greatest increase or decrease in expression (**Figure 7-2** and **Figure 7-3**). Genes and operons that had most changed expression could then be used to derive hypotheses about which genes may be involved in membrane changes in stationary phase.

At 3 hours, the scatter plot shows that most genes that were most highly expressed were methionine related *met* genes, which are spread across different operons across the genome (**Figure 7-2**). Expression of genes from the *dms*ABC and *frd*ABCD operons involved in anaerobic metabolism was also increased. Many genes from the *cbi* operon, involved in cobalamin (vitamin B12) biosynthesis, also showed increased expression. In terms of genes with decreased expression, the most obvious was the abundance of tRNAs. At 5 hours, a larger number of genes had increased expression including the ribosomal modulation factor (RMF), *rmf*, SPI-2 genes, *ompW* and *dadA* and the *lsr* operon encoding for the import of Autoinducer-2 (AI-2) involved in quorum sensing (QS). Many ribosomal genes had decreased expression, as well as SPI-1 and genes involved in spermidine biosynthesis and lipid A modification (**Figure 7-3**).

This gave a brief view of the groups of genes whose expression was most changed at each time point. However, to successfully address the aims and hypotheses of this chapter, the genes considered important for the transition into stationary phase will be discussed further in this chapter specifically those that may be involved in membrane changes.

Figure 7-2 Scatter plot showing DEGs at 1 vs 3 hours in SL1344

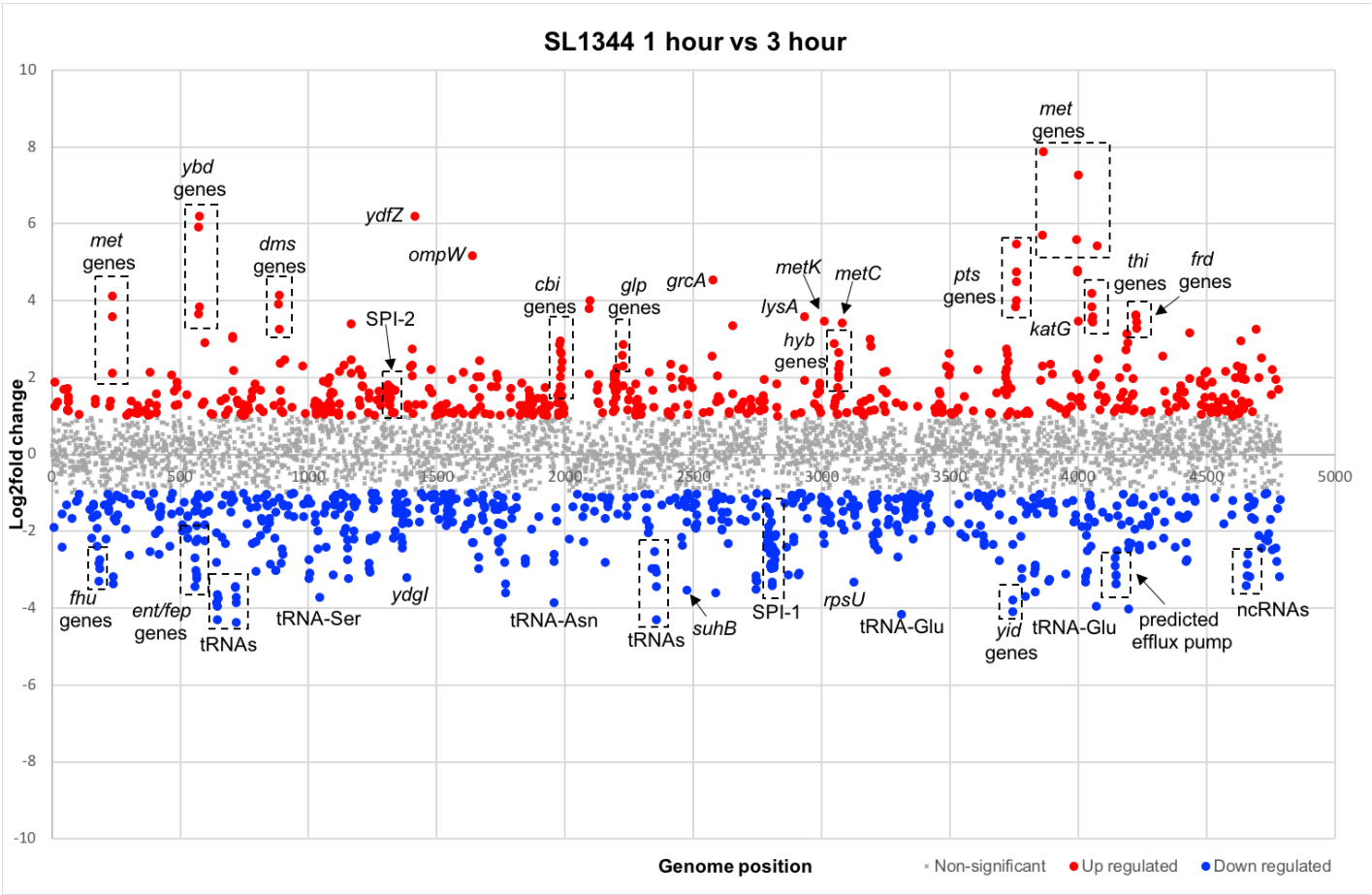

This scatter plot shows upregulated genes at 3 hours compared to 1 hour in red and downregulated genes in blue. The Y-axis shows the log2fold change and the X-axis is based on genome position in SL1344. Genes of interest are labelled and groups of genes are shown in boxes. Many unlabelled downregulated genes are tRNAs.

Figure 7-3 Scatter plot showing DEGs at 1 vs 5 hours in SL1344

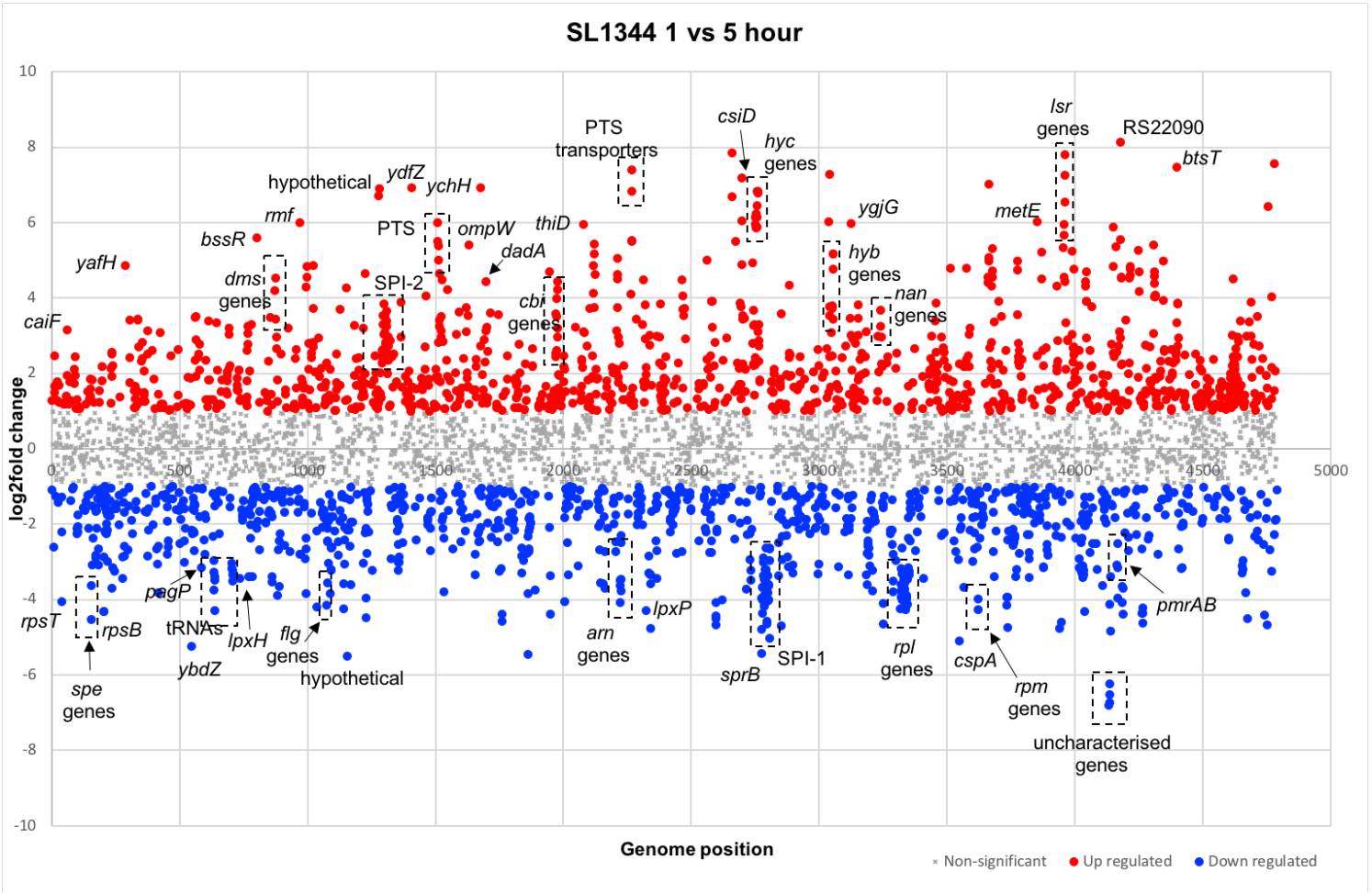

This scatter plot shows upregulated genes at 5 hours compared to 1 hour in red and downregulated genes in blue. The Y-axis shows the log2fold change and the X-axis is based on genome position in SL1344. Genes of interest are labelled and groups of genes are shown in boxes.

7.4.2 Stationary phase changes in gene expression are consistent with previous literature

Many published studies have explored the role and expression level of genes or proteins in stationary phase of various bacterial species but to our knowledge this is the first transcriptomic experiment conducted to specifically study all gene expression changes in stationary phase in *S.* Typhimurium SL1344. To validate this dataset, genes and pathways that have previously been described that change in stationary phase were analysed. This will be described briefly here, but thorough analysis and discussion of stationary phase changes previously described can be found in **Appendix V** .

Firstly, several regulators that had increased expression in stationary phase in previous literature also had increased expression in this dataset. RpoS, which had previously been described in **Chapter 6**, but no evidence could be produced into its role in EtBr accumulation, had increased expression. The expression of *rpoS* increased 2-fold in this dataset, as to be expected based on previous data (Lange and Hengge-Aronis, 1994). Several RpoS dependent genes also showed increased expression. Further to this, it could be concluded that there was an increase in ppGpp in this dataset based on the change in expression of several ppGpp regulated genes. ppGpp and the stringent response are commonly associated with stationary phase (Navarro Llorens et al., 2010). Dps has previously been described as one of the most abundant proteins in stationary phase (Nair and Finkel, 2004), and the 9.81-fold change in expression at 5 hours, validates that this dataset correlates to previously described data.

Changes in ribosome activity in stationary phase is well studied. Most genes encoding 30S and 50S subunits had decreased expression. There was increased expression of the *rpsV* gene which specifically encodes a stationary phase ribosomal protein, and this has been shown previously (Izutsu et al., 2001b). The ribosomal associated gene which had the most increased expression was *rmf.* Ribosomal modulation factor (RMF) has been described as stationary phase specific (Wada et al., 2000) and further validates the dataset presented here. Other ribosome-associated genes previously described to have increased expression in stationary phase include *raiA* (Maki et al., 2000) and *yqjD* (Yoshida et al., 2012) and also had increased expression in this dataset.

Expression of genes involved in responding to carbon starvation also correlated to previous studies. Several sugar transporters involved in increased uptake of sugars have thoroughly been described in **Appendix V** , and are required in glucose-limited environments. Some genes involved in the glyoxylate cycle had increased expression in this dataset and this cycle has previously been described as upregulated in stationary phase (Huisman et al., 1996), to circumvent the carbon utilising steps of the TCA cycle. Glycogen biosynthesis and accumulation is also common to stationary phase and glucose-limited environments, and genes involved in its biosynthesis had increased expression in this dataset.

Anaerobic respiration is key to facultative anaerobes such as *S.* Typhimurium, and is important in stationary phase in batch culture. In the dataset presented here, many genes involved in anaerobic metabolism had increased expression at 5 hours and

correlates to an oxygen-limited environment. Analysis of anaerobic respiration is thoroughly detailed in **Appendix V**

7.4.3 L-methionine and S-adenosyl-L-methionine synthesis pathways had highly increased expression at 3 hours

In the dataset presented here, some of the most DEGs at 3 hours compared to 1 hour were the *met* genes (increased expression), involved in the biosynthesis of L-methionine and *S*-adenosyl-L-methionine. Due to the fold changes seen in these genes, it was possible that they play a significant role in the entrance into stationary phase.

The fold change in expression of the *met* genes is listed in **Table 7-1**. These genes are not within a single operon and are found across the genome of *S.* Typhimurium SL1344. The *metNIQ* operon encodes an ABC importer for L-methionine. This suggests that there is a requirement for L-methionine in the cell in late exponential phase. The following enzymes are involved in the biosynthetic superpathway of L-homoserine, L-homocysteine and L-methionine: MetL, MetA, MetB, MetC and MetE, shown in **Figure 7-4**. Of these, the most highly expressed gene at both 3 and 5 hours was *metE*, which encodes for a methyltransferase converting L-homocysteine into L-methionine. The increased biosynthesis of L-homoserine, L-homocysteine and L-methionine highlights that these compounds must be important at this stage of growth.

It has been suggested that L-homoserine may play a role in the induction of stationary phase. The overall process is that during starvation, signal molecules may be

synthesised due to accumulation of intermediates of amino acid biosynthesis, such as L-homoserine, which can then be turned into cyclic compounds by the binding of tRNA synthetases (Huisman et al., 1996). L-homoserine has been shown to bind tRNA synthetases to produce cyclic homoserine-lactone. Homoserine lactone has been shown to be accumulated in high bacterial cell densities such as stationary phase and is involved in inducing stationary phase RpoS (Huisman and Kolter, 1994). It is possible that this is the reason the genes of the L-methionine pathway were highly upregulated.

Table 7-1 Differentially expressed *met* genes in the RNAseq dataset

Gene	1 hr vs 3 hr fold change	1 hr vs 5 hr fold change
metJ	4.29	2.08
metQ	4.33	2.30
metC	10.71	4.15
metK	11.02	6.20
metI	12.00	4.36
metN	17.43	3.79
metL	27.63	3.20
metA	42.82	13.61
metB	48.08	2.21
metR	51.96	5.54
metF	155.57	37.62
metE	236.20	64.66

Figure 7-4 The superpathway of L-homoserine, L-homocysteine and L-methionine biosynthesis

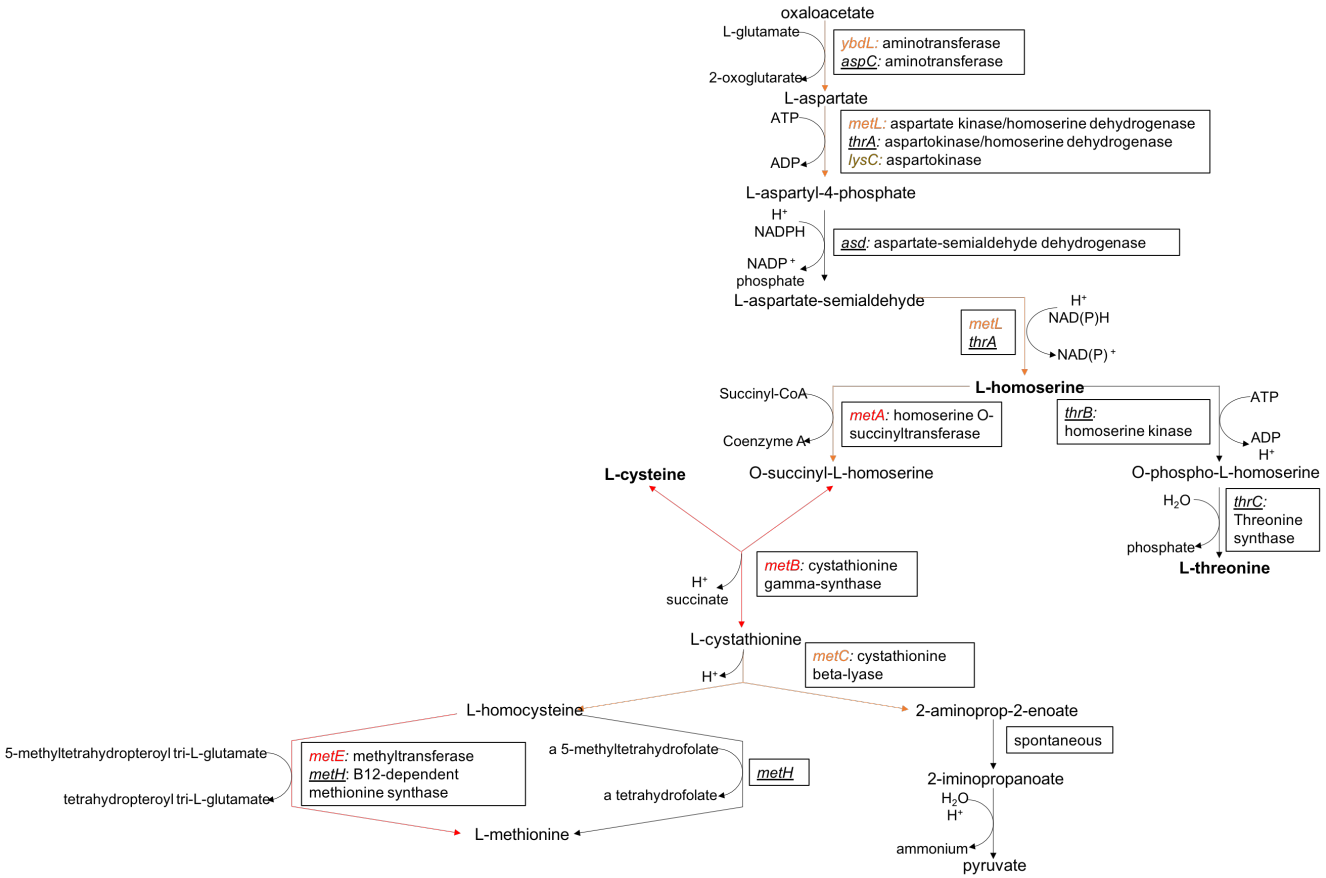

This pathway shows the biosynthesis of L-methionine at 1 vs 3 hours. Reactions that are upregulated in this pathway are shown with an orange arrow, and highly upregulated reactions are shown with a red arrow. The genes encoding enzymes catalysing each reaction are shown in the boxes next to the reaction arrow. Genes that are upregulated are shown in orange/red and unchanged genes are involved in the reaction are shown in black and underlined. The L-cysteine biosynthesis pathway (from L-serine) was not included in diagram because genes involved were not differentially expressed. This figure was produced by EE Whittle using Pathway Tools Software and databases (Karp et al., 2016, Caspi et al., 2020, Fulcher et al., 2018).

However, *metE* is also a gene involved in the biosynthesis of the major methyl donor, *S*-adenosyl-L-methionine (SAM). The reaction for conversion of L-methionine to SAM is facilitated by MetK, an adenosyltransferase. The SAM biosynthesis pathway is shown in **Figure 7-5**. The *metK* gene also had increased expression at 3 and 5 hours compared to 1 hour (**Table 7-1**). It is therefore possible that SAM accumulates in the cell to act as a methyl donor for reactions necessary for stationary phase. Previous literature suggests *metK* is replaced by the *metX* gene in stationary phase however the data presented here did not identify *metX* as a differentially expressed gene. SAM may be involved in several processes important for stationary phase processes including the production of cyclopropane fatty acids, which will be discussed further, and during molybdenum cofactor biosynthesis (important in anaerobic respiration). SAM is involved in the biosynthetic pathway which produces AI-2, a QS molecule. Although there was decreased expression in the *pfs* gene (0.47-fold) which encodes a nucleosidase involved in *S*-adenosyl-L-homocysteine to *S*-ribosyl-L-homocysteine, *luxS* which encodes for a lyase which converts *S*-ribosyl-L-homocysteine to AI-2, remained unchanged. SAM is also involved in the biosynthesis of polyamines, however, genes involved in putrescine and spermidine biosynthesis were downregulated at 5 hours in this dataset.

Assessing the importance of L-methionine and SAM on the cells in preparation for stationary phase would require further investigation. To identify why SAM levels increased, it would be important to identify in what reactions SAM is acting as a methyl donor. This may be possible using stable isotope labelling by amino acids in cell culture (SILAC). Identifying proteins where methyl groups have been donated using this method has previously been described (Ong et al., 2004) where, a heavy

isotope labelled methionine ([$^{13}CD_3$]methionine) could then be converted to [$^{13}CD_3$]SAM and then using Mass Spectrometry, heavy isotope labelled proteins that have had a methyl group donated by [$^{13}CD_3$]SAM could be analysed.

It is difficult to hypothesise the importance of SAM to the EtBr accumulation phenotype across growth phases, however, there may be some use in either measuring the concentrations of SAM over time or to remove these genes from SL1344 and determine whether they affect EtBr accumulation on the entrance into stationary phase.

Figure 7-5 The *S*-adenosyl-L-methionine biosynthesis pathway

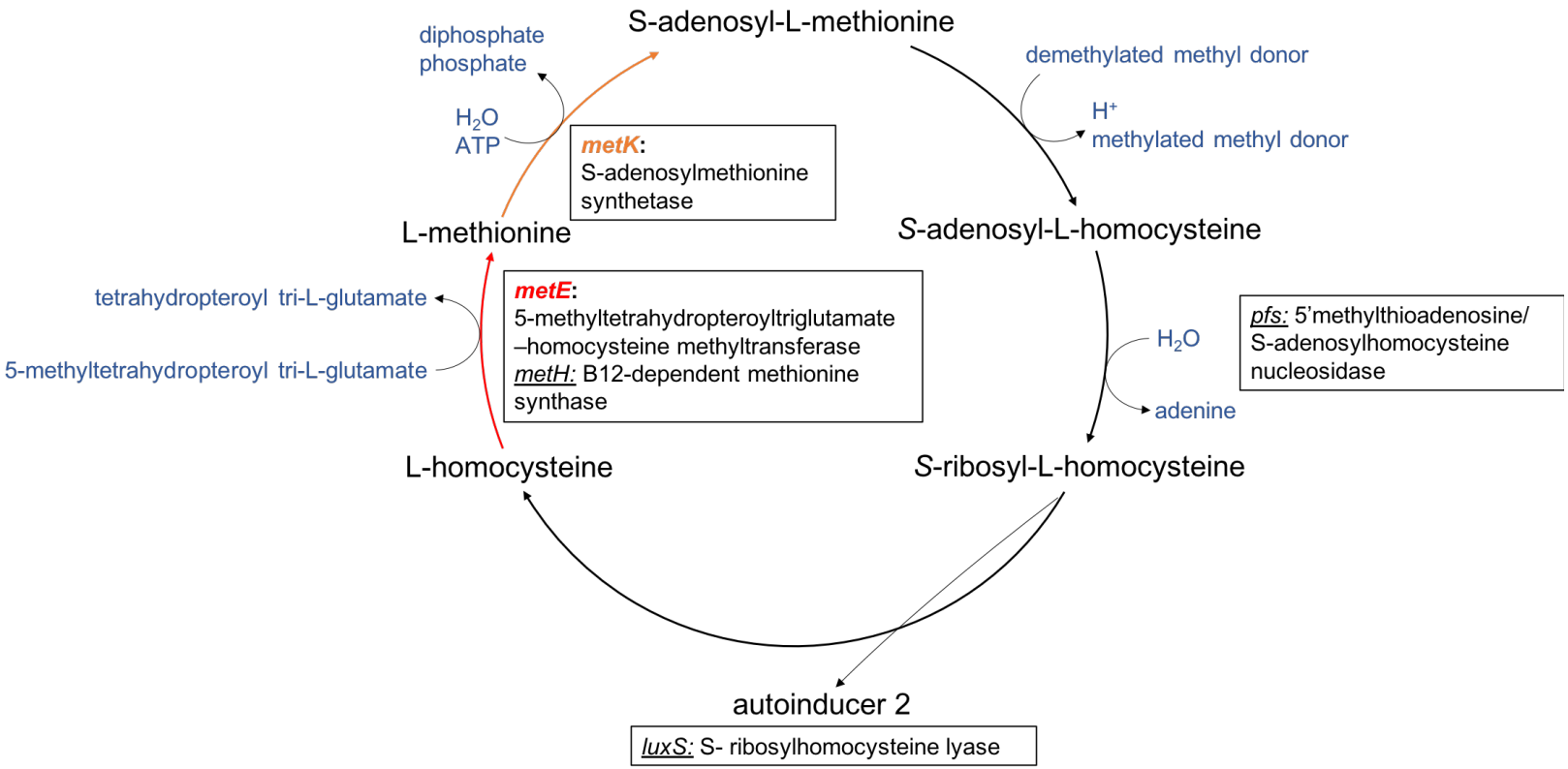

This cycle shows the reactions involved in the biosynthesis of SAM at a vs 3 hours. Reactions that are upregulated in this pathway are shown with an orange arrow, and highly upregulated reactions are shown with a red arrow. The genes encoding enzymes catalysing each reaction are shown in the boxes next to the reaction arrow. Genes that are upregulated are shown in orange/red and unchanged genes are involved in the reaction are shown in black and underlined. It is important to note that the conversion of SAM to *S*-adenosyl-L-homocysteine is not limited to a single reaction, and multiple reactions can occur, depending on where the methyl group is being donated. This figure was produced by EE Whittle using Pathway Tools Software and databases (Karp et al., 2016, Caspi et al., 2020, Fulcher et al., 2018)

7.4.4 Gene expression changes suggest a stationary phase decrease in membrane permeability

This dataset was produced to identify genes and pathways that may be involved with the strengthening of the permeability barrier in stationary phase. There was no single gene that looked likely to provide a major change in permeability, but many genes that could give rise to changes in permeability were found. In addition, genes that could be responsible for changes in multiple sites in the envelope including the IM, peptidoglycan, OM and ECA were identified.

Results will be presented here with subsequent discussion of their possible involvement in decreasing the permeability of the Gram-negative membrane, and therefore possible reasonings for low EtBr accumulation in stationary phase. However, no experiments have been carried out to prove or disprove the involvement of these pathways in permeability and therefore all results and discussion here will be subject to further work.

7.4.4.1 Increased expression of CFA

In this dataset, at 3 and 5 hours of growth, *cfa* had significantly increased expression compared to 1 hour of growth in SL1344 (3.17-fold change and 7.27-fold change respectively). The *cfa* gene encodes a synthase which converts linear unsaturated fatty acids (attached to phospholipids) to cyclopropane fatty acids (**Figure 7-6**). This CFA reaction relies on SAM as a methyl donor.

Figure 7-6 The CFA enzymatic reaction for the biosynthesis of cyclopropane fatty acids

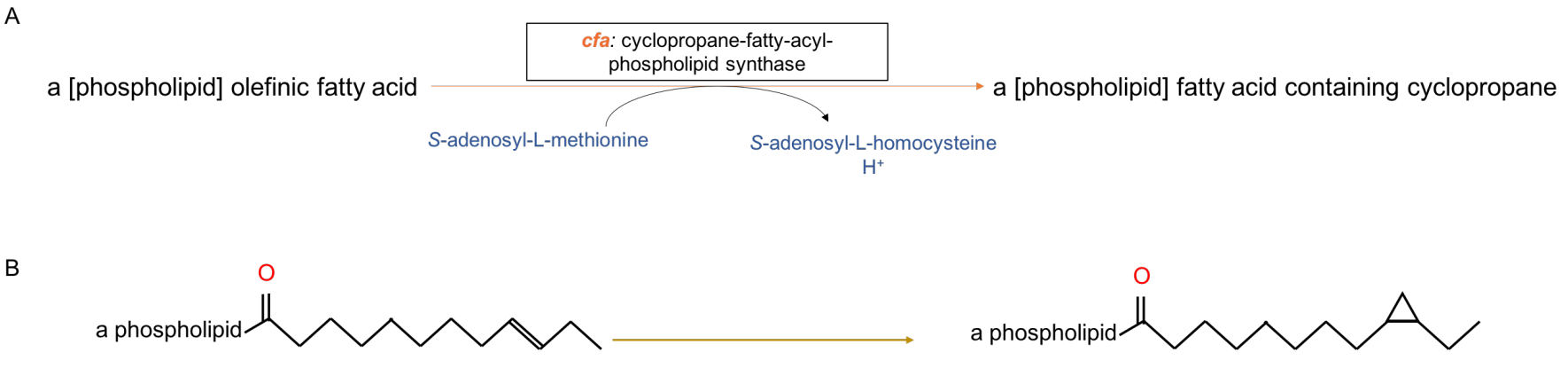

(A) shows the reaction catalysed by CFA (cyclopropane-fatty-acyl-phospholipid synthase) for the biosynthesis of cyclopropane fatty acids from olefinic fatty acids and SAM. Genes that are upregulated are shown in orange. **(B)** shows the difference in the fatty acid structure with the conversion of a carbon-carbon double bond to a cyclopropyl group. This figure was produced by EE Whittle using Pathway Tools Software and databases (Karp et al., 2016, Caspi et al., 2020, Fulcher et al., 2018)

It has previously been shown that cyclopropane fatty acids accumulate in the IM in stationary phase, with the onset of starvation (Huisman et al., 1996). It has also been shown that the *cfa* gene, is in part regulated by RpoS (Wang and Cronan, 1994). An increase in these fatty acids has also been hypothesised to lead to a decrease in membrane fluidity (Bianco et al., 2019, Qi et al., 2019). Mutants lacking *cfa* display increased susceptibility to acid, heat and pressure in stationary phase, further highlighting the importance of cyclopropane fatty acids in tolerating these stresses via membrane mediated mechanisms (Chang and Cronan, 1999, Chen and Ganzle, 2016). Further to this, it was also suggested that CFA is important for ampicillin tolerance of *Shigella sp.* also possibly implicating CFA in resistance to antibiotics in stationary phase (Liu et al., 2019).

This previously published literature highlights the importance of CFA in stationary phase and the results in the dataset presented here confirm this. Therefore, the hypothesis can be drawn that the increase in cyclopropane fatty acids in stationary phase could lead to a decrease in membrane permeability, and therefore a decrease in EtBr accumulation. Further work would be required to confirm this hypothesis. Confirmation of increased transcription of *cfa* could be confirmed with RT-PCR. Deletion of *cfa* and subsequent EtBr accumulation assays using flow cytometry may lead to a different accumulation phenotype in which EtBr accumulation is increased in stationary phase.

7.4.4.2 Stationary phase permeability may be independent of lipid A biosynthesis and modification

Many genes related to lipid A biosynthesis and modification had decreased expression in stationary phase. LPS is key to the permeability of the OM and its crosslinks with divalent cations prevents access to some antibiotics through the OM (Hancock and Bell, 1988). However, it is also a target of the polymyxins, and an antibiotic of last resort, colistin (Fair and Tor, 2014). LPS is also an antigen of bacterial cells and is recognised by Toll-like receptor 4 (TLR-4) on innate immune cells for the development of an immune response (Chow et al., 1999). Modifications of LPS are key to the development of polymyxin resistance but also allow evasion of the immune response (Simpson and Trent, 2019).

The genes shown in **Table 7-2** are involved in lipid A biosynthesis. All DEGs involved in lipid A biosynthesis showed decreased expression after 5 hours of growth. This suggests that in stationary phase, the cell reduces production of lipid A. It is possible that limited turnover in LPS is involved in decreased fluidity and a more stable stationary phase OM. An increase in LPS in stationary phase has previously been linked to increased cell death (Sutterlin et al., 2016). LPS alongside membrane destabilisation through mutations in MlaA leads to membrane blebs, and the loss of phospholipids from the OM leads to increased transport of phospholipids from the IM to the OM causing cells to shrink. Cells eventually die via mechanical stress due to shrinkage and an increase in cytoplasmic concentration (Sutterlin et al., 2016). MlaA and the Mla pathway have previously been shown to maintain the asymmetry of the OM (Malinverni and Silhavy, 2009).The decrease in expression of genes involved in

LPS biosynthesis may be functional in protecting the cell from accumulation of LPS and membrane blebbing, and subsequent cell death in stationary phase.

Many lipid A modification genes are involved in increasing resistance to compounds such as colistin (Olaitan et al., 2014). Therefore, it was expected that enzymes involved in modification of lipid A and LPS would have increased expression in stationary phase, contributing to the decreased permeability of bacterial cells. In the preceding chapter, it was shown that a high concentration of EDTA did not make cells more permeable to EtBr in stationary phase. It was therefore thought that LPS played a role in the strengthening of the permeability barrier. Results from this transcriptomic dataset did not confirm this.

Table 7-2 Differentially expressed genes involved in lipid A biosynthesis

Gene	1 hr vs 3 hr fold change	1 hr vs 5 hr fold change
lpxH	0.28	0.17
lpxB	0.41	0.21
lpxK	0.38	0.21
lpxA	-	0.25
lpxL	-	0.30
lpxD	-	0.41

Genes involved in lipid A modification that were significantly altered in this dataset had decreased expression, meaning that there was less modification of lipid A. All genes involved in modification and their fold changes were shown in **Table 7-3** and how they modify lipid A is shown in **Figure 7-7** (Raetz et al., 2007). PhoPQ activates the two-component regulator system PmrAB. PmrAB has been shown to be important in controlling lipid A modification including incorporation of 4-amino-4-deoxy-L-arabinose (L-Ara4N) (Farizano et al., 2012) and in this dataset had decreased expression at 5 hours. The genes shown in **Table 7-3** for L-Ara4N modification, are involved in the conversion of glucose to L-Ara4N and the subsequent attachment of L-Ara4N to lipid A, catalysed by ArnT (Raetz et al., 2007), and all the DEGs involved in this pathway also had decreased expression in stationary phase. L-Ara4N has been shown to be fundamental for polymyxin resistance (Gunn et al., 1998). The attachment of ethanolamine by EptA is also induced by PmrAB with decreased expression in this dataset. Modification of lipid A by L-Ara4N and ethanolamine acts to neutralise the negative charges of LPS, therefore making cells less susceptible to the action of AMPs and polymyxins. Expression of the gene encoding PagP was decreased in this dataset and is involved in the incorporation of palmitate into lipid A. PagP has been shown to increase the number of acyl chains from 6 to 7, possibly stabilising LPS by increasing hydrophobicity of the cell (Goto et al., 2017).

Figure 7-7 Lipid A and the genes involved in the modification of lipid A

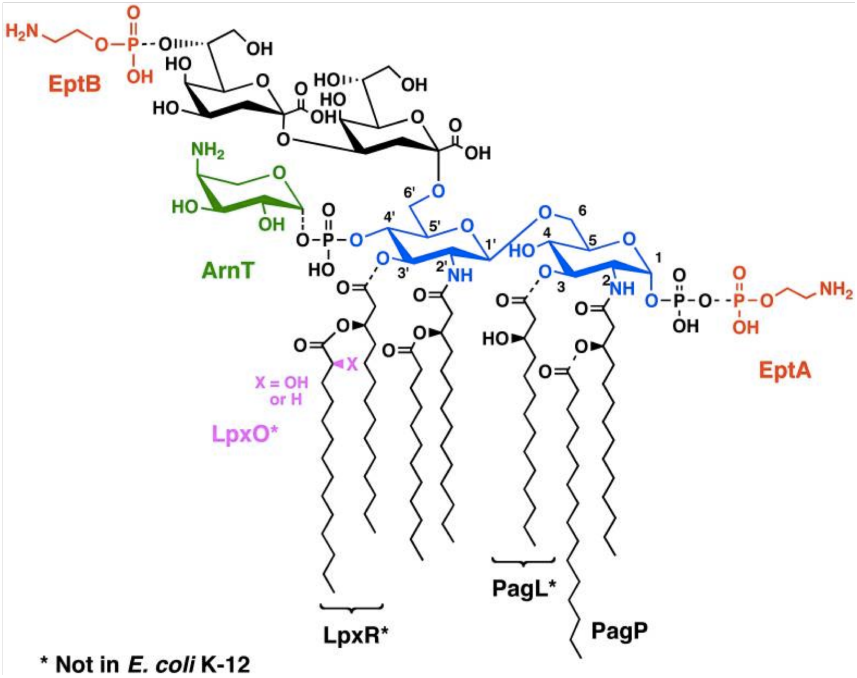

The chemical structure of lipid A is shown here. In red, EptA and EptB is involved in the attachment of ethanolamine, green shows the attachment of L-Ara4N and LpxO (purple) involved in conversion to OH. PagP (black) shows palmitate incorporation and PagL (black) for hydroxymyristoyl chain removal. This figure is taken from Raetz et al, 2007.

Table 7-3 Genes involved in lipid A modifications and their changed in expression

Modification	Gene	1 hr vs 3 hr fold change	1 hr vs 5 hr fold change
Two-component system	*pmrA*	-	0.18
	pmrB	0.49	0.11
L-Ara4N modification	*arnA*	-	0.07
	arnB	-	0.06
	arnC	-	0.09
	arnD	-	-
	udg	-	0.10
	arnT	0.46	-
OH group conversion	*lpxO*	-	2.54
Addition of ethanolamine	*eptA*	-	0.06
Phosphorylation	*LpxT (YeiU)*	-	-
Palmitate incorporation	*pagP*	0.28	0.11
Hydroxymyristoyl chain removal	*pagL*	-	-
Palmitoleote Incorporation	*lpxP*	0.13	0.05

One gene that had increased expression in this dataset was *lpxO*, which hydroxylates the myristic acid chain of LPS. It has previously been hypothesised that this gene, which encodes a hydroxylase/dioxygenase leads to release of 2-hydroxymyristate from *S.* Typhimurium in a macrophage which is subsequently involved in suppression of host cell signaling leading to survival of the bacterial (Gibbons et al., 2000). It is unknown why expression of this gene had increased while all other lipid A modification genes had decreased expression in stationary phase.

The reduced expression of lipid A modifications in stationary phase was not expected but was apparent. It is possible that the expression change is simply due to the decreased expression in lipid A biosynthesis, and therefore there is less lipid A to modify. It can be hypothesised that although LPS is most likely modified in stationary phase, it is not through the mechanisms discussed here. In **Figure 6-6**, it was shown that EDTA could not permeabilise a stationary phase membrane and in addition to the data discussed here, may mean that LPS crosslinking is not the most important mechanism in decreasing permeability to EtBr. In fact, it could be hypothesised that the decrease in membrane permeability has added complexity by a combination of changes in the IM, OM and in peptidoglycan. To identify the importance of LPS in stationary phase, further work would be needed. Since LPS is a target of EDTA, colistin and antimicrobial peptides, it may be possible to test these compounds in terms of resistance in actively growing or stationary phase cells. Another idea may be to overexpress the PmrAB sensor involved in most modifications that make cells resistant to polymyxins. Overexpression of *pmrAB* may be achieved by cloning onto a high copy number plasmid. Overexpressing this system may then lead to increased

modification in all growth phases, and the impact these modifications may have on stationary phase cells may be assessed, including EtBr accumulation.

7.4.4.3 Reduced cell wall remodelling may decrease membrane permeability

A key component of the Gram-negative envelope is the peptidoglycan cell wall. It has previously been shown that the dry weight of peptidoglycan increases in stationary phase (Mengin-Lecreulx and van Heijenoort, 1985). For this reason, it was hypothesised that an increase in peptidoglycan thickness may decrease the permeability of the Gram-negative membrane.

Initial analysis showed that the *dadX* gene involved in the conversion of L-alanine to D-alanine had increased expression. The fold change at 5 hours of growth compared to 1 hour was 8.75. It was initially thought that the change in expression of this gene would mean that there was an increase in D-alanine and therefore an increase in peptidoglycan biosynthesis for an increase in thickness of the cell wall. However, the expression of the *dadA* gene also increased (21.53-fold change), and this encodes a dehydrogenase that converts D-ala to pyruvate and ammonium in SL1344. The genes involved in the formation of the D-ala-D-ala dipeptide (Lugtenberg and v Schijndel-van Dam, 1973), *ddlA* and *ddlB* were not significantly changed at 5 hours. Since these genes were not significantly altered, it suggests that the increase in D-ala was unrelated to peptidoglycan. *S.* Typhimurium contains two alanine racemases, the *alr* racemase is constitutive in maintaining the D-ala required for growth, and the *dadX* racemase that is inducible, most likely by the presence of L-ala when D-ala is required for an energy source (Wild et al., 1985, Barreteau et al., 2008). This is common to *E. coli* and *Pseudomonas aeruginosa* (Barreteau et al., 2008, Trivedi et

al., 2018). The increase in expression of DadA, the dehydrogenase, suggests the importance of D-alanine for energy during stationary phase in a nutrient starved environment, by conversion to pyruvate (Trivedi et al., 2018). However, it has also been shown that the deletion of *dadA* reduces cell stiffness, so therefore may be implicated in stationary phase permeability (Trivedi et al., 2018). However, the expression of *alaE* increased with a fold change of 11.03 at 5 hours compared to 1 hour. AlaE is an L-alanine exporter, suggested to be powered by the PMF and involved in extrusion of L-ala when accumulation of L-ala is at toxic levels (Kim et al., 2015, Katsube et al., 2019). For this reason, we can hypothesise that the *dadX* gene may not be involved in an increase in peptidoglycan biosynthesis, however the *dad* operon has previously been linked to cell stiffness (Trivedi et al., 2018). It is also possible there is too much L-ala in Gram-negative cells in stationary phase, and to reduce the accumulation level, it either induces *dad* genes to convert to D-ala as an energy source or L-ala is removed from cells (**Figure 7-8**).

Figure 7-8 Cytoplasmic pathway for the biosynthesis of peptidoglycan and its insertion into the periplasm

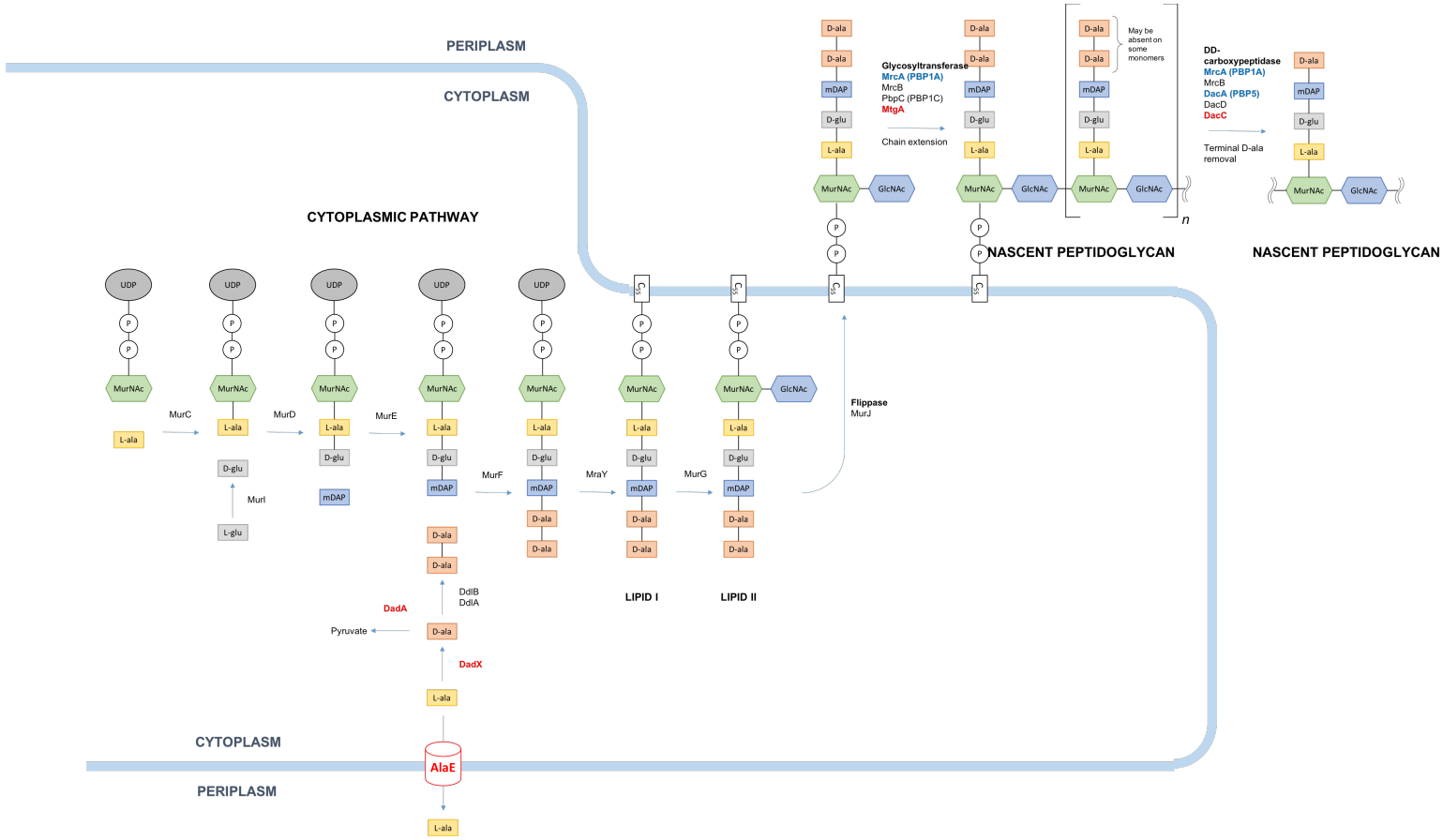

This diagram shows the reactions required for the biosynthesis of peptidoglycan in the cytoplasm. The *dad* operon is also included as well as the AlaE transporter for the removal of L-alanine. The enzymes required for each step are shown above each blue reaction arrow. Enzymes that had unchanged expression in the reaction have black font, upregulated enzymes are shown in red and downregulated in blue. UDP, uridine diphosphate; C_{55}, undecaprenyl phosphate; MurNAc, N-Acetylmuramic acid; GlcNAc, N-Acetylglucosamine; mDAP, *meso*-diaminopimelic acid. This figure was created by Dr. Tim Overton, adapted from Barreteau et al. (2008), Vollmer et al. (2008) and Karp et al. (2014)

It was possible that peptidoglycan played a role in membrane permeability through the maturation pathway. Briefly, the MurNAc lipid with the pentapeptide chain is synthesised in the cytoplasm. Lipid II (MurNAc + GlcNAc) are then flipped on the inner membrane into the periplasm by the flippase, MurJ. None of the enzymes required for these steps were significantly altered in stationary phase compared to 1 hour of growth (**Figure 7-8**). Chain extension of nascent peptidoglycan is produced with glycoslytransferases which add lipid II to the peptidoglycan chain. In this dataset, *mrcA* (PBP1A) expression decreased but *mtgA* expression increased. Since both these genes encode glycosyltransferases, it is unlikely that chain extension increases in stationary phase. D,D-carboxypeptidation of nascent peptidoglycan strands leads to the removal of the terminal D-ala of the pentapeptide. Carboxypeptidases include MrcA, MrcB, DacA, DacC and DacD. Of these, only *mrcA* and *dacA* had decreased expression following 5 hours of growth (**Table 7-4**).

Table 7-4 Genes involved in peptidoglycan maturation and remodelling and the changes in expression

Enzymes	Gene	1 hr vs 3 hr fold change	1 hr vs 5 hr fold change
glycosyltransferases	*mrcA*	0.40	0.29
	mrcB	-	-
	pbpC	-	-
	mtgA	2.41	2.88
D,D-carboxypeptidases	*mrcA*	0.40	0.29
	mrcB	-	-
	dacA	0.46	0.19
	dacC	-	2.34
	dacD	-	-
D,D-transpeptidases	*mrcA*	0.40	0.29
	mrcB	-	-
	mrdA	0.47	0.29
	ftsI	0.29	0.45
L,D-transpeptidases	*ldtA*	-	2.50
	ldtB	0.12	0.10
	ldtD	-	-
	ldtE	2.44	2.96
Amidases	*amiC*	0.49	0.46
	ybjR	-	2.41
Transglycosylases	*mltA*	-	0.26
	mltC	-	0.35
	mltD	0.30	0.11
	mltF	0.38	0.39
D,D-endopeptidases	*mepS*	0.31	0.25
	mepM	0.31	0.26
	pbpG	0.36	0.36

Interestingly, transpeptidase enzymes were differentially expressed. In *E. coli*, the majority of peptidoglycan crosslinks are 4,3 or D,D crosslinks, meaning the crosslink is between D-ala and *meso*-diaminopimelic acid (mDAP) (**Figure 7-9B**). It has previously been shown that a small percentage of crosslinks can occur between mDAP and mDAP, named L,D crosslinks (**Figure 7-9A**). Of the 4 D,D-transpeptidase, *mrcA, mrdA* and *ftsI* had decreased expression at 5 hours, and *mrcB* remained unchanged (**Table 7-4**). LD crosslinks have been shown to increase in stationary phase (More et al., 2019). There are two genes encoding L,D-transpeptidases, *ldtD* and *ldtE* (*ynhG*) that form LD crosslinks. Transcription of *ldtD* was unchanged at 5 hours of growth compared to 1 hour, but *ldtE* expression increased (**Table 7-4**). LdtD has previously been shown to increase L,D crosslinks to decrease cellular permeability and prevent bacterial cell lysis (More et al., 2019). Although it was only *ldtE* with increased expression, it is possible that the increase in L,D crosslinks, produced by LdtE transpeptidase, increases the strength of the Gram-negative membrane barrier in stationary phase. In clinical isolates, it has been found that bacterial cells can be highly resistant to β-lactams, because they do not require PBPs for transpeptidation (Peters et al., 2018). Further to this, it has been suggested that in *E. coli,* the membrane is stabilised by L,D-transpeptidases crosslinking Lpp and peptidoglycan, and this may decrease permeability of the outer membrane (Peters et al., 2018). The enzymes that attach Lpp to mDAP (More et al., 2019) include LdtA which had increased expression at 5 hours and LdtB which had decreased expression (**Table 7-4**). Although a Gram-positive organism, L,D-crosslinks reached 80% in stationary phase *Mycobacterium tuberculosis* and it was suggested that this may be linked to the cells adapting to stationary phase

survival (Lavollay et al., 2008). From this data in addition to previous studies, it can be hypothesised that *S.* Typhimurium has increased L,D-crosslinks in stationary phase. It is therefore possible that the increase in the LdtE transpeptidase, and more L,D-crosslinks, leads to strengthened and impermeable Gram-negative permeability barrier in stationary phase.

Figure 7-9 A schematic for LD and DD transpeptidation reactions of peptidoglycan in the periplasm.

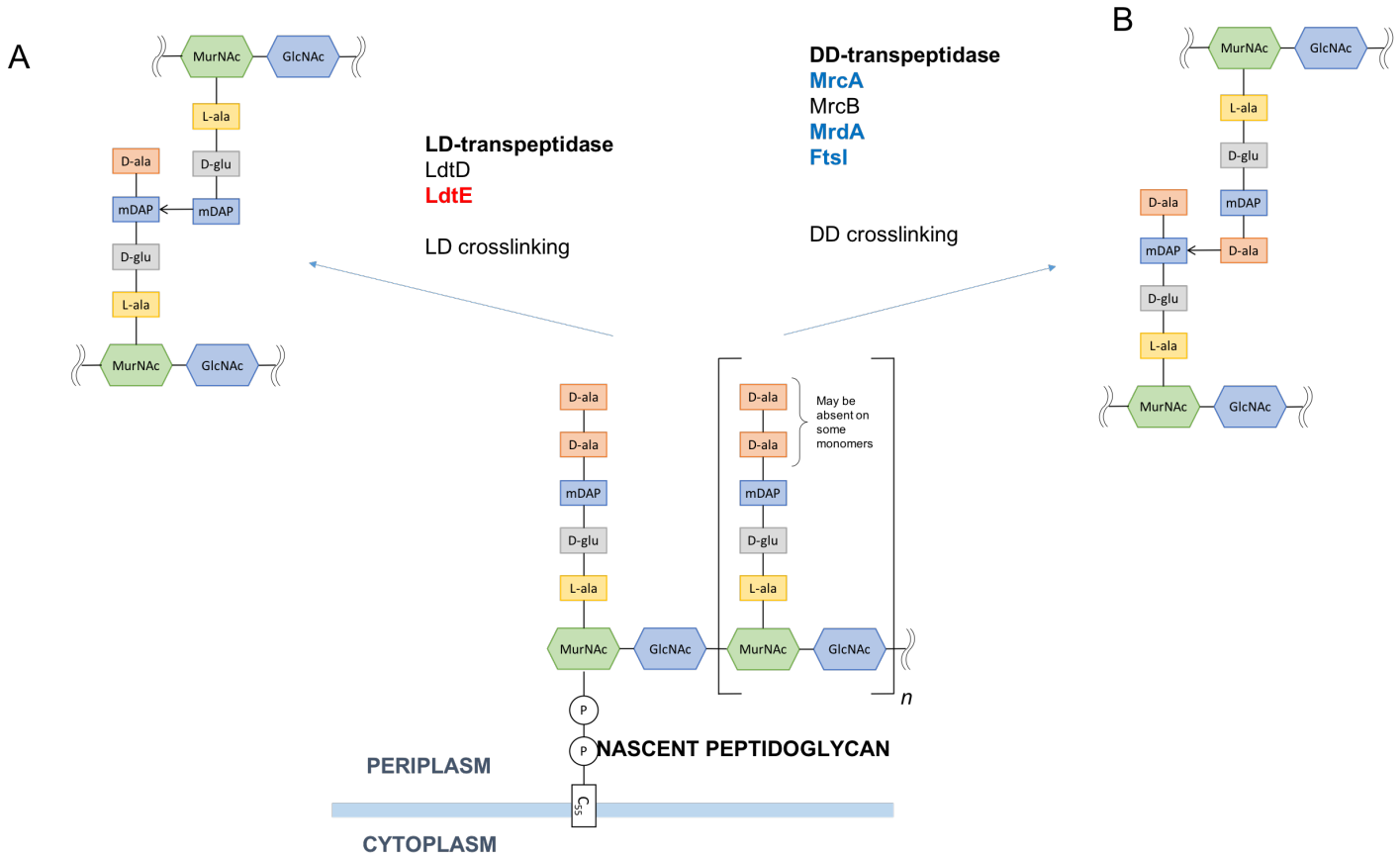

This schematic shows the outcomes of nascent peptidoglycan. (**A**) shows the enzymes required for LD crosslinking. (**B**) shows the enzymes required for DD crosslinking. Enzymes with unchanged expression in the reaction have black font, upregulated enzymes are shown in red and downregulated in blue. C_{55}, undecaprenyl phosphate; MurNAc, N-Acetylmuramic acid; GlcNAc, N-Acetylglucosamine; mDAP, *meso*-diaminopimelic acid. This figure was created by Dr. Tim Overton, adapted from Barreteau et al. (2008), Vollmer et al. (2008) and Karp et al. (2014)

Expression of several hydrolases described in *E. coli* decreased in stationary phase and hydrolases are involved in the degradation and remodelling of peptidoglycan (**Table 7-4**).

The amidase encoding gene, *amiC*, had decreased expression and its role is to degrade peptidoglycan by the removal of the pentapeptide chain from peptidoglycan units (**Figure 7-10A**). AmiC is one of three amidases in *E. coli* and plays the largest role in degradation and peptidoglycan remodelling during cell division, by septum cleavage (Egan et al., 2020). AmiC is activated by NlpD (Uehara et al., 2010), which surprisingly showed an increase in expression in this dataset, even though *amiC* was decreased. However, the decrease in *amiC* transcripts suggests that there is less peptidoglycan remodelling and less cleavage, possibly expected for cells in stationary phase. However, another amidase encoding gene named *ybjR*, had increased expression and it was unknown why this would be.

MltA, MltC, MltD and MltF are lytic transglycosylases (Lommatzsch et al., 1997) involved in the hydrolysis of bonds between peptidoglycan units (**Figure 7-10A**). The genes encoding these transglycosylases showed decreased expression in this dataset and are also involved in septum cleavage, although it has been suggested that their contribution to cleavage and cell division is reduced in comparison to amidases in *E. coli* (Egan et al., 2020). In some organisms, such as *Vibrio cholerae*, amidase activity alone has been shown to be insufficient for cell division and requires MltC also (Weaver et al., 2019). Further to this, D,D-endopeptidases, which break the pentapeptide crosslinks also had decreased expression (MepS, MepM and PbpG) (**Figure 7-10B**). These endopeptidases are essential for cell elongation, by

insertion of new peptidoglycan (Singh et al., 2012, Egan et al., 2020). The genes encoding endopeptidases are less required in stationary phase compared to 1 hour of growth, and it is most likely because cells are no longer growing and dividing exponentially so less peptidoglycan remodelling is required. It is possible that the reduction in hydrolysis of peptidoglycan strands in stationary phase makes the Gram-negative cell more stable, and the increased thickness of the peptidoglycan cell wall makes cells less permeable.

This analysis suggests that *S.* Typhimurium makes more L,D-crosslinks than D,D-crosslinks, and remodelling of the cell wall is reduced in stationary phase, and both may contribute to the decrease in permeability of the cell envelope. The caveat is that most studies of peptidoglycan are carried out in *E. coli*, and *S.* Typhimurium may vary slightly, although most often, there are similarities between these organisms. Further work would be required to confirm whether changes in peptidoglycan do confer reduced EtBr accumulation in stationary phase. However, unpicking the involvement of peptidoglycan will prove challenging because PG synthesis and remodelling is highly dynamic, spatially and temporally regulated, and many enzymatic steps are catalysed by multiple enzymes with different regulation.

Figure 7-10 Reactions and enzymes involved in peptidoglycan degradation and remodelling

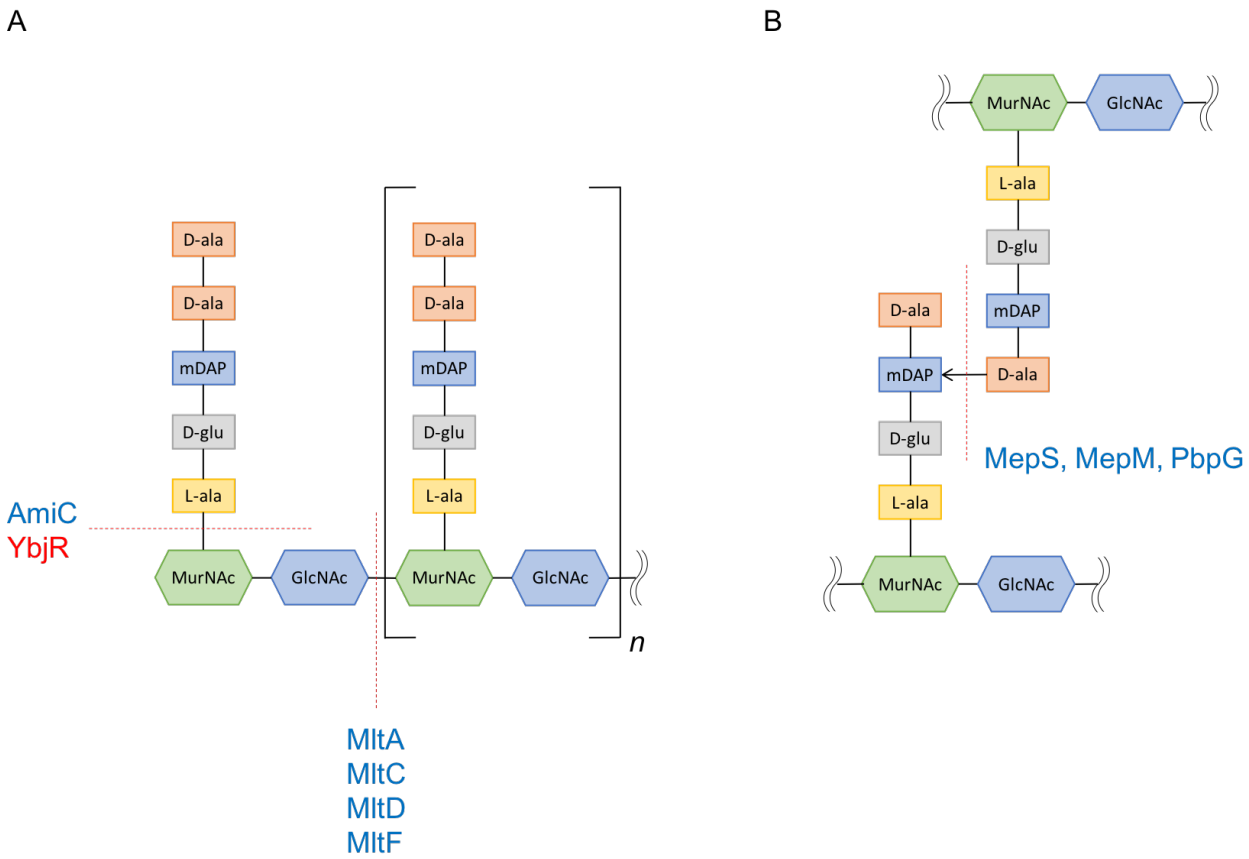

This schematic shows the steps involved in degrading bonds of peptidoglycan. (**A**) shows pentapeptide removal by amidases and degradation of peptidoglycan subunits by lytic transglycosylases. (**B**) shows DD crosslinking degradation by endopeptidases. Enzymes with increased expression at 5 hours are shown in red and decreased expression is shown in blue. MurNAc, N-Acetylmuramic acid; GlcNAc, N-Acetylglucosamine; mDAP, *meso*-diaminopimelic acid. This figure was created by Dr. Tim Overton, adapted from Barreteau et al. (2008), Vollmer et al. (2008) and Karp et al. (2014)

7.4.4.4 Decreased expression of the ECA biosynthesis pathway

In **Chapter 6**, it was discussed that the RpoS dependent gene *yhdP* may play a role in the strength of the permeability barrier in a carbon limited environment. It was hypothesised that cyclic ECA damages the membrane in the absence of YhdP, suggesting that an imbalance of cyclic ECA may lead to membrane damage (Mitchell et al., 2018). Another study implicated ECA and LPS in membrane damage (Klobucar et al., 2020). Increasing evidence from ECA studies, with its previously unknown function, link it to membrane permeability in *E. coli* and *S.* Typhimurium.

For this reason, the role of ECA in stationary phase in the dataset presented here was analysed. In the dataset, the expression of *yhdP* was not significantly altered at 3 or 5 hours of growth compared to 1 hour. However, it was previously shown that YhdP deletion caused susceptibility to antibiotics regardless of growth phase (Mitchell et al., 2018), and therefore may suggest that it is not a gene that is only expressed in stationary phase. YhdP is an unannotated gene with little known about its function. Using pathway tools software, it became apparent that the biosynthesis of ECA was decreased in stationary phase with 5 genes involved in its biosynthesis showing decreased expression. The following genes *wecC, rffG, wecD*, RS20200 and *wecG* have a fold change of 0.40, 0.43, 0.39, 0.21 and 0.47 respectively. The pathway is shown in **Figure 7-11**. This pathway only shows that ECA biosynthesis had decreased expression, however, it is possible that less ECA would be converted to cyclic ECA in stationary phase, if biosynthetic genes had decreased expression. It has previously been shown that ECA is not converted to cyclic ECA in mutants lacking *wecA, wecF* or *wecG* (Erbel et al., 2003), and as expression of the *wecG* is

decreased in this dataset, it may be deduced that there is less cyclic ECA and less ECA in general in stationary phase.

It is possible that the damage caused by ECA may be eliminated in stationary phase to increase the strength of the permeability barrier. To characterise the importance of ECA in stationary phase in *S.* Typhimurium SL1344 would be subject to further work. It would be necessary to confirm decreased expression of genes in stationary phase by RT-PCR, followed by attempts to calculate the concentration of ECA within cells in stationary phase, with subsequent production of mutant strains that cannot produce ECA to identify the effect on EtBr accumulation in stationary phase.

From the results and discussion provided in this section, it is clear that there is a decrease in the permeability of the cell envelope in stationary phase. This process is multi-layered, with changes in the OM, IM, peptidoglycan and in ECA. It is also highly likely that there are more mechanisms involved in altering the membrane, that are highly complex and were unidentified in this dataset. From this, we can conclude that EtBr accumulation in stationary phase remains low due to reduced influx because of decreased permeability (through multiple mechanisms).

Figure 7-11 The ECA biosynthesis pathway in *S.* Typhimurium SL1344

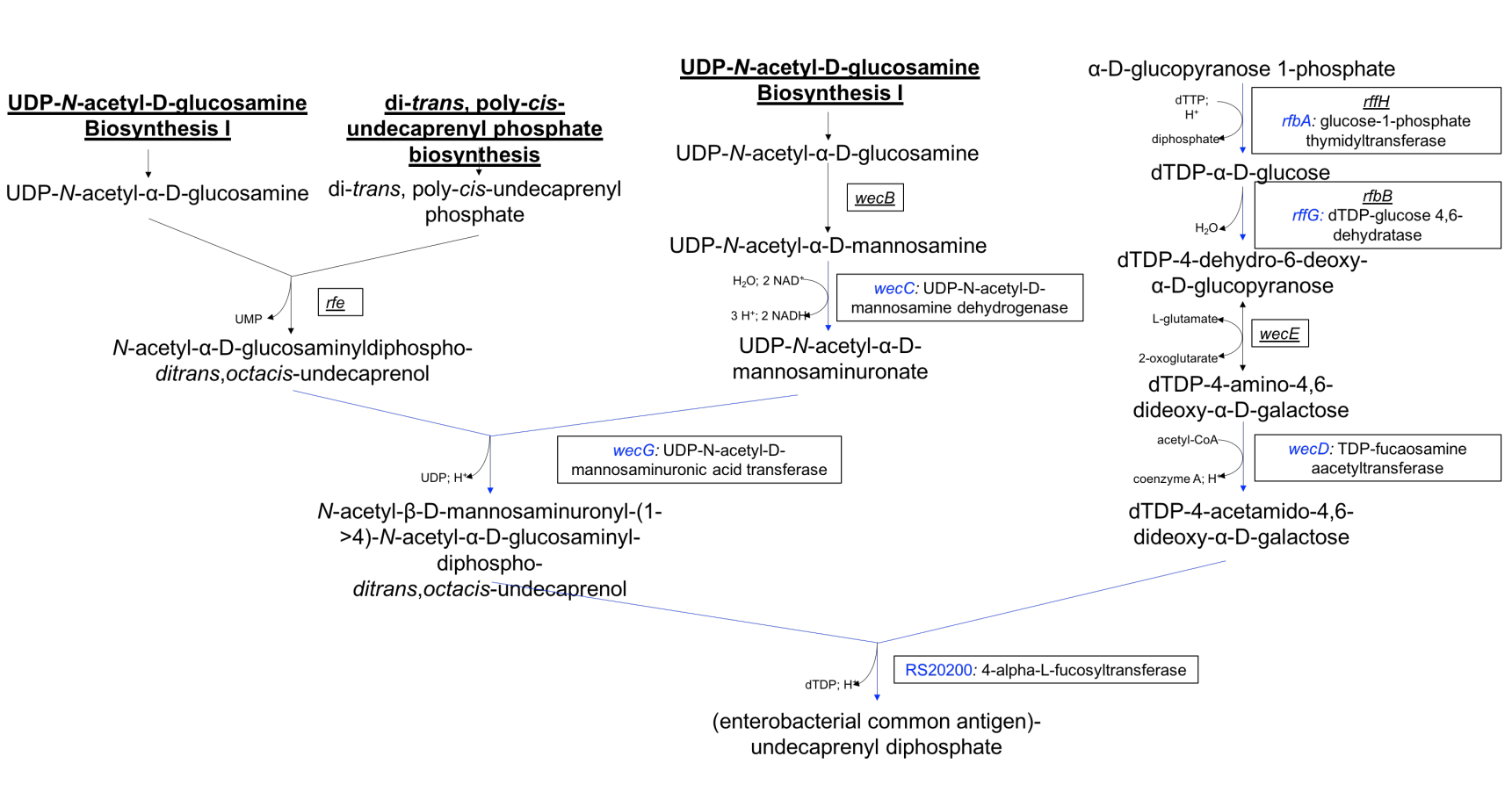

This schematic shows the pathway for biosynthesis of ECA. The genes that were downregulated at 5 hours are shown in blue. Genes that were unchanged are shown in black. This figure was produced by EE Whittle using Pathway Tools Software and databases (Karp et al., 2016, Caspi et al., 2020, Fulcher et al., 2018)

7.4.5 There are limited changes in expression between SL1344 and Δ*acrB*

RNA extraction and transcriptomic analysis was also carried out on SL1344 Δ*acrB* at 1, 3 and 5 hours to determine if there was any differential transcription between the strains. It was also possible that the removal of the AcrB from a cell may contribute to increased permeability of the cell or differences in physiology and so this strain was also analysed.

7.4.5.1 Initial comparisons of SL1344 vs *acrB* mutant at each time point

Commonly, transcriptomic studies compare a bacterial strain against a mutant strain at a single time point (commonly mid-log phase). RNA extractions and transcriptomics analysed here were done at 1, 3 and 5 hours from a growing culture therefore SL1344 Δ*acrB* was compared to WT at each time point.

After 1 hour of growth, only 63 genes were differentially expressed in Δ*acrB* compared to SL1344. Of these, *acrB* had the biggest decrease in expression, and other genes with decreased expression mainly encoded hypothetical proteins. The genes with the biggest increase in expression in SL1344 Δ*acrB* were the *Salmonella* Pathogenicity Island-2 (SPI-2) genes as well as *ramA* and *fljAB*. At 5 hours of growth, only 57 genes were differentially expressed compared to SL1344. Of these, *fljAB* was the most highly expressed in SL1344 Δ*acrB*. The curli producing gene *csgB* also had increased expression as well as SPI-1 genes. The 3 hour time point, equivalent to entrance into stationary phase, was at an OD_{600} of over 0.6 but was the most closely related time point to mid-log phase, the norm for RNAseq analysis. At this time point,

548 genes were differentially expressed compared to SL1344 including many tRNAs, ribosomal genes and SPI-1 genes with increased expression. The *met* genes had the biggest decrease in expression compared to SL1344.

In 2009, Webber et al., analysed the transcriptomics of SL1344 *acrB::aph* compared to SL1344 in minimal media at OD_{600} ~0.7. SL1344 *acrB::aph* only differs to the Δ*acrB* studied in this dataset by the *aph* cassette inserted into *acrB*. It was found that 569 genes were differentially expressed, similar in number to the 548 genes differentially transcribed in this dataset. It was found that 64% of differentially expressed genes related to a decrease in expression in SL1344 *acrB::aph*, showing that genes involved in pathogenicity (SPI-1), anaerobic metabolism, chemotaxis and motility had decreased expression (Webber et al., 2009). Only 32% of DEGs showed decreased expression in this dataset. In comparison to the dataset of this study, genes of *narGHIJK* operon had decreased expression in Δ*acrB* compared to SL1344 at 3 hours of growth but *napABC* and *nirBC* were increased, differing to previous data. There was an overlap in genes with increased expression, as *uhpA* (3 hours)*, malT* (3 hours) and *ramA* (1 hour) in the Δ*acrB* and *acrB::aph* strain in both studies. In this dataset, *ramA* expression only increased at 1 hour, and therefore is common to actively growing cells. The increase in *ramA* expression, a regulator of *acrAB*, due to the inactivation of *acrB* has previously been described, and is a regulator of the production of *acrAB* transcript (Lawler et al., 2013). Based on data presented in this thesis, it is possible that the lack of expression changes in *ramA* in stationary phase compared to SL1344 is due to the lack of dependency on AcrAB-TolC in stationary phase for cell survival.

In 2017, Wang-Kan et al. compared SL1344 AcrB-D408A to SL1344 using RNAseq. The mutation in D408 led to the production of a non-functional protein by impairing proton translocation. This study differed to the one presented here because transcriptional comparisons were made at a single time point (cells that were grown to OD_{600} of 0.6) but MOPs minimal media was used as the growth medium. Similarities to this dataset include upregulation in *csgB* and *nirBD* and a downregulation in *cys* genes and tRNA-met. In contrast, SPI-1 and SPI-2 genes had decreased expression in the D408A mutant (Wang-Kan et al., 2017) but increased expression in the analysis presented here.

This dataset did not perfectly match previously published data but there could be a few reasons for this. The mutants used in the other studies discussed (Webber et al., 2009, Wang-Kan et al., 2017) were genetically different to Δ*acrB*. These experiments were performed in a different media type which has been shown to cause largescale changes to the transcriptome (Blair et al., 2013). In addition, the sampling of the previous studies was different to the time points used here, and relied on a single time point rather than comparing between three. The SalCom database shows that a number of SPI-1 genes have increased expression in late exponential and early stationary phase (Kroger et al., 2013). Therefore, this dataset highlights the limitations of comparing a mutant strain to WT at a single time point when gene expression may differ with growth phase by allowing gene expression to be compared across growth.

The genes with the most decreased expression at 3 hours in SL1344 Δ*acrB* were *met* genes. It has already been shown in **Section 7.4.2** that the *met* genes had a

high increase in expression at 3 hours (late exponential phase) in SL1344. However, when comparing SL1344 Δ*acrB* at each time point, the *met* genes were highly upregulated at 3 hours compared to 1 hour. Therefore, the downregulation of *met* genes in WT vs Δ*acrB* analysis is misleading, as it suggests that the expression of these genes is being switched off by the absence of AcrB, but there is simply less increase in expression at 3 hours and 5 hours compared to SL1344. Fold comparisons for *met* genes can be found in **Table 7-5**. This may be due to the time point of RNA extraction, and *met* gene expression may peak a short time after in SL1344 Δ*acrB*. This analysis highlighted that comparing one strain to another at a single time point is misleading because it may be concluded that genes or pathways are switched off, rather than just due to changes in expression across growth.

For this reason, to be able to identify any changes in SL1344 Δ*acrB* compared to SL1344, relating to growth, SL1344 Δ*acrB* was compared between 1, 3 and 5 hours of growth, like the above analysis on SL1344, and magnitudes of change were compared to the SL1344 dataset.

Table 7-5 Fold changes in met genes when comparing SL1344 to Δ*acrB* and when comparing time points during growth

Gene	SL1344 vs Δ*acrB* fold change at 3 hrs	Δ*acrB* fold change at 1 vs 3 hrs	Δ*acrB* fold change at 1 vs 5 hrs	SL1344 fold change at 1 vs 3 hrs	SL1344 fold change at 1 vs 5 hrs
metJ	0.29	-	-	4.29	2.08
metQ	-	2.53	3.11	4.33	2.30
metC	0.20	-	3.21	10.71	4.15
metK	0.36	3.71	7.08	11.02	6.20
metI	0.22	2.40	4.68	12.00	4.36
metN	0.12	2.03	3.28	17.43	3.79
metL	0.06	-	3.70	27.63	3.20
metA	0.05	-	13.18	42.82	13.61
metB	0.03	-	2.54	48.08	2.21
metR	0.03	-	4.48	51.96	5.54
metF	0.03	5.02	33.64	155.57	37.62
metE	0.03	8.60	104.04	236.20	64.66

7.4.5.2 Some genes with highly similar expression in SL1344 and Δ*acrB*

To identify genes that were similarly expressed in both SL1344 and SL1344 Δ*acrB* at 3 and 5 hours of growth, first, genes that were >50-fold upregulated in WT at 5 h compared to 1h were filtered. Next, the ratio of expression of these genes in SL1344 and SL1344 Δ*acrB* after 5 hours of growth was calculated, and genes with <2-fold different expression (ratio of 0.5-2) were considered not significantly different. Results are shown in **Table 7-6**.

Genes that were similarly expressed at 5 hours of growth, highlight their importance in survival of both strains. RMF expression was not significantly different in SL1344 from Δ*acrB*. The importance of RMF in stabilising ribosomes for stationary phase has been discussed in **Appendix V** This suggests that the shutting down of translation in stationary phase was unaltered by the absence of AcrB. Several genes involved in anaerobic metabolism (**Table 7-6**) were unaltered between strains and this highlights the importance of anaerobic respiration for SL1344 in stationary phase. Furthermore, OmpW was highly expressed to a similar level in both strains, and is another protein suggested to be involved in anaerobic respiration through its uptake of fumarate (Xiao et al., 2016). Analysis also showed that PTS sugar transporters were highly expressed at 5 hours in both strains to a similar level. As previously discussed, sugar transporters are important for the scavenging of sugars for carbon metabolism in a starved stationary phase environment, and this would be key to survival in both strains.

This analysis produced hypotheses that could be explored further. However, the conclusion is that many genes that are differentially expressed at different time points

were expressed similarly in SL1344 and SL1344 Δ*acrB*. This not only highlights the importance of these genes in stationary phase, but also shows that but that normal expression of many genes across growth phases is not significantly altered by the removal of AcrB.

Table 7-6 Genes that had >50-fold increased expression in SL1344 where Δ*acrB* DEGs were <2-fold different (fold differences were calculated by dividing the Δ*acrB* fold change by the SL1344 fold change). Genes are ordered based on chromosome position

Gene	Product	fold change WT 1 hr vs 5 hr	fold change Δ*acr*B 1 hr vs 5 hr	1 hr - 5 hr Δ*acrB* vs WT fold change
bssR	biofilm formation regulator	48.03004	26.49235	0.551579
dmsB	dimethylsulfoxide reductase subunit B	22.97672	36.79017	1.601193
rmf	ribosome modulation factor	63.97515	48.47616	0.757734
RS05370 (STM1093)	hypothetical protein	28.55417	24.87366	0.871104
pipD	dipeptidase	23.48148	23.37286	0.995374
RS06580 (STM1324)	fructosamine kinase family protein	25.05512	15.38411	0.614011
orf408	hypothetical protein	118.7844	66.31137	0.55825
ydfZ	putative selenium delivery protein	121.5918	173.8868	1.430087
RS08035 (STM1612)	aminopeptidase	45.15643	26.11991	0.578432
sseJ	SPI-2 type III secretion system effector	22.34555	15.88857	0.71104
ompW	outer membrane protein	42.21751	37.05637	0.877749
ychH	stress-induced protein	122.1334	114.8599	0.940446
mtfA	DgsA anti-repressor MtfA	25.77601	26.90254	1.043704
thiD	bifunctional hydroxymethylpyrimidine kinase/phosphomethylpyrimidine kinase	61.74884	70.22501	1.137269
RS11230 (STM2186)	NAD(P)-dependent oxidoreductase	28.89164	22.79262	0.7889
mglA	galactose/methyl galactoside ABC transporter ATP-binding protein	36.08547	19.16828	0.531191
mglB	methyl-galactoside ABC transporter substrate-binding protein	42.98767	32.82829	0.763668
galS	DNA-binding transcriptional regulator	24.69407	17.37041	0.703424
glpA	anaerobic glycerol-3-phosphate dehydrogenase subunit A	22.85746	14.07548	0.615794
glpB	glycerol-3-phosphate dehydrogenase subunit GlpB	24.80682	12.77082	0.514811
RS12015 (STM2342)	PTS ascorbate transporter subunit IIC	113.2709	74.53101	0.657989
RS12020 (STM2343)	PTS mannitol transporter subunit IIB	167.5642	150.1628	0.896151
RS12025 (STM2344)	PTS ascorbate transporter subunit IIA	45.80246	29.68573	0.648125

fadI	acetyl-CoA C-acyltransferase	22.35455	14.55297	0.651007
asrA	anaerobic sulfite reductase subunit A	22.3593	27.69181	1.238492
grcA	autonomous glycyl radical cofactor	32.09541	32.33508	1.007468
RS14180 (STM2740)	tyrosine-type recombinase/integrase	230.5484	116.3981	0.504875
RS14280 (STM2759)	peptide ABC transporter substrate-binding protein	44.98997	28.63874	0.636558
srlA	PTS glucitol/sorbitol transporter subunit IIC	30.31045	16.50655	0.544583
hydN	electron transport protein	61.58271	49.39114	0.802029
RS14730 (STM2844)	hypothetical protein	70.50627	56.73931	0.804741
hycI	hydrogenase maturation peptidase	74.77116	69.81799	0.933756
hycH	formate hydrogenlyase maturation protein	58.04262	83.28888	1.434961
hycG	formate hydrogenlyase subunit 7	58.68462	61.77389	1.052642
hycF	formate hydrogenlyase subunit 6	70.05263	73.07097	1.043087
hycE	formate hydrogenlyase subunit 5	87.3801	85.24238	0.975535
hycD	hydrogenase 3 membrane subunit	113.6679	108.3841	0.953515
hycC	formate hydrogenlyase subunit 3	59.04612	57.16628	0.968163
hycB	formate hydrogenlyase subunit 2	113.0147	72.69586	0.643242
hycA	formate hydrogenlyase regulator	109.9628	72.28057	0.657318
fucP	L-fucose:H+ symporter permease	20.20641	17.67293	0.87462
hybB	Ni/Fe-hydrogenase cytochrome b subunit	27.14116	15.93562	0.587138
hybA	hydrogenase 2 operon protein	36.07618	31.83663	0.882483
hybO	hydrogenase 2 small subunit	35.8866	32.96687	0.91864
dctA	dicarboxylate/amino acid:cation symporter	27.79532	19.11987	0.687881
RS19410 (STM3770)	PTS sorbose transporter subunit IIC	31.47596	19.07765	0.606102
RS19415 (STM3771)	PTS sugar transporter subunit IIB	33.72046	45.40774	1.346593
RS19420 (STM3772)	PTS fructose-specific transporter subunit IIA	129.9588	138.7421	1.067585
RS19470 (STM3782)	PTS galactitol transporter subunit IIC	20.01854	10.87683	0.543338
RS19475 (STM3783)	PTS sugar transporter subunit IIB	23.63526	12.24326	0.518008
RS19480 (STM3784)	PTS sugar transporter subunit IIA	26.50835	21.02723	0.79323
RS19485 (STM3785)	GntR family transcriptional regulator	39.41004	42.68038	1.082982
rbsD	D-ribose pyranase	31.32656	32.95951	1.052126
rbsA	ribose ABC transporter ATP-binding protein	26.94843	37.82703	1.403682
metE	5-methyltetrahydropteroyltriglutamate-- homocysteine S-methyltransferase	64.65527	104.0363	1.609092

lsrR	transcriptional regulator	23.6257	16.78057	0.710268
lsrA	AI-2 ABC transporter ATP-binding protein	61.40747	42.4575	0.691406
metF	methylenetetrahydrofolate reductase	37.61624	33.64313	0.894378
frwC	PTS fructose-specific transporter subunit EIIC	27.03165	15.52864	0.574461
thiG	thiazole synthase	21.57164	39.5252	1.832276
thiS	sulfur carrier protein	25.80402	29.06791	1.126488
fdhF	formate dehydrogenase H subunit alpha, selenocysteine-containing	40.77211	35.96321	0.882054
dcuB	anaerobic C4-dicarboxylate transporter	46.43089	32.79077	0.706227
RS22105	molybdopterin-dependent oxidoreductase	23.18101	18.01283	0.777051
frdD	fumarate reductase subunit FrdD	23.23162	11.74676	0.505637
frdA	fumarate reductase (quinol) flavoprotein subunit	28.39094	14.78644	0.520815
aidB	isovaleryl-CoA dehydrogenase	38.12017	25.31198	0.664005
RS22475	DUF1471 domain-containing protein	25.98272	21.51163	0.827921
RS22790 (STM4442)	putative cytoplasmic protein	23.98084	41.2426	1.719815
RS22800 (STM4444)	hypothetical protein	25.727	30.58074	1.188663
RS22805 (STM4445)	amidohydrolase/deacetylase family metallohydrolase	20.81139	18.09454	0.869454
idnT	Gnt-II system L-idonate transporter	31.75324	20.13884	0.63423
btsT	pyruvate/proton symporter	177.2093	88.61197	0.500041
traR	IncI1-type conjugal transfer protein	22.71466	33.88046	1.491568
ypfM	protein YpfM	86.35504	66.3771	0.768653

7.4.5.3 Some genes were not as highly expressed in stationary phase in Δ*acrB* compared to SL1344

A number of genes in SL1344 Δ*acrB* were not as highly expressed as in SL1344 at the time points analysed. However, it is important to note that there were no genes identified that showed increased expression in one strain but decreased expression in another strain.

Genes that were more highly induced at 5 hours in SL1344 than Δ*acrB*, genes were identified. First, genes that were >20-fold induced in SL1344 at 5 h compared to 1 h were filtered. Next, the ratio of expression of these genes in SL1344 and SL1344 Δ*acrB* at 5 h was calculated, and genes that were at least two-fold more highly expressed in SL1344 were selected, giving a total of 24 genes (**Table 7-7**).

Notably, expression of the *dadA* gene was reduced in the Δ*acrB* strain. Analysis of DadA above, suggested its importance in the production of pyruvate and energy from D-alanine and the removal of L-alanine that may accumulate at toxic levels. Its downregulation in stationary phase may be due to a shift in the regulation of some genes, or that accumulation of alanine was not yet at its peak at 5 hours when AcrB is removed. The decreased expression of DadA may also lead to a reduction in cell stiffness. It is hard to assess the importance of this difference by transcriptomic analysis alone but further work may be required to suggest more function and why it may differ in Δ*acrB*. It may be possible to extract RNA from a growing culture at every hour and perform RT-PCR to further investigate if *dadA* never reaches the fold change of SL1344 in the mutant, or if the peak just shifts later. However, previous results in this study and in Wang-Kan et al., (2017) show that there is no growth

defect on the deletion of *acrB* or difference on entry to stationary phase, and therefore this change is not because of different entry times into stationary phase.

Several genes shown in **Table 7-7** are involved in anaerobic respiration including *glpC*, *dmsB*, *frdC* and *frdB*. In **Appendix V** , the importance of anaerobic respiration in stationary phase SL1344 was discussed. The genes that were significantly different in Δ*acrB* mean it may be possible that SL1344 Δ*acrB* enters stationary phase later than SL1344. The suite of RND efflux pumps in *S.* Typhimurium and *E. coli* are similar, except that *E. coli* lacks MdsABC but additionally has RND pumps MdtEF and CusABC. The RND pump, MdtEF, is induced in anaerobic environments, and promotes growth in this environment due to nitrate derived substrates that it exports (Zhang et al., 2011). *S.* Typhimurium does not encode MdtEF, however it does still invade and colonise niches which are oxygen starved. The absence of MdtEF in *Salmonella* may possibly indicate that an RND pump is not required for anaerobic respiration. It has been previously shown deletion of AcrB and TolC lead to differential expression of anaerobic genes (Webber et al., 2009). In **Table 7-6**, it shows that several anaerobic genes were expressed to the same level in both strains, meaning that it is difficult to suggest that the deletion of AcrAB-TolC affects anaerobic respiration by this dataset alone.

Table 7-7 Genes that had >20-fold increased expression in SL1344 and then >2-fold different to Δ*acrB* (fold differences were calculated by dividing the Δ*acrB* fold change by the SL1344 fold change). Genes are ordered based on chromosome position.

Gene	Product	fold change WT 1 hr vs 5 hr	fold change Δ*acr*B 1 hr vs 5 hr	1 hr - 5 hr Δ*acrB* vs WT fold change
yafH	putative acyl-CoA dehydrogenase	29.11537	13.85526	0.475874
agp	bifunctional glucose-1-phosphatase/inositol phosphatase	28.97562	14.31706	0.494107
RS06860 (STM1381)	hypothetical protein	104.5104	29.17025	0.279113
RS08040 (STM1613)	PTS sugar transporter subunit IIB	63.5429	17.96542	0.282729
RS08060 (STM1617)	epimerase	24.97353	5.071294	0.203067
dadA	D-amino acid dehydrogenase small subunit	21.52745	9.476888	0.440223
glpC	anaerobic glycerol-3-phosphate dehydrogenase subunit C	33.30009	15.21148	0.4568
RS1419 (STM2741)	putative periplasmic protein	102.9484	42.02891	0.408252
csiD	carbon starvation induced protein	145.5768	44.01474	0.302347
RS16200 (STM3132)	xylanase deacetylase	65.53634	15.7886	0.240914
RS16205 (STM3133)	putative amidohydrolase	154.4174	44.66729	0.289263
ygjG	putrescine aminotransferase	63.12128	22.29035	0.353135
aldB	aldehyde dehydrogenase	27.44787	12.37959	0.451022
RS19395 (STM3767)	2-dehydro-3-deoxy-phosphogluconate aldolase	21.22651	4.918799	0.231729
fadB	fatty acid oxidation complex subunit alpha FadB	37.43257	15.03725	0.401716
RS20920	cupin domain-containing protein	40.36727	10.54512	0.261229
lsrK	autoinducer-2 kinase	50.99395	16.4998	0.323564
lsrC	autoinducer 2 ABC transporter permease	152.4059	66.3319	0.435232
lsrD	autoinducer 2 ABC transporter permease	223.7729	48.8989	0.21852
acs	acetate--CoA ligase	58.79791	19.95035	0.339304
dmsB	dimethylsulfoxide reductase subunit B	23.46767	8.645667	0.368407
frdC	fumarate reductase subunit F	24.32091	11.89992	0.489288
frdB	succinate dehydrogenase/fumarate reductase iron-sulfur subunit	27.02402	13.27719	0.491311
RS27410	hypothetical protein	187.7924	91.13337	0.485288

Another set of genes which were expressed differently to SL1344 were genes of the *lsrACDBK* operon. The genes *lsrK*, *lsrC* and *lsrD* were expressed with less magnitude in SL1344 Δ*acrB*. This operon encodes products involved in the import and phosphorylation of AI-2. It has previously been suggested that the AcrAB-TolC efflux pump may export QS signalling molecules, but that it does not export AI-2 (Yang et al., 2006). Another study showed that the *lsrABCDK* operon was downregulated in an inactivated AcrB mutant (SL1344 AcrB-D408A), and although not discussed in detail, a link with SPI-1 was suggested (Wang-Kan et al., 2017). It seems clear that the import of AI-2 differs in strains without the function of AcrAB-TolC, but it is unknown why this would be.

Although scientifically interesting, the results and hypotheses that can be drawn from **Table 7-7** do not implicate any genes or pathways that may be involved in changes in membrane permeability. This was a positive result that supports the conclusion that the removal of AcrB does not affect permeability and therefore the accumulation levels of EtBr in stationary phase. Both SL1344 and SL1344 Δ*acrB* must strengthen their permeability barrier in stationary phase, leading to reduced EtBr influx, independent of genes differentially transcribed in the absence of AcrB.

7.4.5.4 SL1344_RS22090 was highly upregulated in stationary phase in both SL1344 and SL1344 Δ*acrB*

There were only 4 genes which had higher expression in SL1344 Δ*acrB* compared to SL1344. These genes were identified when selecting genes that had >20-fold increased expression and were then more than 2-fold different to SL1344. The results of these genes are shown in **Table 7-8**. Of these genes, 3 encoded hypothetical

proteins and one was an unannotated PTS sugar transporter subunit. It is not known why a single PTS sugar transporter was more highly expressed in Δ*acrB* than SL1344, but since many PTS transporters were shown to have increased expression in SL1344, this was not further analysed.

In both SL1344 and Δ*acrB*, an unannotated gene encoding a hypothetical protein was the most upregulated at 5 hours of growth compared to one hour. SL1344_RS22090 (STM4302 in LT2) has a fold change of 281.37 and 661.43 in SL1344 and SL1344 Δ*acrB* respectively. BLAST analysis of the sequence presented the majority of hit alignments with *S. enterica* and *S. bongori* but once those organisms were removed, there was one 100 % match in *E. coli* (STEC_180392) and a 94 % match with a strain of pathogenic *Aerococcus viridans*. Previous studies regarding this gene are limited with some suggestion of this protein being a secreted effector protein (Samudrala et al., 2009, Sato et al., 2011), and transposon insertion studies suggested the gene may be required for colonisation of chicks (Morgan et al., 2004). The fact that this gene is so highly upregulated in both strains at 5 hours compared to 1, highlights its importance in stationary phase. It would be important to carry out further work to identify the function of this gene, through phenotypic checks in a gene deleted strain, and to identify its importance in stationary phase and whether it contributes to membrane permeability in any way.

Table 7-8 Genes that had >20-fold increased expression in Δ*acrB* and then >2-fold different to SL1344 (fold differences were calculated by dividing the Δ*acrB* fold change by the SL1344 fold change). Genes are ordered based on chromosome position

Gene	Product	fold change WT 1 hr vs 5 hr	fold change Δ*acr*B 1 hr vs 5 hr	1 hr – 5 hr Δ*acrB* vs WT fold change
RS22090 (STM4302)	hypothetical protein	281.3744	661.431935	2.351
RS22780 (STM4440)	putative cytoplasmic protein	8.2798521	32.9341061	3.978
RS22785 (STM4441)	hypothetical protein	42.672685	108.428007	2.541
RS23270 (STM4535)	PTS sugar transporter subunit IIA	6.61625217	30.8675503	4.665

7.4.5.5 MlaA may contribute to an increase in membrane permeability in stationary phase

In SL1344 Δ*acrB*, several genes were differentially expressed and a list of these genes can be found in **Appendix VI** . The identification of genes that were differentially expressed across time in SL1344 Δ*acrB* must be followed by further experimental analysis to confirm whether these changes in the transcriptome are directly due to the loss of AcrB.

However, an interesting finding was that the *mlaA* gene was downregulated at 5 hours in SL1344 Δ*acrB* with a 0.47-fold change. The gene was not differentially expressed in SL1344. The *mlaA* gene encodes a lipoprotein that has previously been identified as important in maintaining the asymmetry of the OM in *E. coli,* by transporting phospholipids to the OM (Malinverni and Silhavy, 2009). Previous studies have shown that Δ*mlaA* strains lead to a slight increase in membrane permeability (Malinverni and Silhavy, 2009). More recently, it has been shown that a mutation in *mlaA* leads to the production of an even more permeable cell that is susceptible to detergents and increased cell death on entrance into stationary phase, linked to an increase in LPS in stationary phase (Sutterlin et al., 2016). It is therefore possible that decreased expression of *mlaA* increases the permeability of the membrane. However, this gene was only slightly downregulated, and given that deletion of the gene leads to only a slight increase in permeability, and that accumulation of EtBr was not significantly different from SL1344 in stationary phase, it could be suggested that there is very minimal difference in terms of strength of the permeability barrier between SL1344 and SL1344 Δ*acrB* in stationary phase.

7.5 Final conclusions

Novel findings from the transcriptomic analysis here highlighted that *met* genes were highly expressed in late exponential/early stationary phase and this will be the subject of further work. Furthermore, hypotheses have been produced from this dataset which may begin to unpick genes involved with the strengthening of the permeability barrier in stationary phase, which may suggest the reason for reduced EtBr accumulation in stationary phase. CFA was upregulated and has previously been shown to increase cyclopropane fatty acids in stationary phase and may lead to a decrease in membrane permeability. Furthermore, reduced LPS biosynthesis and peptidoglycan remodelling may be involved with a more stable membrane barrier in stationary phase. All these hypotheses must be explored further to identify their contribution to reduced EtBr accumulation.

This RNAseq analysis has also highlighted that there are limited differences across time in transcriptome between SL1344 and SL1344 Δ*acrB*, and therefore limited alterations to the membrane barrier when AcrB is removed. From this, it can be concluded that the low EtBr accumulation phenotype in SL1344 Δ*acrB* in stationary phase is caused by the same mechanisms that contribute to low EtBr accumulation in SL1344. EtBr accumulation level in stationary phase can be considered AcrAB-TolC and efflux independent in SL1344.

7.6 Key findings

- There is a decrease in permeability in stationary phase and that the mechanisms underlying this are multi-layered and contribute to changes in the OM, IM and PG.
- Increase in cyclopropane fatty acids and peptidoglycan thickness in stationary phase may result in reduced permeability and therefore account for reduced EtBr accumulation.
- There is not an increase in lipid A biosynthesis and modification in stationary suggesting permeability decrease is independent LPS crosslinking
- Methionine genes are upregulated and may be related to the requirement for SAM in stationary phase biochemical pathways.
- It is complex to analyse the differences in SL1344 to SL1344 Δ*acrB*, but limited changes in genes involved in membrane permeability could be identified suggesting stationary phase changes in permeability are independent of AcrAB-TolC

Chapter 8- Final Discussion and Conclusions

8.1 Flow cytometry is a powerful tool for measuring drug accumulation

In this study, a novel assay was developed to measure EtBr accumulation in single bacterial cells (Whittle et al., 2019). Harnessing the fluorescence of RND efflux substrates such as EtBr or Hoescht H3342 has long been a measure of efflux activity in an entire cell population, often where cells have had efflux pumps removed, leading to increased accumulation. The flow cytometry assay presented in this thesis could be adapted to measure EtBr accumulation in both Gram-positive and Gram-negative bacteria, including pathogens considered a global priority. This assay was also able to measure the effect of known efflux inhibitors raising the possibility that it may also be adapted as a high throughput method to screen compound libraries for potential new efflux inhibitors. The strength and novelty of this assay comes from its measurement of accumulation in single cells. A growing body of evidence suggests that expression of efflux pumps within a population is heterogeneous (Sanchez-Romero and Casadesus, 2014), and this assay can identify sub-populations which may accumulate more or less drug than the population as a whole.

8.2 Drug accumulation is growth phase dependent

It has previously been shown that *acrAB* transcription peaks in mid-exponential phase and drops in stationary phase, although the reasons for this are not understood (Bailey et al., 2006). The transcription pattern for *acrAB* across the growth curve was confirmed in this study. Previous studies have shown that strains that overexpress efflux pumps, through mutations in regulators, lead to decreased susceptibility to antibiotics i.e. an increase in efflux pumps leads to an increase in antibiotic removal from cells (Webber and Piddock, 2001). For this reason, it was considered likely that increased transcription of *acrAB* in mid-exponential phase would lead to a decrease in EtBr accumulation. This study is the first to show that drug accumulation in different growth phases does not differ according to normal fluctuations in *acrAB* expression over growth in normal laboratory medium. Investigating whether transcription of efflux pumps remains growth phase dependent in efflux overexpressing strains, and whether this leads to a decrease in drug accumulation may be key to understanding how efflux interferes with antimicrobial treatment of Gram-negative infections.

In the absence of efflux pumps, drug accumulation peaked in mid-exponential phase. Removal of efflux pump components and the introduction of CCCP as an inhibitor, showed the same pattern of accumulation. This clearly highlighted the importance of efflux pumps in maintaining low drug accumulation in actively growing cells. This supports previous findings (Mitchell et al., 2017). By measuring EtBr accumulation in the presence of CCCP, novel findings suggested that efflux inhibition had no impact on the level of drug accumulation in stationary phase. CCCP is a PMF inhibitor which

inhibits the activity PMF-dependent efflux pumps, rather than an efflux inhibitor, therefore it would be important to repeat experimental design with RND specific competitive efflux inhibitors. However, if efflux inhibitors do not increase EtBr accumulation in stationary phase, it can be hypothesised that the addition of efflux inhibitors would have little effect on potentiating the activity of antibiotics for infections where bacteria are slow growing or not actively dividing.

Having shown that low EtBr accumulation in stationary phase was not due to the activity of efflux pumps, it is clear that another mechanism must be causing this phenotype. It is known that the membrane undergoes changes in stationary phase to survive harsh nutrient limited conditions (Huisman et al., 1996), and it has also been suggested that strengthening of the membrane barrier is due to RpoS-directed gene expression (Mitchell et al., 2017).

Initially, it was hypothesised that decreased expression of porins was responsible for the reduction in EtBr accumulation in stationary phase, however, it became clear that EtBr was unlikely to enter cells through porins. It would be interesting to study whether accumulation of antibiotics such as β-lactams, which enter through porins would show reduced accumulation in stationary phase.

It was shown that high concentrations of the membrane permeabiliser, EDTA, increased EtBr accumulation in actively growing cells of SL1344. Efflux is paramount in maintaining low accumulation in actively growing cells, so it is possible that there is less requirement for strength in the permeability barrier at this stage. It is likely that a more permeable membrane in actively growing cells allows more access to nutrients and that a more fluid membrane benefits bacterial cells that are dividing

exponentially. However, high concentrations of EDTA could not permeabilise the Gram-negative membrane in stationary phase, and therefore EtBr accumulation remained low. This shows that a strengthened membrane that has decreased permeability in stationary phase, is most likely the key driver of low drug accumulation in non-growing cells. It was not possible to show that the mechanisms required to strengthen the Gram-negative membrane were RpoS-dependent through deletion of *rpoS*, as suggested by Mitchell et al., 2017. RNAseq analysis highlighted potential biochemical pathways that may be involved in decreased permeability to drugs in a Gram-negative stationary phase cell. A reduction in lipid A biosynthesis and remodelling, as well as a reduction in peptidoglycan remodelling may lead to a reduction in membrane lipid turnover, and fluidity and therefore increased strength in harsh stationary phase environments. Previously characterised increased expression of *cfa* in stationary phase (Wang et al., 1992) was also shown here, and may play a role in reduced influx of drugs in stationary phase cells. This data is subject to further experimental work but supports the hypothesis that bacterial cells rely on decreased membrane permeability for reduced drug accumulation in stationary phase.

It can be concluded that mechanisms to maintain low drug accumulation differ with growth phase. A model of changes to the WT Gram negative bacterial cell (SL1344) predicted by the data in this study is shown in **Figure 8-1A+B**. In exponential phase (**A**), thick blue arrows represent a relatively permeable membrane where drugs and EtBr can enter cells. The thick red arrow represents high efflux activity of AcrAB TolC, allowing export and therefore maintaining low EtBr/drug accumulation. In stationary phase (**B**), the thick red arrow signifies that there is still efflux activity. However, the

dashed blue arrows represent reduced influx of drugs into the cell due to decreased permeability, therefore maintaining low accumulation without the activity of AcrAB-TolC. **C+D** represent RND efflux mutants such as SL1344 Δ*acrB*. In exponential phase (**C**), a permeable membrane allows entrance of drugs (thick blue arrows) into bacterial cells but the absence of AcrAB-TolC activity leads to high accumulation levels. In stationary phase (**D**), AcrAB-TolC still cannot function to export drugs, however drug accumulation is low due to decreased influx and decreased permeability (dashed blue arrows). Altogether, this shows that efflux is only important in maintaining low drug accumulation in actively growing cells. The decrease in membrane permeability in stationary phase tips the balance towards reduced drug influx, meaning that accumulation is efflux independent.

Figure 8-1 Model for the interplay between membrane permeability and efflux in different growth phases and its effect of drug accumulation

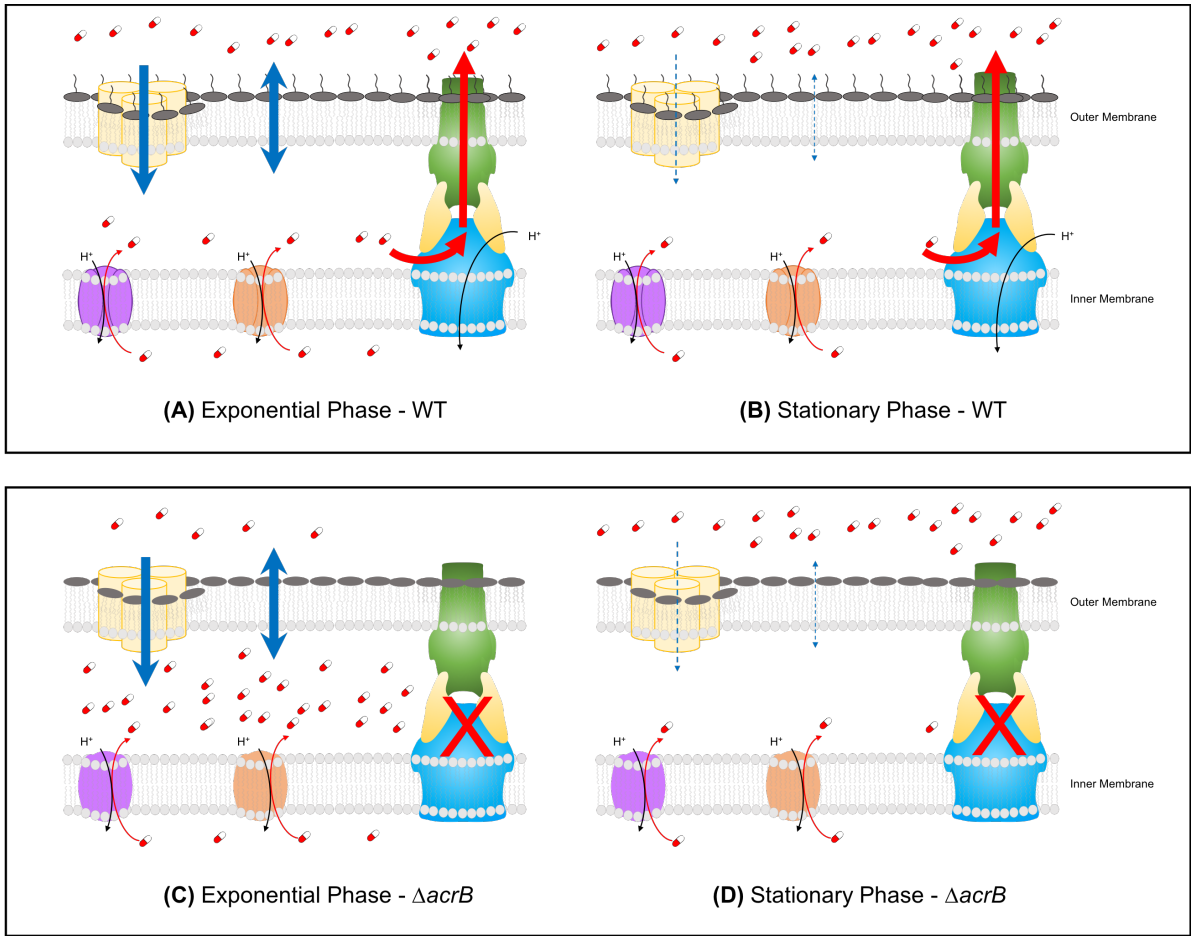

This model outlines the overall conclusions drawn from results of this thesis. This schematic does not contain all the efflux pumps or porins that may be located in the OM and IM to reduce complexity.

8.3 Further Work

- Optimise the described novel flow cytometry method into a high-throughput screen that may be used to identify new efflux inhibitors that lead to an increase in EtBr accumulation in both Gram-negative and Gram-positive cells.
- Investigate sub-populations with different accumulation levels described in **Section 3.10**. Using flow cytometric cell sorting, cells belonging to the sub-population could be separated and then sequenced to identify whether accumulation differences are due to mutations or phenotypic heterogeneity in efflux expression.
- For EtBr accumulation assays across growth phases, it will be important to optimise the assay to measure different fluorescent substrates and fluorescent antibiotics (especially those which enter cells via a different mechanism to EtBr). If the pattern remains the same for all substrates, it would show that membranes strengthen for reduced influx of antibiotics in stationary phase.
- Measure *acrAB* transcription, AcrAB protein level and EtBr accumulation in parallel in single cells using flow cytometry and microscopy. With more powerful flow cytometry and microscopy, it is possible to measure the fluorescence of SL1344 AcrB-GFP and EtBr in parallel. A transcriptional reporter, similar to pMW82-*acrA*, could be constructed with a fluorescent protein (possibly mPlum), which does not overlap with the fluorescence of GFP of EtBr and could be measured alongside them.
- To investigate how growth phase dependence of efflux and permeability is controlled. TraDIS (transposon directed insertion-site sequencing) could be used in combination with the EtBr accumulation assay presented here. A

TraDIS library of the *acrB* mutant could be made and EtBr accumulation measured to identify genes that do not reduce EtBr. A TraDIS library of SL1344 containing a *acrAB-gfp* promoter fusion could also be used, where GFP fluorescence would be measured by flow cytometry in the presence of drugs across the grow curve. Cells could be sorted based on increased GFP fluorescence and sequenced to identify genes that may regulate *acrAB* expression in different growth phases.

Further work on RNAseq analysis:

- To further follow up on hypotheses that *cfa,* reduced lipid A biosynthesis and peptidoglycan remodelling are involved in strengthening the permeability barrier, RT-PCR analysis for the genes would have to be carried out using extracted RNA to further confirm differences in gene expression in stationary phase.
- Measuring EtBr accumulation in SL1344 Δ*cfa* across growth may identify the role cyclopropane fatty acids play in strengthening the permeability barrier.
- Lipid A biosynthesis has decreased expression. Lipid A may be quantified in SL1344 in different growth phases by Nuclear Magnetic Resonance (NMR) spectroscopy. This would determine whether lipid A is at a constant concentration in stationary phase or if concentration decreases with decreased expression. Previous studies have shown that increased LPS in stationary phase may lead to increased cell death and membrane blebbing, and decrease in expression of biosynthetic genes may just to prevent this.

- Investigating why lipid A modification shows decreased expression in stationary phase may be more complex. One possible aim may be to overexpress the PmrAB sensor involved in most modifications that make cells resistant to polymyxins. Overexpression of *pmrAB* may be achieved by cloning onto a high copy number plasmid. Overexpressing this system may then lead to increased modification in all growth phases, the impact this may have on stationary phase cells could be assessed.
- Investigate the importance of reduced peptidoglycan remodelling in stationary phase. It may be possible to show that less remodelling leads to decreased membrane permeability by overexpressing the genes involved in degrading peptidoglycan in stationary phase. It may also be possible to measure EtBr accumulation in strains that undergo peptidoglycan remodelling in stationary phase and identify if changes occur.
- Construct SL1344 Δ*ldtE* to identify whether the increase in L,D-crosslinks affects the levels of EtBr accumulation. An increase in EtBr accumulation in stationary phase could show that increased L,D-crosslinks leads to decreased membrane permeability to EtBr and antibiotics.

8.4 Clinical implications and impact on AMR

The model derived from this thesis should lead to a rethink into the way antibiotics that pass through the membrane, such as aminoglycosides, are used to treat infections. Bacterial infections are complex, and bacterial populations will often not be in a single growth phase, therefore more careful consideration may be required for the most effective antibiotic treatment. Initial mucosal invasion and acute disease

may comprise a population of actively growing cells (Smith, 1998). From the model derived from this study, it shows that stationary phase non-growing cells are impermeable to EtBr and therefore many drugs. Therefore, treatment of chronic infections and biofilms where bacterial cells are slow- or non-growing may need to be considered more carefully. Successful treatment of these infections is already extremely difficult, and careful consideration is already made for treatment of intrinsically impermeable pathogens such as *Pseudomonas aeruginosa* and *Acinetobacter baumanii*. However, administering antibiotics for this kind of infection, with pathogens such as *E. coli* or *Salmonella* may lead to low level intracellular accumulation of antibiotics, which may simply further drive selection of mutations conferring antibiotic resistance. More extensive research into the effects of an impermeable membrane in non-growing infections must be carried out to further improve antimicrobial stewardship.

The model has shown that efflux pumps are only important in maintaining low drug accumulation in actively growing cells. If an infection is actively growing, it seems likely that efflux inhibitors would be effective at increasing the accumulation of antibiotics within cells and potentiate their activity. However, if cells are in a slow-growing or non-growing state, where membrane permeability is fundamental in maintaining low drug accumulation, efflux inhibitors may not be an effective treatment option. It is also possible that administering an efflux inhibitor where it has no effect on treating an infection, may also lead to the development of new mechanisms of AMR.

Together, this study highlights that extensive research is required into how different types of infection with bacteria in different growth states are treated, regardless of whether the infective agent in resistant to antibiotics. The development of efflux inhibitors provides hope in the fight against antibiotic resistant infections, but only when administered in acute, actively growing bacterial infections.

.

Chapter 9–List of References

ABDEL-HAMID, A. M., ATTWOOD, M. M. & GUEST, J. R. 2001. Pyruvate oxidase contributes to the aerobic growth efficiency of *Escherichia coli*. *Microbiology,* 147**,** 1483-1498.

ABEL-SANTOS, E. 2015. Chapter 9 - Endospores, Sporulation and Germination. *In:* YI-WEI TANG, M. S., DONGYOU LIU, IAN POXTON, JOSEPH SCHWARTZMAN (ed.) *Molecular Medical Microbiology (Second Edition).* Academic Press.

ABOUZEED, Y. M., BAUCHERON, S. & CLOECKAERT, A. 2008. *ramR* mutations involved in efflux-mediated multidrug resistance in *Salmonella enterica* serovar Typhimurium. *Antimicrob Agents Chemother,* 52**,** 2428-34.

ABRAHAM, E. P. & CHAIN, E. 1988. An enzyme from bacteria able to destroy penicillin. 1940. *Rev Infect Dis,* 10**,** 677-8.

AESCHBACHER, M., REINHARDT, C. A. & ZBINDEN, G. 1986. A rapid cell membrane permeability test using fluorescent dyes and flow cytometry. *Cell Biol Toxicol,* 2**,** 247-55.

AGRAWAL, A., RANGARAJAN, N. & WEISSHAAR, J. C. 2019. Resistance of early stationary phase *E. coli* to membrane permeabilization by the antimicrobial peptide Cecropin A. *Biochim Biophys Acta Biomembr,* 1861**,** 182990.

AHN, S., JUNG, J., JANG, I. A., MADSEN, E. L. & PARK, W. 2016. Role of Glyoxylate Shunt in Oxidative Stress Response. *J Biol Chem,* 291**,** 11928-38.

AIBA, H. & MIZUNO, T. 1990. Phosphorylation of a bacterial activator protein, OmpR, by a protein kinase, EnvZ, stimulates the transcription of the *ompF* and *ompC* genes in *Escherichia coli*. *FEBS Lett,* 261**,** 19-22.

ALAKOMI, H. L., SAARELA, M. & HELANDER, I. M. 2003. Effect of EDTA on *Salmonella enterica* serovar Typhimurium involves a component not assignable to lipopolysaccharide release. *Microbiology,* 149**,** 2015-2021.

ALEKSHUN, M. N. & LEVY, S. B. 1997. Regulation of chromosomally mediated multiple antibiotic resistance: the mar regulon. *Antimicrob Agents Chemother,* 41**,** 2067-75.

ALLEN, R. J. & SCOTT, G. K. 1979. Biosynthesis and turnover of outer-membrane proteins in *Escherichia coli* ML308-225. *Biochem J,* 182**,** 407-12.

ALONSO-CASAJUS, N., DAUVILLEE, D., VIALE, A. M., MUNOZ, F. J., BAROJA-FERNANDEZ, E., MORAN-ZORZANO, M. T., EYDALLIN, G., BALL, S. & POZUETA-ROMERO, J. 2006. Glycogen phosphorylase, the product of the *glgP* Gene, catalyzes glycogen breakdown by removing glucose units from the nonreducing ends in *Escherichia coli*. *J Bacteriol,* 188**,** 5266-72.

ALTUVIA, S., ALMIRON, M., HUISMAN, G., KOLTER, R. & STORZ, G. 1994. The dps promoter is activated by OxyR during growth and by IHF and sigma S in stationary phase. *Mol Microbiol,* 13**,** 265-72.

ANDERSON, C. J., CLARK, D. E., ADLI, M. & KENDALL, M. M. 2015. Ethanolamine Signaling Promotes *Salmonella* Niche Recognition and Adaptation during Infection. *PLoS Pathog,* 11**,** e1005278.

ANDREWS, J. M. & TESTING, B. W. P. O. S. 2006. BSAC standardized disc susceptibility testing method (version 5). *J Antimicrob Chemother,* 58**,** 511-29.

ANES, J., MCCUSKER, M. P., FANNING, S. & MARTINS, M. 2015. The ins and outs of RND efflux pumps in *Escherichia coli*. *Front Microbiol,* 6**,** 587.

ARNQVIST, A., OLSEN, A. & NORMARK, S. 1994. Sigma S-dependent growth-phase induction of the *csgBA* promoter in *Escherichia coli* can be achieved in vivo by sigma 70 in the absence of the nucleoid-associated protein H-NS. *Mol Microbiol,* 13**,** 1021-32.

ASMAR, A. T., FERREIRA, J. L., COHEN, E. J., CHO, S. H., BEEBY, M., HUGHES, K. T. & COLLET, J. F. 2017. Communication across the bacterial cell envelope depends on the size of the periplasm. *PLoS Biol,* 15**,** e2004303.

ASUQUO, A. E. & PIDDOCK, L. J. 1993. Accumulation and killing kinetics of fifteen quinolones for *Escherichia coli*, *Staphylococcus aureus* and *Pseudomonas aeruginosa*. *J Antimicrob Chemother,* 31**,** 865-80.

AZAM, T. A. & ISHIHAMA, A. 1999. Twelve species of the nucleoid-associated protein from *Escherichia coli*. Sequence recognition specificity and DNA binding affinity. *J Biol Chem,* 274**,** 33105-13.

BAILEY, A. M., IVENS, A., KINGSLEY, R., COTTELL, J. L., WAIN, J. & PIDDOCK, L. J. 2010. RamA, a member of the AraC/XylS family, influences both virulence and efflux in *Salmonella enterica* serovar Typhimurium. *J Bacteriol,* 192**,** 1607-16.

BAILEY, A. M., PAULSEN, I. T. & PIDDOCK, L. J. 2008. RamA confers multidrug resistance in *Salmonella enterica* via increased expression of *acrB*, which is inhibited by chlorpromazine. *Antimicrob Agents Chemother,* 52**,** 3604-11.

BAILEY, A. M., WEBBER, M. A. & PIDDOCK, L. J. V. 2006. Medium plays a role in determining expression of *acrB*, *marA*, and *soxS* in *Escherichia coli*. *Antimicrobial Agents and Chemotherapy,* 50**,** 1071-1074.

BAJAJ, H., SCORCIAPINO, M. A., MOYNIE, L., PAGE, M. G., NAISMITH, J. H., CECCARELLI, M. & WINTERHALTER, M. 2016. Molecular Basis of Filtering Carbapenems by Porins from beta-Lactam-resistant Clinical Strains of *Escherichia coli*. *J Biol Chem,* 291**,** 2837-47.

BARNHART, M. M. & CHAPMAN, M. R. 2006. Curli biogenesis and function. *Annu Rev Microbiol,* 60**,** 131-47.

BARRETEAU, H., KOVAC, A., BONIFACE, A., SOVA, M., GOBEC, S. & BLANOT, D. 2008. Cytoplasmic steps of peptidoglycan biosynthesis. *FEMS Microbiol Rev,* 32**,** 168-207.

BATTESTI, A. & BOUVERET, E. 2009. Bacteria possessing two RelA/SpoT-like proteins have evolved a specific stringent response involving the acyl carrier protein-SpoT interaction. *J Bacteriol,* 191**,** 616-24.

BAUCHERON, S., NISHINO, K., MONCHAUX, I., CANEPA, S., MAUREL, M. C., COSTE, F., ROUSSEL, A., CLOECKAERT, A. & GIRAUD, E. 2014. Bile-mediated activation of the *acrAB* and *tolC* multidrug efflux genes occurs mainly through transcriptional derepression of *ramA* in *Salmonella enterica* serovar Typhimurium. *J Antimicrob Chemother,* 69**,** 2400-6.

BAUCHERON, S., TYLER, S., BOYD, D., MULVEY, M. R., CHASLUS-DANCLA, E. & CLOECKAERT, A. 2004. AcrAB-TolC directs efflux-mediated multidrug resistance in *Salmonella enterica* serovar typhimurium DT104. *Antimicrob Agents Chemother,* 48**,** 3729-35.

BAUGH, S., EKANAYAKA, A. S., PIDDOCK, L. J. & WEBBER, M. A. 2012. Loss of or inhibition of all multidrug resistance efflux pumps of *Salmonella enterica* serovar Typhimurium results in impaired ability to form a biofilm. *J Antimicrob Chemother,* 67**,** 2409-17.

BAUGH, S., PHILLIPS, C. R., EKANAYAKA, A. S., PIDDOCK, L. J. & WEBBER, M. A. 2014. Inhibition of multidrug efflux as a strategy to prevent biofilm formation. *J Antimicrob Chemother,* 69**,** 673-81.

BEKETSKAIA, M. S., BAY, D. C. & TURNER, R. J. 2014. Outer membrane protein OmpW participates with small multidrug resistance protein member EmrE in quaternary cationic compound efflux. *J Bacteriol,* 196**,** 1908-14.

BERGMILLER, T., ANDERSSON, A. M. C., TOMASEK, K., BALLEZA, E., KIVIET, D. J., HAUSCHILD, R., TKACIK, G. & GUET, C. C. 2017. Biased partitioning of the multidrug efflux pump AcrAB-TolC underlies long-lived phenotypic heterogeneity. *Science,* 356**,** 311-315.

BERTANI, B. & RUIZ, N. 2018. Function and Biogenesis of Lipopolysaccharides. *EcoSal Plus,* 8.

BERTRAND, R. L. 2019. Lag Phase Is a Dynamic, Organized, Adaptive, and Evolvable Period That Prepares Bacteria for Cell Division. *J Bacteriol,* 201.

BEVERIDGE, T. J. 1999. Structures of gram-negative cell walls and their derived membrane vesicles. *J Bacteriol,* 181**,** 4725-33.

BIANCO, C. M., FROHLICH, K. S. & VANDERPOOL, C. K. 2019. Bacterial Cyclopropane Fatty Acid Synthase mRNA Is Targeted by Activating and Repressing Small RNAs. *J Bacteriol,* 201.

BLAIR, J. M., LA RAGIONE, R. M., WOODWARD, M. J. & PIDDOCK, L. J. 2009. Periplasmic adaptor protein AcrA has a distinct role in the antibiotic resistance and virulence of *Salmonella enterica* serovar Typhimurium. *J Antimicrob Chemother,* 64**,** 965-72.

BLAIR, J. M. & PIDDOCK, L. J. 2016. How to Measure Export via Bacterial Multidrug Resistance Efflux Pumps. *MBio,* 7.

BLAIR, J. M., RICHMOND, G. E., BAILEY, A. M., IVENS, A. & PIDDOCK, L. J. 2013. Choice of bacterial growth medium alters the transcriptome and phenotype of *Salmonella enterica* Serovar Typhimurium. *PLoS One,* 8**,** e63912.

BLAIR, J. M., SMITH, H. E., RICCI, V., LAWLER, A. J., THOMPSON, L. J. & PIDDOCK, L. J. 2015a. Expression of homologous RND efflux pump genes is dependent upon AcrB expression: implications for efflux and virulence inhibitor design. *J Antimicrob Chemother,* 70**,** 424-31.

BLAIR, J. M., WEBBER, M. A., BAYLAY, A. J., OGBOLU, D. O. & PIDDOCK, L. J. 2015b. Molecular mechanisms of antibiotic resistance. *Nat Rev Microbiol,* 13**,** 42-51.

BLATTNER, F. R., PLUNKETT, G., 3RD, BLOCH, C. A., PERNA, N. T., BURLAND, V., RILEY, M., COLLADO-VIDES, J., GLASNER, J. D., RODE, C. K., MAYHEW, G. F., GREGOR, J., DAVIS, N. W., KIRKPATRICK, H. A., GOEDEN, M. A., ROSE, D. J., MAU, B. & SHAO, Y. 1997. The complete genome sequence of *Escherichia coli* K-12. *Science,* 277**,** 1453-62.

BLEUEL, C., GROSSE, C., TAUDTE, N., SCHERER, J., WESENBERG, D., KRAUSS, G. J., NIES, D. H. & GRASS, G. 2005. TolC is involved in enterobactin efflux across the outer membrane of *Escherichia coli*. *J Bacteriol,* 187**,** 6701-7.

BOGOMOLNAYA, L. M., ANDREWS, K. D., TALAMANTES, M., MAPLE, A., RAGOZA, Y., VAZQUEZ-TORRES, A. & ANDREWS-POLYMENIS, H. 2013. The ABC-type efflux pump MacAB protects *Salmonella enterica* serovar typhimurium from oxidative stress. *MBio,* 4**,** e00630-13.

BOGOMOLNAYA, L. M., TILVAWALA, R., ELFENBEIN, J. R., CIRILLO, J. D. & ANDREWS-POLYMENIS, H. L. 2020. Linearized Siderophore Products Secreted via MacAB Efflux Pump Protect *Salmonella enterica* Serovar Typhimurium from Oxidative Stress. *mBio,* 11.

BOHNERT, J. A., KARAMIAN, B. & NIKAIDO, H. 2010. Optimized Nile Red efflux assay of AcrAB-TolC multidrug efflux system shows competition between substrates. *Antimicrob Agents Chemother,* 54**,** 3770-5.

BOHNERT, J. A., SCHUSTER, S., SZYMANIAK-VITS, M. & KERN, W. V. 2011. Determination of real-time efflux phenotypes in *Escherichia coli* AcrB binding pocket phenylalanine mutants using a 1,2'-dinaphthylamine efflux assay. *PLoS One,* 6**,** e21196.

BOLLA, J. M., ALIBERT-FRANCO, S., HANDZLIK, J., CHEVALIER, J., MAHAMOUD, A., BOYER, G., KIEC-KONONOWICZ, K. & PAGES, J. M. 2011. Strategies for bypassing the membrane barrier in multidrug resistant Gram-negative bacteria. *FEBS Lett,* 585**,** 1682-90.

BONNET, R. 2004. Growing group of extended-spectrum beta-lactamases: the CTX-M enzymes. *Antimicrob Agents Chemother,* 48**,** 1-14.

BOYINGTON, J. C., GLADYSHEV, V. N., KHANGULOV, S. V., STADTMAN, T. C. & SUN, P. D. 1997. Crystal structure of formate dehydrogenase H: catalysis

involving Mo, molybdopterin, selenocysteine, and an Fe4S4 cluster. *Science,* 275**,** 1305-8.

BRAUN, V. 1975. Covalent lipoprotein from the outer membrane of *Escherichia coli*. *Biochim Biophys Acta,* 415**,** 335-77.

BREIDENSTEIN, E. B., DE LA FUENTE-NUNEZ, C. & HANCOCK, R. E. 2011. *Pseudomonas aeruginosa*: all roads lead to resistance. *Trends Microbiol,* 19**,** 419-26.

BRINKMAN, A. B., ETTEMA, T. J., DE VOS, W. M. & VAN DER OOST, J. 2003. The Lrp family of transcriptional regulators. *Mol Microbiol,* 48**,** 287-94.

BROWN, M. H., PAULSEN, I. T. & SKURRAY, R. A. 1999. The multidrug efflux protein NorM is a prototype of a new family of transporters. *Mol Microbiol,* 31**,** 394-5.

BRYAN, L. E. & VAN DEN ELZEN, H. M. 1977. Effects of membrane-energy mutations and cations on streptomycin and gentamicin accumulation by bacteria: a model for entry of streptomycin and gentamicin in susceptible and resistant bacteria. *Antimicrob Agents Chemother,* 12**,** 163-77.

BUCHANAN, C. E. & SOWELL, M. O. 1982. Synthesis of penicillin-binding protein 6 by stationary-phase *Escherichia coli*. *J Bacteriol,* 151**,** 491-4.

BUCKLEY, A. M., WEBBER, M. A., COOLES, S., RANDALL, L. P., LA RAGIONE, R. M., WOODWARD, M. J. & PIDDOCK, L. J. 2006. The AcrAB-TolC efflux system of *Salmonella enterica* serovar Typhimurium plays a role in pathogenesis. *Cell Microbiol,* 8**,** 847-56.

BUGG, T. D., WRIGHT, G. D., DUTKA-MALEN, S., ARTHUR, M., COURVALIN, P. & WALSH, C. T. 1991. Molecular basis for vancomycin resistance in *Enterococcus faecium* BM4147: biosynthesis of a depsipeptide peptidoglycan precursor by vancomycin resistance proteins VanH and VanA. *Biochemistry,* 30**,** 10408-15.

BUMANN, D. & VALDIVIA, R. H. 2007. Identification of host-induced pathogen genes by differential fluorescence induction reporter systems. *Nature Protocols,* 2**,** 770-777.

BUSH, K. 2018. Past and Present Perspectives on beta-Lactamases. *Antimicrob Agents Chemother,* 62.

BYLUND, G. O., WIPEMO, L. C., LUNDBERG, L. A. & WIKSTROM, P. M. 1998. RimM and RbfA are essential for efficient processing of 16S rRNA in *Escherichia coli*. *J Bacteriol,* 180**,** 73-82.

CALDERON, I. L., MORALES, E., CARO, N. J., CHAHUAN, C. A., COLLAO, B., GIL, F., VILLARREAL, J. M., IPINZA, F., MORA, G. C. & SAAVEDRA, C. P. 2011. Response regulator ArcA of *Salmonella enterica* serovar Typhimurium downregulates expression of OmpD, a porin facilitating uptake of hydrogen peroxide. *Res Microbiol,* 162**,** 214-22.

CALVO, J. M. & MATTHEWS, R. G. 1994. The leucine-responsive regulatory protein, a global regulator of metabolism in *Escherichia coli*. *Microbiol Rev,* 58**,** 466-90.

CASPI, R., BILLINGTON, R., KESELER, I. M., KOTHARI, A., KRUMMENACKER, M., MIDFORD, P. E., ONG, W. K., PALEY, S., SUBHRAVETI, P. & KARP, P. D. 2020. The MetaCyc database of metabolic pathways and enzymes - a 2019 update. *Nucleic Acids Res,* 48**,** D445-D453.

CAUILAN, A., RAMOS, K., HARMON, D. E. & RUIZ, C. 2019. Global effect of the AcrAB-TolC multidrug efflux pump of *Escherichia coli* in cell metabolism revealed by untargeted metabolomics. *Int J Antimicrob Agents,* 54**,** 105-107.

CHAI, Q., WEBB, S. R., WANG, Z., DUTCH, R. E. & WEI, Y. 2016. Study of the degradation of a multidrug transporter using a non-radioactive pulse chase method. *Anal Bioanal Chem,* 408**,** 7745-7751.

CHAN, W., COSTANTINO, N., LI, R., LEE, S. C., SU, Q., MELVIN, D., COURT, D. L. & LIU, P. 2007. A recombineering based approach for high-throughput conditional knockout targeting vector construction. *Nucleic Acids Res,* 35**,** e64.

CHANG, L. L., CHEN, H. F., CHANG, C. Y., LEE, T. M. & WU, W. J. 2004. Contribution of integrons, and SmeABC and SmeDEF efflux pumps to multidrug resistance in clinical isolates of *Stenotrophomonas maltophilia*. *J Antimicrob Chemother,* 53**,** 518-21.

CHANG, Y. Y. & CRONAN, J. E., JR. 1999. Membrane cyclopropane fatty acid content is a major factor in acid resistance of *Escherichia coli*. *Mol Microbiol,* 33**,** 249-59.

CHAPMAN, J. S. & GEORGOPAPADAKOU, N. H. 1988. Routes of quinolone permeation in *Escherichia coli*. *Antimicrob Agents Chemother,* 32**,** 438-42.

CHAROENWONG, D., ANDREWS, S. & MACKEY, B. 2011. Role of *rpoS* in the development of cell envelope resilience and pressure resistance in stationary-phase *Escherichia coli*. *Appl Environ Microbiol,* 77**,** 5220-9.

CHEN, Y., AI, L., GUO, P., HUANG, H., WU, Z., LIANG, X. & LIAO, K. 2018. Molecular characterization of multidrug resistant strains of *Acinetobacter baumannii* isolated from pediatric intensive care unit in a Chinese tertiary hospital. *BMC Infect Dis,* 18**,** 614.

CHEN, Y. Y. & GANZLE, M. G. 2016. Influence of cyclopropane fatty acids on heat, high pressure, acid and oxidative resistance in *Escherichia coli*. *Int J Food Microbiol,* 222**,** 16-22.

CHEREPANOV, P. P. & WACKERNAGEL, W. 1995. Gene disruption in *Escherichia coli*: TcR and KmR cassettes with the option of Flp-catalyzed excision of the antibiotic-resistance determinant. *Gene,* 158**,** 9-14.

CHOI, U. & LEE, C. R. 2019. Distinct Roles of Outer Membrane Porins in Antibiotic Resistance and Membrane Integrity in *Escherichia coli*. *Front Microbiol,* 10**,** 953.

CHOPRA, I. & ROBERTS, M. 2001. Tetracycline antibiotics: mode of action, applications, molecular biology, and epidemiology of bacterial resistance. *Microbiol Mol Biol Rev,* 65**,** 232-60 ; second page, table of contents.

CHOW, J. C., YOUNG, D. W., GOLENBOCK, D. T., CHRIST, W. J. & GUSOVSKY, F. 1999. Toll-like receptor-4 mediates lipopolysaccharide-induced signal transduction. *J Biol Chem,* 274**,** 10689-92.

CHOWDHURY, N., SUHANI, S., PURKAYSTHA, A., BEGUM, M. K., RAIHAN, T., ALAM, M. J., ISLAM, K. & AZAD, A. K. 2019. Identification of AcrAB-TolC Efflux Pump Genes and Detection of Mutation in Efflux Repressor AcrR from Omeprazole Responsive Multidrug-Resistant *Escherichia coli I*solates Causing Urinary Tract Infections. *Microbiol Insights,* 12**,** 1178636119889629.

CLSI 2018. M07 Methods for Dilution Antimicrobial Susceptibility Tests for Bacteria that grow Aerobically. *Clinical and Laboratory Standards Institute.*

COHEN, S. P., MCMURRY, L. M. & LEVY, S. B. 1988. *marA* locus causes decreased expression of OmpF porin in multiple-antibiotic-resistant (Mar) mutants of *Escherichia coli*. *J Bacteriol,* 170**,** 5416-22.

COLCLOUGH, A. L., ALAV, I., WHITTLE, E. E., PUGH, H. L., DARBY, E. M., LEGOOD, S. W., MCNEIL, H. E. & BLAIR, J. M. 2020. RND efflux pumps in Gram-negative bacteria; regulation, structure and role in antibiotic resistance. *Future Microbiol,* 15**,** 143-157.

COLDHAM, N. G., WEBBER, M., WOODWARD, M. J. & PIDDOCK, L. J. 2010. A 96-well plate fluorescence assay for assessment of cellular permeability and active efflux in *Salmonella enterica* serovar Typhimurium and *Escherichia coli*. *J Antimicrob Chemother,* 65**,** 1655-63.

CRAWFORD, R. W., ROSALES-REYES, R., RAMIREZ-AGUILAR MDE, L., CHAPA-AZUELA, O., ALPUCHE-ARANDA, C. & GUNN, J. S. 2010. Gallstones play a significant role in *Salmonella* spp. gallbladder colonization and carriage. *Proc Natl Acad Sci U S A,* 107**,** 4353-8.

CRONAN, J. E., JR. 1968. Phospholipid alterations during growth of *Escherichia coli*. *J Bacteriol,* 95**,** 2054-61.

DATSENKO, K. A. & WANNER, B. L. 2000. One-step inactivation of chromosomal genes in *Escherichia coli* K-12 using PCR products. *Proc Natl Acad Sci U S A,* 97**,** 6640-5.

DAURY, L., ORANGE, F., TAVEAU, J. C., VERCHERE, A., MONLEZUN, L., GOUNOU, C., MARREDDY, R. K., PICARD, M., BROUTIN, I., POS, K. M. & LAMBERT, O. 2016. Tripartite assembly of RND multidrug efflux pumps. *Nat Commun,* 7**,** 10731.

DAUVILLEE, D., KINDERF, I. S., LI, Z., KOSAR-HASHEMI, B., SAMUEL, M. S., RAMPLING, L., BALL, S. & MORELL, M. K. 2005. Role of the *Escherichia coli glgX* gene in glycogen metabolism. *J Bacteriol,* 187**,** 1465-73.

DAVIDSON, A. L. & CHEN, J. 2004. ATP-binding cassette transporters in bacteria. *Annu Rev Biochem,* 73**,** 241-68.

DAVIES, S. 2011. Annual Report of the Chief Medical Officer: Infections and the rise of antimicrobial resistance.

DAVIS, B. D., CHEN, L. L. & TAI, P. C. 1986. Misread protein creates membrane channels: an essential step in the bactericidal action of aminoglycosides. *Proc Natl Acad Sci U S A,* 83**,** 6164-8.

DAVIS, K. M. & ISBERG, R. R. 2016. Defining heterogeneity within bacterial populations via single cell approaches. *Bioessays,* 38**,** 782-90.

DE, E., BASLE, A., JAQUINOD, M., SAINT, N., MALLEA, M., MOLLE, G. & PAGES, J. M. 2001. A new mechanism of antibiotic resistance in *Enterobacteriaceae* induced by a structural modification of the major porin. *Mol Microbiol,* 41**,** 189-98.

DE MARTINO, M., ERSHOV, D., VAN DEN BERG, P. J., TANS, S. J. & MEYER, A. S. 2016. Single-Cell Analysis of the Dps Response to Oxidative Stress. *J Bacteriol,* 198**,** 1662-1674.

DE PEDRO, M. A., GRUNFELDER, C. G. & SCHWARZ, H. 2004. Restricted Mobility of Cell Surface Proteins in the Polar Regions of *Escherichia coli*. *J Bacteriol,* 186**,** 2594-602.

DEATH, A. & FERENCI, T. 1993. The importance of the binding-protein-dependent Mgl system to the transport of glucose in *Escherichia coli* growing on low sugar concentrations. *Res Microbiol,* 144**,** 529-37.

DELCOUR, A. H. 2009. Outer membrane permeability and antibiotic resistance. *Biochim Biophys Acta,* 1794**,** 808-16.

DONLAN, R. M. 2002. Biofilms: microbial life on surfaces. *Emerg Infect Dis,* 8**,** 881-90.

DRESSAIRE, C., MOREIRA, R. N., BARAHONA, S., ALVES DE MATOS, A. P. & ARRAIANO, C. M. 2015. BolA is a transcriptional switch that turns off motility and turns on biofilm development. *mBio,* 6**,** e02352-14.

DU, D., WANG-KAN, X., NEUBERGER, A., VAN VEEN, H. W., POS, K. M., PIDDOCK, L. J. V. & LUISI, B. F. 2018. Multidrug efflux pumps: structure, function and regulation. *Nat Rev Microbiol,* 16**,** 523-539.

DUKAN, S. & NYSTROM, T. 1998. Bacterial senescence: stasis results in increased and differential oxidation of cytoplasmic proteins leading to developmental induction of the heat shock regulon. *Genes Dev,* 12**,** 3431-41.

DUNN, M. F., RAMIREZ-TRUJILLO, J. A. & HERNANDEZ-LUCAS, I. 2009. Major roles of isocitrate lyase and malate synthase in bacterial and fungal pathogenesis. *Microbiology,* 155**,** 3166-3175.

DUPONT, H., CHOINIER, P., ROCHE, D., ADIBA, S., SOOKDEB, M., BRANGER, C., DENAMUR, E. & MAMMERI, H. 2017. Structural Alteration of OmpR as a Source of Ertapenem Resistance in a CTX-M-15-Producing *Escherichia coli* O25b:H4 Sequence Type 131 Clinical Isolate. *Antimicrob Agents Chemother,* 61.

DUVAL, V. & LISTER, I. M. 2013. MarA, SoxS and Rob of *Escherichia coli* - Global regulators of multidrug resistance, virulence and stress response. *Int J Biotechnol Wellness Ind,* 2**,** 101-124.

EAVES, D. J., RANDALL, L., GRAY, D. T., BUCKLEY, A., WOODWARD, M. J., WHITE, A. P. & PIDDOCK, L. J. 2004a. Prevalence of mutations within the quinolone resistance-determining region of *gyrA*, *gyrB*, *parC*, and *parE* and association with antibiotic resistance in quinolone-resistant *Salmonella enterica*. *Antimicrob Agents Chemother,* 48**,** 4012-5.

EAVES, D. J., RICCI, V. & PIDDOCK, L. J. 2004b. Expression of *acrB*, *acrF*, *acrD*, *marA*, and *soxS* in *Salmonella enterica* serovar Typhimurium: role in multiple antibiotic resistance. *Antimicrob Agents Chemother,* 48**,** 1145-50.

EGAN, A. J. F., ERRINGTON, J. & VOLLMER, W. 2020. Regulation of peptidoglycan synthesis and remodelling. *Nat Rev Microbiol,* 18**,** 446-460.

EL MEOUCHE, I. & DUNLOP, M. J. 2018. Heterogeneity in efflux pump expression predisposes antibiotic-resistant cells to mutation. *Science,* 362**,** 686-690.

EL-KHANI, M. A. & STRETTON, R. J. 1981. Effect of growth medium on the lipid composition of log and stationary phase cultures of *Salmonella typhimurium*. *Microbios,* 31**,** 161-9.

ENG, R. H., PADBERG, F. T., SMITH, S. M., TAN, E. N. & CHERUBIN, C. E. 1991. Bactericidal effects of antibiotics on slowly growing and nongrowing bacteria. *Antimicrob Agents Chemother,* 35**,** 1824-8.

ERBEL, P. J., BARR, K., GAO, N., GERWIG, G. J., RICK, P. D. & GARDNER, K. H. 2003. Identification and biosynthesis of cyclic enterobacterial common antigen in *Escherichia coli*. *J Bacteriol,* 185**,** 1995-2004.

FAIR, R. J. & TOR, Y. 2014. Antibiotics and bacterial resistance in the 21st century. *Perspect Medicin Chem,* 6**,** 25-64.

FARIZANO, J. V., PESCARETTI MDE, L., LOPEZ, F. E., HSU, F. F. & DELGADO, M. A. 2012. The PmrAB system-inducing conditions control both lipid A remodeling and O-antigen length distribution, influencing the *Salmonella* Typhimurium-host interactions. *J Biol Chem,* 287**,** 38778-89.

FERNANDES, M. M., IVANOVA, K., HOYO, J., PEREZ-RAFAEL, S., FRANCESKO, A. & TZANOV, T. 2017. Nanotransformation of Vancomycin Overcomes the Intrinsic Resistance of Gram-Negative Bacteria. *ACS Appl Mater Interfaces,* 9**,** 15022-15030.

FERNANDEZ-MORA, M., PUENTE, J. L. & CALVA, E. 2004. OmpR and LeuO positively regulate the *Salmonella enterica* serovar Typhi ompS2 porin gene. *J Bacteriol,* 186**,** 2909-20.

FERRO, S., AMORICO, T. & DEO, P. 2018. Role of food sanitising treatments in inducing the 'viable but nonculturable' state of microorganisms. *Food Control,* 91**,** 321-329.

FINN, R. D., COGGILL, P., EBERHARDT, R. Y., EDDY, S. R., MISTRY, J., MITCHELL, A. L., POTTER, S. C., PUNTA, M., QURESHI, M., SANGRADOR-VEGAS, A., SALAZAR, G. A., TATE, J. & BATEMAN, A. 2016. The Pfam protein families database: towards a more sustainable future. *Nucleic Acids Res,* 44**,** D279-85.

FLORES-VALDEZ, M. A., PUENTE, J. L. & CALVA, E. 2003. Negative osmoregulation of the *Salmonella* ompS1 porin gene independently of OmpR in an hns background. *J Bacteriol,* 185**,** 6497-506.

FOOKES, M., SCHROEDER, G. N., LANGRIDGE, G. C., BLONDEL, C. J., MAMMINA, C., CONNOR, T. R., SETH-SMITH, H., VERNIKOS, G. S., ROBINSON, K. S., SANDERS, M., PETTY, N. K., KINGSLEY, R. A., BAUMLER, A. J., NUCCIO, S. P., CONTRERAS, I., SANTIVIAGO, C. A., MASKELL, D., BARROW, P., HUMPHREY, T., NASTASI, A., ROBERTS, M., FRANKEL, G., PARKHILL, J., DOUGAN, G. & THOMSON, N. R. 2011. Salmonella bongori provides insights into the evolution of the *Salmonellae*. *PLoS Pathog,* 7**,** e1002191.

FORAGE, R. G. & LIN, E. C. 1982. DHA system mediating aerobic and anaerobic dissimilation of glycerol in *Klebsiella pneumoniae* NCIB 418. *J Bacteriol,* 151**,** 591-9.

FREIRE, P., VIEIRA, H. L., FURTADO, A. R., DE PEDRO, M. A. & ARRAIANO, C. M. 2006. Effect of the morphogene *bolA* on the permeability of the *Escherichia coli* outer membrane. *FEMS Microbiol Lett,* 260**,** 106-11.

FRIDMAN, O., GOLDBERG, A., RONIN, I., SHORESH, N. & BALABAN, N. Q. 2014. Optimization of lag time underlies antibiotic tolerance in evolved bacterial populations. *Nature,* 513**,** 418-21.

FULCHER, C., SUBHRAVETI, P., KOTHARI, A., PALEY, S., CASPI, R., KESELER, I. & KARP, P. 2018. Summary of *Salmonella enterica*, Subspecies *enterica*, Strain serovar Typhimurium str. LT2, version 24.1. BioCyc Database Collection.

GAL-MOR, O., BOYLE, E. C. & GRASSL, G. A. 2014. Same species, different diseases: how and why typhoidal and non-typhoidal *Salmonella enterica* serovars differ. *Front Microbiol,* 5**,** 391.

GALDIERO, S., FALANGA, A., CANTISANI, M., TARALLO, R., DELLA PEPA, M. E., D'ORIANO, V. & GALDIERO, M. 2012. Microbe-host interactions: structure and role of Gram-negative bacterial porins. *Curr Protein Pept Sci,* 13**,** 843-54.

GEFEN, O., FRIDMAN, O., RONIN, I. & BALABAN, N. Q. 2014. Direct observation of single stationary-phase bacteria reveals a surprisingly long period of constant protein production activity. *Proc Natl Acad Sci U S A,* 111**,** 556-61.

GENTRY, D. R. & CASHEL, M. 1996. Mutational analysis of the *Escherichia coli spoT* gene identifies distinct but overlapping regions involved in ppGpp synthesis and degradation. *Mol Microbiol,* 19**,** 1373-84.

GENTRY, D. R., HERNANDEZ, V. J., NGUYEN, L. H., JENSEN, D. B. & CASHEL, M. 1993. Synthesis of the stationary-phase sigma factor sigma s is positively regulated by ppGpp. *J Bacteriol,* 175**,** 7982-9.

GEORGE, A. M., HALL, R. M. & STOKES, H. W. 1995. Multidrug resistance in *Klebsiella pneumoniae*: a novel gene, *ramA*, confers a multidrug resistance phenotype in *Escherichia coli*. *Microbiology,* 141 (Pt 8)**,** 1909-20.

GIAEVER, H. M., STYRVOLD, O. B., KAASEN, I. & STROM, A. R. 1988. Biochemical and genetic characterization of osmoregulatory trehalose synthesis in *Escherichia coli*. *J Bacteriol,* 170**,** 2841-9.

GIAMMANCO, G. M., PIGNATO, S., MAMMINA, C., GRIMONT, F., GRIMONT, P. A., NASTASI, A. & GIAMMANCO, G. 2002. Persistent endemicity of *Salmonella bongori* 48:z(35):--in Southern Italy: molecular characterization of human, animal, and environmental isolates. *J Clin Microbiol,* 40**,** 3502-5.

GIBBONS, H. S., LIN, S., COTTER, R. J. & RAETZ, C. R. 2000. Oxygen requirement for the biosynthesis of the S-2-hydroxymyristate moiety in *Salmonella typhimurium* lipid A. Function of LpxO, A new Fe2+/alpha-ketoglutarate-dependent dioxygenase homologue. *J Biol Chem,* 275**,** 32940-9.

GIL, F., HERNANDEZ-LUCAS, I., POLANCO, R., PACHECO, N., COLLAO, B., VILLARREAL, J. M., NARDOCCI, G., CALVA, E. & SAAVEDRA, C. P. 2009. SoxS regulates the expression of the *Salmonella enterica* serovar Typhimurium *ompW* gene. *Microbiology,* 155**,** 2490-2497.

GIL, F., IPINZA, F., FUENTES, J., FUMERON, R., VILLARREAL, J. M., ASPEE, A., MORA, G. C., VASQUEZ, C. C. & SAAVEDRA, C. 2007. The *ompW* (porin) gene mediates methyl viologen (paraquat) efflux in *Salmonella enterica* serovar typhimurium. *Res Microbiol,* 158**,** 529-36.

GORITYALA, B. K., GUCHHAIT, G., FERNANDO, D. M., DEO, S., MCKENNA, S. A., ZHANEL, G. G., KUMAR, A. & SCHWEIZER, F. 2016a. Adjuvants Based on Hybrid Antibiotics Overcome Resistance in *Pseudomonas aeruginosa* and Enhance Fluoroquinolone Efficacy. *Angew Chem Int Ed Engl,* 55**,** 555-9.

GORITYALA, B. K., GUCHHAIT, G., GOSWAMI, S., FERNANDO, D. M., KUMAR, A., ZHANEL, G. G. & SCHWEIZER, F. 2016b. Hybrid Antibiotic Overcomes Resistance in *P. aeruginosa* by Enhancing Outer Membrane Penetration and Reducing Efflux. *J Med Chem,* 59**,** 8441-55.

GOTO, R., MIKI, T., NAKAMURA, N., FUJIMOTO, M. & OKADA, N. 2017. *Salmonella* Typhimurium PagP- and UgtL-dependent resistance to antimicrobial peptides contributes to the gut colonization. *PLoS One,* 12**,** e0190095.

GREENE, N. P., KAPLAN, E., CROW, A. & KORONAKIS, V. 2018. Antibiotic Resistance Mediated by the MacB ABC Transporter Family: A Structural and Functional Perspective. *Front Microbiol,* 9**,** 950.

GREENSPAN, P. & FOWLER, S. D. 1985. Spectrofluorometric studies of the lipid probe, nile red. *J Lipid Res,* 26**,** 781-9.

GREER, N. D. 2006. Tigecycline (Tygacil): the first in the glycylcycline class of antibiotics. *Proc (Bayl Univ Med Cent),* 19**,** 155-61.

GRIMSEY, E. M., FAIS, C., MARSHALL, R. L., RICCI, V., CIUSA, M. L., STONE, J. W., IVENS, A., MALLOCI, G., RUGGERONE, P., VARGIU, A. V. & PIDDOCK, L. J. V. 2020. Chlorpromazine and Amitriptyline Are Substrates and Inhibitors of the AcrB Multidrug Efflux Pump. *mBio,* 11.

GRIMSEY, E. M. & PIDDOCK, L. J. V. 2019. Do phenothiazines possess antimicrobial and efflux inhibitory properties? *FEMS Microbiol Rev,* 43**,** 577-590.

GROGAN, D. W. & CRONAN, J. E., JR. 1997. Cyclopropane ring formation in membrane lipids of bacteria. *Microbiol Mol Biol Rev,* 61**,** 429-41.

GUNN, J. S., LIM, K. B., KRUEGER, J., KIM, K., GUO, L., HACKETT, M. & MILLER, S. I. 1998. PmrA-PmrB-regulated genes necessary for 4-aminoarabinose lipid A modification and polymyxin resistance. *Mol Microbiol,* 27**,** 1171-82.

GUO, Q., GOTO, S., CHEN, Y., FENG, B., XU, Y., MUTO, A., HIMENO, H., DENG, H., LEI, J. & GAO, N. 2013. Dissecting the in vivo assembly of the 30S ribosomal subunit reveals the role of RimM and general features of the assembly process. *Nucleic Acids Res,* 41**,** 2609-20.

HALSEY, T. A., VAZQUEZ-TORRES, A., GRAVDAHL, D. J., FANG, F. C. & LIBBY, S. J. 2004. The ferritin-like Dps protein is required for Salmonella enterica serovar Typhimurium oxidative stress resistance and virulence. *Infect Immun,* 72**,** 1155-8.

HANCOCK, R. E. 1984. Alterations in outer membrane permeability. *Annu Rev Microbiol,* 38**,** 237-64.

HANCOCK, R. E. 1998. Resistance mechanisms in *Pseudomonas aeruginosa* and other nonfermentative gram-negative bacteria. *Clin Infect Dis,* 27 Suppl 1**,** S93-9.

HANCOCK, R. E. & BELL, A. 1988. Antibiotic uptake into gram-negative bacteria. *Eur J Clin Microbiol Infect Dis,* 7**,** 713-20.

HANCOCK, R. E., RAFFLE, V. J. & NICAS, T. I. 1981. Involvement of the outer membrane in gentamicin and streptomycin uptake and killing in *Pseudomonas aeruginosa*. *Antimicrob Agents Chemother,* 19**,** 777-85.

HARA-KAONGA, B. & PISTOLE, T. G. 2004. OmpD but not OmpC is involved in adherence of *Salmonella enterica* serovar typhimurium to human cells. *Can J Microbiol,* 50**,** 719-27.

HART, B. R. & BLUMENTHAL, R. M. 2011. Unexpected coregulator range for the global regulator Lrp of *Escherichia coli* and *Proteus mirabilis*. *J Bacteriol,* 193**,** 1054-64.

HARTMAN, B. J. & TOMASZ, A. 1984. Low-affinity penicillin-binding protein associated with beta-lactam resistance in *Staphylococcus aureus*. *J Bacteriol,* 158**,** 513-6.

HASSAN, K. A., CAIN, A. K., HUANG, T., LIU, Q., ELBOURNE, L. D., BOINETT, C. J., BRZOSKA, A. J., LI, L., OSTROWSKI, M., NHU, N. T., NHU TDO, H., BAKER, S., PARKHILL, J. & PAULSEN, I. T. 2016. Fluorescence-Based Flow Sorting in Parallel with Transposon Insertion Site Sequencing Identifies Multidrug Efflux Systems in Acinetobacter baumannii. *MBio,* 7.

HASSAN, K. A., ELBOURNE, L. D., LI, L., GAMAGE, H. K., LIU, Q., JACKSON, S. M., SHARPLES, D., KOLSTO, A. B., HENDERSON, P. J. & PAULSEN, I. T. 2015. An ace up their sleeve: a transcriptomic approach exposes the AceI

efflux protein of *Acinetobacter baumannii* and reveals the drug efflux potential hidden in many microbial pathogens. *Front Microbiol,* 6**,** 333.

HASSAN, K. A., JACKSON, S. M., PENESYAN, A., PATCHING, S. G., TETU, S. G., EIJKELKAMP, B. A., BROWN, M. H., HENDERSON, P. J. & PAULSEN, I. T. 2013. Transcriptomic and biochemical analyses identify a family of chlorhexidine efflux proteins. *Proc Natl Acad Sci U S A,* 110**,** 20254-9.

HASSAN, K. A., LIU, Q., ELBOURNE, L. D. H., AHMAD, I., SHARPLES, D., NAIDU, V., CHAN, C. L., LI, L., HARBORNE, S. P. D., POKHREL, A., POSTIS, V. L. G., GOLDMAN, A., HENDERSON, P. J. F. & PAULSEN, I. T. 2018. Pacing across the membrane: the novel PACE family of efflux pumps is widespread in Gram-negative pathogens. *Res Microbiol,* 169**,** 450-454.

HASSAN, K. A., NAIDU, V., EDGERTON, J. R., METTRICK, K. A., LIU, Q., FAHMY, L., LI, L., JACKSON, S. M., AHMAD, I., SHARPLES, D., HENDERSON, P. J. F. & PAULSEN, I. T. 2019. Short-chain diamines are the physiological substrates of PACE family efflux pumps. *Proc Natl Acad Sci U S A*.

HAYNES, M. K., GARCIA, M., PETERS, R., WALLER, A., TEDESCO, P., URSU, O., BOLOGA, C. G., SANTOS, R. G., PINILLA, C., WU, T. H., LOVCHIK, J. A., OPREA, T. I., SKLAR, L. A. & TEGOS, G. P. 2018. High-Throughput Flow Cytometry Screening of Multidrug Efflux Systems. *Methods Mol Biol,* 1700**,** 293-318.

HEFFRON, F., SUBLETT, R., HEDGES, R. W., JACOB, A. & FALKOW, S. 1975. Origin of the TEM-beta-lactamase gene found on plasmids. *J Bacteriol,* 122**,** 250-6.

HELD, K., RAMAGE, E., JACOBS, M., GALLAGHER, L. & MANOIL, C. 2012. Sequence-verified two-allele transposon mutant library for *Pseudomonas aeruginosa* PAO1. *J Bacteriol,* 194**,** 6387-9.

HENGGE-ARONIS, R. & FISCHER, D. 1992. Identification and molecular analysis of *glgS*, a novel growth-phase-regulated and *rpoS*-dependent gene involved in glycogen synthesis in *Escherichia coli*. *Mol Microbiol,* 6**,** 1877-86.

HENGGE-ARONIS, R., KLEIN, W., LANGE, R., RIMMELE, M. & BOOS, W. 1991. Trehalose synthesis genes are controlled by the putative sigma factor encoded by *rpoS* and are involved in stationary-phase thermotolerance in *Escherichia coli*. *J Bacteriol,* 173**,** 7918-24.

HERBERT, D., ELSWORTH, R. & TELLING, R. C. 1956. The Continuous Culture of Bacteria - a Theoretical and Experimental Study. *Journal of General Microbiology,* 14**,** 601-622.

HERITAGE, J., M'ZALI, F. H., GASCOYNE-BINZI, D. & HAWKEY, P. M. 1999. Evolution and spread of SHV extended-spectrum beta-lactamases in gram-negative bacteria. *J Antimicrob Chemother,* 44**,** 309-18.

HIDALGO, E., LEAUTAUD, V. & DEMPLE, B. 1998. The redox-regulated SoxR protein acts from a single DNA site as a repressor and an allosteric activator. *EMBO J,* 17**,** 2629-36.

HIRAKAWA, H., TAKUMI-KOBAYASHI, A., THEISEN, U., HIRATA, T., NISHINO, K. & YAMAGUCHI, A. 2008. AcrS/EnvR represses expression of the *acrAB* multidrug efflux genes in *Escherichia coli*. *Journal of Bacteriology,* 190**,** 6276-6279.

HOGBERG, L. D., HEDDINI, A. & CARS, O. 2010. The global need for effective antibiotics: challenges and recent advances. *Trends Pharmacol Sci,* 31**,** 509-15.

HOISETH, S. K. & STOCKER, B. A. 1981. Aromatic-dependent *Salmonella typhimurium* are non-virulent and effective as live vaccines. *Nature,* 291**,** 238-9.

HORIYAMA, T. & NISHINO, K. 2014. AcrB, AcrD, and MdtABC multidrug efflux systems are involved in enterobactin export in *Escherichia coli*. *PLoS One,* 9**,** e108642.

HORIYAMA, T., YAMAGUCHI, A. & NISHINO, K. 2010. TolC dependency of multidrug efflux systems in *Salmonella enterica* serovar Typhimurium. *J Antimicrob Chemother,* 65**,** 1372-6.

HOSKISSON, P. A. & HOBBS, G. 2005. Continuous culture - making a comeback? *Microbiology-Sgm,* 151**,** 3153-3159.

HU, Y. & COATES, A. 2012. Nonmultiplying bacteria are profoundly tolerant to antibiotics. *Handb Exp Pharmacol***,** 99-119.

HUISMAN, G., SIEGELE, M., ZAMBRANO, M. & KOLTER, R. 1996. Morphological and Physiological Changes During Stationary Phase. *American Society for Microbiology Press*.

HUISMAN, G. W. & KOLTER, R. 1994. Sensing starvation: a homoserine lactone--dependent signaling pathway in *Escherichia coli*. *Science,* 265**,** 537-9.

IBANEZ-RUIZ, M., ROBBE-SAULE, V., HERMANT, D., LABRUDE, S. & NOREL, F. 2000. Identification of RpoS (sigma(S))-regulated genes in *Salmonella enterica* serovar typhimurium. *J Bacteriol,* 182**,** 5749-56.

ILLINGWORTH, A. *What is MFI and how is it calculated?* [Online]. International Clinical Cytometry Society: Ask an Expert. Available: https://www.cytometry.org/web/q_view.php?id=152&filter=Analysis%20Techniques [Accessed 2020].

IPINZA, F., COLLAO, B., MONSALVA, D., BUSTAMANTE, V. H., LURASCHI, R., ALEGRIA-ARCOS, M., ALMONACID, D. E., AGUAYO, D., CALDERON, I. L., GIL, F., SANTIVIAGO, C. A., MORALES, E. H., CALVA, E. & SAAVEDRA, C. P. 2014. Participation of the *Salmonella* OmpD porin in the infection of RAW264.7 macrophages and BALB/c mice. *PLoS One,* 9**,** e111062.

IUCHI, S., COLE, S. T. & LIN, E. C. 1990. Multiple regulatory elements for the *glpA* operon encoding anaerobic glycerol-3-phosphate dehydrogenase and the *glpD* operon encoding aerobic glycerol-3-phosphate dehydrogenase in *Escherichia coli*: further characterization of respiratory control. *J Bacteriol,* 172**,** 179-84.

IVNITSKI-STEELE, I., HOLMES, A. R., LAMPING, E., MONK, B. C., CANNON, R. D. & SKLAR, L. A. 2009. Identification of Nile red as a fluorescent substrate of the Candida albicans ATP-binding cassette transporters Cdr1p and Cdr2p and the major facilitator superfamily transporter Mdr1p. *Anal Biochem,* 394**,** 87-91.

IZUTSU, K., WADA, A. & WADA, C. 2001a. Expression of ribosome modulation factor (RMF) in *Escherichia coli* requires ppGpp. *Genes Cells,* 6**,** 665-76.

IZUTSU, K., WADA, C., KOMINE, Y., SAKO, T., UEGUCHI, C., NAKURA, S. & WADA, A. 2001b. *Escherichia coli* ribosome-associated protein SRA, whose copy number increases during stationary phase. *J Bacteriol,* 183**,** 2765-73.

JACKSON, D. W., SUZUKI, K., OAKFORD, L., SIMECKA, J. W., HART, M. E. & ROMEO, T. 2002. Biofilm formation and dispersal under the influence of the global regulator CsrA of *Escherichia coli*. *J Bacteriol,* 184**,** 290-301.

JAISHANKAR, J. & SRIVASTAVA, P. 2017. Molecular Basis of Stationary Phase Survival and Applications. *Front Microbiol,* 8**,** 2000.

JANISSEN, R., ARENS, M. M. A., VTYURINA, N. N., RIVAI, Z., SUNDAY, N. D., ESLAMI-MOSSALLAM, B., GRITSENKO, A. A., LAAN, L., DE RIDDER, D., ARTSIMOVITCH, I., DEKKER, N. H., ABBONDANZIERI, E. A. & MEYER, A. S. 2018. Global DNA Compaction in Stationary-Phase Bacteria Does Not Affect Transcription. *Cell,* 174**,** 1188-1199 e14.

JECKELMANN, J. M. & ERNI, B. 2020. Transporters of glucose and other carbohydrates in bacteria. *Pflugers Arch*.

JISHAGE, M., KVINT, K., SHINGLER, V. & NYSTROM, T. 2002. Regulation of sigma factor competition by the alarmone ppGpp. *Genes Dev,* 16**,** 1260-70.

JONAS, K., TOMENIUS, H., KADER, A., NORMARK, S., ROMLING, U., BELOVA, L. M. & MELEFORS, O. 2007. Roles of curli, cellulose and BapA in *Salmonella* biofilm morphology studied by atomic force microscopy. *BMC Microbiol,* 7**,** 70.

JONES, D. M., SUTCLIFFE, E. M. & CURRY, A. 1991. Recovery of viable but non-culturable *Campylobacter jejuni*. *J Gen Microbiol,* 137**,** 2477-82.

KAMIO, Y. & NIKAIDO, H. 1976. Outer membrane of *Salmonella typhimurium*: accessibility of phospholipid head groups to phospholipase c and cyanogen bromide activated dextran in the external medium. *Biochemistry,* 15**,** 2561-70.

KANDROR, O., DELEON, A. & GOLDBERG, A. L. 2002. Trehalose synthesis is induced upon exposure of *Escherichia coli* to cold and is essential for viability at low temperatures. *Proc Natl Acad Sci U S A,* 99**,** 9727-32.

KARIUKI, S., OKORO, C., KIIRU, J., NJOROGE, S., OMUSE, G., LANGRIDGE, G., KINGSLEY, R. A., DOUGAN, G. & REVATHI, G. 2015. Ceftriaxone-resistant *Salmonella enterica* serotype typhimurium sequence type 313 from Kenyan patients is associated with the blaCTX-M-15 gene on a novel IncHI2 plasmid. *Antimicrob Agents Chemother,* 59**,** 3133-9.

KARP, P. D., LATENDRESSE, M., PALEY, S. M., KRUMMENACKER, M., ONG, Q. D., BILLINGTON, R., KOTHARI, A., WEAVER, D., LEE, T., SUBHRAVETI, P., SPAULDING, A., FULCHER, C., KESELER, I. M. & CASPI, R. 2016.

Pathway Tools version 19.0 update: software for pathway/genome informatics and systems biology. *Brief Bioinform,* 17**,** 877-90.

KARP, P. D., WEAVER, D., PALEY, S., FULCHER, C., KUBO, A., KOTHARI, A., KRUMMENACKER, M., SUBHRAVETI, P., WEERASINGHE, D., GAMA-CASTRO, S., HUERTA, A. M., MUNIZ-RASCADO, L., BONAVIDES-MARTINEZ, C., WEISS, V., PERALTA-GIL, M., SANTOS-ZAVALETA, A., SCHRODER, I., MACKIE, A., GUNSALUS, R., COLLADO-VIDES, J., KESELER, I. M. & PAULSEN, I. 2014. The EcoCyc Database. *EcoSal Plus,* 6.

KASCAKOVA, S., MAIGRE, L., CHEVALIER, J., REFREGIERS, M. & PAGES, J. M. 2012. Antibiotic transport in resistant bacteria: synchrotron UV fluorescence microscopy to determine antibiotic accumulation with single cell resolution. *PLoS One,* 7**,** e38624.

KASHKET, E. R. 1981. Effects of aerobiosis and nitrogen source on the proton motive force in growing *Escherichia coli* and *Klebsiella pneumoniae* cells. *J Bacteriol,* 146**,** 377-84.

KATAYAMA, Y., ITO, T. & HIRAMATSU, K. 2000. A new class of genetic element, staphylococcus cassette chromosome *mec*, encodes methicillin resistance in *Staphylococcus aureus*. *Antimicrob Agents Chemother,* 44**,** 1549-55.

KATSUBE, S., ANDO, T. & YONEYAMA, H. 2019. L-Alanine Exporter, AlaE, of *Escherichia coli* Functions as a Safety Valve to Enhance Survival under Feast Conditions. *Int J Mol Sci,* 20.

KEENEY, D., RUZIN, A., MCALEESE, F., MURPHY, E. & BRADFORD, P. A. 2008. MarA-mediated overexpression of the AcrAB efflux pump results in decreased susceptibility to tigecycline in *Escherichia coli*. *J Antimicrob Chemother,* 61**,** 46-53.

KERN, W. V., STEINKE, P., SCHUMACHER, A., SCHUSTER, S., VON BAUM, H. & BOHNERT, J. A. 2006. Effect of 1-(1-naphthylmethyl)-piperazine, a novel putative efflux pump inhibitor, on antimicrobial drug susceptibility in clinical isolates of *Escherichia coli*. *J Antimicrob Chemother,* 57**,** 339-43.

KIM, B. H., KIM, S., KIM, H. G., LEE, J., LEE, I. S. & PARK, Y. K. 2005. The formation of cyclopropane fatty acids in *Salmonella enterica* serovar Typhimurium. *Microbiology,* 151**,** 209-218.

KIM, S., IHARA, K., KATSUBE, S., HORI, H., ANDO, T., ISOGAI, E. & YONEYAMA, H. 2015. Characterization of the l-alanine exporter AlaE of *Escherichia coli* and its potential role in protecting cells from a toxic-level accumulation of l-alanine and its derivatives. *Microbiologyopen,* 4**,** 632-43.

KIM, W. & LEE, Y. 2020. Mechanism for coordinate regulation of *rpoS* by sRNA-sRNA interaction in *Escherichia coli*. *RNA Biol,* 17**,** 176-187.

KLOBUCAR, K., FRENCH, S., COTE, J. P., HOWES, J. R. & BROWN, E. D. 2020. Genetic and Chemical-Genetic Interactions Map Biogenesis and Permeability Determinants of the Outer Membrane of *Escherichia coli*. *mBio,* 11.

KOBAYASHI, A., HIRAKAWA, H., HIRATA, T., NISHINO, K. & YAMAGUCHI, A. 2006. Growth phase-dependent expression of drug exporters in *Escherichia coli* and its contribution to drug tolerance. *Journal of Bacteriology,* 188**,** 5693-5703.

KOBAYASHI, N., NISHINO, K. & YAMAGUCHI, A. 2001. Novel macrolide-specific ABC-type efflux transporter in *Escherichia coli*. *Journal of Bacteriology,* 183**,** 5639-5644.

KOLTER, R., SIEGELE, D. A. & TORMO, A. 1993. The stationary phase of the bacterial life cycle. *Annu Rev Microbiol,* 47**,** 855-74.

KORONAKIS, V., SHARFF, A., KORONAKIS, E., LUISI, B. & HUGHES, C. 2000. Crystal structure of the bacterial membrane protein TolC central to multidrug efflux and protein export. *Nature,* 405**,** 914-9.

KROGER, C., COLGAN, A., SRIKUMAR, S., HANDLER, K., SIVASANKARAN, S. K., HAMMARLOF, D. L., CANALS, R., GRISSOM, J. E., CONWAY, T., HOKAMP, K. & HINTON, J. C. 2013. An infection-relevant transcriptomic compendium for *Salmonella enterica* Serovar Typhimurium. *Cell Host Microbe,* 14**,** 683-95.

KRONER, G. M., WOLFE, M. B. & FREDDOLINO, P. L. 2019. *Escherichia coli* Lrp Regulates One-Third of the Genome via Direct, Cooperative, and Indirect Routes. *J Bacteriol,* 201.

KUDVA, R., DENKS, K., KUHN, P., VOGT, A., MULLER, M. & KOCH, H. G. 2013. Protein translocation across the inner membrane of Gram-negative bacteria: the Sec and Tat dependent protein transport pathways. *Res Microbiol,* 164**,** 505-34.

KUMAR, S., HE, G., KAKARLA, P., SHRESTHA, U., RANJANA, K. C., RANAWEERA, I., WILLMON, T. M., BARR, S. R., HERNANDEZ, A. J. & VARELA, M. F. 2016. Bacterial Multidrug Efflux Pumps of the Major Facilitator Superfamily as Targets for Modulation. *Infect Disord Drug Targets,* 16**,** 28-43.

KURODA, T. & TSUCHIYA, T. 2009. Multidrug efflux transporters in the MATE family. *Biochim Biophys Acta,* 1794**,** 763-8.

KVIST, M., HANCOCK, V. & KLEMM, P. 2008. Inactivation of efflux pumps abolishes bacterial biofilm formation. *Appl Environ Microbiol,* 74**,** 7376-82.

LACROIX, F. J., CLOECKAERT, A., GREPINET, O., PINAULT, C., POPOFF, M. Y., WAXIN, H. & PARDON, P. 1996. *Salmonella typhimurium acrB*-like gene: identification and role in resistance to biliary salts and detergents and in murine infection. *FEMS Microbiol Lett,* 135**,** 161-7.

LAIBLE, G. & HAKENBECK, R. 1991. Five independent combinations of mutations can result in low-affinity penicillin-binding protein 2x of *Streptococcus pneumoniae*. *J Bacteriol,* 173**,** 6986-90.

LAMBERT, P. A. 2005. Bacterial resistance to antibiotics: modified target sites. *Adv Drug Deliv Rev,* 57**,** 1471-85.

LAN, C. Y. & IGO, M. M. 1998. Differential expression of the OmpF and OmpC porin proteins in *Escherichia coli* K-12 depends upon the level of active OmpR. *J Bacteriol,* 180**,** 171-4.

LANDGRAF, J. R., WU, J. & CALVO, J. M. 1996. Effects of nutrition and growth rate on Lrp levels in *Escherichia coli*. *J Bacteriol,* 178**,** 6930-6.

LANGE, R. & HENGGE-ARONIS, R. 1991a. Growth phase-regulated expression of *bolA* and morphology of stationary-phase *Escherichia coli* cells are controlled by the novel sigma factor sigma S. *J Bacteriol,* 173**,** 4474-81.

LANGE, R. & HENGGE-ARONIS, R. 1991b. Identification of a central regulator of stationary-phase gene expression in *Escherichia coli*. *Mol Microbiol,* 5**,** 49-59.

LANGE, R. & HENGGE-ARONIS, R. 1994. The cellular concentration of the sigma S subunit of RNA polymerase in *Escherichia coli* is controlled at the levels of transcription, translation, and protein stability. *Genes Dev,* 8**,** 1600-12.

LAURINAVICHENE, T. V. & TSYGANKOV, A. A. 2001. H2 consumption by *Escherichia coli* coupled via hydrogenase 1 or hydrogenase 2 to different terminal electron acceptors. *FEMS Microbiol Lett,* 202**,** 121-4.

LAVOLLAY, M., ARTHUR, M., FOURGEAUD, M., DUBOST, L., MARIE, A., VEZIRIS, N., BLANOT, D., GUTMANN, L. & MAINARDI, J. L. 2008. The peptidoglycan of stationary-phase *Mycobacterium tuberculosis* predominantly contains cross-links generated by L,D-transpeptidation. *J Bacteriol,* 190**,** 4360-6.

LAWLER, A. J., RICCI, V., BUSBY, S. J. & PIDDOCK, L. J. 2013. Genetic inactivation of *acrAB* or inhibition of efflux induces expression of *ramA*. *J Antimicrob Chemother,* 68**,** 1551-7.

LEBEL, M. 1988. Ciprofloxacin: chemistry, mechanism of action, resistance, antimicrobial spectrum, pharmacokinetics, clinical trials, and adverse reactions. *Pharmacotherapy,* 8**,** 3-33.

LEE, S. Y., LIM, C. J., DROGE, P. & YAN, J. 2015. Regulation of Bacterial DNA Packaging in Early Stationary Phase by Competitive DNA Binding of Dps and IHF. *Sci Rep,* 5**,** 18146.

LEIVE, L. 1974. The barrier function of the gram-negative envelope. *Ann N Y Acad Sci,* 235**,** 109-29.

LEMKE, J. J., SANCHEZ-VAZQUEZ, P., BURGOS, H. L., HEDBERG, G., ROSS, W. & GOURSE, R. L. 2011. Direct regulation of *Escherichia coli* ribosomal protein promoters by the transcription factors ppGpp and DksA. *Proc Natl Acad Sci U S A,* 108**,** 5712-7.

LEMONNIER, M., LEVIN, B. R., ROMEO, T., GARNER, K., BAQUERO, M. R., MERCANTE, J., LEMICHEZ, E., BAQUERO, F. & BLAZQUEZ, J. 2008. The evolution of contact-dependent inhibition in non-growing populations of *Escherichia coli*. *Proc Biol Sci,* 275**,** 3-10.

LI, B., QIU, Y., SHI, H. & YIN, H. 2016. The importance of lag time extension in determining bacterial resistance to antibiotics. *Analyst,* 141**,** 3059-67.

LI, X. Z., NIKAIDO, H. & POOLE, K. 1995. Role of mexA-mexB-oprM in antibiotic efflux in *Pseudomonas aeruginosa*. *Antimicrob Agents Chemother,* 39**,** 1948-53.

LI, X. Z., POOLE, K. & NIKAIDO, H. 2003. Contributions of MexAB-OprM and an EmrE homolog to intrinsic resistance of *Pseudomonas aeruginosa* to aminoglycosides and dyes. *Antimicrob Agents Chemother,* 47**,** 27-33.

LIBERATI, N. T., URBACH, J. M., MIYATA, S., LEE, D. G., DRENKARD, E., WU, G., VILLANUEVA, J., WEI, T. & AUSUBEL, F. M. 2006. An ordered, nonredundant library of *Pseudomonas aeruginosa* strain PA14 transposon insertion mutants. *Proc Natl Acad Sci U S A,* 103**,** 2833-8.

LIN, T. Y., CHIU, C. H., LIN, P. Y., WANG, M. H., SU, L. H. & LIN, T. Y. 2003. Short-term ceftriaxone therapy for treatment of severe non-typhoidal *Salmonella enterocolitis*. *Acta Paediatr,* 92**,** 537-40.

LISTER, P. D., WOLTER, D. J. & HANSON, N. D. 2009. Antibacterial-resistant *Pseudomonas aeruginosa*: clinical impact and complex regulation of chromosomally encoded resistance mechanisms. *Clin Microbiol Rev,* 22**,** 582-610.

LIU, Q., HASSAN, K. A., ASHWOOD, H. E., GAMAGE, H., LI, L., MABBUTT, B. C. & PAULSEN, I. T. 2018. Regulation of the *acel* multidrug efflux pump gene in *Acinetobacter baumannii*. *J Antimicrob Chemother,* 73**,** 1492-1500.

LIU, Q., LI, M., TENG, Y., YANG, H., XI, Y., CHEN, S. & DUAN, G. 2019. The role of cfa gene in ampicillin tolerance in *Shigella*. *Infect Drug Resist,* 12**,** 2765-2774.

LIU, X. & FERENCI, T. 2001. An analysis of multifactorial influences on the transcriptional control of *ompF* and *ompC* porin expression under nutrient limitation. *Microbiology,* 147**,** 2981-9.

LIU, Y. Y., WANG, Y., WALSH, T. R., YI, L. X., ZHANG, R., SPENCER, J., DOI, Y., TIAN, G., DONG, B., HUANG, X., YU, L. F., GU, D., REN, H., CHEN, X., LV, L., HE, D., ZHOU, H., LIANG, Z., LIU, J. H. & SHEN, J. 2016. Emergence of plasmid-mediated colistin resistance mechanism MCR-1 in animals and human beings in China: a microbiological and molecular biological study. *Lancet Infect Dis,* 16**,** 161-8.

LLANES, C., HOCQUET, D., VOGNE, C., BENALI-BAITICH, D., NEUWIRTH, C. & PLESIAT, P. 2004. Clinical strains of *Pseudomonas aeruginosa* overproducing MexAB-OprM and MexXY efflux pumps simultaneously. *Antimicrob Agents Chemother,* 48**,** 1797-802.

LLOYD, C. R., PARK, S., FEI, J. & VANDERPOOL, C. K. 2017. The Small Protein SgrT Controls Transport Activity of the Glucose-Specific Phosphotransferase System. *J Bacteriol,* 199.

LOMMATZSCH, J., TEMPLIN, M. F., KRAFT, A. R., VOLLMER, W. & HOLTJE, J. V. 1997. Outer membrane localization of murein hydrolases: MltA, a third lipoprotein lytic transglycosylase in *Escherichia coli*. *J Bacteriol,* 179**,** 5465-70.

LOMOVSKAYA, O., LEWIS, K. & MATIN, A. 1995. EmrR is a negative regulator of the *Escherichia coli* multidrug resistance pump EmrAB. *J Bacteriol,* 177**,** 2328-34.

LOMOVSKAYA, O., WARREN, M. S., LEE, A., GALAZZO, J., FRONKO, R., LEE, M., BLAIS, J., CHO, D., CHAMBERLAND, S., RENAU, T., LEGER, R., HECKER, S., WATKINS, W., HOSHINO, K., ISHIDA, H. & LEE, V. J. 2001. Identification and characterization of inhibitors of multidrug resistance efflux pumps in *Pseudomonas aeruginosa*: novel agents for combination therapy. *Antimicrob Agents Chemother,* 45**,** 105-16.

LUGTENBERG, E. J. & V SCHIJNDEL-VAN DAM, A. 1973. Temperature-sensitive mutant of *Escherichia coli* K-12 with an impaired D-alanine:D-alanine ligase. *J Bacteriol,* 113**,** 96-104.

LULI, G. W. & STROHL, W. R. 1990. Comparison of growth, acetate production, and acetate inhibition of *Escherichia coli* strains in batch and fed-batch fermentations. *Appl Environ Microbiol,* 56**,** 1004-11.

MA, D., ALBERTI, M., LYNCH, C., NIKAIDO, H. & HEARST, J. E. 1996. The local repressor AcrR plays a modulating role in the regulation of *acrAB* genes of *Escherichia coli* by global stress signals. *Mol Microbiol,* 19**,** 101-12.

MACHEBOEUF, P., CONTRERAS-MARTEL, C., JOB, V., DIDEBERG, O. & DESSEN, A. 2006. Penicillin binding proteins: key players in bacterial cell cycle and drug resistance processes. *FEMS Microbiol Rev,* 30**,** 673-91.

MADIGAN, M. M., JM; PARKER, J; 2000. Brock Biology of Micro-organisms. p 135-162.

MAHAMOUD, A., CHEVALIER, J., ALIBERT-FRANCO, S., KERN, W. V. & PAGES, J. M. 2007. Antibiotic efflux pumps in Gram-negative bacteria: the inhibitor response strategy. *J Antimicrob Chemother,* 59**,** 1223-9.

MAIER, R. M. 2009. Bacterial Growth. Edition 3. *Environmental Microbiology.* Elsevier.

MAJOWICZ, S. E., MUSTO, J., SCALLAN, E., ANGULO, F. J., KIRK, M., O'BRIEN, S. J., JONES, T. F., FAZIL, A., HOEKSTRA, R. M. & INTERNATIONAL COLLABORATION ON ENTERIC DISEASE 'BURDEN OF ILLNESS, S. 2010. The global burden of nontyphoidal *Salmonella* gastroenteritis. *Clin Infect Dis,* 50**,** 882-9.

MAKI, Y., YOSHIDA, H. & WADA, A. 2000. Two proteins, YfiA and YhbH, associated with resting ribosomes in stationary phase *Escherichia coli*. *Genes Cells,* 5**,** 965-74.

MALINVERNI, J. C. & SILHAVY, T. J. 2009. An ABC transport system that maintains lipid asymmetry in the gram-negative outer membrane. *Proc Natl Acad Sci U S A,* 106**,** 8009-14.

MANDIN, P. & GOTTESMAN, S. 2010. Integrating anaerobic/aerobic sensing and the general stress response through the ArcZ small RNA. *EMBO J,* 29**,** 3094-107.

MANEEWANNAKUL, K. & LEVY, S. B. 1996. Identification for *mar* mutants among quinolone-resistant clinical isolates of *Escherichia coli*. *Antimicrob Agents Chemother,* 40**,** 1695-8.

MANGAN, M. W., LUCCHINI, S., DANINO, V., CROININ, T. O., HINTON, J. C. & DORMAN, C. J. 2006. The integration host factor (IHF) integrates stationary-phase and virulence gene expression in *Salmonella enterica* serovar Typhimurium. *Mol Microbiol,* 59**,** 1831-47.

MARSHALL, R. L., LLOYD, G. S., LAWLER, A. J., ELEMENT, S. J., KAUR, J., CIUSA, M. L., RICCI, V., TSCHUMI, A., KUHNE, H., ALDERWICK, L. J. & PIDDOCK, L. J. V. 2020. New Multidrug Efflux Inhibitors for Gram-Negative Bacteria. *mBio,* 11.

MARTIN, D. S. 1932. The Oxygen Consumption of *Escherichia coli* during the Lag and Logarithmic Phases of Growth. *J Gen Physiol,* 15**,** 691-708.

MARTINEZ-GARCIA, E., TORMO, A. & NAVARRO-LLORENS, J. M. 2003. GASP phenotype: presence in enterobacteria and independence of sigmaS in its acquisition. *FEMS Microbiol Lett,* 225**,** 201-6.

MASI, M., WINTERHALTER, M. & PAGES, J. M. 2019. Outer Membrane Porins. *Subcell Biochem,* 92**,** 79-123.

MCKAY, S. L. & PORTNOY, D. A. 2015. Ribosome hibernation facilitates tolerance of stationary-phase bacteria to aminoglycosides. *Antimicrob Agents Chemother,* 59**,** 6992-9.

MCMURRY, L. M., OETHINGER, M. & LEVY, S. B. 1998. Overexpression of marA, soxS, or acrAB produces resistance to triclosan in laboratory and clinical strains of Escherichia coli. *FEMS Microbiol Lett,* 166**,** 305-9.

MCNEIL, H. E., ALAV, I., TORRES, R. C., ROSSITER, A. E., LAYCOCK, E., LEGOOD, S., KAUR, I., DAVIES, M., WAND, M., WEBBER, M. A., BAVRO, V. N. & BLAIR, J. M. A. 2019. Identification of binding residues between periplasmic adapter protein (PAP) and RND efflux pumps explains PAP-pump promiscuity and roles in antimicrobial resistance. *PLoS Pathog,* 15**,** e1008101.

MENGIN-LECREULX, D. & VAN HEIJENOORT, J. 1985. Effect of growth conditions on peptidoglycan content and cytoplasmic steps of its biosynthesis in *Escherichia coli*. *J Bacteriol,* 163**,** 208-12.

MIKI, T. & HARDT, W. D. 2013. Outer membrane permeabilization is an essential step in the killing of gram-negative bacteria by the lectin RegIIIbeta. *PLoS One,* 8**,** e69901.

MIKOLOSKO, J., BOBYK, K., ZGURSKAYA, H. I. & GHOSH, P. 2006. Conformational flexibility in the multidrug efflux system protein AcrA. *Structure,* 14**,** 577-87.

MIL-HOMENS, D., BARAHONA, S., MOREIRA, R. N., SILVA, I. J., PINTO, S. N., FIALHO, A. M. & ARRAIANO, C. M. 2018. Stress Response Protein BolA Influences Fitness and Promotes *Salmonella enterica* Serovar Typhimurium Virulence. *Appl Environ Microbiol,* 84.

MISRA, R., MORRISON, K. D., CHO, H. J. & KHUU, T. 2015. Importance of Real-Time Assays To Distinguish Multidrug Efflux Pump-Inhibiting and Outer Membrane-Destabilizing Activities in *Escherichia coli*. *J Bacteriol,* 197**,** 2479-88.

MITCHELL, A. M., SRIKUMAR, T. & SILHAVY, T. J. 2018. Cyclic Enterobacterial Common Antigen Maintains the Outer Membrane Permeability Barrier of *Escherichia coli* in a Manner Controlled by YhdP. *mBio,* 9.

MITCHELL, A. M., WANG, W. & SILHAVY, T. J. 2017. Novel RpoS-Dependent Mechanisms Strengthen the Envelope Permeability Barrier during Stationary Phase. *J Bacteriol,* 199.

MITCHELL, J. E., OSHIMA, T., PIPER, S. E., WEBSTER, C. L., WESTBLADE, L. F., KARIMOVA, G., LADANT, D., KOLB, A., HOBMAN, J. L., BUSBY, S. J. & LEE, D. J. 2007. The *Escherichia coli* regulator of sigma 70 protein, Rsd, can up-regulate some stress-dependent promoters by sequestering sigma 70. *J Bacteriol,* 189**,** 3489-95.

MIZUNOE, Y., WAI, S. N., TAKADE, A. & YOSHIDA, S. 1999. Restoration of culturability of starvation-stressed and low-temperature-stressed *Escherichia coli* O157 cells by using H2O2-degrading compounds. *Arch Microbiol,* 172**,** 63-7.

MORE, N., MARTORANA, A. M., BIBOY, J., OTTEN, C., WINKLE, M., SERRANO, C. K. G., MONTON SILVA, A., ATKINSON, L., YAU, H., BREUKINK, E., DEN BLAAUWEN, T., VOLLMER, W. & POLISSI, A. 2019. Peptidoglycan Remodeling Enables *Escherichia coli* To Survive Severe Outer Membrane Assembly Defect. *mBio,* 10.

MOREIRA, R. N., DRESSAIRE, C., BARAHONA, S., GALEGO, L., KAEVER, V., JENAL, U. & ARRAIANO, C. M. 2017. BolA Is Required for the Accurate Regulation of c-di-GMP, a Central Player in Biofilm Formation. *mBio,* 8.

MORGAN, E., CAMPBELL, J. D., ROWE, S. C., BISPHAM, J., STEVENS, M. P., BOWEN, A. J., BARROW, P. A., MASKELL, D. J. & WALLIS, T. S. 2004. Identification of host-specific colonization factors of *Salmonella enterica* serovar Typhimurium. *Mol Microbiol,* 54**,** 994-1010.

MORITA, Y., KODAMA, K., SHIOTA, S., MINE, T., KATAOKA, A., MIZUSHIMA, T. & TSUCHIYA, T. 1998. NorM, a putative multidrug efflux protein, of *Vibrio parahaemolyticus* and its homolog in *Escherichia coli*. *Antimicrob Agents Chemother,* 42**,** 1778-82.

MORUNO ALGARA, M., KUCZYNSKA-WISNIK, D., DEBSKI, J., STOJOWSKA-SWEDRZYNSKA, K., SOMINKA, H., BUKREJEWSKA, M. & LASKOWSKA, E. 2019. Trehalose protects *Escherichia coli* against carbon stress manifested by protein acetylation and aggregation. *Mol Microbiol,* 112**,** 866-880.

MUHEIM, C., GOTZKE, H., ERIKSSON, A. U., LINDBERG, S., LAURITSEN, I., NORHOLM, M. H. H. & DALEY, D. O. 2017. Increasing the permeability of *Escherichia coli* using MAC13243. *Sci Rep,* 7**,** 17629.

MUNITA, J. M. & ARIAS, C. A. 2016. Mechanisms of Antibiotic Resistance. *Microbiol Spectr,* 4.

MUNOZ-ELIAS, E. J. & MCKINNEY, J. D. 2006. Carbon metabolism of intracellular bacteria. *Cell Microbiol,* 8**,** 10-22.

MURAKAMI, S., NAKASHIMA, R., YAMASHITA, E., MATSUMOTO, T. & YAMAGUCHI, A. 2006. Crystal structures of a multidrug transporter reveal a functionally rotating mechanism. *Nature,* 443**,** 173-9.

NA, S. H., MIYANAGA, K., UNNO, H. & TANJI, Y. 2006. The survival response of *Escherichia coli* K12 in a natural environment. *Appl Microbiol Biotechnol,* 72**,** 386-92.

NAIR, S. & FINKEL, S. E. 2004. Dps protects cells against multiple stresses during stationary phase. *J Bacteriol,* 186**,** 4192-8.

NAKAJIMA, H., KOBAYASHI, K., KOBAYASHI, M., ASAKO, H. & AONO, R. 1995. Overexpression of the *robA* gene increases organic solvent tolerance and multiple antibiotic and heavy metal ion resistance in *Escherichia coli*. *Appl Environ Microbiol,* 61**,** 2302-7.

NAVARRO LLORENS, J. M., TORMO, A. & MARTINEZ-GARCIA, E. 2010. Stationary phase in gram-negative bacteria. *FEMS Microbiol Rev,* 34**,** 476-95.

NEIDHARDT, F. C., BLOCH, P. L. & SMITH, D. F. 1974. Culture medium for enterobacteria. *J Bacteriol,* 119**,** 736-47.

NICOLOFF, H., GOPALKRISHNAN, S. & ADES, S. E. 2017. Appropriate Regulation of the sigma(E)-Dependent Envelope Stress Response Is Necessary To Maintain Cell Envelope Integrity and Stationary-Phase Survival in *Escherichia coli*. *J Bacteriol,* 199.

NIKAIDO, E., YAMAGUCHI, A. & NISHINO, K. 2008. AcrAB multidrug efflux pump regulation in *Salmonella enterica* serovar Typhimurium by RamA in response to environmental signals. *J Biol Chem,* 283**,** 24245-53.

NIKAIDO, H. 1989. Outer membrane barrier as a mechanism of antimicrobial resistance. *Antimicrob Agents Chemother,* 33**,** 1831-6.

NIKAIDO, H. 2003. Molecular basis of bacterial outer membrane permeability revisited. *Microbiol Mol Biol Rev,* 67**,** 593-656.

NIKAIDO, H. 2009. The Limitations of LB Medium. *American Society for Microbiology*.

NIKAIDO, H. & THANASSI, D. G. 1993. Penetration of lipophilic agents with multiple protonation sites into bacterial cells: tetracyclines and fluoroquinolones as examples. *Antimicrob Agents Chemother,* 37**,** 1393-9.

NISHINO, K., HAYASHI-NISHINO, M. & YAMAGUCHI, A. 2009a. H-NS Modulates Multidrug Resistance of *Salmonella enterica* Serovar Typhimurium by Repressing Multidrug Efflux Genes *acrEF*. *Antimicrobial Agents and Chemotherapy,* 53**,** 3541-3543.

NISHINO, K., LATIFI, T. & GROISMAN, E. A. 2006. Virulence and drug resistance roles of multidrug efflux systems of *Salmonella enterica* serovar Typhimurium. *Mol Microbiol,* 59**,** 126-41.

NISHINO, K., NIKAIDO, E. & YAMAGUCHI, A. 2007. Regulation of multidrug efflux systems involved in multidrug and metal resistance of *Salmonella enterica* serovar typhimurium. *Journal of Bacteriology,* 189**,** 9066-9075.

NISHINO, K., NIKAIDO, E. & YAMAGUCHI, A. 2009b. Regulation and physiological function of multidrug efflux pumps in *Escherichia coli* and *Salmonella*. *Biochim Biophys Acta,* 1794**,** 834-43.

NISHINO, K. & YAMAGUCHI, A. 2001. Analysis of a complete library of putative drug transporter genes in *Escherichia coli*. *J Bacteriol,* 183**,** 5803-12.

NOSEK, V. & MISEK, J. 2019. Enzymatic kinetic resolution of chiral sulfoxides - an enantiocomplementary approach. *Chem Commun (Camb),* 55**,** 10480-10483.

NYSTROM, T. 2004. Stationary-phase physiology. *Annu Rev Microbiol,* 58**,** 161-81.

O' NEILL, J. 2016. Tackling Drug-Resistant Infections Globally: Final report and recommendations. *Review on Antimicrobial Resistance*.

O'TOOLE, G. A. 2011. Microtiter dish biofilm formation assay. *J Vis Exp*.

OKUSU, H., MA, D. & NIKAIDO, H. 1996. AcrAB efflux pump plays a major role in the antibiotic resistance phenotype of *Escherichia coli* multiple-antibiotic-resistance (Mar) mutants. *J Bacteriol,* 178**,** 306-8.

OLAITAN, A. O., MORAND, S. & ROLAIN, J. M. 2014. Mechanisms of polymyxin resistance: acquired and intrinsic resistance in bacteria. *Front Microbiol,* 5**,** 643.

OLLIVER, A., VALLE, M., CHASLUS-DANCLA, E. & CLOECKAERT, A. 2004. Role of an *acrR* mutation in multidrug resistance of in vitro-selected fluoroquinolone-resistant mutants of *Salmonella enterica* serovar Typhimurium. *FEMS Microbiol Lett,* 238**,** 267-72.

OLMSTED, J., 3RD & KEARNS, D. R. 1977. Mechanism of ethidium bromide fluorescence enhancement on binding to nucleic acids. *Biochemistry,* 16**,** 3647-54.

ONG, S. E., MITTLER, G. & MANN, M. 2004. Identifying and quantifying in vivo methylation sites by heavy methyl SILAC. *Nat Methods,* 1**,** 119-26.

OPPERMAN, T. J., KWASNY, S. M., KIM, H. S., NGUYEN, S. T., HOUSEWEART, C., D'SOUZA, S., WALKER, G. C., PEET, N. P., NIKAIDO, H. & BOWLIN, T. L. 2014. Characterization of a novel pyranopyridine inhibitor of the AcrAB efflux pump of *Escherichia coli*. *Antimicrob Agents Chemother,* 58**,** 722-33.

OPPERMAN, T. J. & NGUYEN, S. T. 2015. Recent advances toward a molecular mechanism of efflux pump inhibition. *Front Microbiol,* 6**,** 421.

PA14.MGH.HARVARD.EDU. *PA14 Transposon Insertion Mutant Library* [Online]. Available: http://ausubellab.mgh.harvard.edu/cgi-bin/pa14/home.cgi [Accessed].

PAGET, M. S. & HELMANN, J. D. 2003. The sigma70 family of sigma factors. *Genome Biol,* 4**,** 203.

PAIVA, J. B., PENHA FILHO, R. A., PEREIRA, E. A., LEMOS, M. V., BARROW, P. A., LOVELL, M. A. & BERCHIERI, A., JR. 2009. The contribution of genes required for anaerobic respiration to the virulence of *Salmonella enterica* serovar Gallinarum for chickens. *Braz J Microbiol,* 40**,** 994-1001.

PAIXAO, L., RODRIGUES, L., COUTO, I., MARTINS, M., FERNANDES, P., DE CARVALHO, C. C., MONTEIRO, G. A., SANSONETTY, F., AMARAL, L. & VIVEIROS, M. 2009. Fluorometric determination of ethidium bromide efflux kinetics in *Escherichia coli*. *J Biol Eng,* 3**,** 18.

PAO, S. S., PAULSEN, I. T. & SAIER, M. H., JR. 1998. Major facilitator superfamily. *Microbiol Mol Biol Rev,* 62**,** 1-34.

PARKER, A. & GOTTESMAN, S. 2016. Small RNA Regulation of TolC, the Outer Membrane Component of Bacterial Multidrug Transporters. *J Bacteriol,* 198**,** 1101-13.

PAULSEN, I. T., PARK, J. H., CHOI, P. S. & SAIER, M. H., JR. 1997. A family of gram-negative bacterial outer membrane factors that function in the export of proteins, carbohydrates, drugs and heavy metals from gram-negative bacteria. *FEMS Microbiol Lett,* 156**,** 1-8.

PEDELACQ, J. D., CABANTOUS, S., TRAN, T., TERWILLIGER, T. C. & WALDO, G. S. 2006. Engineering and characterization of a superfolder green fluorescent protein. *Nat Biotechnol,* 24**,** 79-88.

PETERS, K., PAZOS, M., EDOO, Z., HUGONNET, J. E., MARTORANA, A. M., POLISSI, A., VANNIEUWENHZE, M. S., ARTHUR, M. & VOLLMER, W. 2018. Copper inhibits peptidoglycan LD-transpeptidases suppressing beta-lactam resistance due to bypass of penicillin-binding proteins. *Proc Natl Acad Sci U S A,* 115**,** 10786-10791.

PHE 2017. Enteric fever (typhoid and paratyphoid) England, Wales and Northern Ireland: 2017. PHE.

PHE 2018. *Salmonella* data 2007 to 2016. Public Health England.

PI, H., JONES, S. A., MERCER, L. E., MEADOR, J. P., CAUGHRON, J. E., JORDAN, L., NEWTON, S. M., CONWAY, T. & KLEBBA, P. E. 2012. Role of catecholate siderophores in gram-negative bacterial colonization of the mouse gut. *PLoS One,* 7**,** e50020.

PIDDOCK, L. J. 2006. Clinically relevant chromosomally encoded multidrug resistance efflux pumps in bacteria. *Clin Microbiol Rev,* 19**,** 382-402.

PIDDOCK, L. J., JIN, Y. F., RICCI, V. & ASUQUO, A. E. 1999. Quinolone accumulation by *Pseudomonas aeruginosa, Staphylococcus aureus* and *Escherichia coli*. *J Antimicrob Chemother,* 43**,** 61-70.

PIDDOCK, L. J., WHITE, D. G., GENSBERG, K., PUMBWE, L. & GRIGGS, D. J. 2000. Evidence for an efflux pump mediating multiple antibiotic resistance in *Salmonella enterica* serovar Typhimurium. *Antimicrob Agents Chemother,* 44**,** 3118-21.

PIIR, K., PAIER, A., LIIV, A., TENSON, T. & MAIVALI, U. 2011. Ribosome degradation in growing bacteria. *EMBO Rep,* 12**,** 458-62.

PISABARRO, A. G., DE PEDRO, M. A. & VAZQUEZ, D. 1985. Structural modifications in the peptidoglycan of *Escherichia coli* associated with changes in the state of growth of the culture. *J Bacteriol,* 161**,** 238-42.

PLUMBRIDGE, J. 2002. Regulation of gene expression in the PTS in *Escherichia coli*: the role and interactions of Mlc. *Curr Opin Microbiol,* 5**,** 187-93.

PONTEL, L. B., AUDERO, M. E., ESPARIZ, M., CHECA, S. K. & SONCINI, F. C. 2007. GolS controls the response to gold by the hierarchical induction of *Salmonella*-specific genes that include a CBA efflux-coding operon. *Mol Microbiol,* 66**,** 814-25.

PRATT, L. A., HSING, W., GIBSON, K. E. & SILHAVY, T. J. 1996. From acids to osmZ: multiple factors influence synthesis of the OmpF and OmpC porins in *Escherichia coli*. *Mol Microbiol,* 20**,** 911-7.

PRICE-CARTER, M., TINGEY, J., BOBIK, T. A. & ROTH, J. R. 2001. The alternative electron acceptor tetrathionate supports B12-dependent anaerobic growth of *Salmonella enterica* serovar typhimurium on ethanolamine or 1,2-propanediol. *J Bacteriol,* 183**,** 2463-75.

PROUTY, A. M., BRODSKY, I. E., MANOS, J., BELAS, R., FALKOW, S. & GUNN, J. S. 2004. Transcriptional regulation of *Salmonella enterica* serovar Typhimurium genes by bile. *FEMS Immunol Med Microbiol,* 41**,** 177-85.

PURVIS, J. E., YOMANO, L. P. & INGRAM, L. O. 2005. Enhanced trehalose production improves growth of *Escherichia coli* under osmotic stress. *Appl Environ Microbiol,* 71**,** 3761-9.

QI, Y., LIU, H., CHEN, X. & LIU, L. 2019. Engineering microbial membranes to increase stress tolerance of industrial strains. *Metab Eng,* 53**,** 24-34.

RAETZ, C. R., REYNOLDS, C. M., TRENT, M. S. & BISHOP, R. E. 2007. Lipid A modification systems in gram-negative bacteria. *Annu Rev Biochem,* 76**,** 295-329.

RAMI, A., TOUTAIN, C. M. & JACQ, A. 2005. An increased level of alternative sigma factor RpoS partially suppresses drug hypersensitivity associated with inactivation of the multidrug resistance pump AcrAB in *Escherichia coli*. *Res Microbiol,* 156**,** 356-60.

RAMOS, J. L., MARTINEZ-BUENO, M., MOLINA-HENARES, A. J., TERAN, W., WATANABE, K., ZHANG, X., GALLEGOS, M. T., BRENNAN, R. & TOBES, R. 2005. The TetR family of transcriptional repressors. *Microbiol Mol Biol Rev,* 69**,** 326-56.

RAND, J. D., DANBY, S. G., GREENWAY, D. L. & ENGLAND, R. R. 2002. Increased expression of the multidrug efflux genes *acrAB* occurs during slow growth of *Escherichia coli*. *FEMS Microbiol Lett,* 207**,** 91-5.

REEVE, C. A., BOCKMAN, A. T. & MATIN, A. 1984. Role of protein degradation in the survival of carbon-starved *Escherichia coli* and *Salmonella typhimurium*. *J Bacteriol,* 157**,** 758-63.

REEVES, M. W., EVINS, G. M., HEIBA, A. A., PLIKAYTIS, B. D. & FARMER, J. J., 3RD 1989. Clonal nature of *Salmonella typhi* and its genetic relatedness to other salmonellae as shown by multilocus enzyme electrophoresis, and proposal of *Salmonella bongori* comb. nov. *J Clin Microbiol,* 27**,** 313-20.

RENAU, T. E., LEGER, R., FLAMME, E. M., SANGALANG, J., SHE, M. W., YEN, R., GANNON, C. L., GRIFFITH, D., CHAMBERLAND, S., LOMOVSKAYA, O., HECKER, S. J., LEE, V. J., OHTA, T. & NAKAYAMA, K. 1999. Inhibitors of efflux pumps in *Pseudomonas aeruginosa* potentiate the activity of the fluoroquinolone antibacterial levofloxacin. *J Med Chem,* 42**,** 4928-31.

RHEE, S., MARTIN, R. G., ROSNER, J. L. & DAVIES, D. R. 1998. A novel DNA-binding motif in MarA: the first structure for an AraC family transcriptional activator. *Proc Natl Acad Sci U S A,* 95**,** 10413-8.

RICCI, V., ATTAH, V., OVERTON, T., GRAINGER, D. C. & PIDDOCK, L. J. V. 2017. CsrA maximizes expression of the AcrAB multidrug resistance transporter. *Nucleic Acids Res,* 45**,** 12798-12807.

RICCI, V., BLAIR, J. M. & PIDDOCK, L. J. 2014. RamA, which controls expression of the MDR efflux pump AcrAB-TolC, is regulated by the Lon protease. *J Antimicrob Chemother,* 69**,** 643-50.

RICCI, V. & PIDDOCK, L. J. 2009. Ciprofloxacin selects for multidrug resistance in *Salmonella enterica* serovar Typhimurium mediated by at least two different pathways. *J Antimicrob Chemother,* 63**,** 909-16.

RICHMOND, G. E., CHUA, K. L. & PIDDOCK, L. J. 2013. Efflux in *Acinetobacter baumannii* can be determined by measuring accumulation of H33342 (bis-benzamide). *J Antimicrob Chemother,* 68**,** 1594-600.

RILEY, E. E., DAS, D. & LAUGA, E. 2018. Swimming of peritrichous bacteria is enabled by an elastohydrodynamic instability. *Sci Rep,* 8**,** 10728.

ROCARD, J. M., ASADISHAD, B., SAMONTE, P. R. V., GHOSHAL, S. & TUFENKJI, N. 2018. Natural freeze-thaw cycles may increase the risk associated with *Salmonella* contamination in surface and groundwater environments. *Water Res X,* 1**,** 100005.

RODRIGUES, L., RAMOS, J., COUTO, I., AMARAL, L. & VIVEIROS, M. 2011. Ethidium bromide transport across *Mycobacterium smegmatis* cell-wall: correlation with antibiotic resistance. *BMC Microbiol,* 11**,** 35.

RODRIGUEZ-MORALES, O., FERNANDEZ-MORA, M., HERNANDEZ-LUCAS, I., VAZQUEZ, A., PUENTE, J. L. & CALVA, E. 2006. *Salmonella enterica* serovar Typhimurium ompS1 and ompS2 mutants are attenuated for virulence in mice. *Infect Immun,* 74**,** 1398-402.

ROLFE, M. D., RICE, C. J., LUCCHINI, S., PIN, C., THOMPSON, A., CAMERON, A. D., ALSTON, M., STRINGER, M. F., BETTS, R. P., BARANYI, J., PECK, M. W. & HINTON, J. C. 2012. Lag phase is a distinct growth phase that prepares bacteria for exponential growth and involves transient metal accumulation. *J Bacteriol,* 194**,** 686-701.

ROMEO, T. & PREISS, J. 1989. Genetic regulation of glycogen biosynthesis in *Escherichia coli*: in vitro effects of cyclic AMP and guanosine 5'-diphosphate 3'-diphosphate and analysis of in vivo transcripts. *J Bacteriol,* 171**,** 2773-82.

ROSENBERG, E. Y., BERTENTHAL, D., NILLES, M. L., BERTRAND, K. P. & NIKAIDO, H. 2003. Bile salts and fatty acids induce the expression of *Escherichia coli* AcrAB multidrug efflux pump through their interaction with Rob regulatory protein. *Mol Microbiol,* 48**,** 1609-19.

ROTTENBERG, H. & STEINER-MORDOCH, S. 1986. Free fatty acids decouple oxidative phosphorylation by dissipating intramembranal protons without inhibiting ATP synthesis driven by the proton electrochemical gradient. *FEBS Lett,* 202**,** 314-8.

RUDKIN, J. K., EDWARDS, A. M., BOWDEN, M. G., BROWN, E. L., POZZI, C., WATERS, E. M., CHAN, W. C., WILLIAMS, P., O'GARA, J. P. & MASSEY, R. C. 2012. Methicillin resistance reduces the virulence of healthcare-associated methicillin-resistant *Staphylococcus aureus* by interfering with the *agr* quorum sensing system. *J Infect Dis,* 205**,** 798-806.

RUIZ, C. & LEVY, S. B. 2014. Regulation of acrAB expression by cellular metabolites in Escherichia coli. *J Antimicrob Chemother,* 69**,** 390-9.

RUIZ, N., GRONENBERG, L. S., KAHNE, D. & SILHAVY, T. J. 2008. Identification of two inner-membrane proteins required for the transport of lipopolysaccharide to the outer membrane of *Escherichia coli*. *Proc Natl Acad Sci U S A,* 105**,** 5537-42.

RUMBO, C., GATO, E., LOPEZ, M., RUIZ DE ALEGRIA, C., FERNANDEZ-CUENCA, F., MARTINEZ-MARTINEZ, L., VILA, J., PACHON, J., CISNEROS, J. M., RODRIGUEZ-BANO, J., PASCUAL, A., BOU, G., TOMAS, M., SPANISH GROUP OF NOSOCOMIAL, I., MECHANISMS OF, A., RESISTANCE TO, A., SPANISH SOCIETY OF CLINICAL, M., INFECTIOUS, D. & SPANISH NETWORK FOR RESEARCH IN INFECTIOUS, D. 2013. Contribution of efflux pumps, porins, and beta-lactamases to multidrug resistance in clinical isolates of *Acinetobacter baumannii*. *Antimicrob Agents Chemother,* 57**,** 5247-57.

RUZIN, A., VISALLI, M. A., KEENEY, D. & BRADFORD, P. A. 2005. Influence of transcriptional activator RamA on expression of multidrug efflux pump AcrAB and tigecycline susceptibility in *Klebsiella pneumoniae*. *Antimicrob Agents Chemother,* 49**,** 1017-22.

RYAN, M. P., O'DWYER, J. & ADLEY, C. C. 2017. Evaluation of the Complex Nomenclature of the Clinically and Veterinary Significant Pathogen *Salmonella*. *Biomed Res Int,* 2017**,** 3782182.

SABETI AZAD, M., OKUDA, M., CYRENNE, M., BOURGE, M., HECK, M. P., YOSHIZAWA, S. & FOURMY, D. 2020. Fluorescent Aminoglycoside Antibiotics and Methods for Accurately Monitoring Uptake by Bacteria. *ACS Infect Dis,* 6**,** 1008-1017.

SABNIS, A., KLÖCKNER, A., BECCE, M., HAGART, K. L. H., EVANS, L. E., FURNISS, R. C. D., MAVRIDOU, D. A. I., LARROUY-MAUMUS, G. J.,

STEVENS, M. M. & EDWARDS, A. M. 2020. Colistin kills bacteria by targeting lipopolysaccharide in the cytoplasmic membrane. *bioRxiv*, 479618.

SAHA, P., XIAO, X., YEOH, B. S., CHEN, Q., KATKERE, B., KIRIMANJESWARA, G. S. & VIJAY-KUMAR, M. 2019. The bacterial siderophore enterobactin confers survival advantage to *Salmonella* in macrophages. *Gut Microbes,* 10, 412-423.

SALMONELLA SUBCOMMITTEE OF THE NOMENCLATURE COMMITTEE OF THE INTERNATIONAL SOCIETY FOR, M. 1934. The Genus *Salmonella* Lignieres, 1900. *J Hyg (Lond),* 34, 333-50.

SAMUDRALA, R., HEFFRON, F. & MCDERMOTT, J. E. 2009. Accurate prediction of secreted substrates and identification of a conserved putative secretion signal for type III secretion systems. *PLoS Pathog,* 5, e1000375.

SANCHEZ-ROMERO, M. A. & CASADESUS, J. 2014. Contribution of phenotypic heterogeneity to adaptive antibiotic resistance. *Proc Natl Acad Sci U S A,* 111, 355-60.

SANCHEZ-VAZQUEZ, P., DEWEY, C. N., KITTEN, N., ROSS, W. & GOURSE, R. L. 2019. Genome-wide effects on *Escherichia coli* transcription from ppGpp binding to its two sites on RNA polymerase. *Proc Natl Acad Sci U S A,* 116, 8310-8319.

SANTIVIAGO, C. A., FUENTES, J. A., BUENO, S. M., TROMBERT, A. N., HILDAGO, A. A., SOCIAS, L. T., YOUDERIAN, P. & MORA, G. C. 2002. The *Salmonella enterica* sv. Typhimurium *smvA*, *yddG* and *ompD* (porin) genes are required for the efficient efflux of methyl viologen. *Mol Microbiol,* 46, 687-98.

SANTIVIAGO, C. A., TORO, C. S., HIDALGO, A. A., YOUDERIAN, P. & MORA, G. C. 2003. Global regulation of the *Salmonella enterica* serovar typhimurium major porin, OmpD. *J Bacteriol,* 185, 5901-5.

SANTOS, J. M., FREIRE, P., VICENTE, M. & ARRAIANO, C. M. 1999. The stationary-phase morphogene *bolA* from *Escherichia coli* is induced by stress during early stages of growth. *Mol Microbiol,* 32, 789-98.

SANTOS, J. M., LOBO, M., MATOS, A. P., DE PEDRO, M. A. & ARRAIANO, C. M. 2002. The gene *bolA* regulates *dacA* (PBP5), *dacC* (PBP6) and *ampC* (AmpC), promoting normal morphology in *Escherichia coli*. *Mol Microbiol,* 45, 1729-40.

SATO, Y., TAKAYA, A. & YAMAMOTO, T. 2011. Meta-analytic approach to the accurate prediction of secreted virulence effectors in gram-negative bacteria. *BMC Bioinformatics,* 12, 442.

SCHNEIDERS, T., AMYES, S. G. & LEVY, S. B. 2003. Role of AcrR and *ramA* in fluoroquinolone resistance in clinical *Klebsiella pneumoniae* isolates from Singapore. *Antimicrob Agents Chemother,* 47, 2831-7.

SENIOR, K. 2000. FDA approves first drug in new class of antibiotics. *Lancet,* 355, 1523.

SEOANE, A. S. & LEVY, S. B. 1995. Characterization of MarR, the repressor of the multiple antibiotic resistance (mar) operon in Escherichia coli. *J Bacteriol,* 177**,** 3414-9.

SEYFZADEH, M., KEENER, J. & NOMURA, M. 1993. *spoT*-dependent accumulation of guanosine tetraphosphate in response to fatty acid starvation in *Escherichia coli*. *Proc Natl Acad Sci U S A,* 90**,** 11004-8.

SHAFA, F. & SALTON, M. R. 1960. Disaggregation of bacterial cell walls by anionic detergents. *J Gen Microbiol,* 23**,** 137-41.

SHARMA, A., GUPTA, V. K. & PATHANIA, R. 2019. Efflux pump inhibitors for bacterial pathogens: From bench to bedside. *Indian J Med Res,* 149**,** 129-145.

SHARMA, P., HAYCOCKS, J. R. J., MIDDLEMISS, A. D., KETTLES, R. A., SELLARS, L. E., RICCI, V., PIDDOCK, L. J. V. & GRAINGER, D. C. 2017. The multiple antibiotic resistance operon of enteric bacteria controls DNA repair and outer membrane integrity. *Nat Commun,* 8**,** 1444.

SHI, X., CHEN, M., YU, Z., BELL, J. M., WANG, H., FORRESTER, I., VILLARREAL, H., JAKANA, J., DU, D., LUISI, B. F., LUDTKE, S. J. & WANG, Z. 2019. In situ structure and assembly of the multidrug efflux pump AcrAB-TolC. *Nat Commun,* 10**,** 2635.

SHU-KEE ENG, P. P., NURUL-SYAKIMA AB MUTALIB, HOOI- LENG SER, KOK-GAN CHAN & LEARN-HAN LEE 2015. *Salmonella*: A review on pathogenesis, epidemiology and antibiotic resistance. *Frontiers in Life Science,* 8**,** 284-293.

SILHAVY, T. J., KAHNE, D. & WALKER, S. 2010. The bacterial cell envelope. *Cold Spring Harb Perspect Biol,* 2**,** a000414.

SILVA, I. J., BARAHONA, S., EYRAUD, A., LALAOUNA, D., FIGUEROA-BOSSI, N., MASSE, E. & ARRAIANO, C. M. 2019. SraL sRNA interaction regulates the terminator by preventing premature transcription termination of rho mRNA. *Proc Natl Acad Sci U S A,* 116**,** 3042-3051.

SILVA, I. J., ORTEGA, A. D., VIEGAS, S. C., GARCIA-DEL PORTILLO, F. & ARRAIANO, C. M. 2013. An RpoS-dependent sRNA regulates the expression of a chaperone involved in protein folding. *RNA,* 19**,** 1253-65.

SIMPSON, B. W. & TRENT, M. S. 2019. Pushing the envelope: LPS modifications and their consequences. *Nat Rev Microbiol,* 17**,** 403-416.

SINGH, R., SMITHA, M. S. & SINGH, S. P. 2014. The role of nanotechnology in combating multi-drug resistant bacteria. *J Nanosci Nanotechnol,* 14**,** 4745-56.

SINGH, S. K., SAISREE, L., AMRUTHA, R. N. & REDDY, M. 2012. Three redundant murein endopeptidases catalyse an essential cleavage step in peptidoglycan synthesis of *Escherichia coli* K12. *Mol Microbiol,* 86**,** 1036-51.

SITTKA, A., PFEIFFER, V., TEDIN, K. & VOGEL, J. 2007. The RNA chaperone Hfq is essential for the virulence of *Salmonella typhimurium*. *Mol Microbiol,* 63**,** 193-217.

SMITH, H. 1998. What happens to bacterial pathogens in vivo? *Trends Microbiol,* 6**,** 239-43.

SMITH, H. E. & BLAIR, J. M. 2014. Redundancy in the periplasmic adaptor proteins AcrA and AcrE provides resilience and an ability to export substrates of multidrug efflux. *J Antimicrob Chemother,* 69**,** 982-7.

SOARES, C. M., BJORKSTEN, J. & TAPIA, O. 1995. L3 loop-mediated mechanisms of pore closing in porin: a molecular dynamics perturbation approach. *Protein Eng,* 8**,** 5-12.

SONG, S., LEE, B., YEOM, J. H., HWANG, S., KANG, I., CHO, J. C., HA, N. C., BAE, J., LEE, K. & KIM, Y. H. 2015. MdsABC-Mediated Pathway for Pathogenicity in *Salmonella enterica* Serovar Typhimurium. *Infect Immun,* 83**,** 4266-76.

SOON, R. L., NATION, R. L., COCKRAM, S., MOFFATT, J. H., HARPER, M., ADLER, B., BOYCE, J. D., LARSON, I. & LI, J. 2011a. Different surface charge of colistin-susceptible and -resistant *Acinetobacter baumannii* cells measured with zeta potential as a function of growth phase and colistin treatment. *J Antimicrob Chemother,* 66**,** 126-33.

SOON, R. L., NATION, R. L., HARPER, M., ADLER, B., BOYCE, J. D., TAN, C. H., LI, J. & LARSON, I. 2011b. Effect of colistin exposure and growth phase on the surface properties of live *Acinetobacter baumannii* cells examined by atomic force microscopy. *Int J Antimicrob Agents,* 38**,** 493-501.

SPIRA, B., SILBERSTEIN, N. & YAGIL, E. 1995. Guanosine 3',5'-bispyrophosphate (ppGpp) synthesis in cells of *Escherichia coli* starved for Pi. *J Bacteriol,* 177**,** 4053-8.

STOCK, J. B., RAUCH, B. & ROSEMAN, S. 1977. Periplasmic space in *Salmonella typhimurium* and *Escherichia coli*. *J Biol Chem,* 252**,** 7850-61.

STONE, M. R. L., PHETSANG, W., COOPER, M. A. & BLASKOVICH, M. A. T. 2020. Visualization of Bacterial Resistance using Fluorescent Antibiotic Probes. *J Vis Exp*.

SUTTERLIN, H. A., SHI, H., MAY, K. L., MIGUEL, A., KHARE, S., HUANG, K. C. & SILHAVY, T. J. 2016. Disruption of lipid homeostasis in the Gram-negative cell envelope activates a novel cell death pathway. *Proc Natl Acad Sci U S A,* 113**,** E1565-74.

SUZUKI, H., NISHIMURA, Y., YASUDA, S., NISHIMURA, A., YAMADA, M. & HIROTA, Y. 1978. Murein-lipoprotein of *Escherichia coli*: a protein involved in the stabilization of bacterial cell envelope. *Mol Gen Genet,* 167**,** 1-9.

SWICK, M. C., MORGAN-LINNELL, S. K., CARLSON, K. M. & ZECHIEDRICH, L. 2011. Expression of multidrug efflux pump genes *acrAB-tolC, mdfA*, and *norE* in *Escherichia coli* clinical isolates as a function of fluoroquinolone and multidrug resistance. *Antimicrob Agents Chemother,* 55**,** 921-4.

SYMMONS, M. F., BOKMA, E., KORONAKIS, E., HUGHES, C. & KORONAKIS, V. 2009. The assembled structure of a complete tripartite bacterial multidrug efflux pump. *Proc Natl Acad Sci U S A,* 106**,** 7173-8.

TAKATSUKA, Y. & NIKAIDO, H. 2009. Covalently linked trimer of the AcrB multidrug efflux pump provides support for the functional rotating mechanism. *J Bacteriol,* 191**,** 1729-37.

TANI, T. H., KHODURSKY, A., BLUMENTHAL, R. M., BROWN, P. O. & MATTHEWS, R. G. 2002. Adaptation to famine: a family of stationary-phase genes revealed by microarray analysis. *Proc Natl Acad Sci U S A,* 99**,** 13471-6.

TEGOS, G. P., HAYNES, M., STROUSE, J. J., KHAN, M. M., BOLOGA, C. G., OPREA, T. I. & SKLAR, L. A. 2011. Microbial efflux pump inhibition: tactics and strategies. *Curr Pharm Des,* 17**,** 1291-302.

TELENTI, A., IMBODEN, P., MARCHESI, F., LOWRIE, D., COLE, S., COLSTON, M. J., MATTER, L., SCHOPFER, K. & BODMER, T. 1993. Detection of rifampicin-resistance mutations in *Mycobacterium tuberculosis*. *Lancet,* 341**,** 647-50.

THIENNIMITR, P., WINTER, S. E., WINTER, M. G., XAVIER, M. N., TOLSTIKOV, V., HUSEBY, D. L., STERZENBACH, T., TSOLIS, R. M., ROTH, J. R. & BAUMLER, A. J. 2011. Intestinal inflammation allows *Salmonella* to use ethanolamine to compete with the microbiota. *Proc Natl Acad Sci U S A,* 108**,** 17480-5.

TIAN, H., SIX, D. A., KRUCKER, T., LEEDS, J. A. & WINOGRAD, N. 2017. Subcellular Chemical Imaging of Antibiotics in Single Bacteria Using C60-Secondary Ion Mass Spectrometry. *Anal Chem,* 89**,** 5050-5057.

TIPPER, D. J. & STROMINGER, J. L. 1965. Mechanism of action of penicillins: a proposal based on their structural similarity to acyl-D-alanyl-D-alanine. *Proc Natl Acad Sci U S A,* 54**,** 1133-41.

TRAXLER, M. F., SUMMERS, S. M., NGUYEN, H. T., ZACHARIA, V. M., HIGHTOWER, G. A., SMITH, J. T. & CONWAY, T. 2008. The global, ppGpp-mediated stringent response to amino acid starvation in *Escherichia coli*. *Mol Microbiol,* 68**,** 1128-48.

TRIVEDI, R. R., CROOKS, J. A., AUER, G. K., PENDRY, J., FOIK, I. P., SIRYAPORN, A., ABBOTT, N. L., GITAI, Z. & WEIBEL, D. B. 2018. Mechanical Genomic Studies Reveal the Role of d-Alanine Metabolism in *Pseudomonas aeruginosa* Cell Stiffness. *mBio,* 9.

TURLIN, E., HEUCK, G., SIMOES BRANDAO, M. I., SZILI, N., MELLIN, J. R., LANGE, N. & WANDERSMAN, C. 2014. Protoporphyrin (PPIX) efflux by the MacAB-TolC pump in *Escherichia coli*. *Microbiologyopen,* 3**,** 849-59.

TURNBULL, K. J., DZHYGYR, I., LINDEMOSE, S., HAURYLIUK, V. & ROGHANIAN, M. 2019. Intramolecular Interactions Dominate the Autoregulation of *Escherichia coli* Stringent Factor RelA. *Front Microbiol,* 10**,** 1966.

TYAGI, D., KRAFT, A. L., LEVADNEY SMITH, S., ROOF, S. E., SHERWOOD, J. S., WIEDMANN, M. & BERGHOLZ, T. M. 2019. Pre-Harvest Survival and Post-Harvest Chlorine Tolerance of Enterohemorrhagic *Escherichia coli* on Lettuce. *Toxins (Basel),* 11.

UEHARA, T., PARZYCH, K. R., DINH, T. & BERNHARDT, T. G. 2010. Daughter cell separation is controlled by cytokinetic ring-activated cell wall hydrolysis. *EMBO J,* 29**,** 1412-22.

UETA, M., YOSHIDA, H., WADA, C., BABA, T., MORI, H. & WADA, A. 2005. Ribosome binding proteins YhbH and YfiA have opposite functions during 100S formation in the stationary phase of *Escherichia coli*. *Genes Cells,* 10**,** 1103-12.

URDANETA, V. & CASADESUS, J. 2018. Adaptation of *Salmonella enterica* to bile: essential role of AcrAB-mediated efflux. *Environ Microbiol,* 20**,** 1405-1418.

VAARA, M., VAARA, T., JENSEN, M., HELANDER, I., NURMINEN, M., RIETSCHEL, E. T. & MAKELA, P. H. 1981. Characterization of the lipopolysaccharide from the polymyxin-resistant *pmrA* mutants of *Salmonella typhimurium*. *FEBS Lett,* 129**,** 145-9.

VAN DER STRAATEN, T., JANSSEN, R., MEVIUS, D. J. & VAN DISSEL, J. T. 2004. Salmonella gene *rma* (*ramA*) and multiple-drug-resistant *Salmonella enterica* serovar typhimurium. *Antimicrob Agents Chemother,* 48**,** 2292-4.

VAN MELDEREN, L. & AERTSEN, A. 2009. Regulation and quality control by Lon-dependent proteolysis. *Res Microbiol,* 160**,** 645-51.

VASTERMARK, A. & SAIER, M. H., JR. 2014. The involvement of transport proteins in transcriptional and metabolic regulation. *Curr Opin Microbiol,* 18**,** 8-15.

VIEIRA, H. L., FREIRE, P. & ARRAIANO, C. M. 2004. Effect of *Escherichia coli* morphogene *bolA* on biofilms. *Appl Environ Microbiol,* 70**,** 5682-4.

VIRLOGEUX-PAYANT, I., BAUCHERON, S., PELET, J., TROTEREAU, J., BOTTREAU, E., VELGE, P. & CLOECKAERT, A. 2008. TolC, but not AcrB, is involved in the invasiveness of multidrug-resistant *Salmonella enterica* serovar Typhimurium by increasing type III secretion system-1 expression. *Int J Med Microbiol,* 298**,** 561-9.

VIVEIROS, M., MARTINS, A., PAIXAO, L., RODRIGUES, L., MARTINS, M., COUTO, I., FAHNRICH, E., KERN, W. V. & AMARAL, L. 2008. Demonstration of intrinsic efflux activity of *Escherichia coli* K-12 AG100 by an automated ethidium bromide method. *Int J Antimicrob Agents,* 31**,** 458-62.

VOGEL, J. & LUISI, B. F. 2011. Hfq and its constellation of RNA. *Nat Rev Microbiol,* 9**,** 578-89.

VOLLMER, W., BLANOT, D. & DE PEDRO, M. A. 2008. Peptidoglycan structure and architecture. *FEMS Microbiol Rev,* 32**,** 149-67.

WADA, A., IGARASHI, K., YOSHIMURA, S., AIMOTO, S. & ISHIHAMA, A. 1995. Ribosome modulation factor: stationary growth phase-specific inhibitor of ribosome functions from *Escherichia coli*. *Biochem Biophys Res Commun,* 214**,** 410-7.

WADA, A., MIKKOLA, R., KURLAND, C. G. & ISHIHAMA, A. 2000. Growth phase-coupled changes of the ribosome profile in natural isolates and laboratory strains of *Escherichia coli*. *J Bacteriol,* 182**,** 2893-9.

WANG, A. Y. & CRONAN, J. E., JR. 1994. The growth phase-dependent synthesis of cyclopropane fatty acids in *Escherichia coli* is the result of an RpoS(KatF)-dependent promoter plus enzyme instability. *Mol Microbiol,* 11**,** 1009-17.

WANG, A. Y., GROGAN, D. W. & CRONAN, J. E., JR. 1992. Cyclopropane fatty acid synthase of *Escherichia coli*: deduced amino acid sequence, purification, and studies of the enzyme active site. *Biochemistry,* 31**,** 11020-8.

WANG, X., BISWAS, S., PAUDYAL, N., PAN, H., LI, X., FANG, W. & YUE, M. 2019. Antibiotic Resistance in *Salmonella* Typhimurium Isolates Recovered From the Food Chain Through National Antimicrobial Resistance Monitoring System Between 1996 and 2016. *Front Microbiol,* 10**,** 985.

WANG-KAN, X., BLAIR, J. M. A., CHIRULLO, B., BETTS, J., LA RAGIONE, R. M., IVENS, A., RICCI, V., OPPERMAN, T. J. & PIDDOCK, L. J. V. 2017. Lack of AcrB Efflux Function Confers Loss of Virulence on *Salmonella enterica* Serovar Typhimurium. *MBio,* 8.

WEAVER, A. I., JIMENEZ-RUIZ, V., TALLAVAJHALA, S. R., RANSEGNOLA, B. P., WONG, K. Q. & DORR, T. 2019. Lytic transglycosylases RlpA and MltC assist in *Vibrio cholerae* daughter cell separation. *Mol Microbiol,* 112**,** 1100-1115.

WEBBER, M. A., BAILEY, A. M., BLAIR, J. M., MORGAN, E., STEVENS, M. P., HINTON, J. C., IVENS, A., WAIN, J. & PIDDOCK, L. J. 2009. The global consequence of disruption of the AcrAB-TolC efflux pump in *Salmonella enterica* includes reduced expression of SPI-1 and other attributes required to infect the host. *J Bacteriol,* 191**,** 4276-85.

WEBBER, M. A., BUCKNER, M. M. C., REDGRAVE, L. S., IFILL, G., MITCHENALL, L. A., WEBB, C., IDDLES, R., MAXWELL, A. & PIDDOCK, L. J. V. 2017. Quinolone-resistant gyrase mutants demonstrate decreased susceptibility to triclosan. *J Antimicrob Chemother,* 72**,** 2755-2763.

WEBBER, M. A. & PIDDOCK, L. J. 2001. Absence of mutations in *marRAB* or *soxRS* in *acrB*-overexpressing fluoroquinolone-resistant clinical and veterinary isolates of *Escherichia coli*. *Antimicrob Agents Chemother,* 45**,** 1550-2.

WEBBER, M. A., TALUKDER, A. & PIDDOCK, L. J. 2005. Contribution of mutation at amino acid 45 of AcrR to *acrB* expression and ciprofloxacin resistance in clinical and veterinary *Escherichia coli* isolates. *Antimicrob Agents Chemother,* 49**,** 4390-2.

WEIGEL, L. M., STEWARD, C. D. & TENOVER, F. C. 1998. *gyrA* mutations associated with fluoroquinolone resistance in eight species of *Enterobacteriaceae*. *Antimicrob Agents Chemother,* 42**,** 2661-7.

WEISS, M. S., WACKER, T., WECKESSER, J., WELTE, W. & SCHULZ, G. E. 1990. The three-dimensional structure of porin from *Rhodobacter capsulatus* at 3 A resolution. *FEBS Lett,* 267**,** 268-72.

WENSINK, J., GILDEN, N. & WITHOLT, B. 1982. Attachment of lipoprotein to the murein of *Escherichia coli*. *Eur J Biochem,* 122**,** 587-90.

WESTON, N., SHARMA, P., RICCI, V. & PIDDOCK, L. J. V. 2018. Regulation of the AcrAB-TolC efflux pump in *Enterobacteriaceae*. *Res Microbiol,* 169**,** 425-431.

WHITE, D. G., GOLDMAN, J. D., DEMPLE, B. & LEVY, S. B. 1997. Role of the *acrAB* locus in organic solvent tolerance mediated by expression of *marA*, *soxS*, or *robA* in *Escherichia coli*. *J Bacteriol,* 179**,** 6122-6.

WHITTLE, E. E., LEGOOD, S. W., ALAV, I., DULYAYANGKUL, P., OVERTON, T. W. & BLAIR, J. M. A. 2019. Flow Cytometric Analysis of Efflux by Dye Accumulation. *Front Microbiol,* 10**,** 2319.

WHO. 2015. *Typhoid* [Online]. Available: http://www.who.int/immunization/diseases/typhoid/en/ [Accessed].

WHO 2017a. GLOBAL PRIORITY LIST OF ANTIBIOTIC-RESISTANT BACTERIA TO GUIDE RESEARCH, DISCOVERY, AND DEVELOPMENT OF NEW ANTIBIOTICS.

WHO 2017b. Prioritization of pathogens to guide discovery, research and development of new antibiotics for drug resistant bacterial infections, including tuberculosis. World Health Organisation.

WILD, J., HENNIG, J., LOBOCKA, M., WALCZAK, W. & KLOPOTOWSKI, T. 1985. Identification of the *dadX* gene coding for the predominant isozyme of alanine racemase in *Escherichia coli* K12. *Mol Gen Genet,* 198**,** 315-22.

WILSON, W. A., ROACH, P. J., MONTERO, M., BAROJA-FERNANDEZ, E., MUNOZ, F. J., EYDALLIN, G., VIALE, A. M. & POZUETA-ROMERO, J. 2010. Regulation of glycogen metabolism in yeast and bacteria. *FEMS Microbiol Rev,* 34**,** 952-85.

WINTER, S. E., THIENNIMITR, P., WINTER, M. G., BUTLER, B. P., HUSEBY, D. L., CRAWFORD, R. W., RUSSELL, J. M., BEVINS, C. L., ADAMS, L. G., TSOLIS, R. M., ROTH, J. R. & BAUMLER, A. J. 2010. Gut inflammation provides a respiratory electron acceptor for *Salmonella*. *Nature,* 467**,** 426-9.

WRAY, C. & SOJKA, W. J. 1978. Experimental *Salmonella typhimurium* infection in calves. *Res Vet Sci,* 25**,** 139-43.

XIAO, H., KALMAN, M., IKEHARA, K., ZEMEL, S., GLASER, G. & CASHEL, M. 1991. Residual guanosine 3',5'-bispyrophosphate synthetic activity of *relA* null mutants can be eliminated by *spoT* null mutations. *J Biol Chem,* 266**,** 5980-90.

XIAO, M., LAI, Y., SUN, J., CHEN, G. & YAN, A. 2016. Transcriptional Regulation of the Outer Membrane Porin Gene *ompW* Reveals its Physiological Role during the Transition from the Aerobic to the Anaerobic Lifestyle of *Escherichia coli*. *Front Microbiol,* 7**,** 799.

XIONG, A., GOTTMAN, A., PARK, C., BAETENS, M., PANDZA, S. & MATIN, A. 2000. The EmrR protein represses the *Escherichia coli emrRAB* multidrug resistance operon by directly binding to its promoter region. *Antimicrob Agents Chemother,* 44**,** 2905-7.

YAMADA, J., YAMASAKI, S., HIRAKAWA, H., HAYASHI-NISHINO, M., YAMAGUCHI, A. & NISHINO, K. 2010. Impact of the RNA chaperone Hfq on multidrug resistance in *Escherichia coli*. *J Antimicrob Chemother,* 65**,** 853-8.

YAMAGISHI, A., NAKANO, S., YAMASAKI, S. & NISHINO, K. 2020. An efflux inhibitor of the MacAB pump in *Salmonella enterica* serovar Typhimurium. *Microbiol Immunol,* 64**,** 182-188.

YAMANAKA, H., KOBAYASHI, H., TAKAHASHI, E. & OKAMOTO, K. 2008. MacAB is involved in the secretion of *Escherichia coli* heat-stable enterotoxin II. *J Bacteriol,* 190**,** 7693-8.

YAMASAKI, S., NAGASAWA, S., HAYASHI-NISHINO, M., YAMAGUCHI, A. & NISHINO, K. 2011. AcrA dependency of the AcrD efflux pump in *Salmonella enterica* serovar Typhimurium. *J Antibiot (Tokyo),* 64**,** 433-7.

YANG, D., JENNINGS, A. D., BORREGO, E., RETTERER, S. T. & MANNIK, J. 2018. Analysis of Factors Limiting Bacterial Growth in PDMS Mother Machine Devices. *Front Microbiol,* 9**,** 871.

YANG, S., LOPEZ, C. R. & ZECHIEDRICH, E. L. 2006. Quorum sensing and multidrug transporters in *Escherichia coli*. *Proc Natl Acad Sci U S A,* 103**,** 2386-91.

YASUFUKU, T., SHIGEMURA, K., SHIRAKAWA, T., MATSUMOTO, M., NAKANO, Y., TANAKA, K., ARAKAWA, S., KINOSHITA, S., KAWABATA, M. & FUJISAWA, M. 2011. Correlation of overexpression of efflux pump genes with antibiotic resistance in *Escherichia coli* Strains clinically isolated from urinary tract infection patients. *J Clin Microbiol,* 49**,** 189-94.

YOCUM, R. R., RASMUSSEN, J. R. & STROMINGER, J. L. 1980. The mechanism of action of penicillin. Penicillin acylates the active site of *Bacillus stearothermophilus* D-alanine carboxypeptidase. *J Biol Chem,* 255**,** 3977-86.

YONG, D., TOLEMAN, M. A., GISKE, C. G., CHO, H. S., SUNDMAN, K., LEE, K. & WALSH, T. R. 2009. Characterization of a new metallo-beta-lactamase gene, *bla*(NDM-1), and a novel erythromycin esterase gene carried on a unique genetic structure in *Klebsiella pneumoniae* sequence type 14 from India. *Antimicrob Agents Chemother,* 53**,** 5046-54.

YOON, E. J., COURVALIN, P. & GRILLOT-COURVALIN, C. 2013. RND-type efflux pumps in multidrug-resistant clinical isolates of *Acinetobacter baumannii*: major role for AdeABC overexpression and AdeRS mutations. *Antimicrob Agents Chemother,* 57**,** 2989-95.

YOSHIDA, H., MAKI, Y., FURUIKE, S., SAKAI, A., UETA, M. & WADA, A. 2012. YqjD is an inner membrane protein associated with stationary-phase ribosomes in *Escherichia coli*. *J Bacteriol,* 194**,** 4178-83.

YOSHIDA, H., MAKI, Y., KATO, H., FUJISAWA, H., IZUTSU, K., WADA, C. & WADA, A. 2002. The ribosome modulation factor (RMF) binding site on the 100S ribosome of *Escherichia coli*. *J Biochem,* 132**,** 983-9.

YOSHIDA, H., WADA, A., SHIMADA, T., MAKI, Y. & ISHIHAMA, A. 2019. Coordinated Regulation of Rsd and RMF for Simultaneous Hibernation of Transcription Apparatus and Translation Machinery in Stationary-Phase *Escherichia coli*. *Front Genet,* 10**,** 1153.

YOSHIDA, T., QIN, L., EGGER, L. A. & INOUYE, M. 2006. Transcription regulation of *ompF* and *ompC* by a single transcription factor, OmpR. *J Biol Chem,* 281**,** 17114-23.

ZAMBRANO, M. M., SIEGELE, D. A., ALMIRON, M., TORMO, A. & KOLTER, R. 1993. Microbial competition: *Escherichia coli* mutants that take over stationary phase cultures. *Science,* 259**,** 1757-60.

ZHANG, Y. L., XIAO, M. F., HORIYAMA, T., ZHANG, Y. F., LI, X. C., NISHINO, K. & YAN, A. X. 2011. The Multidrug Efflux Pump MdtEF Protects against Nitrosative Damage during the Anaerobic Respiration in *Escherichia coli*. *Journal of Biological Chemistry,* 286**,** 26576-26584.

ZIHA-ZARIFI, I., LLANES, C., KOHLER, T., PECHERE, J. C. & PLESIAT, P. 1999. In vivo emergence of multidrug-resistant mutants of *Pseudomonas aeruginosa* overexpressing the active efflux system MexA-MexB-OprM. *Antimicrob Agents Chemother,* 43**,** 287-91.

ZINSER, E. R. & KOLTER, R. 2000. Prolonged stationary-phase incubation selects for lrp mutations in *Escherichia coli* K-12. *J Bacteriol,* 182**,** 4361-5.

ZUPAN, J. R., CAMERON, T. A., ANDERSON-FURGESON, J. & ZAMBRYSKI, P. C. 2013. Dynamic FtsA and FtsZ localization and outer membrane alterations during polar growth and cell division in *Agrobacterium tumefaciens*. *Proc Natl Acad Sci U S A,* 110**,** 9060-5.

Chapter 10 Appendices

Appendix I Representative scatter plot of EtBr accumulation in SL1344 across growth

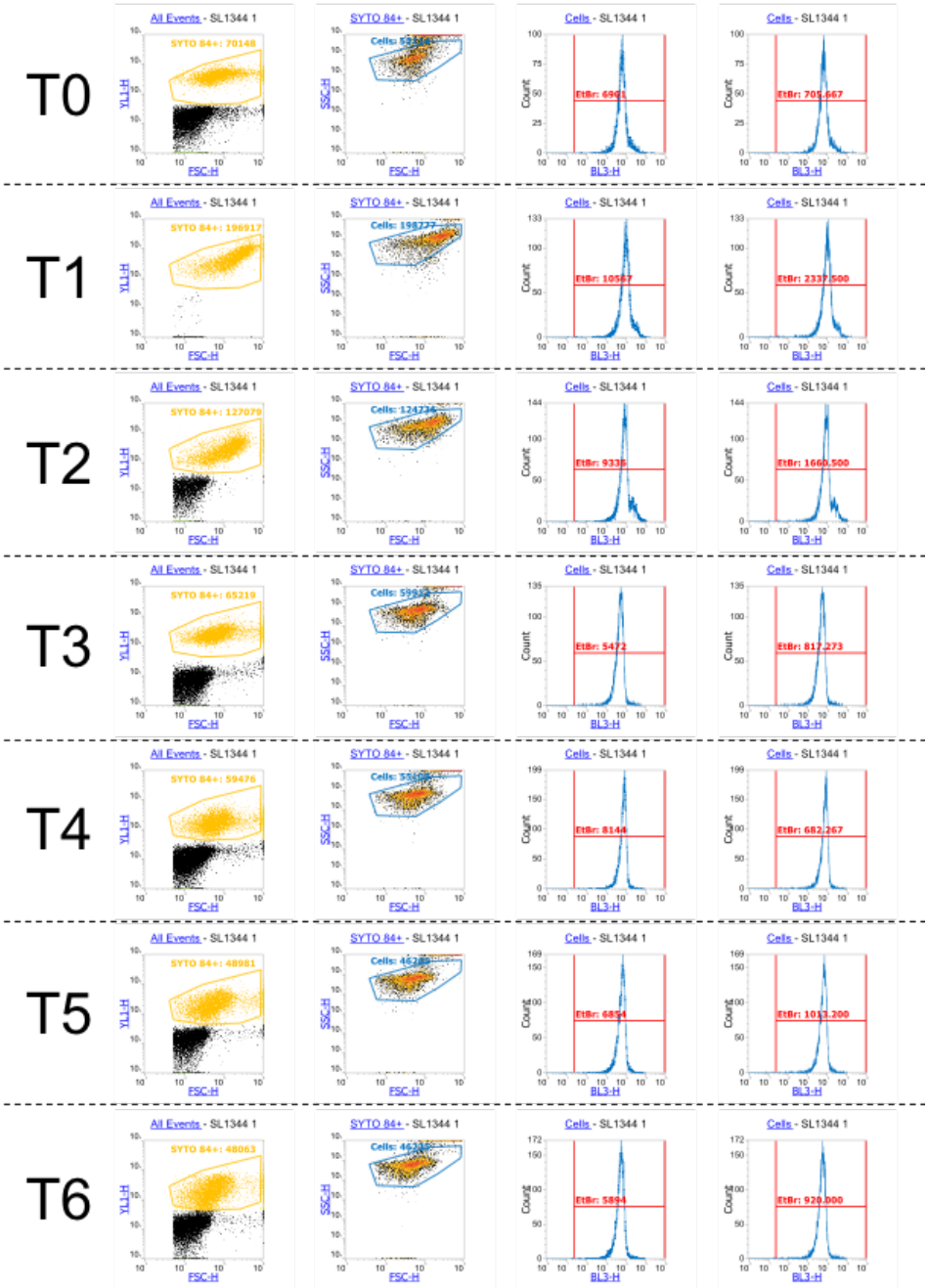

Representative scatter plots of gating and EtBr accumulation in SL1344 over 6 hours of growth. This is one replicate. At each there is initial SYTO-84+ gating, followed by FSC vs SSC gating for a population based on size. EtBr accumulation is plotted on a logarithmic histogram where the X-median is shown in the 3rd across plot and events/μL is shown in each 4th across plot.

Appendix II Representative scatter plot of EtBr accumulation in SL1344 ΔacrB across growth

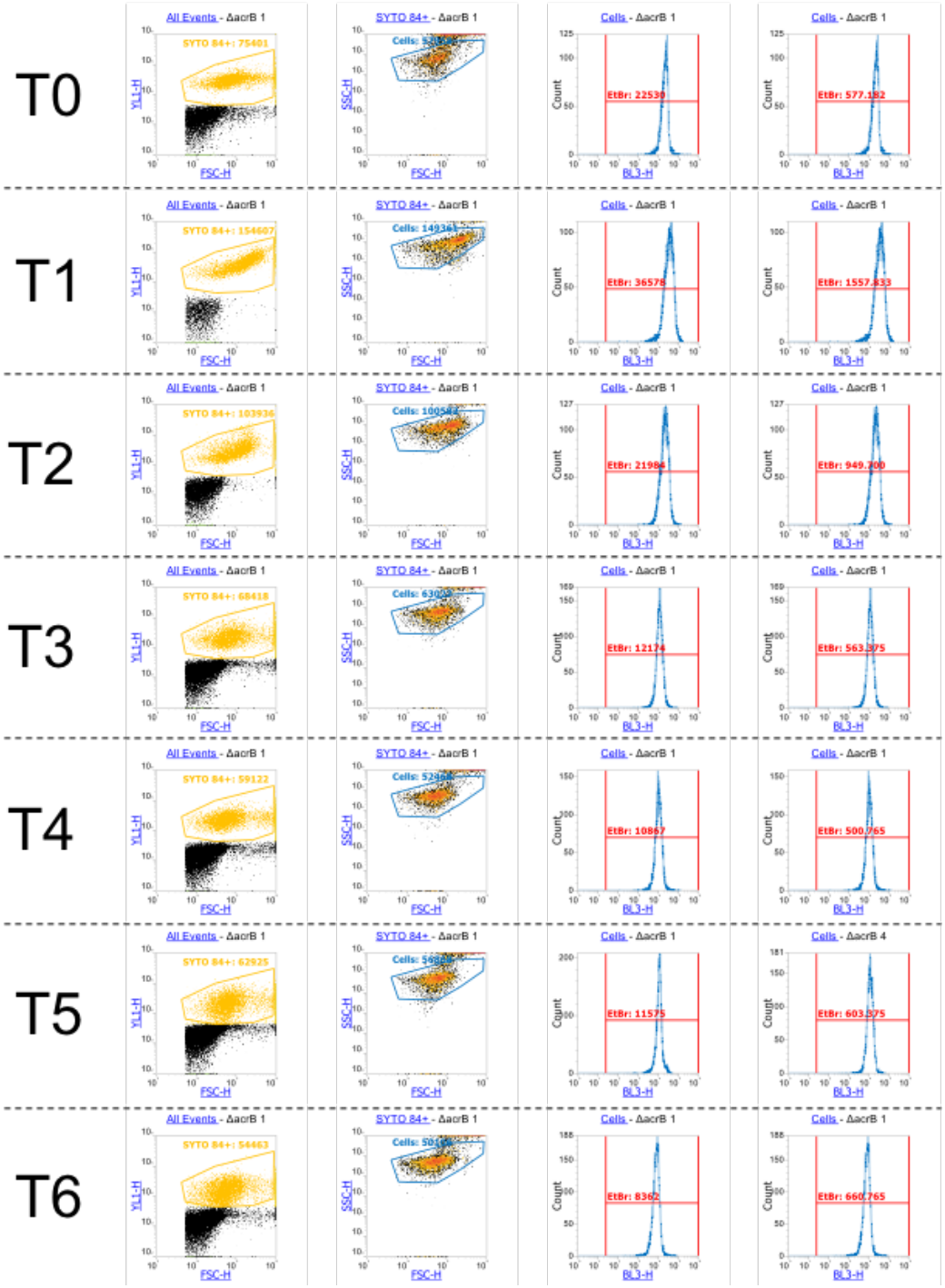

Representative scatter plots of gating and EtBr accumulation in SL1344 Δ*acrB* over 6 hours of growth. This is one replicate. At each there is initial SYTO-84+ gating, followed by FSC vs SSC gating for a population based on size. EtBr accumulation is plotted on a logarithmic histogram where the X-median is shown in the 3rd across plot and events/μL is shown in each 4th across plot.

Appendix III Gene alignment for SL1344 AcrB-GFP

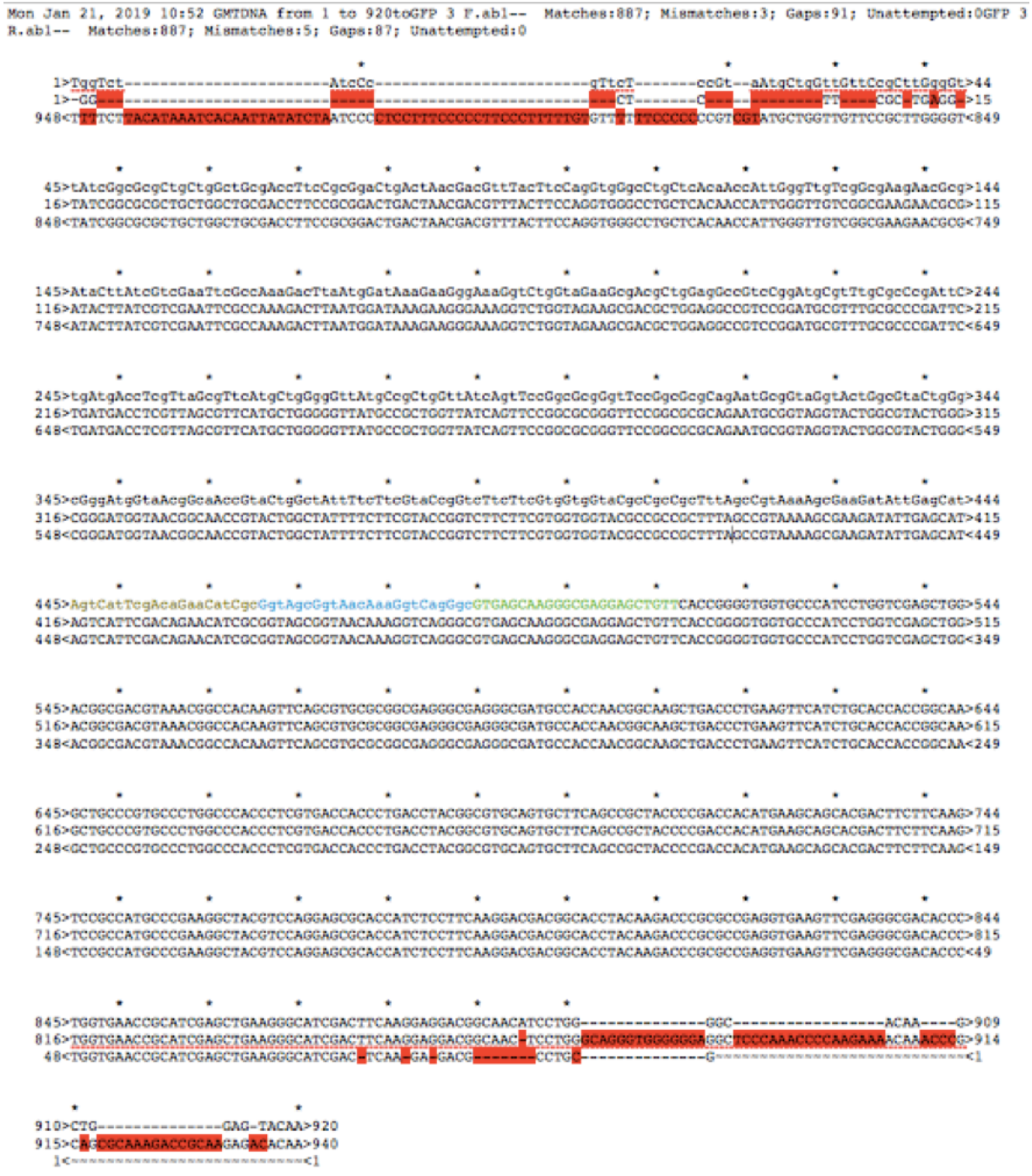

Gene alignment for candidate 3 of SL1344 AcrB-GFP minus the *aph* cassette. The first sequence line represents the expected sequence. Yellow represents AcrB homology, blue represents the poly-linker and green represents GFP. The second line is sequencing results and alignment based on the forward strand. The third line is alignment based on the reverse strand.

Appendix IV Whole population AcrB protein level based on GFP fluorescence

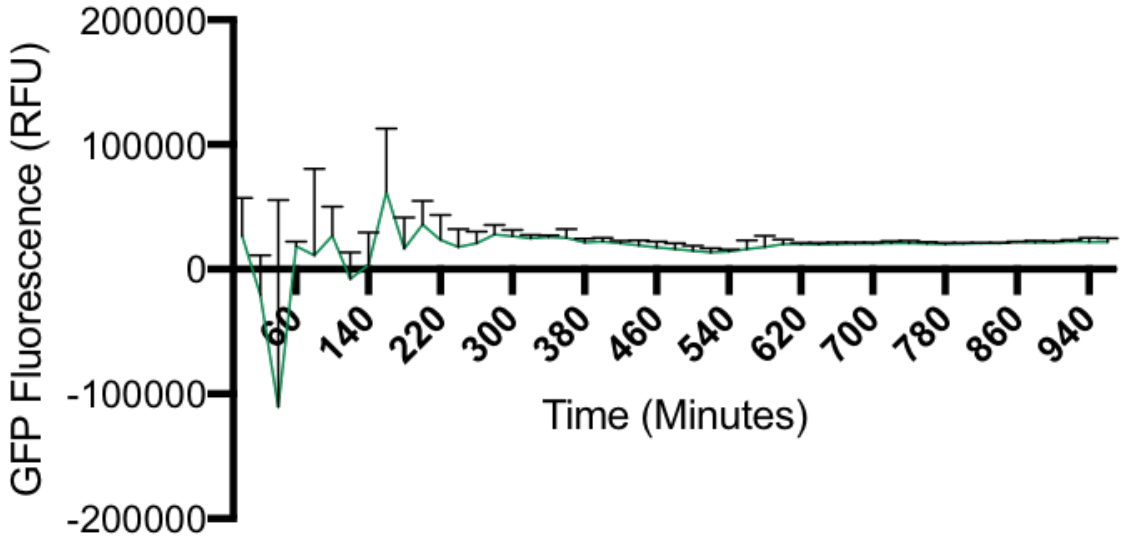

*T*his graph shows GFP fluorescence from AcrB-GFP from 0 hours to 16 hours of growth, measuring OD_{600} and fluorescence intensity every 30 minutes. The Green line shows FI/ OD_{600}. SL1344 autofluorescence was subtracted from this data.

Appendix V Supplementary chapter detailing stationary phase changes identified in the data-described and in previous literature.

Many published studies have explored the role and expression level of particular genes or proteins in stationary phase of various bacterial species but to our knowledge this is the first transcriptomic experiment conducted to specifically study all gene expression changes in stationary phase in *S.* Typhimurium. Therefore, the dataset is compared to known expression changes allowing broader conclusions about stationary phase gene expression to be drawn.

Genes involved in stationary phase regulation correlate to previous literature

It is well known that entrance into stationary is controlled by a number of different regulators. To confirm that the RNAseq dataset presented here correlated to previously published information about regulation in stationary phase, the dataset was searched for these known regulators.

The role of the stationary phase sigma factor, RpoS, was discussed in **Chapter 6**. **Table 10-1** shows that at 3 hours, expression of *rpoS* does not significantly differ from one hour. At 5 hours, the fold change of *rpoS* compared to at 1 hour was 2.06. This correlates to previous studies that show that there is increased expression of this sigma factor in stationary phase (Lange and Hengge-Aronis, 1994). However, the 2-fold difference is lower than expected. This may be due to increased expression further into stationary phase, and a limitation to the time when the sample was taken or the genes that are regulated by RpoS may show a higher increase in expression than the sigma factor itself. In this dataset, *rsd* which encodes for an anti-RNA polymerase σ^{70} factor had a fold increase of 2.45 at 5 hours compared to 1 hour of

growth in SL1344 **(Table 10-1**). Rsd has been shown to remove σ^{70} from RNA polymerase and promote the σ^{s} bound RNA polymerase holoenzyme (Mitchell et al., 2007). This shows that there is increased expression of genes involved in the transition of σ^{70} to σ^{s}. A number of RpoS regulated genes were found to have increased expression at 5 hours in this dataset including *bolA* (Lange and Hengge-Aronis, 1991a), *katG* , *otsA* (Ibanez-Ruiz et al., 2000) and the curli producing *csg* operon (Barnhart and Chapman, 2006, Arnqvist et al., 1994).

The stringent response is commonly associated with stationary phase. It is a phenomenon in which cells respond to starvation by downregulating rRNA biosynthesis and ribosomal proteins and increasing expression of RpoS (Navarro Llorens et al., 2010). The stringent response includes the accumulation of guanosine 3',5'-bispyrophosphate (ppGpp). A recent study showed that ppGpp altered transcription of 757 genes including the activation of *csgDEF* (curli genes), *raiA* and *rsd* (Sanchez-Vazquez et al., 2019). It has been shown that ppGpp regulates Rsd through the sequestering and competition of sigma factor binding the RNA polymerase core (Jishage et al., 2002).

RelA is a protein which synthesises ppGpp when responding to amino acid starvation (Navarro Llorens et al., 2010) whereas SpoT can both synthesise and degrade ppGpp in response to carbon and phosphorus starvation, as well as fatty acid shortage (Xiao et al., 1991, Spira et al., 1995, Seyfzadeh et al., 1993). The biosynthetic pathway for ppGpp is shown in **Figure 10-1**.

Salmonella sp and *E. coli* produce both of these proteins however this is not conserved across all bacteria (Battesti and Bouveret, 2009). In summary, ppGpp

accumulates in stationary phase to further adapt the cell to stationary phase and starvation. In this dataset however, the *relA* gene encoding a ppGpp synthetase did not have significantly altered expression at 3 or 5 hours compared to 1 hour. However, in *E. coli*, it was shown that the activity of RelA is subject to allosteric control (Turnbull et al., 2019) and therefore explain why transcript level does not differ. The *spoT* gene had decreased expression at 5 hours, which does not correlate to previous literature. However, there are a number of genes in this dataset with increased expression that respond to increased ppGpp such as *rpoS* (Gentry et al., 1993) and with decreased expression in response to ppGpp such as ribosomal genes (Lemke et al., 2011). In order to identify whether downregulation of *spoT* was expected in *Salmonella enterica* serovar Typhimurium, the gene was queried using the Salcom online tool (Kroger et al., 2013) which also showed a gradual decrease in *spoT* transcripts from early exponential to late stationary phase. This correlated with the RNAseq data. It may be hypothesised that the degrading activity of SpoT may contribute to the downregulation of this gene for an increased accumulation of ppGpp. . It may be hypothesised that the ppGpp-degrading activity of SpoT predominates in these conditions, thus *spoT* expression is repressed to allow increased ppGpp concentrations

Figure 10-1 The ppGpp biosynthesis pathway

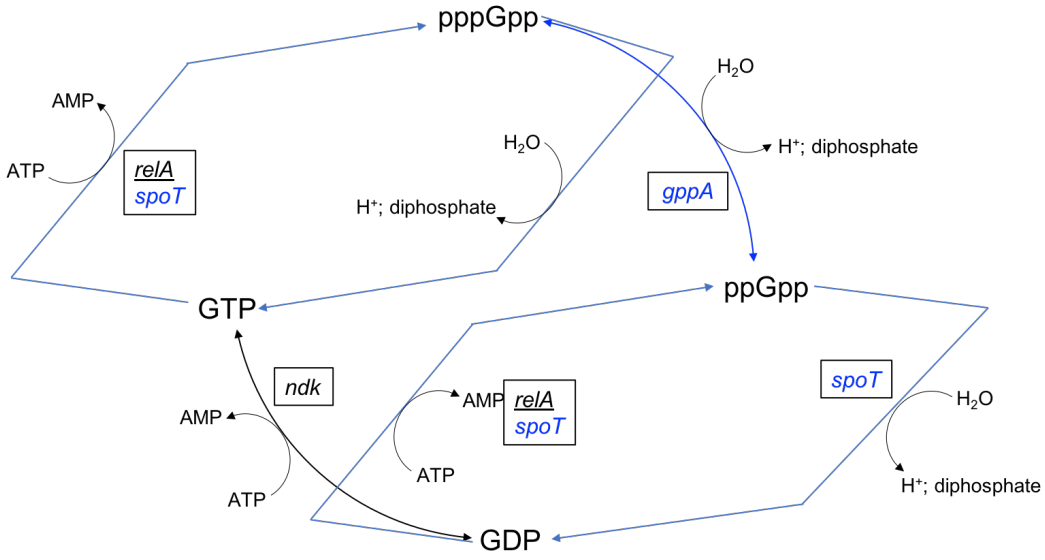

This pathway shows the biosynthesis pathway of ppGpp. Blue arrows are reactions where genes are downregulated. Genes for each reaction are shown in boxes next to their reaction arrow. Genes coloured blue are downregulated, and unchanged genes are shown as black and underlined.

Table 10-1 Differentially expressed regulatory genes in stationary phase

Regulators	Gene	1 hr vs 3 hr fold change	1 hr vs 5 hr fold change
σ^s	*rpoS*	-	2.06
Lrp	*lrp*	-	0.41
IHF	*ihfA*	-	-
	ihfB	2.13	-
Dps	*dps*	3.56	9.81
ppGpp	*relA*	-	-
	spoT	-	0.25
Anti-σ^{70} factor	*rsd*	-	2.45

Other regulators that have been linked to stationary phase are Lrp, IHF and Dps (Navarro Llorens et al., 2010). Lrp has been shown to play an important role in stationary phase, regulating around 200 *E. coli* stationary phase genes (Tani et al., 2002). **Table 10-1** shows that in this data set, *lrp* had decreased expression at 5 hours, suggesting that it is not playing a role in SL1344 stationary phase. However, regulators of stationary phase appear to only have only a slight increase in expression and therefore it may be the case that Lrp plays more of a role in the preparation for stationary phase in this case, and that experimental design meant the point of increased expression was missed. IHF (one subunit, *ihfB*) had increased expression at 3 hours **(Table 10-1)** and therefore it is possible that it correlates with previous data suggesting IHF plays a role in entrance into stationary phase (Mangan et al., 2006, Lee et al., 2015). In *E. coli*, Dps is one of the most abundant proteins in stationary phase (Nair and Finkel, 2004). It is induced by RpoS and IHF in stationary phase, but also protects from oxidative stress in exponentially growing cells (Altuvia et al., 1994). It was clear that in SL1344, at 3 hour and 5 hours, that the expression of Dps increased on entrance into stationary phase and is therefore in agreement with previous literature.

The downregulation of ribosomes suggests the shutdown of protein translation in stationary phase

Protein translation is reduced in stationary phase (Navarro Llorens et al., 2010, Huisman et al., 1996). Genes required for translation, namely genes that encode ribosomal proteins or tRNAs were analysed to determine whether transcript level correlated to information previously described in the literature.

When comparing SL1344 transcription at 1 vs 3 and 1 vs 5 hours, a large number of *rps* genes encoding 30S ribosomal proteins and *rpm* and *rpl* genes encoding 50S ribosomal proteins were downregulated in stationary phase. A number of these genes in *E. coli* have been shown to be directly repressed by the dual action of ppGpp and the RNA polymerase binding protein, DksA (Lemke et al., 2011), and ppGpp increases in stationary phase.

The ribosomal 30S subunit genes are shown in **Table 10-2**. Of these genes, only one, *rpsV*, had increased expression. The gene *rpsV* encodes the 30S ribosomal protein S22 and had a 3.27-fold change at 3 hours which increased to 16.57 at 5 hours. Previously, the *rpsV* copy number for the ribosomal protein was shown to increase in stationary phase and was therefore named the stationary-phase-induced ribosome-associated (SRA) protein (Izutsu et al., 2001b). The same study showed that increased transcription of *rpsV* on entrance into stationary phase was partly dependent on regulation by RpoS as well as Fis (factor inversion stimulation), IHF and ppGpp (Izutsu et al., 2001b). All other 30S subunit genes had a <0.15-fold change at 5 hours (decreased expression), except *rpsP*. Stationary phase bacteria shut down protein translation on entrance into stationary phase, and therefore it is possible that the decreased expression of these genes may be linked to reduced ribosomal activity and entrance into ribosomal hibernation (Yoshida et al., 2019). All 50S ribosomal subunit genes that were differentially expressed had decreased expression (**Table 10-3**) apart from *rpmJ2*. This feeds into the well accepted hypothesis that 30S and 50S ribosomes are produced in exponentially growing cells, and are stable in this phase. In stationary phase, these subunits are mostly degraded

or are ‘hibernating’ (Piir et al., 2011), therefore the requirement for transcription of these genes is limited.

Other ribosome associated genes in this dataset are *rimM* (ribosome maturation factor M), with a fold change of 0.05 and *rbfA* (ribosome binding factor A), with a fold difference of 0.23. RimM has been implicated as a factor involved in the late-stage assembly of the 30S ribosome (Guo et al., 2013), as well as RimM and RfbA also being essential for 16S processing (Bylund et al., 1998). Again, if ribosomes are shutting down in stationary phase, it would be expected that genes involved in ribosomal processing would show decreased expression.

Table 10-2 Differentially expressed genes that encode for 30S ribosomal subunits

Genes	Protein unit	1 hr vs hr 3 fold change	1 hr vs 5 hr fold change
rpsA	S1	0.16	0.08
rpsB	S2	0.40	0.05
rpsC	S3	-	0.06
rpsD	S4	0.38	0.08
rpsE	S5	0.41	0.08
rpsF	S6	0.28	0.05
rpsG	S7	0.36	0.10
rpsH	S8	0.42	0.09
rpsI	S9	0.28	0.04
rpsJ	S10	0.35	0.09
rpsK	S11	0.35	0.07
rpsL	S12	0.32	0.10
rpsM	S13	0.38	0.11
rpsN	S14	0.38	0.09
rpsO	S15	0.23	0.08
rpsP	S16	0.26	
rpsQ	S17	0.49	0.06
rpsR	S18	0.30	0.05
rpsS	S19	0.49	0.06
rpsT	S20	0.19	0.06
rpsU	S21	0.10	0.10
rpsV	**S22**	**3.27**	**16.57**

Table 10-3 Differentially expressed genes that encode for 50S ribosomal subunits

Genes	Protein unit	1 hr vs 3 hr fold change	1 hr vs 5 hr fold change
rplA	L1	0.44	0.09
rplB	L2	0.48	0.07
rplC	L3	0.33	0.06
rplD	L4	0.38	0.06
rplE	L5	0.36	0.08
rplF	L6	0.39	0.08
rplI	L9	0.29	0.05
rplJ	L10	0.44	0.10
rplK	L11	0.43	0.12
rplL	L7/L12	0.42	0.11
rplM	L13	0.31	0.06
rplN	L14	0.35	0.08
rplO	L15	0.39	0.06
rplP	L16	-	0.06
rplQ	L17	0.31	0.05
rplR	L18	0.39	0.08
rplS	L19	0.35	0.04
rplT	L20	0.49	0.32
rplU	L21	0.18	0.11
rplV	L22	0.45	0.05
rplW	L23	0.44	0.07
rplX	L24	0.35	0.08
rplY	L25	0.39	0.08
rpmA	L27	0.24	0.07
rpmB	L28	0.21	0.06
rpmC	L29	-	0.07
rpmD	L30	0.40	0.07
rpmE	L31	0.30	0.24
rpmF	L32	0.45	0.11
rpmG	L33	0.19	0.05
rpmH	L34	0.20	0.06
rpmI	L35	-	0.36
rpmJ	L36	0.44	0.16
rpmJ2	L36	-	2.12

The most upregulated gene at 5 hours in this dataset that was ribosome associated was *rmf* which encodes the ribosome modulation factor (RMF). Expression of *rmf* was increased by 63-fold at 5 hours compared to 1 hour. RMF is directly activated by ppGpp (Izutsu et al., 2001a) and is considered stationary phase specific (Wada et al., 1995). Previously it has been shown that RMF promotes the production of 100S ribosome dimers from 70S subunits (Wada et al., 2000). 100S ribosomes are considered inactive and their formation leads to the inhibition of translation. Stationary phase RMF inhibits translation and inactivates ribosomes by binding the 100S ribosome and blocking the peptidyl transferase centre and peptide exit tunnel (Yoshida et al., 2002). Mutations in the *rmf* gene prevent survival in prolonged stationary phase (Wada et al., 2000) and deletion of this gene in *E. coli* leads to increased susceptibility to gentamicin (McKay and Portnoy, 2015), highlighting that cells can be more tolerant of antibiotics in stationary phase.

Other genes associated with stationary phase ribosomes are *raiA* (also known as *yfiA*) and *ybhH*. They were shown to have increased copy number in stationary phase compared to exponential phase (Maki et al., 2000) with YbhH in *E.coli* involved in the stabilisation of 100S ribosomes and RaiA preventing 70S dimer formation in stationary phase (Ueta et al., 2005). With regards to the RNAseq dataset presented here, *raiA* had increased expression in stationary phase (at 5 hours) with 15.07-fold change, in agreement to previous literature. However, *ybhH* was not a differentially expressed.

The final ribosome related gene that is associated with stationary phase is *yqjD*, which produces the protein YqjD. Proteins paralogous to YqjD in *E. coli* include ElaB

and YgaM (Yoshida et al., 2012). YqjD has been identified as an inner membrane protein, however it has also been found to associate with 70S and 100S ribosomes in stationary phase (Yoshida et al., 2012). The function of YqjD is unknown but it has been suggested that it may inactivate ribosomes. Both *yqjD* and *elaB* had increased expression in the data presented in this chapter (fold change: 3.06 and 4.63 respectively at 5 hours when compared to 1 hour).

This data suggests that at 5 hours, stationary phase has been entered and that in SL1344 in stationary phase, translation is shut down and ribosomes hibernate as previously described in the literature.

Responding to carbon starvation in stationary phase

Stationary phase in batch culture signifies the start of nutrient starvation, namely glucose limitation or carbon starvation, and the Gram-negative cell response to carbon starvation has been extensively studied.

Carbon metabolism requires the uptake of sugars such as glucose into the cytoplasm, for progression of glycolytic pathways. Phosphotransferase systems (PTS) couple the transport of sugars across the membrane with phosphorylation of sugars (Vastermark and Saier, 2014). PTS sugars include glucose, fructose, mannose and mannitol. Briefly, the PTS transport system is a phosphorylation cascade which begins with a kinase, named Enzyme II, which catalyzes the transfer of phosphate from phospho*enol*pyruvate to HPr, a phosphoryl carrier (Vastermark and Saier, 2014) (This first phosphorylation step is not specific to different sugars). From this, the first of 3 PTS subunits is then phosphorylated (subunit IIA), followed subunit IIB and the sugar is phosphorylated and transported to the cytoplasm by IIC

(Vastermark and Saier, 2014). These subunits are specific to different sugars. These phosphorylated sugars are then converted to fructose-1,6-bisphospate and utilised in the glycolytic pathways (Jeckelmann and Erni, 2020, Vastermark and Saier, 2014). Glycolysis then produces phospho*enol*pyruvate which further facilitates sugar transport (Vastermark and Saier, 2014). In a glucose rich environment, cells will favourably transport glucose, and if PTS-glucose specific transporters are expressed, will only take up glucose even in the presence of other sugars (Jeckelmann and Erni, 2020). In this dataset, at 5 hours, *ptsG*, which encodes for a glucose specific PTS transporter subunit IIBC, had decreased expression (fold change of 0.22). This gene has previously been shown to be induced by the presence of glucose in the environment (Plumbridge, 2002) and therefore at 5 hours when glucose is limited in stationary phase, *ptsG* is not being induced. It has also been shown that SgrT acts to inhibit the expression of *ptsG* (Lloyd et al., 2017), and *sgrT* had increased expression in this dataset (2.46-fold change). It is possible that it may be unfavourable to express glucose specific transporters in stationary phase as they prevent the uptake of other sugars (Jeckelmann and Erni, 2020), and this may be why SgrT was upregulated.

Table 10-4 shows other sugar transporters that had highly increased transcription in this dataset. For example, genes of the *frwABCD* fructose PTS transporter were had increased expression as well as and alternative sugar transporter, *uhpT,* a hexose transport protein. Furthermore, expression of several unannotated PTS sugar transporters increased, possibly due to these transporters being non-specific in scavenging for sugars in a glucose limited environment. Increased expression of the transporter for galactose, MglABC, has previously been shown in glucose limited

batch culture (Death and Ferenci, 1993), and can also uptake glucose. Expression of *mglABC* was significantly increased in this dataset, possibly due to this transporter being able to uptake glucose if still present without inhibiting the uptake of other sugars.

The glycolytic pathways allow the utilisation of sugars following uptake into the cell. The glycolytic pathways of SL1344 include glycolysis and the Entner-Doudoroff pathways, the TCA cycle and the pentose phosphate pathway. At 5 hours, the genes involved in the Entner-Doudoroff pathway were not significantly changed from 1 hour. However, 2 genes had increased expression in the glycolysis pathway: *pfkB* (6-phosphofructokinase II) involved in the conversion of β-D-fructofuranose 6-phosphate to β-D-fructose 1,6-bisphosphate and *fbaB* (fructose bisphosphate aldolase) involved in the conversion of β-D-fructose 1,6-bisphosphate to D-glyceraldehyde 3-phosphate. These genes may be upregulated for the catabolism of carbon for energy in nutrient limiting conditions, however, it is also possible that the involvement of *fbaB* in gluconeogenesis is the reason for increased expression during starvation. Other than *fbaB*, *maeB* and *pckA* also had increased expression in the gluconeogenesis pathway. Gluconeogenesis is an important pathway in the production of sugars from pyruvate a carbon starved environment. Since genes in both the glycolytic and gluconeogenic pathways have increased expression at 5 hours, it is possible that the balance between the two is important in stationary phase. The TCA cycle also contains a number of genes with increased expression, notably *mdh* of the gluconeogenesis pathway and but also *gltA* and *acnA*, and all genes are required for the glyoxylate cycle.

Table 10-4 The differential expression of sugar transporters at 3 and 5 hours in SL1344

Transporters	Gene	1 hr vs 3 hr fold change	1 hr vs 5 hr fold change
PTS fructose transporter	*frwA*	-	-
	frwB	-	5.62
	frwC	2.79	27.03
	frwD	-	3.64
Hexose transporter	*uhpT*	-	0.42
Galactose transporter	*mglA*	-	36.09
	mglB	-	42.99
	mglC	-	13.45
PTS sugar transporters	RS08040	-	63.54
	RS08055	2.16	31.85
	RS19415	-	33.72
	RS19475	-	23.64
	RS19480	-	26.51
	RS23270	-	6.62
	RS23275	-	14.58
	RS23280	-	14.31

Table 10-5 Differentially expressed genes of carbon metabolism pathways in stationary phase

Pathway	Gene	1 hr vs 3 hr fold change	1 hr vs 5 hr fold change
Glycogen accumulation	*glgC*	-	7.98
	glgA	-	5.27
	glgB	-	3.17
	glgX	-	4.32
	glgP	-	4.05
Glyoxylate Cycle	*aceB*	5.64	4.58
	mdh	-	4.87
	gltA	-	2.84
	acnB	-	-
	acnA	-	5.23
	aceA	2.92	2.69

The upregulation of the glyoxylate cycle in stationary phase has been discussed previously (Huisman et al., 1996). It has been suggested that this pathway is more favourable than the TCA cycle because it circumvents the need for carbon producing conversion of isocitrate to 2-oxoglutarate to succinyl-CoA. Instead, isocitrate is converted to glyoxylate which can then be converted to malate, and further be used in gluconeogenesis. The genes involved in the glyoxylate cycle are shown in **Table 10-5** and those which had increased expression include *mdh*, *gltA* and *acnA*. The upregulation of this pathway in stationary phase agrees with previous literature (Huisman et al., 1996). It is also suggested that in glucose rich environments, where cells are rapidly dividing, glucose can be stored as acetate, which can then feed into the glyoxylate cycle during carbon starvation (Huisman et al., 1996).

At 5 hours, the genes involved in glycogen biosynthesis and accumulation, *glgC*, *glgA* and *glgB*, had increased expression (**Table 10-5**). This data correlates to previous studies that show that glycogen accumulates during nutrient deprived stationary phase, so that it can act as a sugar storage molecule (Huisman et al., 1996). However, in this dataset, *glgX*, encoding a debranching enzyme and *glgP*, encoding a phosphorylase, also showed increased expression. These genes are involved in the degradation of glycogen to glucose (Dauvillee et al., 2005, Alonso-Casajus et al., 2006). It is likely that they were also upregulated to provide glucose to the cell in glucose-limited environments.

Fatty acid β-oxidation genes in this dataset also showed increased expression. The genes include *fadA*, *fadB*, *fadD*, *fadE*, *fadI* and *fadJ*. Products from this oxidation can be utilised within the TCA cycle (Munoz-Elias and McKinney, 2006). It is possible that

the upregulation of oxidation in stationary phase is due to the increased need for energy in a nutrient deprived environment.

Genes involved in anaerobic respiration were upregulated in oxygen starved stationary phase

Within batch culture, stationary phase can lead to an oxygen limited environment. Anaerobic respiration is also required for *Salmonella* infection of a host (Paiva et al., 2009, Winter et al., 2010). In the dataset presented here, a large number of genes involved in anaerobic respiration had increased expression at 5 hours and these results will be discussed.

The genes required for glycerol utilisation were upregulated and are shown in Error! Reference source not found.. Glycerol can be used in both anaerobic and aerobic respiration. The transporters for glycerol-3-phosphate include *glpF* and *glpT*. GlpT decreased in expression at both 3 and 5 hours suggesting glycerol-3-phosphate does not use this transporter in stationary phase. GlpF also imports glycerol, which is then phosphorylated by GlpK, and both these genes had increased expression at 5 hours and allow for glycerol-3-phosphate to be utilised by glycolysis. However, *sn*-glycerol-3-phosphate can also be transported into the cell via the ABC transporter with subunits including UgpA, UgpB, UgpC and UgpE, where expression also increased in stationary phase. It is likely that the transport of *sn*-glycerol-3-phosphate accumulates more within the cell as it can be used as an electron donor directly in the electron transport chain during anaerobic respiration (Karp et al., 2016, Caspi et al., 2020, Iuchi et al., 1990). Using the GlpCBA glycerol dehydrogenase, *sn*-glycerol-3-phosphate can donate 2 electrons into chain, and 2 H^+ where fumarate can then

be used as the terminal electron acceptor, where succinate is produced to feed into the TCA cycle (Iuchi et al., 1990, Caspi et al., 2020). The upregulation of glycerol utilisation genes suggest its importance in anaerobic respiration in stationary phase.

Table 10-6 Differentially expressed genes of involved in glycerol utilisation in stationary phase

Gene	Product	1 hr vs 3 hr fold change	1 hr vs 5 hr fold change
glpC	anaerobic glycerol-3-phosphate dehydrogenase subunits	7.23	33.30
glpB		4.95	24.81
glpA		5.99	22.86
glpF	glycerol kinase	0.30	7.47
glpK	Porin/transporter	-	7.34
glpD	glycerol-3-phosphate dehydrogenase	-	3.15
glpT	transporter	0.28	0.28
ugpA	sn-glycerol 3-phosphate transport system permease protein	-	5.91
ugpB		-	14.48
ugpC		-	2.97
ugpE		-	4.58
gldA	glycerol dehydrogenase	3.86	4.93

The expression of the formate dehydrogenase, FdhF, was increased by 40.77-fold change at 5 hours, suggesting that formate could be another electron donator for the production of energy during anaerobic respiration. This enzyme is a molybdenum and selenium containing enzyme (Boyington et al., 1997) and may be linked to the upregulation in genes encoding the molybdenum cofactor pathway and the upregulation of *ydfZ* which is involved in selenium scavenging.

S. Typhimurium can use several terminal electron acceptors in place of O_2 during anaerobic respiration, due to a number of alternative terminal reductases. As previously mentioned, fumarate is a terminal electron acceptor, but other terminal acceptors include dimethyl sulphoxide (DMSO), trimethylamine N-oxide (TMAO), nitrate, nitrite and thiosulphate/tetrathionate. The reductases for these are FrdABCD, DmsABC, NarGHIJ and NarXYZ and TtrABC respectively (**Table 10-7** and **Table 10-8**). The *frd* and *dms* operons contain some of the most highly increased expressed in the dataset at 5 hours. Not only does the fumarate reductase have highly increased expression but also, at 5 hours, *ompW*, had a 42.22-fold change. This porin has been implicated in the uptake of fumarate and the cells transition to an anaerobic lifestyle (Xiao et al., 2016). The DmsABC operon has previously been shown to have increased expression in stationary phase (Nosek and Misek, 2019). The NarGHIJ and NarZ reductases also had increased expression at 5 hours (**Table 10-7**). This highlights the requirement for anaerobic growth at 5 hours or during stationary phase. These reductases have also been shown to be required for anaerobic respiration in *Salmonella* when infecting the intestinal tract of an avian host (Paiva et al., 2009). Further to this, operons encoding hydrogenases (*hyp* and *hyb*) increased in expression at 5 hours. These hydrogenases accept electrons off H_2 that can then be

accepted by fumarate or DMSO-trimethylamine N-oxide (Laurinavichene and Tsygankov, 2001).

Table 10-7 Genes encoding S. Typhimurium terminal reductases in anaerobic respiration

Alternative terminal reductases	Gene	1 hr vs 3 hr fold change	1 hr vs 5 hr fold change
Fumarate Reductase	*frdA*	9.70	28.39
	frdB	10.86	27.02
	frdC	12.20	24.32
	frdD	12.33	23.23
DMSO-trimethylamine N-oxide reductase	*dmsA*	15.08	18.45
	dmsB	17.54	22.98
	dmsC	9.60	10.90
Nitrate/nitrite reductase	*narG*	2.37	2.58
	narH	4.09	4.50
	narI	2.79	2.01
	narJ	5.47	5.15
	narX	-	-
	narY	-	-
	narZ	-	3.19

Table 10-8 Genes involved in anaerobic respiration using tetrathionate

operon	Gene	1 hr vs 3 hr fold change	1 hr vs 5 hr fold change
ttrRSABC	*ttrR*	-	2.77
	ttrS	-	4.02
	ttrA	-	2.49
	ttrB	-	-
	ttrC	-	-
phsABC	*phsA*	-	4.52
	phsB	-	3.41
	phsC	-	5.53
asrABC	*asrA*	-	22.36
	asrB	2.07	12.98
	asrC	2.45	16.50

Ethanolamine and 1,2-propanediol can be used as a carbon source in anaerobic environments. Ethanolamine has been shown to be abundant in mammalian cells and is utilised by *Salmonella* during infection in the intestine (Anderson et al., 2015, Thiennimitr et al., 2011). Genes involved in the degradation of these compounds had increased expression in this dataset. EutC and EutB had increased expression for the degradation of ethanolamine, and PduC, PduD and PduP had increased expression for the degradation of L-1,2-propanediol. The *pdu* genes are also involved in the degradation of glycerol to 3,4-propanediol. However, it has been shown that neither of these compounds alone can be used for cells to grow anaerobically. Utilisation of both is reliant of the production of vitamin B_{12}, which is produced *de novo* in *S*. Typhimurium in anaerobic conditions (Price-Carter et al., 2001). It was shown that in the presence of the terminal electron acceptor, tetrathionate, ethanolamine and 1,2-propanediol could be used as a carbon energy source anaerobically (Price-Carter et al., 2001). The tetrathionate reductase, TtrABC, did not have significantly changed gene expression in this dataset. However, the TtrRS sensor histidine kinase had increased expression at 5 hours (**Table 10-8**), required for sensing tetrathionate and production of the tetrathionate reductase. The cascade of reactions that allow tetrathionate to produce energy involve two further operons. Tetrathionate is converted to thiosulphate with the *ttr* operon, followed by thiosulphate conversion to sulphite and sulphide (using the *phs* operon). Sulphite and NADH are then converted to sulphide, H_2O and NAD^+ using the *asr* operon. Both the *phsABC* and the *asrABC* operons had highly increased expression at 5 hours compared to 1 hour in this dataset (**Table 10-8**). It has previously been shown that tetrathionate can be produced in an inflamed host intestine when *S.* Typhimurium

causes infection which allows the pathogen to survive anaerobically (Winter et al., 2010).

All these genes, operons and pathways relating to anaerobic respiration have increased expression showing the importance of anaerobic respiration in stationary phase in batch culture, where oxygen becomes limited

Appendix VI Table DEGs only changed in SL1344 Δ*acrB* and not found changed in SL1344

Gene	Product	Fold change (1 hr vs 5 hr)
glnA	glutamate--ammonia ligase	0.25
lamB	maltoporin	0.28
sucC	ADP-forming succinate--CoA ligase subunit beta	0.34
iraM	anti-adapter protein IraM	0.36
btuB	TonB-dependent vitamin B12 receptor BtuB	0.36
yifK	amino acid permease	0.36
odhB	2-oxoglutarate dehydrogenase complex dihydrolipoyllysine-residue succinyltransferase	0.37
yfaZ	putative inner membrane protein	0.39
recF	DNA replication/repair protein RecF	0.41
dapE	succinyl-diaminopimelate desuccinylase	0.41
bacA	undecaprenyl-diphosphate phosphatase	0.42
dsbI	protein-disulfide oxidoreductase DsbI	0.42
sucD	succinate--CoA ligase subunit alpha	0.42
amiA	N-acetylmuramoyl-L-alanine amidase AmiA	0.42
lipB	lipoyl(octanoyl) transferase LipB	0.43
pheT	phenylalanine--tRNA ligase subunit beta	0.43
lpxM	lauroyl-Kdo(2)-lipid IV(A) myristoyltransferase	0.44
msgA	virulence protein	0.45
ispB	octaprenyl diphosphate synthase	0.45
yiaH	acetyltransferase	0.45
cmoA	carboxy-S-adenosyl-L-methionine synthase CmoA	0.45
fre	NAD(P)H-flavin reductase	0.45
sdaA	L-serine ammonia-lyase	0.46
yneJ	putative LysR family transcriptional regulator	0.46
rlmI	23S rRNA (cytosine(1962)-C(5))-methyltransferase RlmI	0.46
rfaQ	lipopolysaccharide core heptosyltransferase RfaQ	0.46
hybD	HyaD/HybD family hydrogenase maturation endopeptidase	0.46

pldA	phospholipase A	0.46
minE	cell division topological specificity factor MinE	0.46
stpA	DNA-binding protein StpA	0.47
nudB	dihydroneopterin triphosphate diphosphatase	0.47
sitB	iron/manganese ABC transporter ATP-binding protein SitB	0.47
minD	septum site-determining protein MinD	0.47
nudE	ADP compounds hydrolase NudE	0.47
mlaA	phospholipid-binding lipoprotein MlaA	0.47
cpoB	cell division protein CpoB	0.47
glpG	rhomboid family intramembrane serine protease GlpG	0.47
slmA	nucleoid occlusion factor SlmA	0.47
asnC	transcriptional regulator AsnC	0.48
hslO	Hsp33 family molecular chaperone HslO	0.48
nikR	nickel-responsive transcriptional regulator NikR	0.48
ftsN	cell division protein FtsN	0.48
epmA	elongation factor P--(R)-beta-lysine ligase	0.48
smpB	SsrA-binding protein SmpB	0.48
zipA	cell division protein ZipA	0.48
coaBC	phosphopantothenoylcysteine decarboxylase/phosphopantothenate--cysteine ligase	0.48
tyrP	tyrosine transporter TyrP	0.49
lolE	lipoprotein-releasing ABC transporter permease subunit LolE	0.49
pyrG	CTP synthase (glutamine hydrolyzing)	0.49
yrdA	gamma carbonic anhydrase family protein	0.49
lolB	lipoprotein localization protein LolB	0.49
gshA	glutamate--cysteine ligase	0.49
citC	[citrate (pro-3S)-lyase] ligase	0.49
mobB	molybdopterin-guanine dinucleotide biosynthesis protein B	0.50
creD	cell envelope integrity protein CreD	0.50
traC	type IV secretion system protein TraC	0.50
ygcY	putative d-glucarate dehydratase	2.00
ssrA	hybrid sensor histidine kinase/response regulator	2.01

iroB	salmochelin biosynthesis C-glycosyltransferase IroB	2.02
ymdB	O-acetyl-ADP-ribose deacetylase	2.03
traU	conjugal transfer pilus assembly protein TraU	2.03
mtlD	mannitol-1-phosphate 5-dehydrogenase	2.04
pdxK	pyridoxine/pyridoxal/pyridoxamine kinase	2.05
hdeB	acid-activated periplasmic chaperone HdeB	2.05
traB	conjugal transfer protein TraB	2.08
pmrD	signal transduction protein PmrD	2.08
traR	conjugal transfer protein TraR	2.09
lrgA	murein hydrolase regulator LrgA	2.09
yfcF	glutathione transferase	2.10
pduK	propanediol utilization microcompartment protein PduK	2.12
rtcA	RNA 3'-terminal phosphate cyclase	2.13
rhtC	threonine export protein RhtC	2.13
trpS2	AraC family transcriptional regulator	2.16
ydiP	colanic acid biosynthesis acetyltransferase WcaB	2.17
wcaB	homoserine/homoserine lactone efflux protein	2.18
rthB	major pilin PefA	2.18
pefA	curli production assembly/transport protein CsgF	2.20
csgF	2-keto-myo-inositol isomerase IolI1	2.23
iolI1	citrate lyase holo-[acyl-carrier protein] synthase	2.23
citX2	exodeoxyribonuclease V subunit alpha	2.24
recD	cobalamin reductase PduS	2.25
pduS	cobalt ABC transporter substrate-binding protein CbiN	2.27
cbiN	acetylglutamate kinase	2.27
argB	homoserine kinase	2.28
thrB	fimbrial minor subunit StfF	2.29
stfF	DNA-binding response regulator	2.34
ssrB	acetolactate synthase 2 catalytic subunit	2.65
ilvG	threonine synthase	2.68
thrC	bifunctional aspartate kinase/homoserine dehydrogenase I	2.75

thrA	branched-chain-amino-acid transaminase	2.91
ilvE	ketol-acid reductoisomerase	2.93
ilvC	dihydroxy-acid dehydratase	3.20
ilvD	acetolactate synthase 2 small subunit	3.43
ilvM	acetolactate synthase 2 small subunit	3.52
		4.00
		4.22
		4.38
		7.03